Conductive Anodic Filament (CAF) Formation

by

Antonio Caputo

A thesis submitted in conformity with the requirements
for the degree of Doctor of Philosophy

Materials Science and Engineering
University of Toronto

Conductive Anodic Filament (CAF) Formation

Antonio Caputo

Doctor of Philosophy

Department of Materials Science and Engineering
University of Toronto

2010

Abstract

Conductive anodic filament (CAF) is a failure mode in printed wiring boards (PWBs) which occurs under high humidity and high voltage gradient conditions. The filament, a copper salt, grows from anode to cathode along the epoxy-glass interface. Ready and Turbini (2000) identified this copper salt as the $Cu_2(OH)_3Cl$, atacamite compound. This work has investigated the influence of polyethylene glycol (PEG) and polyethylene propylene glycol (PEPG) fluxing agents on the chemical nature of CAF. For coupons processed with PEPG flux, with and without chloride, a copper-chloride containing compound was formed in the polymer matrix. This compound was characterized using x-ray photoelectron spectroscopy (XPS) as CuCl and an electrochemical mechanism for the formation of the chloride-containing CAF has been proposed. For PEG flux, with and without chloride, it has been shown that CAF only formed, but no copper containing compound formed in the matrix. It appears for PEG fluxed coupons, a PEG-Cu-Cl complex forms, binds the available Cu and acts as a barrier to the formation of CuCl in the polymer matrix. Meeker and Lu Valle (1995) have previously proposed that CAF failure is best represented by two competing reactions – the formation of a copper

chloride corrosion compound (now identified as $Cu_2(OH)_3Cl$) and the formation of innocuous trapped chlorine compounds. Since no evidence of any trapped chloride compounds has been found, we propose that the formation of CAF is best represented by a single non-reversible reaction.

For coupons processed with a high bromide-containing flux, bromide containing CAF was created and characterized using transmission electron microscopy (TEM) to be $Cu_2(OH)_3Br$. In addition, a copper-containing compound was formed in the polymer matrix and characterized using XPS as CuBr. An electrochemical mechanism for the formation of bromide-containing CAF has been proposed based on the XPS data.

.

Dedicated to my Parents, Domenico & Maria Caputo & my brother Roberto Caputo

Acknowledgements

I would like to thank Dr. Laura J. Turbini for her guidance, time and great support. Her great patience and investment in ensuring my success has been invaluable. She has taught me the key skills that are necessary to succeed in academics. Her advice and knowledge has taught me great scientific and logical thought.

I would like to thank Professor Doug D. Perovic for his great guidance and support throughout my academic career in the Department of Materials Science and Engineering at the University of Toronto. If it were not for his great enthusiasm as my instructor in the introductory Materials Science and Engineering course I would not have found a home and a great passion for materials science.

I would like to extend my sincerest gratitude to Dr. Jim E. Clemans from Alcatel-Lucent Technologies for his thorough review of my thesis and his very insightful comments which have aided in the improvement of my thesis.

I would like to thank my committee members, Professor M. Thompson, Professor M. Kortschot and Professor T. North for taking time out of their busy schedules to participate on my committee. Their time, effort, support and suggestions have been very valuable.

I would like to thank Professor Jun Nogami, chairman of the Department of Materials Science and Engineering for all his time, effort, guidance and support in ensuring my success. I would like to thank Professor Steven J. Thorpe, the MSE graduate chair, for all his time and patience in aiding me in the improvement of my thesis.

I would like to thank the entire administrative staff in the Department of Materials Science and Engineering, in particular Maria Fryman, Fanny Strumas, and Jody Prentice for all their help.

I would like to thank all my friends and colleagues, in particular Dr. Dwayne Shirley, Dr. Adrian Gerlich, Ibraheem Khan, Peter Su, David Lau, Alex Liu, Zain Aleem, and Nelson To who have provided great support and friendship. I would also like to thank Sal Boccia for all his friendship, great advice and all his technical support. I would like to thank Peter Brodersen for all his technical assistance in obtaining x-ray photoelectron spectroscopy (XPS) data.

I would like to thank the entire Materials Interconnect Lab at Research in Motion, in particular Dr. Bev Christian, Andrew Ryzynski, Alex Romanov, Deepchand Ramjattan, and Edmund Zygalo for welcoming me into their lab and providing invaluable technical assistance.

I would also like to thank the Centre for Microelectronics, Assembly, and Packaging (CMAP), Materials and Manufacturing Ontario (MMO), the Ontario Graduate Scholarship (OGS) for funding this work and the University of Toronto Open Fellowship Program.

I would like to thank my parents, Domenico and Maria Caputo for all their support and guidance throughout my academic career. I would like to thank my brother, Roberto Caputo for all his great support and being the greatest little brother in the whole world.

Table of Contents

List of Acronyms

CAF – conductive anodic filament
PWB(s) – printed wiring board(s)
PEG – polyethylene glycol
PEG/Cl – polyethylene glycol with chloride
PEPG – polyethylene polypropylene glycol
PEPG/Cl – polyethylene polypropylene glycol with chloride
LAP – linear aliphatic polyether
HASL – hot air solder leveling
XPS – x-ray photoelectron spectroscopy
TEM – transmission electron microscopy
SEM - scanning electron microscopy
EDS – energy dispersive spectroscopy
FIB – focused ion beam
FTIR – Fourier transform infrared spectroscopy
T-H-B – temperature-humidity-bias
SIR – surface insulation resistance
IR - insulation resistance
FR-4 - flame resistant composite laminate consisting of a brominated epoxy matrix reinforced with E-glass fibers.
MC-2 - a blended polyester and epoxy matrix with woven glass face sheets, and a chopped glass core.
G-10 - non-fire retardant epoxy/woven glass.
BT - bis-maleimide triazine
CE- cyanate esters
CEM-3 - a substrate similar to G-10 except with chopped glass.
DICY – dicyamide
IEC – International Electrotechnical Commission
JPCA – Japan Printed Circuit Association
IPC – Association Connecting Electronics Industries
DOPO – 9,10-dihydro-9-oxa-10-phosphenanthrene-10-oxide
WSF – water soluble flux
BSE – backscattered electrons
SE – secondary electrons
H-H – hole-to-hole
H-T – hole-to-trace
T-H – trace -to-hole
T-T – trace-to-trace
RH – relative humidity
CTE – coefficient of thermal expansion
ac – alternating current
dc – direct current
ICDD – International Centre for Diffraction Data
BE – binding energy

List of Symbols

T_g – glass transition temperature
t_F – failure time
E_a – activation energy
H- relative humidity
V- voltage
T- temperature
L- conductor spacing
a,b,d – material dependent constants
R – universal gas constant
t_1 – represents the failure time due to weakening of the epoxy/glass interafce
t_2 – represents the failure time due to the electrochemical process
MTTF – mean time to failure
A_1 – chlorine salt
A_2 – CAF
A_3 – innocuous trapped chlorine compounds
r - measured ring radius on the diffraction pattern in mm
d - interplanar spacing in nm
L_{CL}- the camera length of the TEM
λ - the wavelength of incident radiation
E_b - binding energy
KE – kinetic energy
w - work function of the spectrometer
ν - frequency
h – Planck's constant
M – molarity (mols/liter)
K_s – solubility product constant
$\Delta G°_f$ - standard free energies of formation
ΔG° - standard free energy change for a reaction
k – rate constant

List of Figures

List of Tables

Chapter 1 – Introduction

1.1 Organization of Thesis

Chapter 1 – Introduction

This chapter will introduce conductive anodic filament (CAF) formation and its importance in modern day electronics. The objectives and motivations of this thesis will also be provided.

Chapter 2 – Background

This chapter provides a detailed historical background of CAF from when it was first discovered in 1976 to present. This chapter will also survey the literature and previous experimental experience to identify the limitations in designing a PWB for CAF testing and will provide a recommendation for a suitable hole-hole edge spacing.

Chapter 3 – Experimental

This chapter provides all the test methods and experimental testing apparatus used in this work.

Chapter 4 – Results

This chapter evaluates coupons that were processed with 5 different solder flux formulations. Two different analytical techniques are used to show that there is an interaction between the substrate material and solder flux. Several characterization techniques are used to observe CAF.

Chapter 5 – Discussion

This chapter discusses all the findings presented in chapter 4. The relevant chemical reactions in the formation of CAF will be discussed for the various fluxes tested and a model explaining the results will be proposed.

Chapter 6 – Summary and Conclusions

This chapter will list all the major contributions of this thesis.

Chapter 7 – Industrial Significance and Impact

This chapter provides insight on the industrial significance and impact of the findings of this work.

Chapter 8 – Future Work

This chapter provides important test methodologies that must be incorporated in future CAF testing.

1.2 Conductive Anodic Filament

In the mid 1970's, Bell Lab researchers [1-5] discovered a new failure mode in printed wiring boards (PWBs), the creation of a subsurface short, later termed conductive anodic filament (CAF) [3]. CAF is an electrochemically induced failure in which a conductive copper-containing [3] salt grows from the anode to the cathode along the epoxy/glass fiber interface in the PWB.

1.3 Factors Accelerating CAF

The rate of CAF formation is influenced by mechanical stress, processing temperature, solder flux, accelerated temperature aging conditions, humidity and bias (T-H-B) and conductor spacing. These will be discussed in more detail in Chapter 2.

1.4 Importance of CAF in Modern Day Electronics

Traditionally in the electronics industry PWB materials have been processed using lead-tin soldering conditions where the board material was exposed to a temperature range of 201°C - 220°C. However, the European Union mandated that after July 1st, 2006 all electronics sold in Europe must use lead-free soldering (with only a few exemptions). This has resulted in PWB's being exposed to process temperatures from 240°C - 260°C. These higher processing temperatures pose a reliability threat when it comes to CAF failure [6].

During the soldering process a solder flux is used to clean the surface of the metal enabling the solder to wet more effectively with the metal pads. Water soluble fluxes are used by some companies because of their ability to produce high yields and create flux residues that are easily removed with water. Since there is an interaction between the flux and the board, careful consideration in flux selection must be taken to avoid reliability issues related to CAF [6-10].

The movement to increased circuit density, creating more compact designs has reduced component size and conductor spacing considerably. Closer conductor spacing has resulted in higher voltage gradients, which is a key element in the rate of CAF formation [9, 10].

1.5 Objectives and Motivations

The goal of this work is to develop and understand the electrochemical processes involved in the formation of both chloride and bromide containing CAF by studying the interaction between the solder flux and laminate material. The objectives and motivations to accomplish these goals are listed in the paragraphs below.

1.5.1 – Interaction of Board Material and Solder Flux

Ready [9, 10] has found that for certain water soluble fluxes, CAF forms at the epoxy/glass fiber interface, and in addition a copper containing compound is found within the polymer matrix. The present work will characterize that compound in detail and determine its composition.

1.5.2 – Electrochemical Mechanism for Chloride Containing CAF Formation

Ready identified CAF to contain copper and chlorine [8], and further identified it to be $Cu_2(OH)_3Cl$ using Transmission Electron Microscopy (TEM) [9, 10]. The present work will further consider the electrochemical mechanism for CAF formation.

1.5.3– Characterization and Electrochemical Mechanism for Bromide CAF

Previously Ready [8] has shown when a high bromide-containing flux is used, CAF containing copper and bromine is found. This work will create bromide CAF and determine its composition and mechanism of formation.

Chapter 2 – Background

2.1- Printed Wiring Boards (PWBs)

The printed wiring board (PWB) has been used in the electronics industry for over 50 years [11]. A PWB is defined as a "printed board that provides point-to-point connections but not printed components in a predetermined arrangement on a common base" [12]. This section will discuss the issues related to PWBs as they pertain to this thesis.

2.1.1 – What Are Printed Wiring Boards (PWB's)?

A PWB is a polymer resin composite (typical constructions contain epoxy) with reinforced glass (E-glass) fibres.

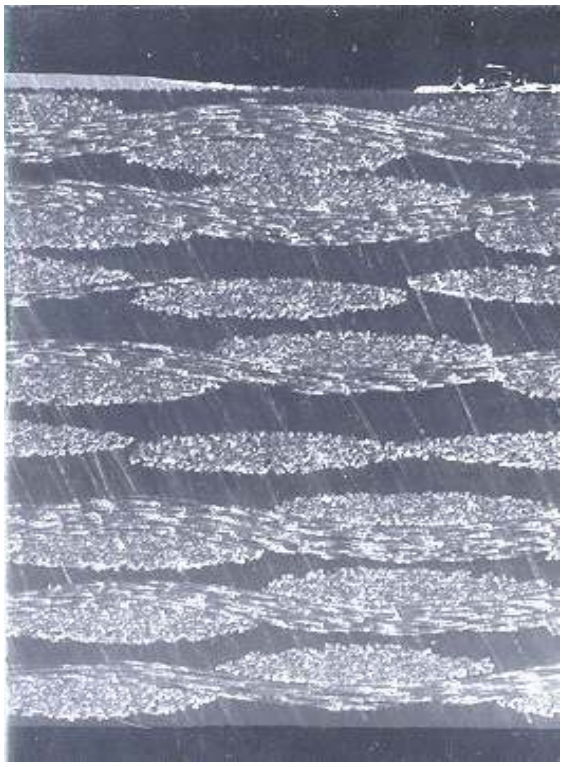

Figure 2.1: Cross-section of a PWB [8].

PWBs can be classified into three main types:

(1) Single-sided boards –boards that have circuitry on only one side.

(2) Double-sided boards – a board with a conductive pattern on both sides. For the purposes of this thesis, metalized holes were used. Typically double-sided PWBs use 8 sheets of 7628-glass cloth with a thickness of 0.175 mm (0.007”) to create a 1.5 mm (0.062”] thick board. The glass to resin ratio in this case is higher than that of a multilayer board, where the glass cloth thickness might range from 0.025 to 0.10mm (0.001” to 0.004 “) per layer and there might be 1-3 sheets used in each layer of the core and the prepreg (i.e. a sheet material, such as glass fabric impregnated with a resin cured to an intermediate stage).

(3) Multilayer boards - boards containing three or more circuit layers. This type of construction is employed in PWB designs in consumer products such as portable video games, cellular phones and audio discs. The advantage of this is reduction in costs, increase in features within a smaller size, flexibile resin content, and variation in glass style. These become very important when constructing PWBs for CAF analysis.

For the purpose of this thesis, CAF testing was performed on a double sided board with plated through holes. In design related issues pertaining to CAF resistant materials, a multi-layer board design is recommended and used in the industry test methods.

2.1.2 - PWB Laminate Materials

CAF testing has been performed on several different laminate materials over the last 30 years. The bulk of the work has focused on FR-4 and other traditional laminates. In the last 10 years, several studies have evaluated a new class of laminates, mainly CAF

resistant laminates and halogen free laminates. The following sections will discuss FR-4 and traditional laminates, CAF resistant materials and halogen free materials.

2.1.2.1 – FR- 4 and Other Traditional Laminates

Over the last 30 years many different laminate materials have been evaluated. The predominant laminate used in the electronics industry is FR-4. FR-4 is a term used by laminate manufacturers to describe the flame resistant composite laminate consisting of a brominated epoxy matrix reinforced with E-glass fibers. Lando [3], Rudra [13] and Ready [8] have investigated the susceptibility of FR-4 to CAF failure compared to CAF failure for different laminate materials. Lando compared conventional FR-4 to G-10 (non-fire retardant epoxy/woven glass), polyimide/woven glass, polyester/woven and chopped glass, epoxy/ kevlar and triazine/woven glass. Rudra compared conventional FR-4 to bis-maleimide triazine (BT), and cyanate esters (CE). Ready compared FR-4 with CEM-3 (a substrate similar to G-10 except with chopped glass) and MC-2 (a blended polyester and epoxy matrix with woven glass face sheets, and a chopped glass core). Based on all their findings, CAF formation is most resistant in bismaleimide triazine (BT) and most susceptible in MC-2. The susceptibility of CAF failure in each of these materials follows the trend:

MC-2 >> Epoxy/Kevlar > FR-4 ≈ PI > G-10 > CEM-3 > CE > BT

These studies show that careful consideration in material choice is required when CAF failure is a possibility. For the designer, this depends on both cost and application.

2.1.2.2 – CAF Resistant Materials

A new class of materials termed “CAF resistant materials” has emerged in the last 10 years. These materials tend to have superior thermal properties. Traditional FR-4 has

a glass transition temperature (T_g) ranging between 125 °C - 135 °C. For some applications, materials which have a T_g ranging between 175 °C - 180 °C are required. These higher T_g can be achieved by using a phenolic curing process with a poly-functional epoxy in place of the traditional DICY (dicyandiamide) curing process used in FR-4 materials. In addition, traditional epoxy is manufactured by the reaction of epichlorohydrin and bisphenol-A forming difunctional epoxy (Figure 2.2) From the reaction below it can be seen that chlorine is left behind as a by-product from the reaction that forms epoxy. Since chlorine is required to form CAF, an additional cleaning step has been added in the processing of CAF resistant materials to eliminate the chlorine present.

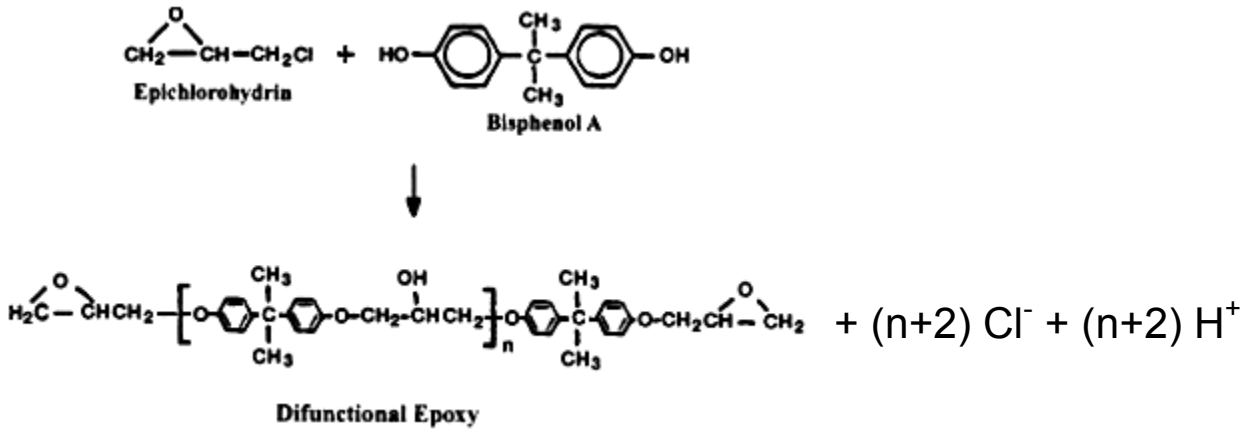

Figure 2.2: Reaction between epichlorohydrin and bisphenol A to form epoxy[14].

2.1.2.3 – Halogen-Free Materials

More recently there has been a push for halogen-free electronic materials from computer manufacturers who have mandated that they will offer bromine and chlorine free consumer products. Several international organizations have defined halogen-free as bromine and chlorine-free, and have set different maximum allowable concentrations

in the product. The IEC (International Electrotechnical Commission) 61249-2-21 and the IPC have set a maximum allowable concentration of 900 ppm bromine or chlorine with the total concentration of both these elements not to exceed 1500 ppm. The JPCA ES-01 (Japan Printed Circuit Association) defines halogen-free as a maximum concentration of 900 ppm for bromine or chlorine. Halogen-free epoxy replaces the brominated epoxy with phosphorus doped epoxy and metal hydroxide fillers such as aluminum and magnesium hydroxide. DOPO (9,10-dihydro-9-oxa-10-phosphenanthren e-10-oxide) is commonly used in halogen-free epoxy as flame retardant replacements [15]. Since the focus of this work is not on halogen free materials, these laminate materials will not be discussed further.

2.2 – Fluxes

Soldering [12] is defined as the process of joining metallic surfaces without melting the base metals. In order for the joining to take place the metallic surface needs to be clean of contaminants and oxides. The flux [12] is a chemically active compound that, when heated, removes minor surface oxidation, minimizes oxidation of the basis metal, and promotes the formation of an intermetallic layer between solder and basis metal.

2.2.1 – Flux Types

The three main types of fluxes are: (a) rosin fluxes, (b) low solid/no clean fluxes, and (c) water soluble fluxes. The rosin flux contains naturally occurring resin from the sap of pine trees, which contains a unique blend of organic acids with the two most common ones being pimaric acid and abietic acid. Rosin fluxes are useful because they tend to liquefy during soldering and solidify upon cooling entrapping harmful contaminants.

These fluxes tend to be used in high reliability military applications or for medical electronics.

In the mid 1980's a new class of fluxes termed (low solid or no-clean) was developed. The initial formulations contained 5-8 wt% solids compared with the traditional fluxes which used 25% solids. Today's formulations contain 1-2 wt% solids. These fluxes tend to remove the need to clean because of the low level of contaminants left on the board after processing. Neither rosin nor low solid fluxes are the focus of this thesis, so no further details will be provided on them. Water soluble fluxes will be discussed in the next section of this thesis because they are the focus of this thesis.

2.2.2 – Water Soluble Flux

Water soluble fluxes (WSF) are sometimes referred to as "organic acid fluxes". This name can be misleading because most fluxes used in electronics are organic based. These fluxes may contain a wide range of halide, organic acid or amine activators, with an alcohol based solvent and a polyglycol vehicle. The constituents of WSF and the role of each constituent (i.e. solvent, vehicle and activators) will be discussed further in the coming sections. Water soluble fluxes have gained acceptance in the electronics industry due to their wider processing window, higher soldering yield, and ability to be cleaned with water. The main issues with these fluxes are they tend to be more aggressive, leaving harmful residues that if not cleaned properly can lead to corrosion in the field and long term reliability issues. Water soluble fusing fluids are used as the flux for hot air solder leveling (HASL), where solder is applied to the board to preserve its solderability.

2.2.2.1 – Solvent

The solvent serves to dissolve the vehicle, activators, and other additives. It evaporates during the soldering process. The solvent is chosen based on its ability to dissolve the flux constituents and its boiling point. Typical, solvents used are alcohols, glycols, glycol esters, glycol ethers, and water. An alcohol based solvent was used in this work.

2.2.2.2 – Vehicle

The vehicle is the non-volatile liquid that coats the basis metal to be soldered, and dissolves metal salts formed during the reaction between the activators with the surface oxides. It also serves as a heat transfer medium between the solder and the components. Typical WSF vehicles are glycols, polyglycols, polyglycol surfactants, polyethers, and glycerine. The vehicles chosen for this study were polyethylene glycol (PEG) and poly(ethylene/propylene) glycol (PEPG) and a polyglycol in the HASL fluid which was not fully identified in the material safety data sheet.

2.2.2.3 – Activator

The activator is used to enhance the removal of surface oxides during the soldering process. Activators can be reactive at room temperature, but their activity is enhanced at elevated temperatures. There are many different activators that can be chosen, but for the purposes of this study chlorine or bromine were chosen as the activators.

2.2.3 – Postproduction Cleaning

The cleaning step for water soluble fluxes is critical for removing harmful residues. Movement to a lead-free world poses additional challenges in the cleaning process because the higher processing temperature results in greater polymerization of the flux constituents, producing residues that are more difficult to remove. Adjusting the water

bath temperature, introducing agitation, and increasing the time the board is exposed to the cleaning steps are all things that must be considered.

2.3 – CAF

Conductive Anodic Filament (CAF) is an electrochemically induced failure mode in which a conductive copper containing salt grows from the anode to the cathode along the epoxy/glass fiber interface. Figure 2.3 (a) illustrates the formation of CAF in a hole-to-hole pattern, and (b) shows the cross section of a PWB with CAF visible around the glass fibers. Scanning electron microscopy using back scattered electrons (SEM/BSE) was used to generate this image.

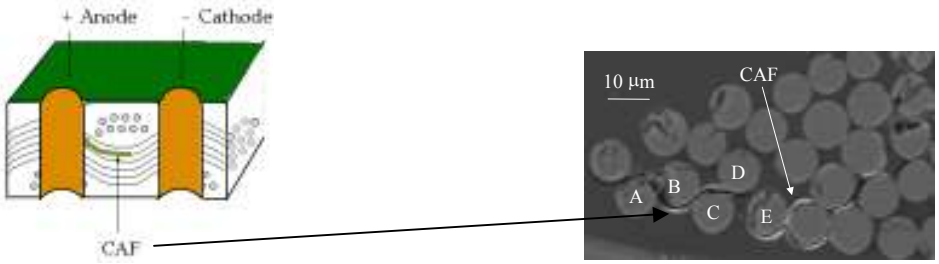

(a) (b)

Figure 2.3: (a) Formation of CAF, and (b) Cross section of a PWB showing CAF surrounding the epoxy/glass fiber interface using SEM/BSE [9].

2.3.1 – Early Work on CAF

The first work on CAF was done by the Bell Lab researchers in the mid 1970's. Boddy et al [1] conducted a failure analysis study using FR-4 fine-line flexible printed circuits coated with different UV-cured resins. Figure 2.4 shows several flexible printed circuits illustrating the various factors studied: covercoat, number of glass reinforcement layers, and thickness of the epoxy buttercoat[1] layer.

---

[1]**Buttercoat:** A layer of epoxy applied over the glass-reinforced core of the substrate [1].

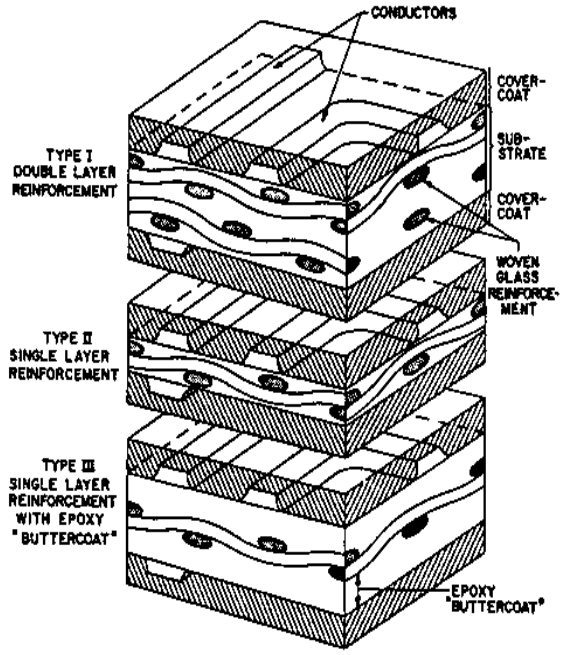

Figure 2.4: Typical flexible printed wiring construction which makes use of woven glass reinforcement [1]. © 1976 IEEE

Boddy first examined flexible printed circuits with covercoat. These were exposed to a series of processing operations to simulate the normal assembly process (i.e. fluxing, wave soldering, and cleaning). The processed coupons were then exposed to accelerated test condition ranging from 35ºC–95ºC, 25%-95% relative humidity (RH) and voltages of up to 400V. It was found that if the operating voltage was 100 V, failure of the printed circuits under normal use conditions (i.e. 40%-60% RH and 25ºC–35ºC) would take tens of years. They determined that time to failure (t_F) could be modeled by a log-normal plot and that an increase in temperature, humidity, or bias accelerated the failure of the printed circuits.

Boddy [1] also evaluated two different covercoats (i.e. one with a reactive additive and one without a reactive additive) on FR-4. Four substrate related failures were

described: (a) through-substrate shorts, (b) sub-surface shorts, (c) covercoat-related failures, and (d) interface related failures (Figure 2.5). Through-substrate shorts are a problem in systems containing little or no buttercoat and dominate only at a minimum 80% RH and temperatures above 75ºC.

It was not until 1979 that Lando et al [3] first termed these subsurface shorts CAF. He investigated (a) different material PWB substrates and identified their susceptibility to CAF, and (b) different conductor orientations. He monitored CAF failure using insulation resistance (IR) tests to create a model for CAF failure. The different conductor orientations are illustrated in Figure 2.6.

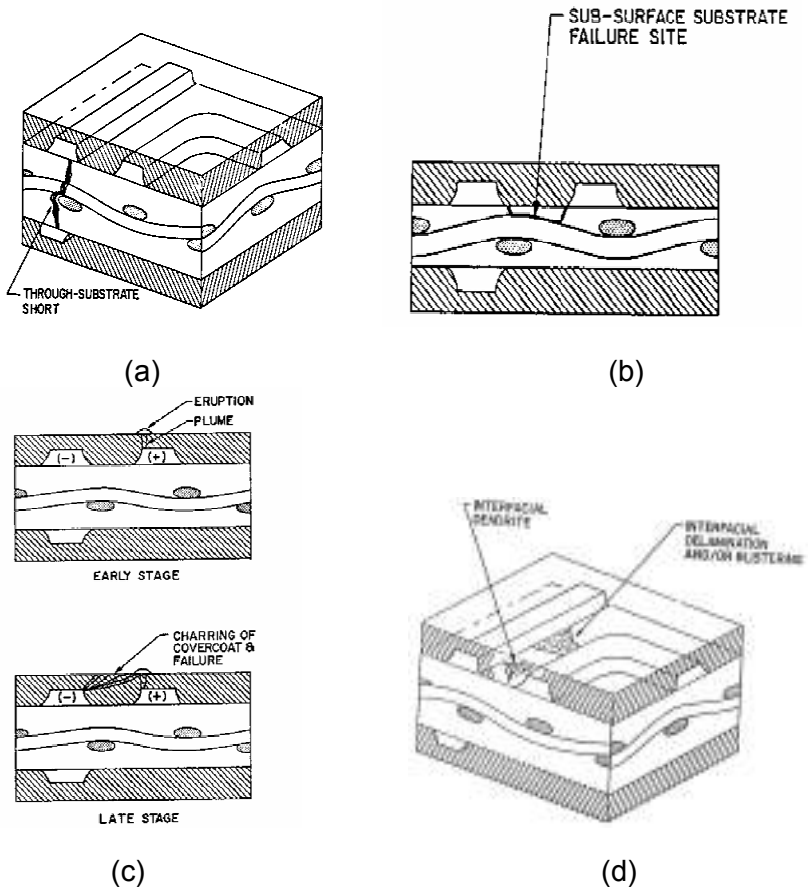

Figure 2.5: Illustration of (a) through substrate shorts, (b) sub-surface shorts, (c) covercoat related shorts, and (d) interface related failures [1]. © 1976 IEEE

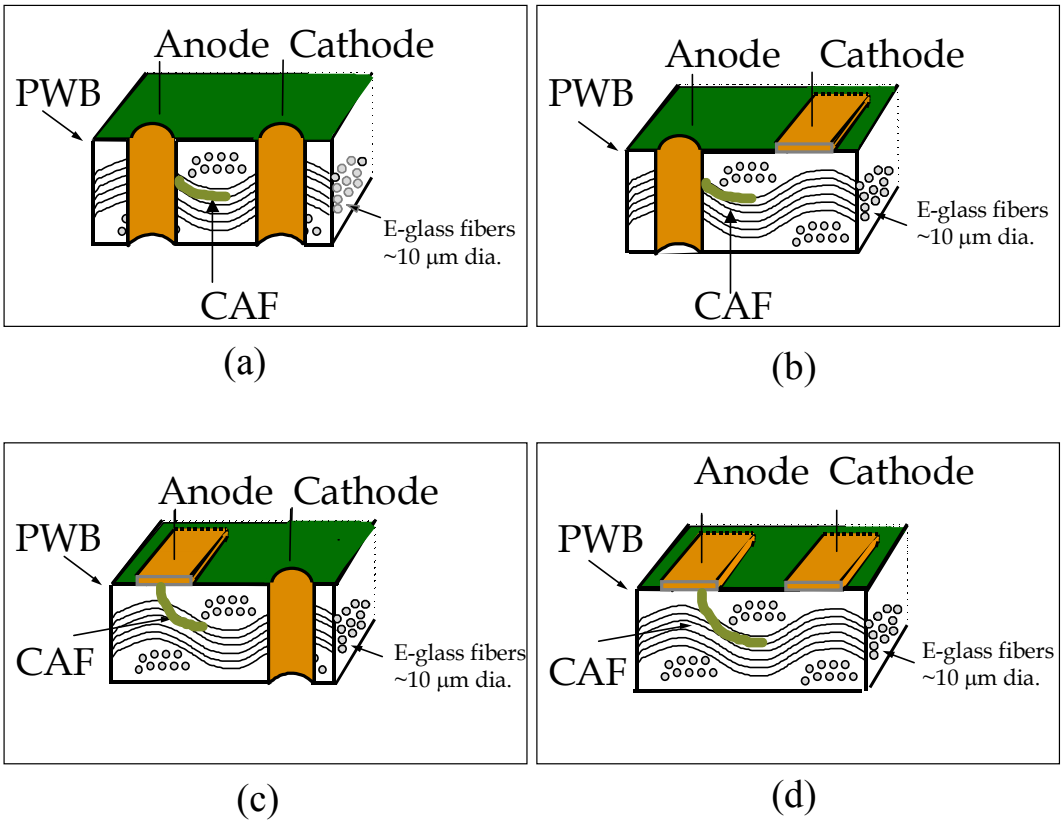

Figure 2.6: Different conductor orientations used for CAF formation for (a) hole-hole (H-H), (b) hole-trace (H-T), (c) trace-hole (T-H), and (d) trace-trace (T-T) [9, 10].

Based on the different conductor orientations presented in Figure 2.6, the incidence of CAF formation occurs as follows:

H-H > H-T ≈ T-H > T-T (0.008" space) > T-T (0.015" space).

Lando et al [3] proposed a two step model for the formation of CAF. In the first step, there is weakening of the epoxy-glass fiber interface which creates a path for the migration of the copper containing conductive filament. In the second step, water absorption provides an aqueous medium where the electrochemical reactions occur. The possible electrode reactions they proposed were:

Anode: $Cu \rightarrow Cu^{n+} + ne^{-}$ (2.1)

$H_2O \rightarrow 0.5O_2 + 2H^{+} + 2e^{-}$ (2.2)

Cathode:

$H_2O + e^{-} \rightarrow 0.5H_2 + OH^{-}$ (2.3)

The electrolysis of water creates a PH gradient between the anode (i.e. acidic) and the cathode (i.e. basic). This is illustrated by the PH gradient diagram in Figure 2.7.

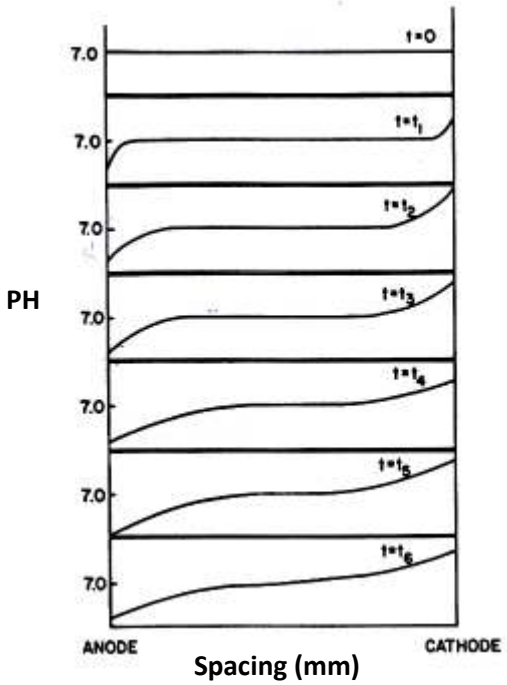

Figure 2.7: PH gradient diagram for CAF formation [3]. © 1979 IEEE

Lahti et al [2] reviewed long-term performance of high density PWBs fabricated with glass-reinforced epoxy dielectrics. In his study PWBs such as single sided, double sided and multilayer board designs with and without plated through holes were used. The conductor spacing ranged between 0.005”-0.050”. The PWBs were aged at temperatures ranging between 23ºC-95ºC and relative humidity’s between 2-95%. The

voltage was varied between 10-600V, with the majority tested at voltages between 45-400V. The electrical data is characterized by a gradual decline in insulation resistance (IR) with exposure to aging conditions, followed by a sudden drop in IR. A typical IR plot from the Bell Labs work is illustrated in Figure 2.8. The data indicate that below 60ºC and 80% RH, the samples show little evidence of thermal activation (i.e E_a = 0-0.2 eV). For temperature ranges greater than 60ºC-65ºC and 80% RH the CAF failure is strongly temperature dependent (i.e. E_a = 1.0-2.5 eV). The study did not produce sufficient data to correlate the dependence of CAF failure on humidity; however a reduction in humidity by 20% (i.e. 80%→60%) at 50ºC produced a 100x increase in the failure time. At 85ºC a 20% reduction in humidity results only in 2-3x increase in failure time. Data at 85ºC, 85% RH, and 45V shows that for conductor spacings below 0.005" there begins to be a drastic drop in lifetime. This study gives a dependence of failure time on voltage as: $t_F = V^{-1}$. The type of raw material used shows a variation in the failure time by two orders of magnitude.

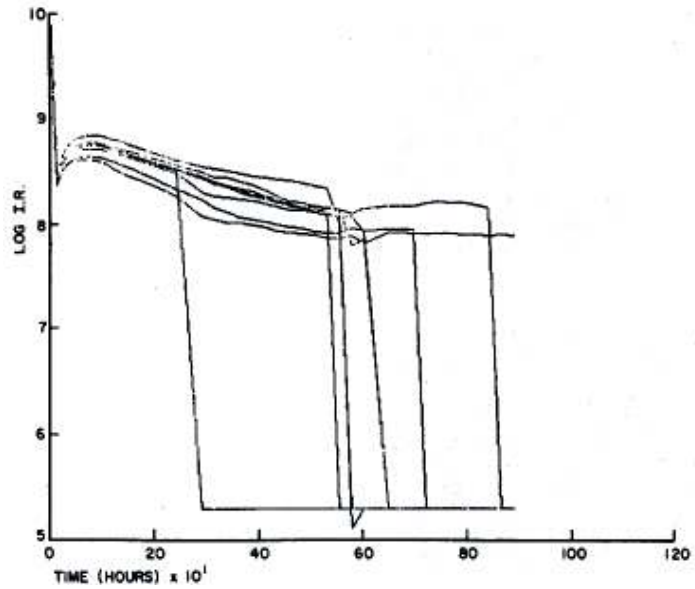

Figure 2.8: Typical SIR plot from Bell Labs work [3]. © 1979 IEEE

Welsher et al [4, 5] performed a series of tests on FR-4 substrate material to characterize the dependence of time to failure, temperature, relative humidity, applied bias, and conductor spacing. For three commercially available FR-4 laminates tested at temperatures ranging between 50 ºC -100 ºC at 200V and 95% RH the materials show Arrhenius behavior with activation energy of 1 eV. The relationship between failure time and voltage was found to be: $t_F = a + b/V$ where a and b depends on material, temperature and humidity. Furthermore, temperature-humidity life data were analyzed by a multiple regression of the function: $t_F = a(H)^b \exp(E_a/RT)$ where H is the relative humidity, T is the temperature in Kelvin, and R is the universal gas constant. Welsher also performed thermal shock tests that showed reduction in a materials life. This study supports the two step model proposed by Lando which can be expressed in terms of time to failure (i.e. $t_F = t_1 + t_2$) where t_1 represents the mechanical failure and t_2 represents the electrochemical reactions. He concluded:

(i) the Arrhenius behavior suggests the temperature dependence is dominated by interfacial degradation
(ii) The voltage, a + b/V, does not affect interfacial degradation
(iii) Thermal transients cause instantaneous loss of adhesion due to CTE mismatch
(iv) $t_1 >> t_2$
(v) $t_2 \sim L^2/V$ and t_1 is independent of L

The data in this study predict the mean time to failure (MTTF) as follows:

$$MTTF = a(H)^b \exp(E_a/RT) + d(L^2/V) \quad (2.4)$$

where L is the conductor spacing, V is the bias and d is a material dependent constant and all other variables have the same meaning as defined earlier.

Meeker et al [16] proposed a 2 step kinetic model for CAF failure. In their model, a chlorine salt can form either a copper chlorine compound (i.e. CAF) or an innocuous trapped chlorine compound. The model is illustrated schematically in Figure 2.9. Since $k_1, k_2 >> k_3$ the forward reactions are favoured.

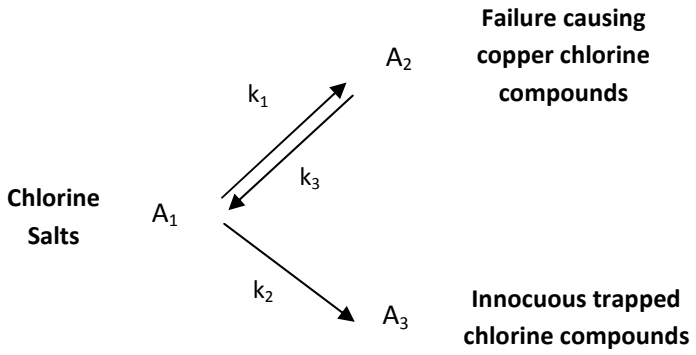

Figure 2.9: Kinetic model for CAF failure [16].

At the same time that Bell Lab researchers were studying subsurface shorts, Der Marderosian [17] at Raytheon investigated measling[2] of multilayer PWBs from three different vendors. He aged the boards at 65ºC and 95 % RH, with one set exposed to a 100V dc, a second set exposed to a 100V ac, and a third set exposed to no bias.

The boards exposed to a 100V dc created a failure which he termed “punch thru” since the filament grew from the anode (surface of board) to the cathode (ground plane) along the epoxy glass fibers. This was later shown to be the same as CAF and is illustrated in Figure 2.10.

---

[2]**Measling:** A white spot on the base laminate which indicates a separation of glass fibers at the weave intersection [17].

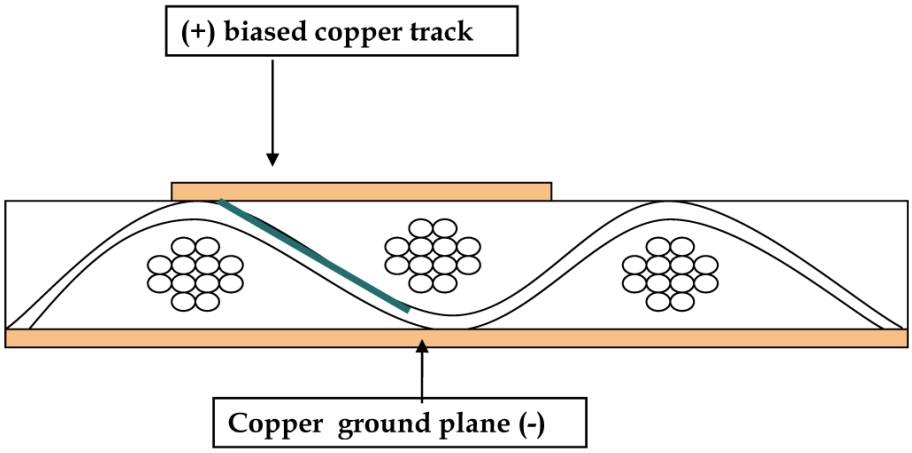

Figure 2.10: Illustration of punch thru [17]. Source: Reprinted with kind permission of Springer Science and Business Media.

For the sets of coupons exposed to either 100V ac or no bias, no CAF was observed. These results illustrate that CAF is created by an electrochemical process which occurs only under dc bias conditions.

The following mechanism was proposed by Der Marderosian [17]:

$$Cu + 3H_2O = CuO\downarrow + Cu(OH)_2\downarrow + 2H_2\uparrow \qquad (2.5)$$

$$Cu(OH)_2 = CuO\downarrow + H_2O \qquad (2.6)$$

In reaction (2.5), CuO and $Cu(OH)_2$ are formed at the anode. In the presence of heat (i.e. ~ 60 ºC), $Cu(OH)_2$ decomposes to CuO and H_2O (i.e reaction 2.6).

Jachim [7] showed that solder flux choice affects CAF formation. IPC-B-24 (i.e this is illustrated in Figure 2.14) coupons were fluxed with water soluble flux, soldered, cleaned, electrified and aged at 85ºC, 85% RH, and 100V bias. She noted that more CAF was created on the coupons that were fluxed than those coupons that were processed without flux.

Bent [6] studied the effect of CAF formation on various water soluble fluxes containing different flux vehicles. The fluxes studied were formulated with and without halide activator (2 wt% chloride activator, or 2wt% bromide). The coupons were processed under both lead-based soldering conditions (201°C -205°C) and lead-free (241°C - 245°C). The key result is that the incidence of CAF was orders of magnitudes higher for many coupons processed under lead-free conditions.

2.3.2 – Chemical Nature of CAF

Ready [8, 10] examined two different substrate materials processed with four different water soluble fluxes. He found that CAF formation on MC-2 substrate material with and without flux was severe in all cases. However, CAF susceptibility for FR4 was found to be less severe. SEM/BSE and energy dispersive spectroscopy (EDS) was used to determine that CAF contained copper, chlorine, and sometimes bromine.

2.3.3 – Chloride Containing CAF

Using TEM, Ready [9, 10] identified CAF to be synthetic atacamite, $CuCl_2 \cdot 5Cu(OH)_2 \cdot H_2O$ from the powder diffraction data base from 1971 [18]. More recently, the x-ray diffraction data base containing the synthetic atacamite was replaced with the following atacamite formula $Cu_2(OH)_3Cl$ [19].

2.3.4 – Copper Compound in the Polymer Matrix for Fluxed Coupons

Ready [9, 10] also investigated the effect of flux chemistry, applied voltage, conductor spacing, and temperature on CAF formation for FR-4 board material. He discovered that different CAF morphologies were present. For boards processed with no flux, CAF formed only at the epoxy/glass fiber interface. This is illustrated in Figure 2.11.

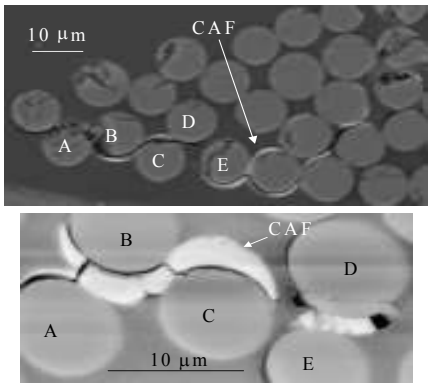

Figure 2.11: CAF surrounds epoxy/glass fiber interface for PWBs with no flux [9, 10].

2.3.4.1 – Polyethylene Polypropylene Glycol (PEPG)

For boards processed with polyethylene polypropylene glycol (PEPG) flux without halide, a stratified morphology was observed, with an EDS elemental analysis revealing copper and chlorine in the epoxy. For boards processed with PEPG flux containing 2 wt% bromide activator, a stratified CAF morphology composed predominantly of chlorine and copper was observed. This is illustrated in Figure 2.12.

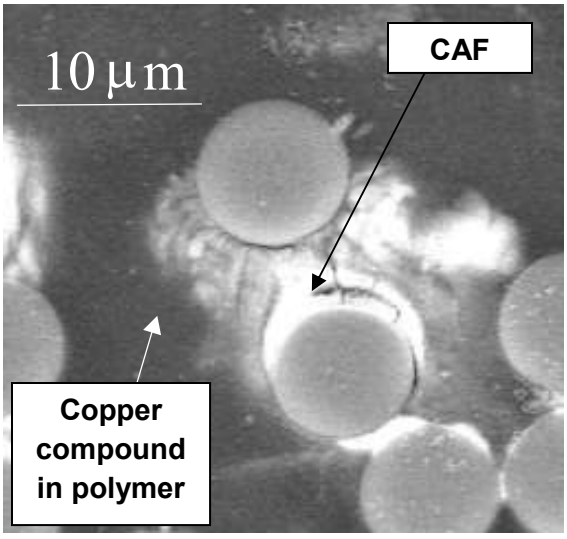

Figure 2.12: Stratified morphology for FR-4 treated with PEPG containing Br^- activator [9, 10].

2.3.4.2 – Linear Aliphatic Polyether (LAP)

For boards that were processed with a linear aliphatic polyether (LAP) with 2 wt% chloride activator contained a striated morphology. This is illustrated in Figure 2.13.

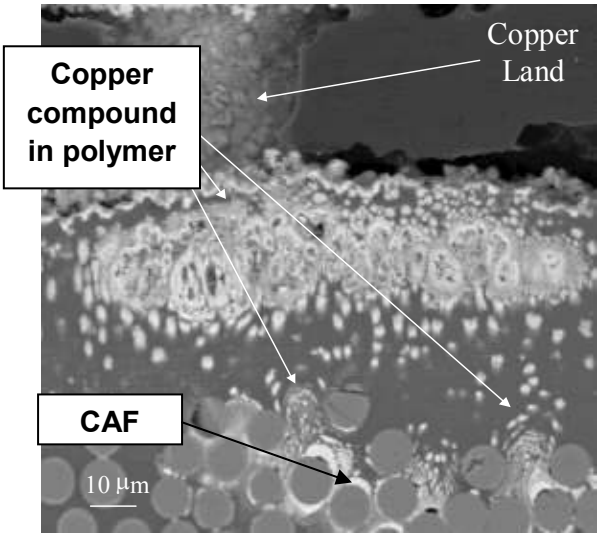

Figure 2.13: Striated morphology for FR-4 treated with LAP flux with Cl^- activator [9, 10].

2.4 – Summary of Factors Accelerating CAF Formation

This section summarizes the most important factors that enhance CAF failure. All factors have been shown experimentally to accelerate CAF failure.

2.4.1 - Processing Temperature

Processing temperature weakens the epoxy-glass fiber interface due to the mismatch in the coefficients of thermal expansion (CTE) between the epoxy and glass fibers resulting in an easier path for CAF to grow.

2.4.2 – Water Soluble Flux

Some water-soluble solder flux residues diffuse into the PWB during the soldering process. These residues are hydrophilic in nature enhancing moisture absorption into

the resin, causing it to swell. This creates stress between the epoxy and glass weakening this interface.

2.4.3 – Aging Temperature

The rate of a chemical reaction increases with increasing temperature and CAF has been shown to follow an Arrhenius behaviour. The early work by Bell labs used an aging temperature of 35 ^{0}C. The IPC standard test methods requires an aging temperature of 85 ^{0}C.

2.4.4 – Humidity

Humid conditions cause moisture to diffuse into the printed wiring board (PWB). This causes swelling of the resin, which adds further stress to the epoxy-glass fiber interface causing further weakening. In addition, moisture provides an aqueous medium for ions to migrate in the presence of a bias voltage.

2.4.5 – Voltage

CAF is an electrochemically induced failure mode. CAF failure can be accelerated by (a) increasing voltage, or (b) reducing the conductor spacing. Either (a) or (b) will result if there is an increase in the voltage gradient, resulting in enhanced CAF formation.

2.4.6 – Mechanical Damage

During the hole drilling process mechanical stress displaces the glass fibers which results in cracking and weakening of the epoxy/glass fiber interface, thus providing an easier path for CAF growth.

2.5 – CAF PWB Design

The present trend in modern day electronics is towards a more complex, denser package design to provide more features. This means that the conductor spacings are

decreasing. The IPC 2008-2009 roadmap for mechanically drilled holes [20] indicates that the conductor spacing is rapidly shrinking (Table 2.1). It is projected that the hole to hole spacing between 2008 and 2018 will be reduced by 25%.

Table 2.1 – Mechanical Hole Formation in a Conventional Board of 1.5 mm Thickness

Attribute	2008/2009	Current 2010/2011	Midterm 2012/2013	Long Term 2014-2018
Via Size Min (mm)	0.25	0.23	0.225	0.212
Aspect Ratio	6:1	7:1	7:1	8:1
Via Pitch (mm)	0.50	0.45	0.40	0.40
Hole-to-Hole (mm)	0.25	0.22	0.175	0.188

Closer conductor spacing, combined with the higher processing temperatures for lead-free soldering [6] can be problematic when it comes to electrochemically induced failures such as CAF. The voltage gradient is greater as the spacing is reduced. Work by Ready [10] found the mean time-to-failure (MTTF) for a hole-to-hole conductor orientation can be represented by the following proportionality:

$$MTTF \alpha (L^4/V^2) \quad (2.7)$$

where L, conductor spacing and V, voltage.

2.5.1 – Trace – Trace

Traditionally a trace-trace or line-line pattern has been used in CAF testing. This test pattern is very easy to design and most IPC test specification uses this test pattern. It

has been shown that CAF failure is not most susceptible when utilizing this test pattern. The layout of this test pattern is shown later in Figure 2.14 in section 2.6.1.1.

2.5.2 – Hole – Hole

Many CAF studies dealing with the statistics of failure have used hole-to-hole patterns on double-sided boards. These boards have higher glass content than multilayer boards. Typically, double-sided PWBs use 8 sheets of 7628-glass cloth with a thickness of 0.175 mm (0.007”) to create a 1.5mm [0.062”] board. The glass to resin ratio in this case is higher than that of a multilayer board, where the glass cloth thickness might range from 0.025 to 0.10mm (0.001” to 0.004 “) per layer and there might be 1-3 sheets used in each layer of the core and the prepreg.

2.5.3 – Materials Issues

CAF resistant substrates are frequently more expensive, and therefore are used for products that require high reliability, optimizing both cost and performance. Designs are multilayer boards, rather than double-sided rigid boards. Typical, double-sided PWBs have resin contents in the range of 41%-48 %. A multilayer board, on the other hand, has a resin content around 50%-70 %. The higher resin content means less glass fibers, reducing the stress during the drilling process where damage can occur at the epoxy-glass interface. Table 2.2 contains a listing of several glass cloth style types, thicknesses and typical resin content.

Table 2.2 – Effect of Glass Style on the Resin content

Glass Style	Fiberglass Thickness	%Resin
7628	0.175mm	41 – 48%
2116	0.095mm	45 – 53%
1080	0.056mm	61 – 64%
2113	0.0725mm	~ 56%
106	0.035mm	~ 70%

Sauter [21] developed a multilayer CAF test board and evaluated both CAF resistant and standard FR-4 materials using different conductor orientation. He found that for closer spacing (<0.5mm) CAF resistant materials show higher CAF failure than standard FR-4 materials. However, when spacing was increased this effect fell off and the two laminates performed equally well. Thus, hole spacing coupled with laminate materials properties are important consideration for board design. However, at larger spacing (0.5mm) the incidence of CAF failure for CAF resistant materials as compared with traditional FR-4 materials was about the same. This observation is attributed to an increase in fracture during drilling observed in the CAF resistant materials because they are more brittle. When using CAF resistant and high T_g materials, careful PWB manufacturer selection and/or conservative PWB spacing designs are required to avoid increased risk of CAF failure. Sauter also found that altering the drilling direction from the weave direction to a direction diagonal to the weave reduces the susceptibility for CAF failure.

Rogers and Pecht [22] evaluated both traditional FR-4 and CAF resistant materials that had 0.076 mm and 0.1 mm spacing. They saw no evidence of CAF failure, but they found that for spacing less than 4 mil (0.1 mm), the insulation resistance (IR) values dropped immediately after a bias was applied at 85°C and 85% R.H., indicating internal

premature shorting had occurred. They suggested that the closer spacing resulted in moisture ingress which caused the drop in insulation resistance, probably due to plating salts in cracks between the holes.

Hinds and Treanor [23] showed that the glass style choice is an another important parameter to consider. Thicker glass styles such as the 7628 require almost 2.5x more force during drilling than finer glass styles such as the 106. In addition, thicker glass fibers cannot be used for drill bit sizes of 0.1 mm or less. Work by Merix which used a 0.25 mm drill bit has shown CAF growth more frequently when 1080 glass style was used.

2.5.4 – Hole Drilling

The design of a circuit board in which both holes and vias are required, results in the interaction of the polymer, glass fibers, and the drill. The material choice has a strong influence on whether mechanical damage will result during hole drilling. The drilling process itself is a very complex issue where many factors need to be considered in order to help minimize stresses that cause cracking.

2.5.5– Factors Affecting Hole Drilling

Hinds and Treanor [23] also investigated drilling related issues and identified a number of important factors to consider.

2.5.5.1 – Drill Wear

As the drill bit wears the amount of force required for hole drilling increases. The greater the force exerted during hole drilling, the greater the mechanical damage such as crack formation between barrels. During the subsequent plating process, copper salts, and other plating fluids are deposited in these cracks. When boards are later powered up

under a humid environment, the plating salts become conductive and cause premature shorts.

A drill bit can drill 4000 holes before it requires re-sharpening. Considerable drill bit wear occurs in drilling the first 200 holes. Thereafter, the drill bit wear increases linearly to the point where the drill bit is no longer effective (i.e. 0 – 4000 drilled goles). The drill wear for both the end load and torque increases 70% above the new or re-sharpened drill which is reflected by a linear increase in the applied load and torque for approximately every 1000 holes drilled.

2.5.5.2 – Chip Load

The chip load is defined as the distance traveled by the drill bit into the board in each revolution. It is very important to select a chip load that is not too low, or the drill bit will cause greater temperature build-up, greater drill wear, and lower productivity. Increasing the chip load increases the force on the board material, which can eventually cause mechanical damage. For drill bit size of 0.25 mm in diameter, a chip load of 0.015 mm is recommended, while for drill bit size of 0.15 mm in diameter, a chip load of 0.0065 mm is recommended. This will ensure optimum productivity, minimal drill wear, and less mechanical damage.

2.5.5.3 – Copper Layers

The thickness of copper present will affect the amount of mechanical damage that results during drilling. Increased copper thickness will result in greater force, greater drill bit wear, and more mechanical damage.

2.5.5.4 – Aspect Ratio

The aspect ratio represents the ratio of the board thickness to the hole diameter. The

greater the board thickness, the greater the distance required for the drill bit to travel during hole drilling. A thicker board will thus result in greater wear on the drill bit, thus resulting in greater force exerted during the drilling process, which increase the potential for internal cracking in the board. Murai et al [24] have found that for thinner boards (4 layers of 1080 glass style of 0.05 mm thickness), hole spacings between 0.05 mm – 0.1 mm can be produced with great accuracy using 0.1 mm drill bit diameters on halogen free materials.

Gopalakrishnan et al [25] evaluated a CAF resistant material using various drill bit sizes and hole-to-hole spacing. For drill bit diameters of 0.20 mm and 0.25 mm the failures for hole-hole spacings of 0.38 mm to 0.495 mm were in excess of 80%. However, when 0.495 mm spacing were created using a larger drill bit (0.635 mm) the number of failures was reduced by half. This shows that both spacing and drill bit size have an effect on the quality of hole drilling.

Karavakis and Bertling [26] investigated laminate structures that used 6 plies of 2116 glass style and 18 mm thick copper. They evaluated a range of spacings from 0.178 mm to 0.5 mm holes drilled in both the warp and fill direction. They found that the insulation resistance is lower for holes in the fill direction, independent of hole spacing. In addition, they found that the insulation resistance was much lower for hole spacings of 0.178 mm compared to 0.5 mm. These results are consistent with previous studies. In addition, they found that for laminate materials which have greater ability to absorb moisture there is a greater failure rate than for those materials that are moisture resistant. Lastly, drilling needs to be optimized for via diameters less than 0.127 mm. Alternative drilling methods such as laser drilling used for high aspect ratio holes create

less stress between the glass and resin interface.

2.5.6 – Recommended Hole Spacing

Several factors must be considered in designing a coupon for CAF testing. In designing a double sided CAF test coupon using a hole-edge-to-hole-edge spacing of approximately 0.18 mm, it was found that significant deviation in spacing from the intended spacing occurred (Figure 2.14 (b)). In addition, due to both the rotational and end load on the drills chisel edge, mechanical stress resulted in the tearing of one or more fibers which caused cracking. A multimeter was used to show that premature shorting occurred between the adjacent holes (Figure 2.14 (b)) from copper filling these cracks during the plating process. It was learned that that a spacing of 0.18 mm could not be achieved, so Parry et al [27] designed a new CAF test coupon using a multilayer board design and recommended an edge-to-edge spacing of 0.35 mm. This value took into account hole-drilling tolerances of ±0.075 mm and ensured that the hole-hole tolerances did not exceed 20%. It was later found that when this spacing was used, premature shorting resulted from mechanical damage caused by drilling that created cracks between the holes. When the hole to hole spacing was increased to 0.5 mm, the premature shorting disappeared. Thus, this is the minimum spacing recommended for future test coupons [28].

2. 6 – Characterization and Analytical Techniques

This section will provide background information on all the characterization techniques used in this work.

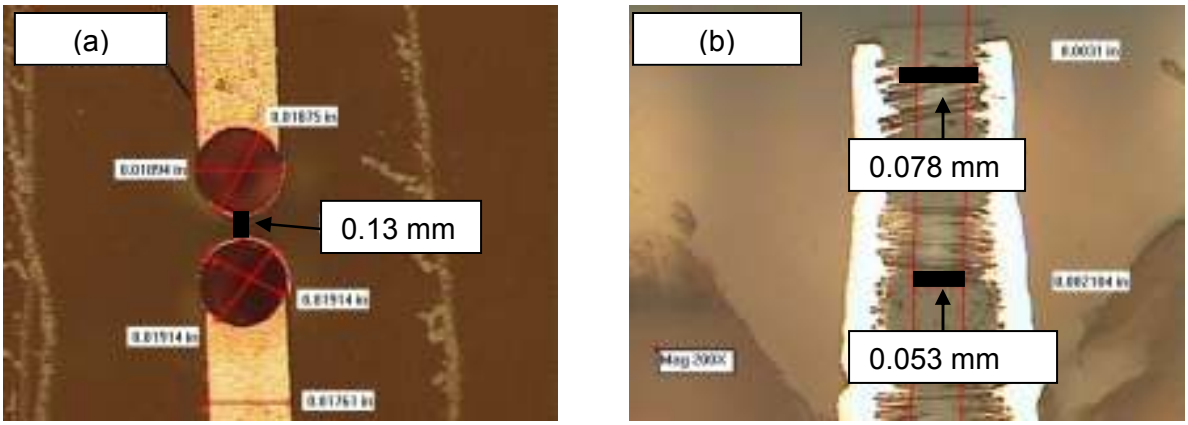

Figure 2.14: Optical image showing (a) hole-edge-to-hole-edge spacing of 0.13 mm, and (b) wicking which resulted in a premature short. (Courtesy of G. Hoepel, Coretec)

2.6.1 - Surface Insulation Resistance (SIR) Testing

Traditionally in the electronics industry the electrical properties of laminate materials has been evaluated using IPC standard electrical test methods. The electrical test methods and accelerated aging conditions as they apply to CAF in this thesis will be discussed further in the next two sections.

2.6.1.1 – IPC Electrochemical Migration Testing

Traditionally an interdigited comb pattern (Figure 2.15) is used for electrical testing. When using this coupon layout, a surface insulation resistance (SIR) test is employed to measure the resistance to the flow of current across the surface of a printed wiring board (PWB) substrate. For a hole-to-hole test coupon, the copper metallization is plated through a hole in the board, and hence the bulk insulation resistance (IR) will be measured. The IPC defines surface insulation resistance as “the electrical resistance between two conductors separated by some dielectric material(s)”. For the purpose of this thesis, since a hole-to-hole test coupon was used, we will refer to the insulation resistance.

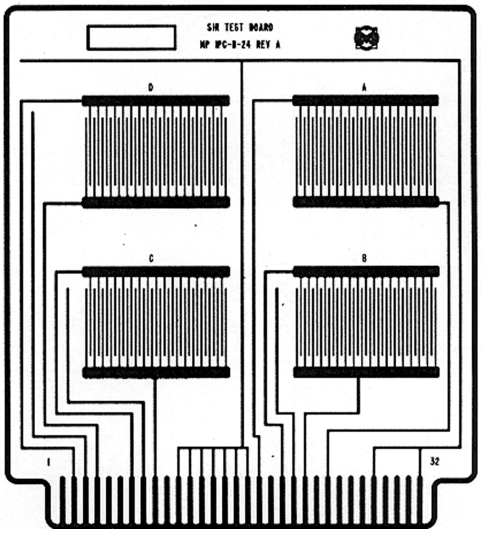

Figure 2.15: Interdigited comb pattern used in SIR testing.

2.6.1.2 Temperature-Humidity-Bias (T-H-B) Testing

Historically insulation resistance (IR) testing began as a material property that measured the base material, regardless of test conditions imposed on the sample. Present day usage of IR testing refers primarily to temperature-humidity-bias (THB) accelerated aging tests. All IR testing for CAF is done under (T-H-B) conditions where the aging and relative humidity (RH) conditions of 85 °C and 85% are consistent with (IPC-TM-650, TM 2.6.3.3., Revision B) with the bias modified to 200V for the purpose of this study and the testing time modified to 28 days. Since the purpose of this work was to create CAF, the electrical data was not of interest. A higher voltage was used to accelerate CAF growth, and a 28 day testing period was used to provide a sufficient time period to create CAF. It must be noted that the standard SIR test involves taking measurements following elapsed times of 1, 4 , and 7 days with a failure being represented by an IR value below 10^8 Ω after day 4 or day 7.

2.6.2 – Scanning Electron Microscopy (SEM)

SEM is a characterization technique used to image the surface of bulk materials with electrons. Typically there is a primary electron beam gun which accelerates electrons from the tip of the filament (typically tungsten) toward the positively charged anode, through electromagnetic lenses onto the sample in vacuum. The SEM can be operated in either secondary electron (SE) mode or backscattered electron (BSE) mode. In secondary mode, secondary electrons are used to image the surface of the sample from an escape depth between 1nm-10 nm resulting in ideal conditions for surface topography imaging with high depth-of-field. In BSE mode, electrons have a deeper penetration depth, which ranges anywhere between 0.1 μm – 1 μm. This allows atomic number contrast (i.e. higher atomic number elements such as copper appear brighter than lower atomic number elements like chlorine). Typically the accelerating voltage used in SEM's is 20 kV, and was employed in this work. Previous work on CAF used BSE mode to identify the a copper-containing compound in the polymer matrix. In this work, due to sample preparation and the SEM used, SE mode was sufficient to identify the CAF microstructure.

SEM samples are coated with a conductive carbon coating. Alternatively gold coating can be used, however, since CAF contains copper and chloride, working with a carbon coating was preferred to ensure than the heavier atomic number gold did not mask out these elements in elemental analysis. All samples were placed on a conductive metal holder and carbon tape was used to make contact between the sample cross section and conductive metallic sample. The SEM work was used to identify the CAF at the

epoxy/glass fiber interface, as well as the copper containing compound found in the polymer matrix.

2.6.3 – Energy Dispersive Spectroscopy (EDS)

When the SEM is operated in SE mode, both qualitative and quantitative elemental analyses can be performed. The EDS detector is typically a silicon-lithium detector where the sample is tilted approximately 15° relative to the x-ray detector. There is a beryllium (Be) window which prevents contamination of the detector crystal. In analysis for elements such as sodium (Na) and below, the beryllium (Be) window must be opened. The incident electron beam is located at the area of interest, which excites outer core electrons, creating x-rays which travel back through a cooled Si(Li) detector and a spectra is generated based on energy in keV. The x-axis corresponds to the appropriate element of the x-rays detected and the intensity (i.e. y-axis) corresponding to the amount of each element present in the sampled volume. EDS was used in this work to confirm the presence of copper, chlorine, or bromine in the CAF samples at the epoxy/glass fiber interface and the copper compound in the polymer matrix.

2.6.4 – Focused Ion Beam (FIB)

Transmission electron microscopic sample preparation in the past has been time consuming and challenging. Following the advancement and acceptance of FIBs, TEM samples can be produced in a matter of hours. The dual beam (FIB-SEM) is one set-up that is used in preparing TEM samples. This set-up utilizes a vertical electron column as illustrated in Figure 2.16. In this set-up the sample is tilted 52° for milling normal to the sample surface.

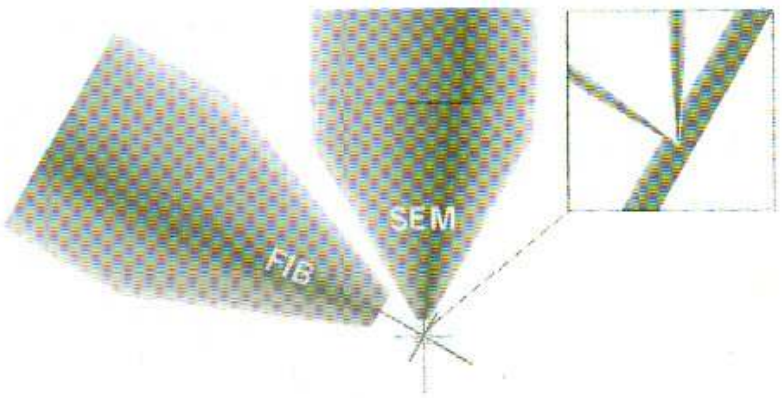

Figure 2.16: Set-up of a dual beam FIB-SEM system [29]. Source: Reprinted with kind permission of Springer Science and Business Media.

A vacuum system is required for FIB and it is similar to a field emission SEM (i.e. on the order of 1 x 10^{-8} torr). The probe sputtering is made possible by a liquid metal ion source (LMIS) which provides an ion source at a diameter of ~5nm. Typically the LMIS contains a tungsten needle and is attached to a reservoir that holds the metal source material. Gallium (Ga) is currently the most common LMIS due to its low melting point (29.8 °C) minimizing interdiffusion between the liquid and tungsten needle, it has low volatility giving it a long lifetime, low surface energy promoting viscous behavior on tungsten, excellent mechanical, electrical and vacuum properties and lastly its emission characteristics enable high angular intensity with small energy spread.

This system allows the area of interest to be magnified at high resolution and then utilize the fine ion beam to make a thin cross-section (~100 nm) by sputtering. A typical 3-D image obtained during the milling process of a bromide CAF sample is illustrated in Figure 2.17. The sample is then further thinned and polished by FIB milling. The un-thinned and thinned bromide CAF is illustrated in Figures 2.18 (a) and Figure 2.18 (b), respectively.

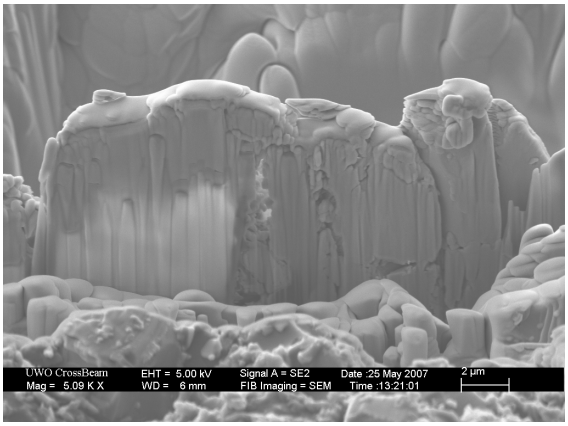

Figure 2.17: 3-D image of a TEM bromide CAF section prepared using FIB.

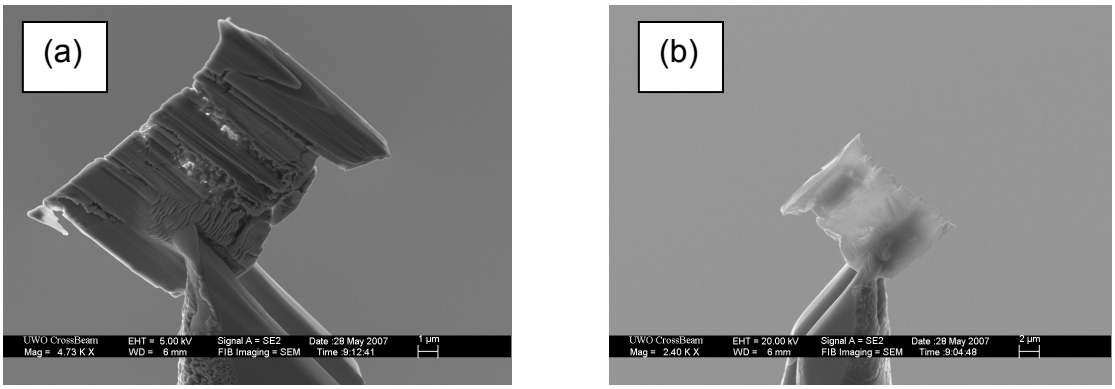

Figure 2.18: TEM Bromide CAF sample (a) un-thinned, and (b) thinned.

2.6.5 –Transmission Electron Microscopy (TEM)

TEM is a characterization technique that can be used to determine crystallographic structure and identify material phases. The set up is analogous to a light microscope where electrons are accelerated at 200 keV from an electron beam with a condenser lens used to form the beam and an objective lens to focus and magnify the beam on the area of interest on the specimen. A projector lens is used to further magnify the image onto the imaging system employed. One of the major challenges of TEM is the requirement of a very thin sample (100 nm or less) since the electrons must be effectively transmitted through the sample. There are two imaging modes that can be

used, bright field and dark field. For the purpose of this work, only bright field imaging was used. In bright field, the image is generated from elastically scattered and inelastically scattered electrons passing through the sample. The bright field images were used to identify the areas where selected area diffraction (SAD) was performed on the bromide containing CAF. EDS was performed on the bromide CAF samples to confirm the presence of copper, oxygen, and bromine. In SAD the electrons are passed through an aperture that has a diameter of 50 μm which results in a spot size of 1 μm on the sample. In analyzing the diffraction pattern the following relationship is used:

$$\lambda L_{CL} = dr \qquad (2.8)$$

where r is the measured ring radius on the diffraction pattern in mm, d is the interplanar spacing in nm, λ is the wavelength of incident radiation, and L_{CL} is the camera length of the TEM. The λL_{CL} term is constant and was determined to be 13.04 mm·nm using a standard gold diffraction pattern. The tabulated d values are compared to the standard accepted d values published by the International Centre for Diffraction Data (ICDD) to identify the bromide containing CAF**.**

2.6.6 – X-ray Photoelectron Spectroscopy (XPS)

XPS is a surface analysis technique, also referred to as ESCA (electron spectroscopy for chemical analysis), which is used to identify chemical compounds. In this technique, monochromatic x-rays are bombarded on the surface (~100 angstrom penetration depth) of a material resulting in the emission of valence or core photoelectrons (Figure 2.19). The XPS spectrum is produced by measuring both the kinetic energy (KE) and

the number of released electrons from the surface. The binding energy (E_b) of the emitted electrons is related to the energy of the x-ray photons ($h\nu$), the KE, and the work function (w) of the spectrometer by the following equation:

$$E_b = h\nu - KE - w \qquad (2.9)$$

Each element has a characteristic binding energy which produces characteristic energy peaks in the XPS spectra allowing one to identify the characteristic elements in a chemical compound. It is important to note that XPS is a surface sensitive technique, so care must be taken in ensuring that the sample is not contaminated. Prior to the characterization of the copper compound in the polymer matrix, the XPS spectrometer was calibrated using a two step method.

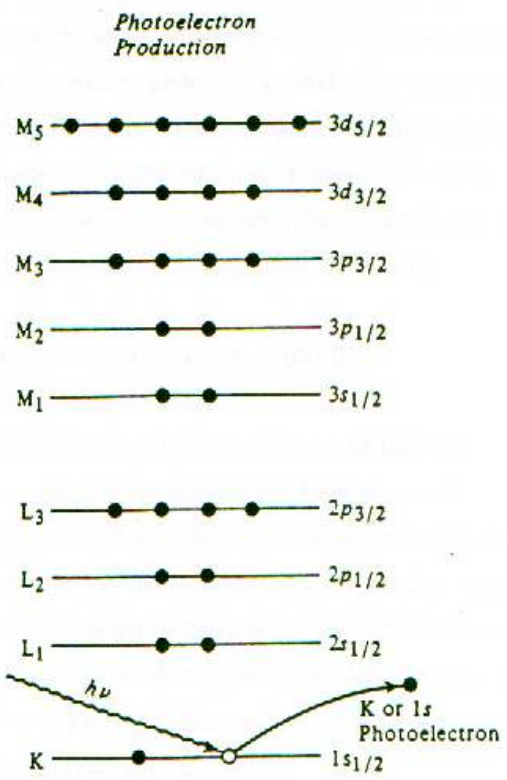

Figure 2.19: Schematic demonstrating the ejection of primary electrons in an atom.

2.6.7 – Fourier Transform Infrared Spectroscopy (FTIR)

FTIR is a technique that is used to analyze organic constituents. Traditionally in infrared spectroscopy the infrared beam passes through the sample. The advancement in infrared spectroscopy in the last decade and the development of FTIR has resulted in much progress. In FTIR the radiation source is split into two beams: a beam of fixed length and one of variable length (movable mirror). This set-up results in the two path lengths to result in constructive and destructive interference and variability in intensities (an interferogram). The Fourier transformation converts the interferogram from the time domain into a single spectral point on the more familiar form of the frequency domain. The adjustment of the movable mirror varies the beam length and allows Fourier transformation at successive points and gives rise to a complete spectrum. The elimination of the monochromator in FTIR, allows the entire radiation range (5000 cm^{-1} – 400 cm^{-1}) to be passed through the sample saving time. A spectrum of intensity (y-axis) and wavelength (x-axis) is generated.

2.6.8 – Ion Chromatography

The presence of ionic constituents in a PWB can affect the electrical performance of the material under T-H-B testing conditions. Ion chromatography can we subdivided into anion and cation exchange chromatography. For the purposes this work, only anion exchange chromatography was used and will be discussed. In anion exchange chromatography, a buffered solution, known as the mobile phase carrier carries the anions (i.e. Cl^-,Br^- etc), where they bind to a positively charged resin. The analytes are then removed by introducing an anion with the same charge as the analytes, where the conductivity of the analytes is recorded. At equal ionic charge, the elution strength sequence depends primarily on the anion size and the ion exchanger. The elution

power of anions increases with their increasing interaction with the ion exchange column according to the following sequence:

$$NO_3^- > Br^- > NO_2^- > Cl^- > F^-$$

but the order can change depending on hydrophobicity and the crosslinking of the resin. The retention time follows the reverse order, with fluoride ions being exchanged the quickest and the nitrate ions being exchanged the slowest in this work.

2.7 – Chapter Summary

This chapter has provided the necessary background information for all the chapters to follow in this thesis. A historically perspective on CAF has been provided in this chapter. The factors that accelerate CAF formation (i.e. processing temperature, voltage, humidity, conductor spacing, aging temperature, and water soluble flux) have been described. Three very important discoveries by Ready et al have been presented in this chapter: (i) CAF has been identified using TEM to be $Cu_2(OH)_3Cl$, (ii) for coupons processed a water soluble flux, a copper compound is observed in the polymer matrix, and (iii) for coupons processed with a high bromide containing flux, bromide CAF was observed.

A new class of CAF resistant materials has been discussed briefly, since these are materials that are available for high reliability application, but were not the focus of this thesis. New classes of halogen free materials, which are not to be confused with CAF resistant materials, have also been discussed briefly. These halogen free materials are being pushed forward by the computer manufacturers, and will play a vital role in the electronics industry in the future. Even though these halogen free materials are not part of this work, their importance warrants mention. Since the main focus of this work is to

evaluate different solder flux formulations, the role of the flux, and the constituents that make up the flux have been discussed.

It is projected by IPC that hole-hole spacings will reach 0.188 mm by 2018. These closer spacings pose a serious reliability threat when it comes to CAF failure. CAF resistant materials tend to be more expensive and will be used for high reliability applications. These materials tend to be more brittle and extra care must be taken into account in design and hole drilling. The board thickness, glass style, and resin content all affect the brittleness of substrate materials. In addition, drill wear, chip load, aspect ratio, and the number of copper layers all affect the ability to drill reliable holes with minimal mechanical damage. Some studies have evaluated CAF resistant materials using hole-to-hole spacings as small 0.076 mm. Mechanical drilling remains the predominant method, and spacings below 0.5 mm can result in cracking between barrels. Hole-to-hole separations no smaller than 0.5 mm are recommended unless special methods are used to eliminate cracking through the barrel. Lastly, a brief background literature survey has been provided on the key fundamentals for all the analytical and characterization techniques used in this work.

Chapter 3 – Experimental

3.0 – Overview

This chapter will discuss the details of the test vehicle used in this work. It will also provide the chemical formulations of the solder fluxes used. The procedure for the lead-free processing of the test coupons will be explained. The electrical testing apparatus will be discussed and all the analytical characterization techniques employed in this thesis will be presented.

3.1 – Test Vehicle Assembly

A double sided hole-to-hole test board developed by Ready [9] with an edge-to-edge spacing of 0.5 mm was used in this investigation. The test vehicle dimensions are 48.3 mm x 68.6 mm x 1.5 mm. The board was composed of 8 plies of 7628-glass embedded in epoxy resin. The board material tested was FR-4, which is a common board material used in the electronics industry and was discussed in the preceding chapter. The FR-4 coupons employ bare copper metallization for the conductors and plated through holes. The test pattern is illustrated in Figure 3.1.

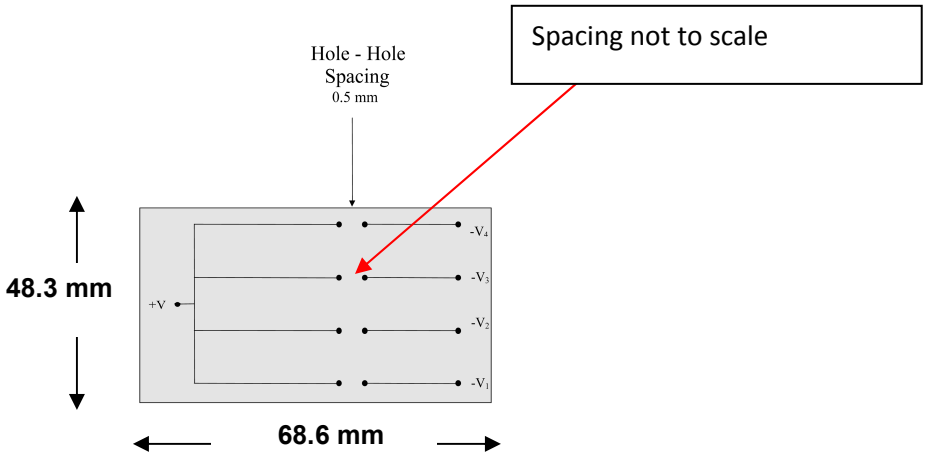

Figure 3.1: Test vehicle assembly used in this study [9, 10].

3.2 – Coupon Processing

The test coupons were exposed to different flux formulations and then exposed to thermal processing to mimic the soldering process encountered in an industrial environment. The sections below will highlight the details of the flux formulations, the thermal processing and cleaning procedures.

3.2.1 Flux Application

A variety of water soluble flux formulations were used in the experimental testing. The flux types are highlighted in Table 3.1. Approximately 1 ml of flux was applied using a syringe over each adjacent hole pair. For the more viscous HASL fluid, the flux was spread throughout the entire set of the four hole pairs.

Table 3.1 – Solder Flux Formulations Tested

Solder Flux	Isopropyl alcohol content	Test Vehicle	Halide Content
Polyethylene Glycol (PEG)	80 wt%	20% PEG	-
PEG with 2 wt% Cl^-	80 wt%	18 wt% PEG	2 wt% Cl
Polyethylene Polypropylene (PEPG)	80 wt%	20% PEPG	-
PEPG with 2 wt% Cl^-	80 wt%	18 wt% PEPG	2 wt% Cl
HASL Fluid*	-	50 -75 wt% polyol	1-15 wt% HBr

* Hot air solder leveling fluid

3.2.2 Soldering

To mimic the manufacturing soldering process a Conceptronics 7-zone oven reflow oven, model HVN_2 102 was used to process the coupons. The lead-free soldering

temperature profile was obtained using the Super M.O.L.E.® which is a multichannel thermal profiling logger distributed by ECD (Electronic Controls Design, Inc.). Two k-type thermocouples were placed on the test vehicle using a polymer adhesive. The adhesive was allowed to cure by applying slight heat using a heat gun and then sealed with kapton tape. The M.O.L.E. was programmed to take temperature readings every second as the M.O.L.E. ran through the reflow oven. The thermocouples were then connected to the M.O.L.E. and the M.O.L.E. was turned on and placed in an insulating sleeve. The M.O.L.E. and the test coupon were then placed in the reflow oven and allowed to run through the oven. Once the M.O.L.E. and coupon came through the oven, the M.O.L.E. was turned off and the thermal profile was generated using data acquisition program, M.O.L.E. Data Manager, version 2.1 to obtain the data points which were plotted using Microsoft Excel (e.g. Figure 3.2). The optimal thermal profile exposed the test board to a temperature in the lead-free range between 240^{o}C – 250^{o}C. The optimal air temperature zones for the oven used in the coupon processing were as follows: Zone 1: 100^{o}C, Zone 2: 120^{o}C, Zone 3: 150^{o}C, Zone 4: 170^{o}C, Zone 5: 190^{o}C, Zone 6: 200^{o}C, and Zone 7: 270^{o}C. The oven conveyor belt speed was set to 10.6 mm/s (25”/min.) for all coupon processing. A total of 14 separate batches of coupons were processed using the above conditions. Each time a new batch of coupons was processed a thermal profile of the coupon temperature was collected to ensure that it was the same as the profile shown in Figure 3.2. A final batch of coupons was processed at Research in Motion using a bench top forced convection reflow oven PRO 1600 manufactured by Advanced Techniques U.S. Inc.. The profile was programmed to give a lead-free soldering temperature profile consistent to that mentioned above. The

oven settings were as follows: a ramp rate 0.6 ^{o}C/s was used to get to a temperature of 220^{o}C, the temperature was held at 220^{o}C for 70 seconds, then ramped to an air temperature of 280^{o}C using a ramp rate of 1^{o}C/s, held at 280^{o}C for 60 seconds, followed by a cool down for 60 seconds. The temperature profile for the coupon temperature was generated using the M.O.L.E. as before and is illustrated in Figure 3.3.

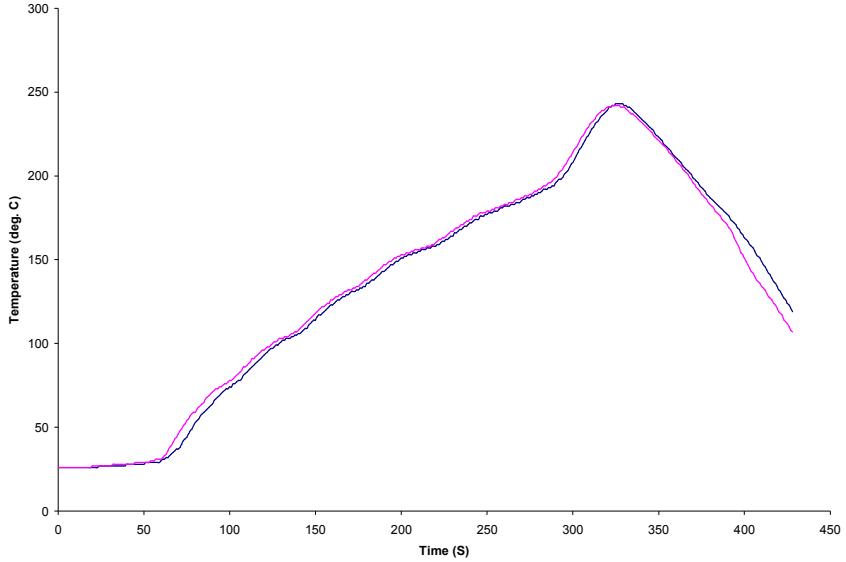

Figure 3.2: Lead-Free soldering profile using a reflow oven to process test coupons.

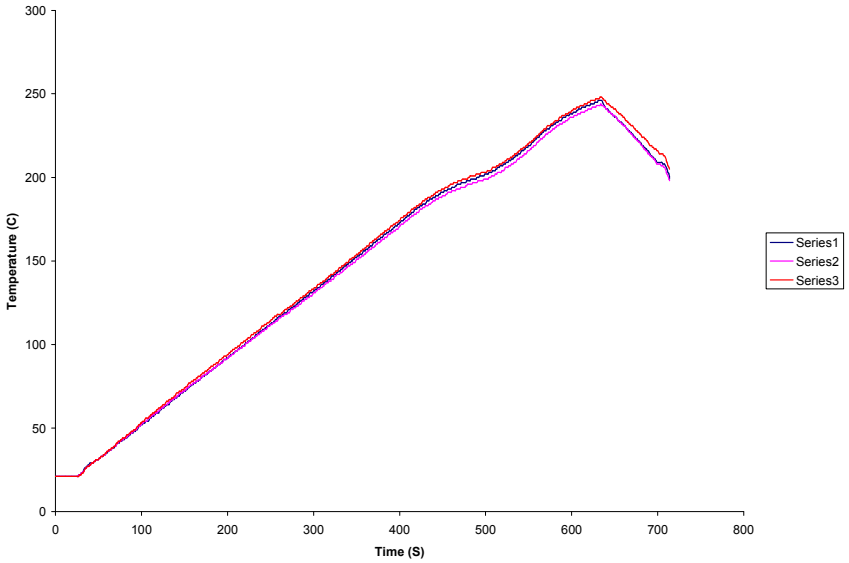

Figure 3.3: Lead-Free soldering profile using a forced convection oven.

3.2.3 Cleaning

After the reflow process, the coupons were allowed to cool for approximately 10 minutes. The coupons processed at George Brown College (GBC) had an initial cleaning performed at GBC by rinsing the coupons with deionized water at 80^{o}C. This initial cleaning was required to remove the bulk of the flux residues, which were easily removed once the coupons were processed. Once a temperature of 80 ^{o}C was achieved the individual coupons were immersed into the water bath and scrubbed using a toothbrush for approximately five minutes. To maintain a clean water bath the PEPG processed coupons were cleaned first followed by the PEPG/Cl processed coupons. The water was then changed and re-heated to 80^{o}C and the PEG processed coupons were cleaned first followed by the PEG/Cl processed coupons. Lastly, the water bath was changed and the HASL processed coupons were cleaned. The coupons were allowed to air dry on a coupon rack and were then stored individually in Kapak® bags and brought to the University of Toronto for additional cleaning. For the second cleaning step, a Branson 5210 ultrasonic cleaner was used. The bath used deionized water heated to 65^{o}C. Coupons in sets of 3 were placed in the water bath based on flux chemistry (i.e. PEPG, PEPG/Cl etc) and ultrasonically cleaned for 10 minutes. The water bath was changed in the same sequence as described above. The coupons were rinsed in isopropyl alcohol (IPA) and allowed to air dry on a coupon rack and then placed individual in new Kapak® bags.

3.3 – Accelerated Aging Tests

3.3.1 – SIR Testing

Wires were hand soldered to the processed coupons, both at the voltage points and the measurement points. The coupon was designed in such a manner that there was one voltage point and 4 measurements points. For the system used in the testing, each cable had 16 measurement channels (i.e. each port could measure a maximum of 16 points). Either 3 or 4 coupons were wired up per cable, depending on the number of coupons being tested. In addition, the system had a single voltage port, so all voltage wires were ganged together and then connected to the main site that connected to the test system. Once the coupons were wired to the cables they were connected to a Concoat AutoSIR® 128 and then placed in a Thermotron 2800 temperature-humidity (T-H) chamber on coupon racks. The testing was performed at 85^0C/ 85%RH and +200 V bias. Insulation resistance measurements were taken approximately every 8 hours using a +100V test voltage.

3.3.1.1 – Temperature – Humidity Chamber

A Thermotron 2800 temperature-humidity (T-H) chamber was used during the SIR testing. The chamber was normally ramped up to 85 °C first, while holding humidity at 40%. Once the chamber reached 85 °C, the humidity was increased by increments of 15%, and held for 15 minutes (i.e. once 55% was reached, the humidity is held there for 15 minutes) until 85% RH was reached. When 85 °C and 85% RH was reached, the chamber was allowed to equilibrate for 3 hours before the voltage was applied. The coupons remained in the chamber under accelerated aging for 28 days.

3.4 Characterization Techniques

3.4.1 – Optical Microscopy

The coupons were examined optically using a Wild Heerbrugg microscope with a Nikon coolpix E955 camera attachment. A backlighting source was used to locate CAF. A typical backlighting image illustrating a CAF shadow is shown in Figure 3.4. For the SIR tests performed at Research in Motion, a Nikon eclipse MA 100 optical microscope with a Nikon D5 Fi 1 camera attachment and a polarized light source was used to locate the CAF. A typical CAF image generated using polarized light is illustrated in Figure 3.5.

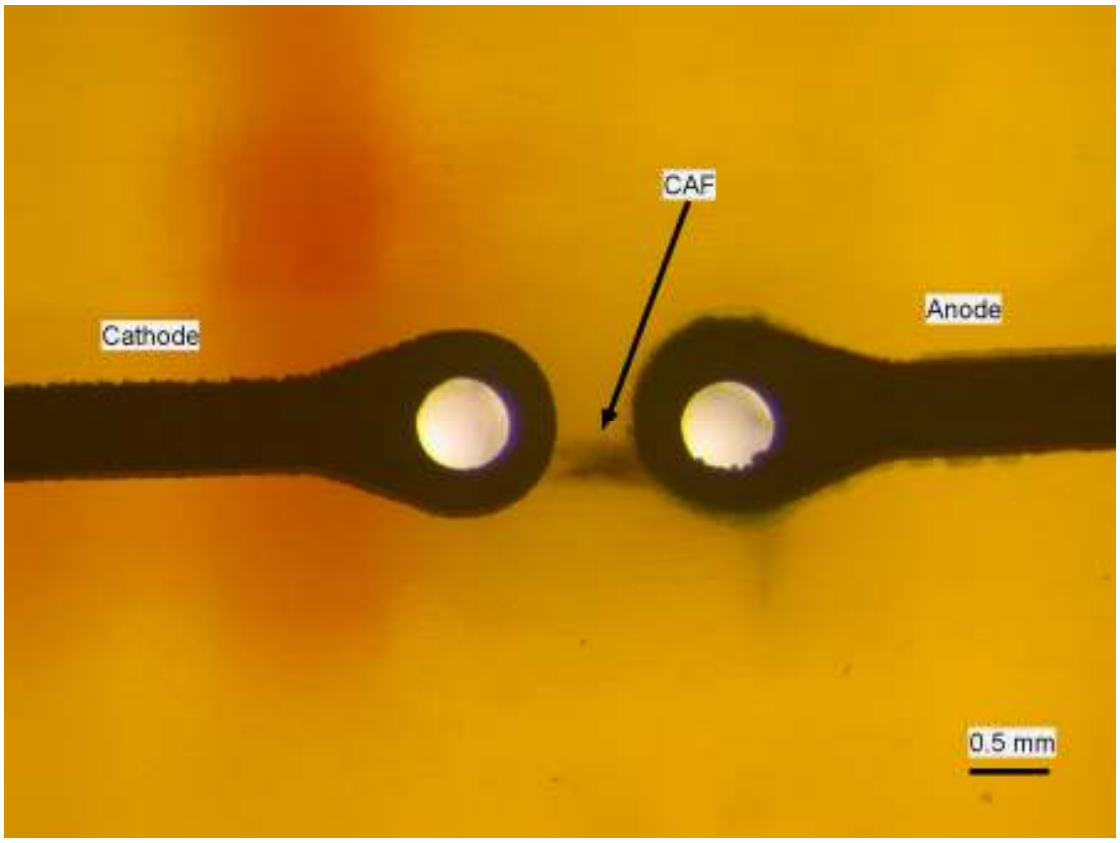

Figure 3.4: Typical backlighting image illustrating CAF [33]. Source: Reprinted with kind permission of Springer Science and Business Media.

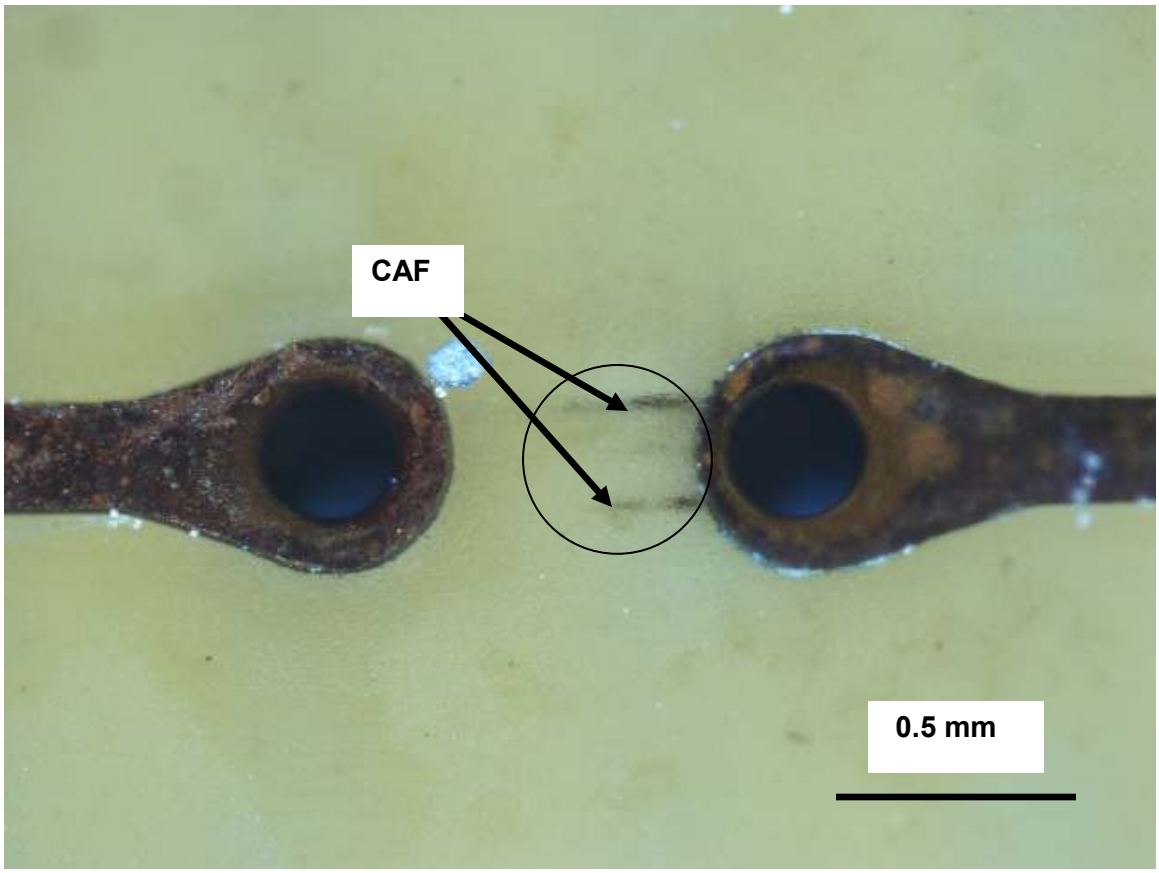

Figure 3.5: Typical image generated using polarized light showing CAF.

3.4.2 – Scanning Electron Microscopy (SEM)

A Hitachi S-570 scanning electron microscope (SEM) with an accelerating voltage of 20 kV was used to observe cross-sections of CAF at the epoxy-glass interface and the compound in the polymer matrix. The SEM can be operated in either secondary electron mode or backscattered mode. All cross-sections were carbon coated. Previous work on CAF used the backscattered imaging mode, which gives elemental contrast, resulting in heavier elements such as copper appearing brighter. In this work, the backscattered mode was used on the samples prepared at RIM after July 7th, 2009 using the JEOL, JSM – 6460 LV variable pressure SEM to characterize the CAF. For the SEM performed at RIM, the samples were not carbon coated since a variable

pressure SEM allows samples to be analyzed using low pressure. The pressure used to analyze the samples at RIM ranged between 60 Pa - 70 Pa. The bulk of this work was performed using secondary mode, and the CAF was easily observed due to the very smooth surface achieved during polishing.

3.4.3 - Energy Dispersive Spectroscopy (EDS)

Energy dispersive spectroscopy (EDS), which was coupled with the Hitachi S-570 and JEOL, JSM – 6460 LV SEMs, was used to confirm that both CAF and the compound in the polymer matrix contained copper, and either chlorine or bromide deepening on the flux used. The elemental analysis was performed either at (a) a specific spot, (b) over an area or (c) a concentration map of an area was obtained. The EDS was used strictly to confirm that the CAF contained copper, and chloride and/or bromide. The presence of silicon or calcium was from the E-glass fibers of the PWB.

3.4.4 – Focused Ion Beam (FIB)

Two separate bromide CAF samples were prepared for transmission electron microscopy (TEM) analysis at the University of Western Ontario using the Leo 1540 focused ion beam (FIB) SEM cross beam microscope. The samples were milled and the milled sample was then removed by placing it on molybdenum using nano-manipulators for further polishing and thinning of the sample to ~ 100 nm or less. The sample on the molybdenum holder was then ready for TEM analysis.

3.4.5 – Transmission Electron Microscopy (TEM)

TEM was performed using a FEI, Model - Tecnai 20 with and EDS detector built into the system. The accelerating voltage used was 200 kV. EDS was performed on samples tilted to 15° to confirm the presence of bromine, oxygen, and copper. Once these

elements were confirmed, the sample was tilted to 0° and selected area diffraction (SAD) was performed at several points to generate diffraction patterns.

3.4.6 – X-ray Photoelectron Spectroscopy (XPS)

X-ray photoelectron spectroscopy (XPS) was used to characterize the copper containing compound found in the polymer matrix. A Thermo Scientific K-alpha probe XPS spectrometer (ThermoFisher, E.Grinstead, UK) with a spot size of 30 μm was used to characterize the copper compound for the coupon processed with PEPG. A Thermo Scientific theta probe (ThermoFisher, E. Grinstead, UK) with a spot size of 15 μm was used to characterize the copper compound for the coupon processed with PEPG/Cl and HASL fluxes. A monochromatic Al Kα X-ray source was used to characterize all samples. Prior to the characterization of the copper compound in the polymer matrix, the XPS spectrometer was calibrated using a two step method. The first part of the calibration is referred to an absolute calibration where metals of known binding energies (BE) with excellent conductivity and clean surface are used. The three metals used to do the absolute calibration were: (i) Au which has a $4f^{7/2}$ low BE of 84.0 eV, (ii) Ag which has a $3d^{5/2}$ mid-range BE of 368.3 eV, and (iii) Cu which has a $2p^{3/2}$ high BE of 932.7 eV. The absolute calibration step ensures that the energy scale is linearized. The second part of the calibration ensures that charge compensation is taken into account for low energy electrons and ions. This step is needed for non-conductive samples and uses adventitious carbon with a known BE of 285.0 eV to determine the small energy shift and then define all shifting relative to the low BE shift.

3.4.7 – Fourier Transform Infrared Spectroscopy (FTIR)

Coupons that were processed with HASL flux under 1 or 2 reflows were compared to unprocessed coupons for both organic and ionic residues. The processed coupons, unprocessed coupons, and a sample of HASL fluid were soaked in acetonitrile for 24 hours. The acetonitrile was then allowed to evaporate in air, and the remaining extracted glycols were analyzed using a Bruker Tensor 27 FTIR. This was repeated for all other fluxes presented in Table 1, which were only processed under one reflow.

3.4.8 – Ion Chromatography

Ion chromatography was performed using a Dionex CD20 conductivity detector to determine if ionics from the flux had diffused into the board. Two coupons per flux (Table 3.1) were processed using a single reflow. For the HASL processed coupons, two additional coupons exposed to two reflows were also analyzed. Two "as received coupons" were used as the control coupons. Extraction was done by placing the coupons in Kapak polyester bags and covering them with a measured volume of 50/50 v/v solution of isopropyl alcohol (IPA) and deionized (DI) water solution. In addition, a Kapak bag with only IPA/DI water solution was run to ensure that the Kapak bags were not contaminated. The bags were then sealed and placed in a water bath at 80 ^{0}C for one hour. Five milliliters of the extracted solution was placed in a vial and evaporated until 1 ml of solution remained. To ensure full removal of the IPA before ion chromatography an additional 4 ml of DI water was added and the solution was evaporated again to 1 ml. Before the samples were run through the ion chromatography apparatus, the anion exchange column was calibrated using the following standard parameters:

Eluent: 8mM Na_2CO_3/1mM NaH CO_3

Flow rate: 1.0 mL/min

Operating temperature: 30 °C

Detection: Suppressed conductivity at 10 μSFS

Injection Volume: 10 μL

Storage Solution: Eluent

Once the apparatus was calibrated, the samples were run at room temperature.

3.5 – Chapter Summary

This chapter has summarized the details of the test vehicle, flux formulations used, the experimental procedure for all coupon processing and electrical testing and the characterization techniques used in this thesis.

Chapter 4 – Results

4.0 – Overview

This chapter will present all the experimental data that has been obtained for coupons processed with five different water soluble fluxes after temperature-humidity-bias testing. The results were obtained using various analytical and characterization techniques.

4.1 Insulation Resistance (IR) Testing

In the electronics industry the electrical integrity of a material is tested using temperature, humidity, bias (T-H-B) testing. This section will provide the details of the electrical data that was compiled in this work.

4.1.1 Overview of IR Testing Including Measurement Issues

The background information on insulation resistance testing was previously discussed in Section 2.6.1. Throughout the course of this work, 15 different insulation resistance tests were run as outlined in Section 3.3. The first 14 of these tests were run using the AutoSIR 128 at the University of Toronto. It was learned through discussions with technical staff at Research In Motion (RIM) and other companies in the electronics industry, who employed the same equipment, that there was a glitch in the software resulting in inconsistent insulation resistance data. It was confirmed that the software caused inaccurate insulation resistance readings to be generated. Due to these equipment issues, the 14 tests run at the University of Toronto were used only to create CAF for characterization purposes. RIM recently upgraded the software on their AutoSIR 128 unit to correct this deficiency. Thus, the testing subsequently completed at

Table 4.1 –Insulation Resistance Values and Number of CAF

Flux Chemistry	Average SIR Value per 3 Coupons (Ω)		# of CAF
Control – 1	2.11×10^{11}		0
Control – 2			0
Control – 3			0
		Total CAF	**0**
Control Processed - 4	2.99×10^{11}		0
Control Processed – 5			0
Control Processed – 6			0
		Total CAF	**0**
PEPG – 7	7.11×10^{10}		1
PEPG – 8			2
PEPG – 9			1
		Total CAF	**4**
PEPG/Cl – 10	6.09×10^{10}		3
PEPG/Cl – 11			2
PEPG/Cl – 12			0
		Total CAF	**5**
PEG – 13	8.50×10^{9}		1
PEG – 14			2
PEG – 15			3
		Total CAF	**6**
PEG/Cl – 16	6.51×10^{9}		0
PEG/Cl – 17			0
PEG/Cl – 18			0
		Total CAF	**0**
HASL – 19	2.63×10^{10}		4
HASL – 20			4
HASL – 21			3
		Total CAF	**11**

RIM generated good insulation resistance data which is included in this work to provide the actual values for control coupons and coupons processed with various fluxes. The detailed plots are presented in Appendix A. Table 4.1 summarizes the average insulation resistance values and the number of CAF created during the 28-day accelerated aging test run at RIM for the control fluxed coupons.

4.1.2 – Insulation Resistance Plot where CAF almost Bridged

On one coupon that was processed with the HASL flux, one of the hole-to-hole plots showed an example where CAF almost bridged (Figure 4.1). This insulation resistance degradation was followed by a restoration which took place 7 times, as shown in Figure 4.1.

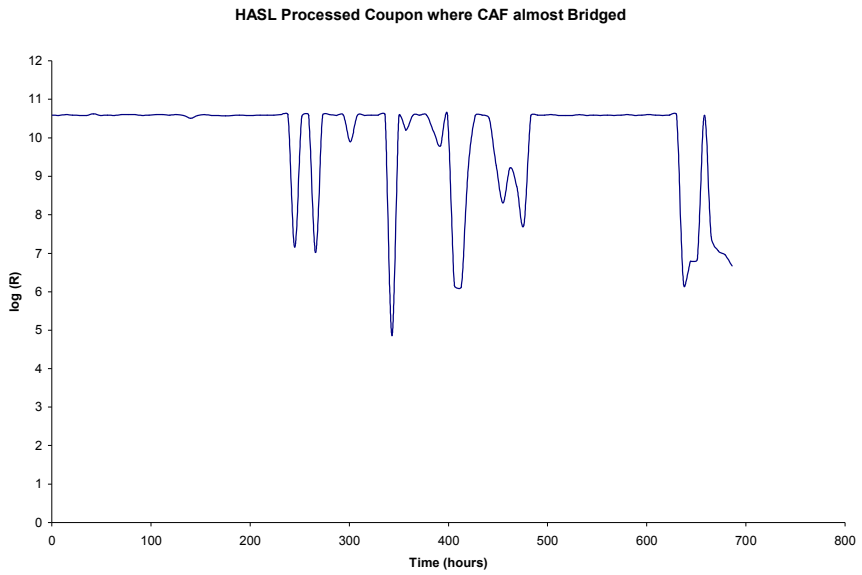

Figure 4.1: Insulation resistance plot for a coupon processed with the high bromide containing flux (i.e. HASL flux) where CAF almost bridged.

4.2 - Extraction of Organic Flux Constituents from Processed Boards Compared with the Flux Itself

This section will present FTIR data showing that during the coupon processing stage there is an interaction between the PWB and the flux. The organic constituents of the

flux were extracted as outlined in Section 3.4.7 and analyzed using FTIR. The FTIR spectra from the flux extracted from the processed board matched the as-received flux, thus showing that the flux diffused into the PWB during processing.

The FTIR spectra for the PEPG (i.e. Figure 4.2) extract from the processed coupon and the as-received flux showed a match between the extract and the raw material, thus demonstrating that the polyglcol from the flux had diffused into the substrate. This will be discussed in section 5.1.2. It must be noted that the presence of chloride does not affect the FTIR spectra between PEPG and PEPG/Cl, since FTIR evaluates the organic constituents (i.e. the PEPG vehicle). For this reason the FTIR spectra for PEPG/Cl has been included in Appendix B.

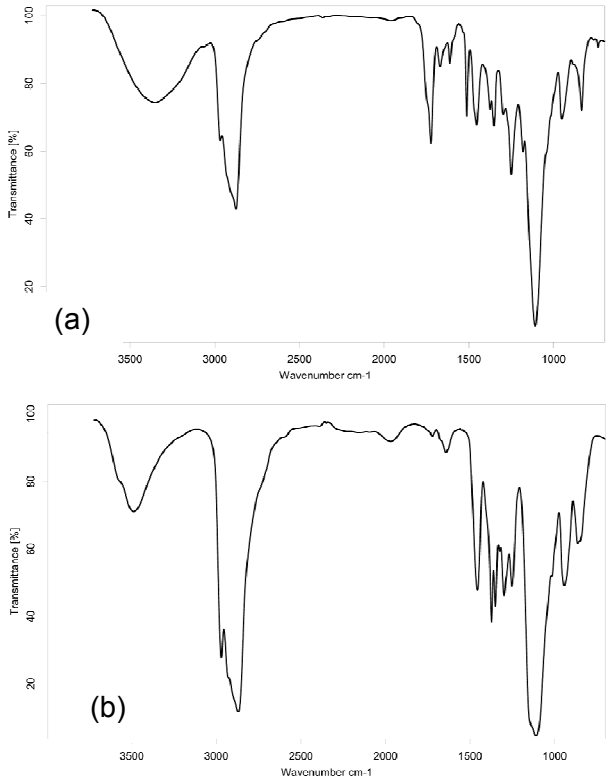

Figure 4.2: FTIR spectra for (a) PEPG flux extracted from the processed coupon, and (b) PEPG flux [33]. Source: Reprinted with kind permission of Springer Science and Business Media.

In a similar manner the PEG FTIR spectra (i.e. Figure 4.3) showed a match between the extract and the raw material, thus demonstrating that the polyglycol from the flux has diffused into the substrate. This will be discussed in section 5.2.3. The PEG/Cl spectra have been included in Appendix B.

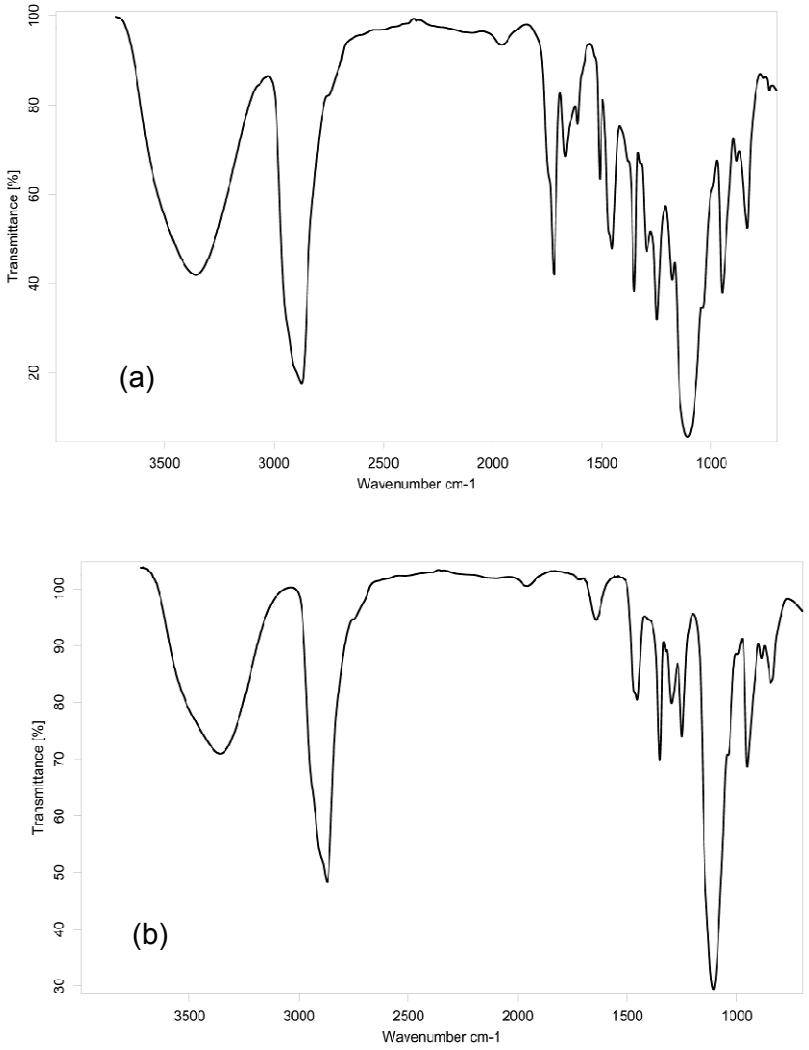

Figure 4.3: FTIR spectra for (a) PEG flux extracted from the processed coupon, and (b) PEG flux [33]. Source: Reprinted with kind permission of Springer Science and Business Media.

The FTIR spectra for the coupons processed following 1 or 2 reflows and the unprocessed coupon were compared to the spectra of the HASL fluid. The polyglycol spectra for the HASL flux showed a match to the polglycol spectra for the extract from the processed coupons (Figure 4.4). This proved that the polyglycol from the HASL fluid diffused into the substrate during soldering.

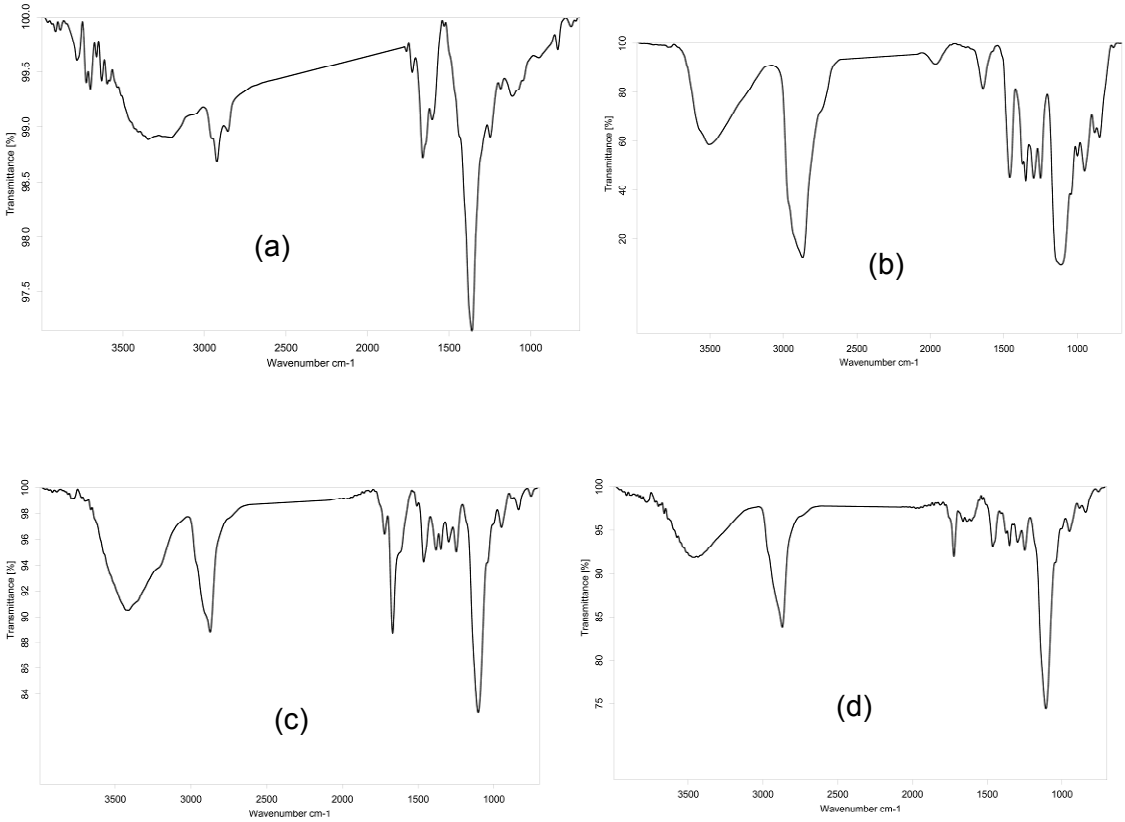

Figure 4.4: FTIR spectra for the extract from (a) unprocessed board, (b) HASL flux, (c) coupon processed under 1 reflow, and (d) coupon processed under 2 reflows.

4.3 Extraction of Ionic Flux Constituents from Processed Boards

The ionic constituents for the as received PEPG, PEPG/Cl, PEG, PEG/Cl and HASL fluxes were analyzed using ion chromatography and compared to the ion constituents that were extracted from the PWB which were processed with each respective flux. The detection limit of the detector was 0.02 ppm. The results are summarized in Table 4.2.

Table 4.2 – Extraction of Chloride and Bromide from Fluxed and Control Coupons

	Cl^-(ppm)	Br^-(ppm)
Control	0.67	0.09
As received PEPG flux	0.04	-
As received PEPG with 2 wt% Cl^-	878	-
Coupons processed with PEPG	0.23	0.48
Coupons processed PEPG with 2 wt% Cl^-	0.44	0.66
As received PEG flux	0.07	0.51
As received PEG with 2 wt% Cl^-	946	-
Coupons processed with PEG	0.19	0.18
Coupons processed with PEG with 2 wt% Cl^-	0.44	0.53
As received HASL fluid	36	19, 500
1 reflow with HASL fluid	0.46	10.46
2 reflows with HASL fluid	0.30	5.52

4.4 – SEM and EDS Characterization for Coupons Processed with PEPG, PEPG/Cl, PEG, PEG/Cl and HASL Fluxes

CAF was defined in Chapter 2 to be a copper salt that grows along the epoxy-glass interface. When CAF cross-sections are prepared and polished to the tip of the CAF, it will appear as a very fine filament that surrounds the epoxy-glass interface. As the sample is further polished, the CAF becomes thicker at the epoxy/glass fiber interface. SEM and EDS were used to show CAF evolution for all the fluxes tested.

4.4.1 – PEPG

Figure 4.5 is an example of a CAF mage generated using SEM for a coupon processed with PEPG. The spot EDS microanalysis confirms the presence of copper and chloride in the CAF compound. The bromide originates from the bromide found in the epoxy backbone, while silicon and calcium are from the E-glass. For coupons processed with PEPG fluxes, a copper compound is also found in the polymer matrix. This compound is not to be confused with CAF, as CAF grows only at the epoxy/glass fiber interface. The compound in the polymer matrix will be discussed further in Section 4.4.3.

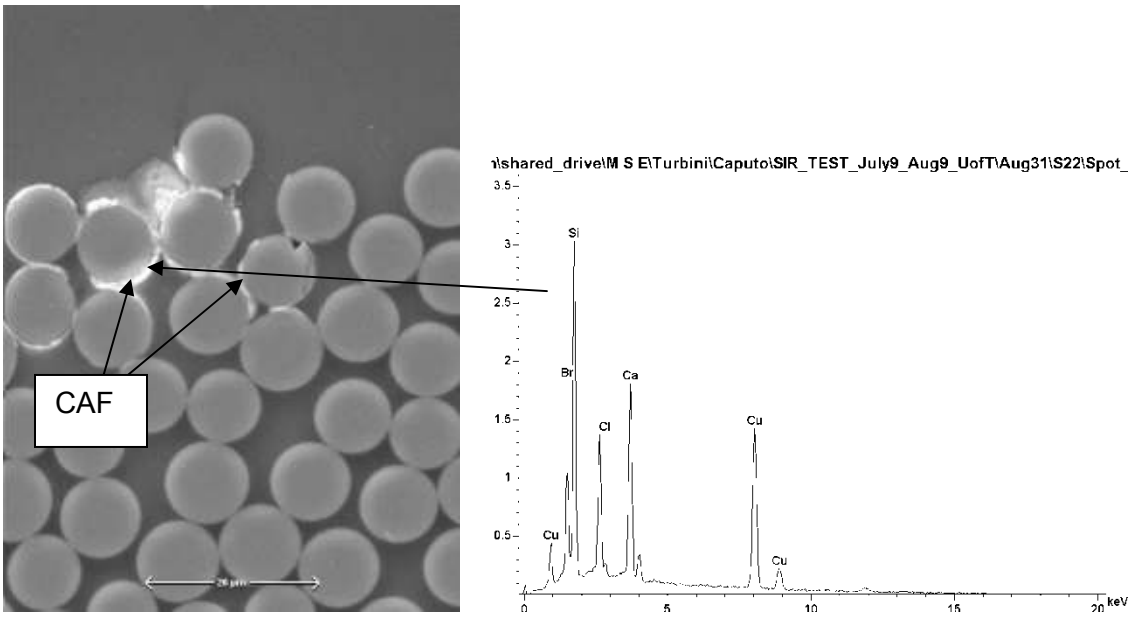

Figure 4.5: SEM image showing CAF and EDS spectrum confirming the presence of copper and chlorine at the epoxy/glass fiber interface for a coupon processed with PEPG.

Figure 4.6 exhibits a second example where CAF was observed for a PEPG processed coupon. To show the CAF thickening phenomena, sequential cross-sections were prepared for SEM analysis. The SEM image for Section A is illustrated in Figure 4.7. This image reveals the presence of CAF surrounding the epoxy/glass fiber interface and

a compound in the polymer matrix starting to be observed in the polymer matrix. The EDS map (Figure 4.8) confirms the presence of copper and chlorine. The cross-section was further polished toward the anode (i.e. Section B in Figure 4.6). The SEM image for this section revealed that the CAF is thicker, and the compound in the polymer matrix becomes more prevalent (Figure 4.9). In addition, the EDS map confirmed the presence of both copper and chlorine (Figure 4.10). Further SEM serial cross-sections and images showing CAF for PEPG processed coupons can be found in Appendix C.

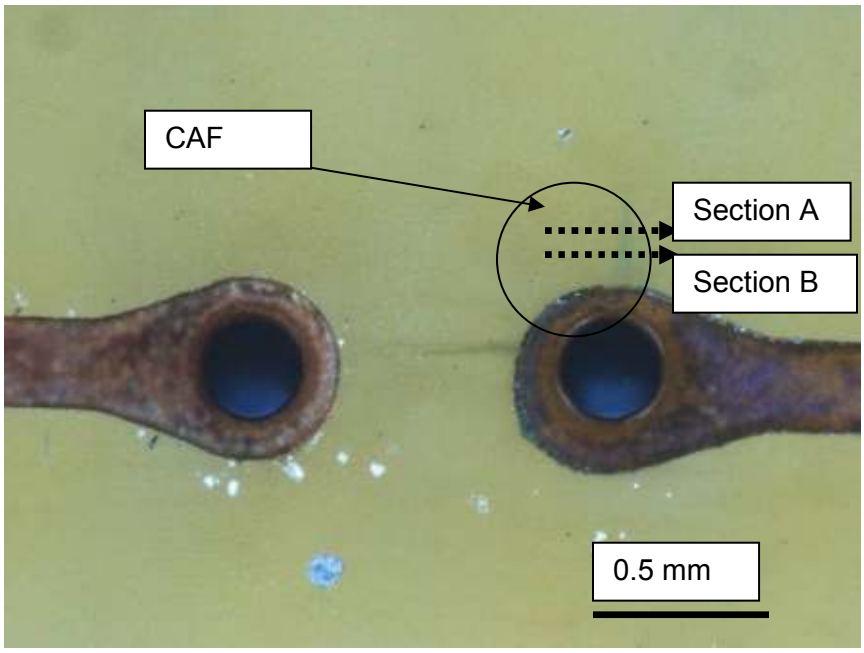

Figure 4.6: Optical image demonstrating CAF for a PEPG processed coupon.

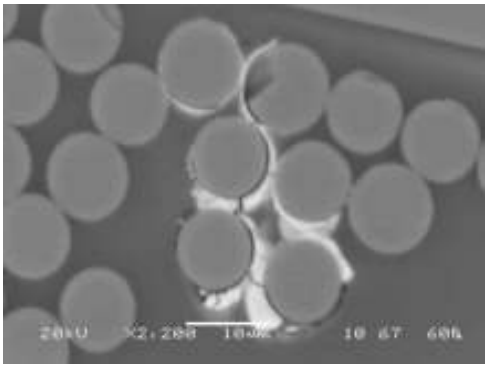

Figure 4.7: A PEPG processed coupon showing CAF and a copper compound in the polymer matrix for section A.

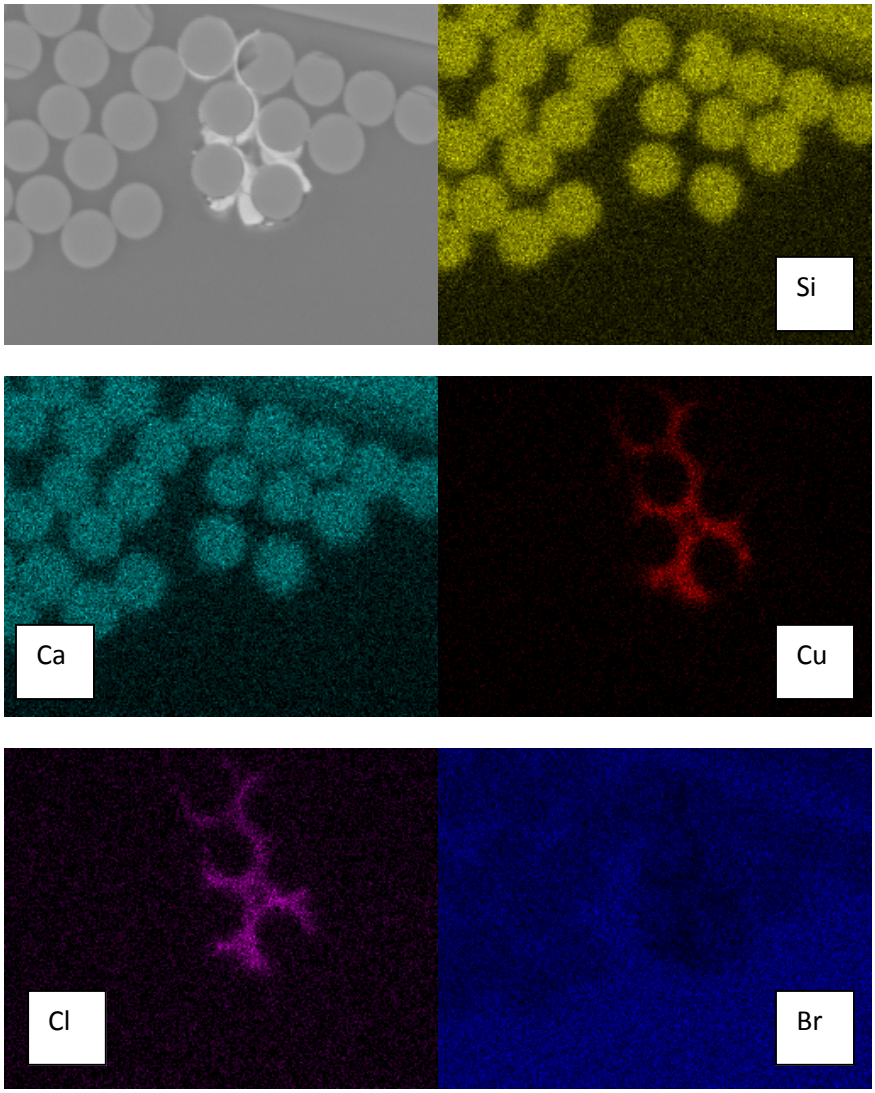

Figure 4.8: EDS map for a PEPG processed coupon showing CAF and a copper compound in the polymer for section A.

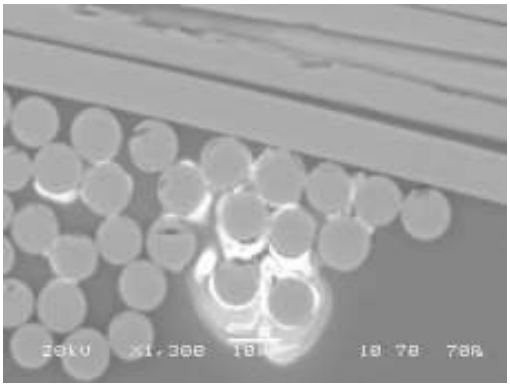

Figure 4.9: PEPG processed coupon showing CAF and a copper compound in the polymer matrix for section B.

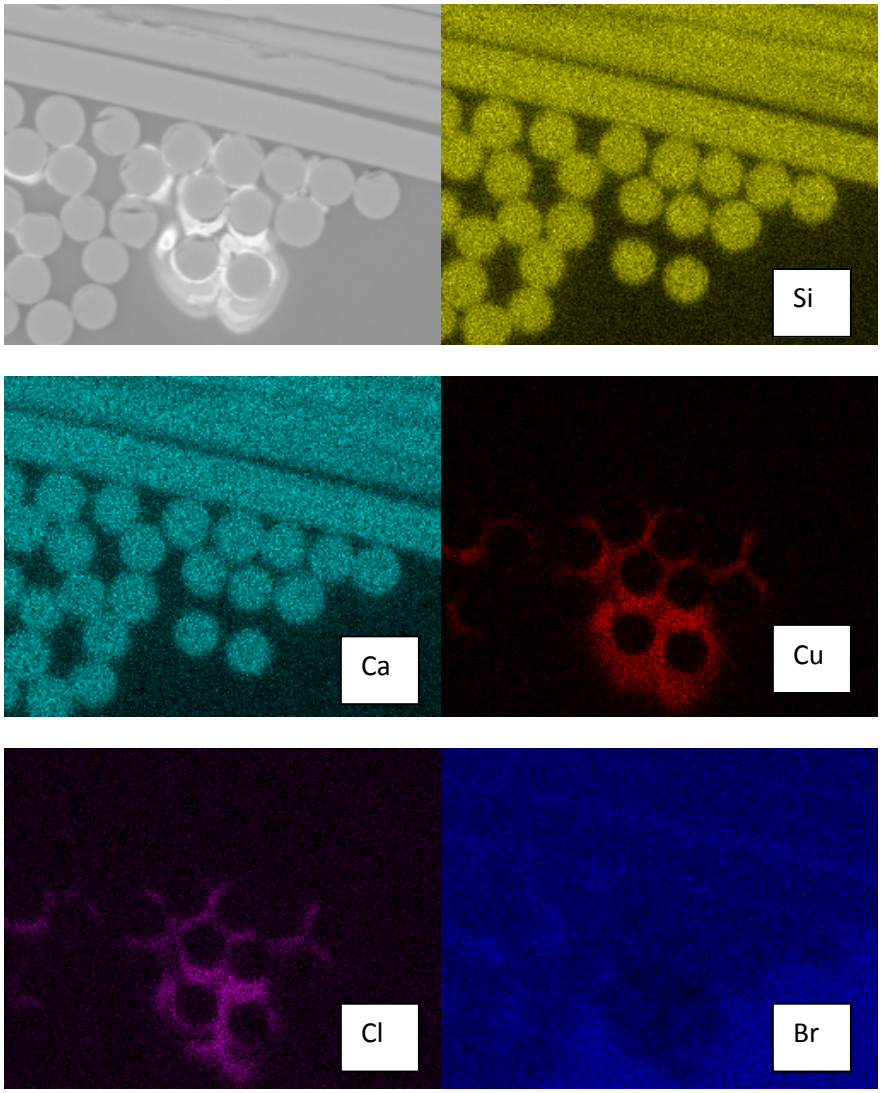

Figure 4.10: EDS map of a PEPG processed coupon for the CAF and copper compound in the polymer for section B.

4.4.2 - PEPG/Cl

As is the case for PEPG, coupons processed with PEPG containing 2wt% chloride (PEPG/Cl) formed CAF. An SEM image where CAF was formed on a coupon processed with PEPG/Cl is illustrated in Figure 4.11. The spot EDS confirms the presence of both copper and chlorine. Figure 4.13 shows a second example of a cross-section that was made at the tip of the CAF (i.e. section C) in Figure 4.12. The EDS

map (Figure 4.14) confirms the presence of copper and chlorine. With further polishing toward the anode (i.e. section D), the CAF becomes thicker, and a copper compound in the polymer matrix becomes evident (Figure 4.15). The EDS map (Figure 4.16) confirms the presence of copper and chlorine. Further SEM serial cross-sections and images showing CAF for PEPG/Cl processed coupons can be found in Appendix D.

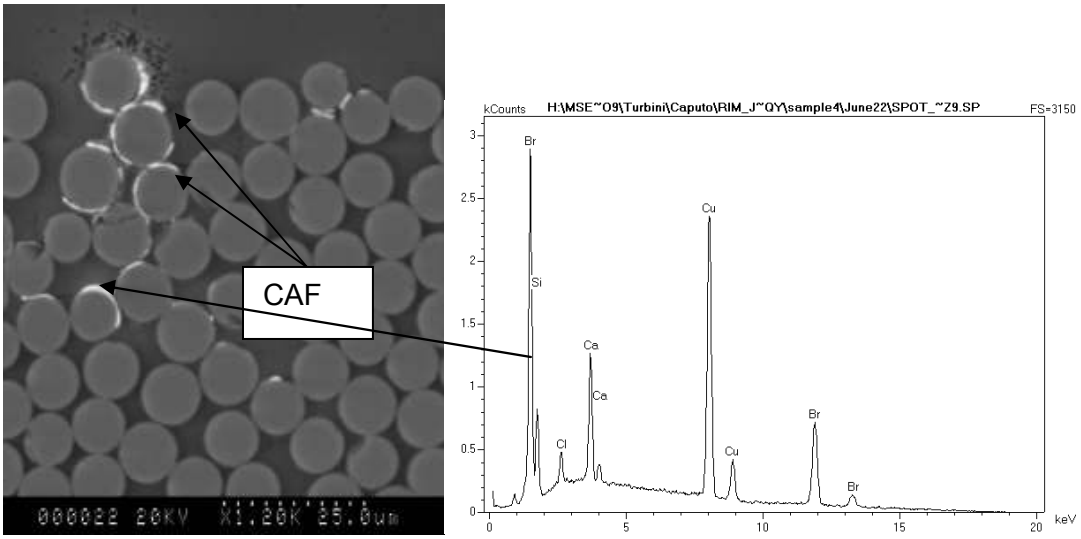

Figure 4.11: SEM image showing CAF and a spot EDS confirming the presence of copper and chlorine for a PEPG/Cl processed coupon.

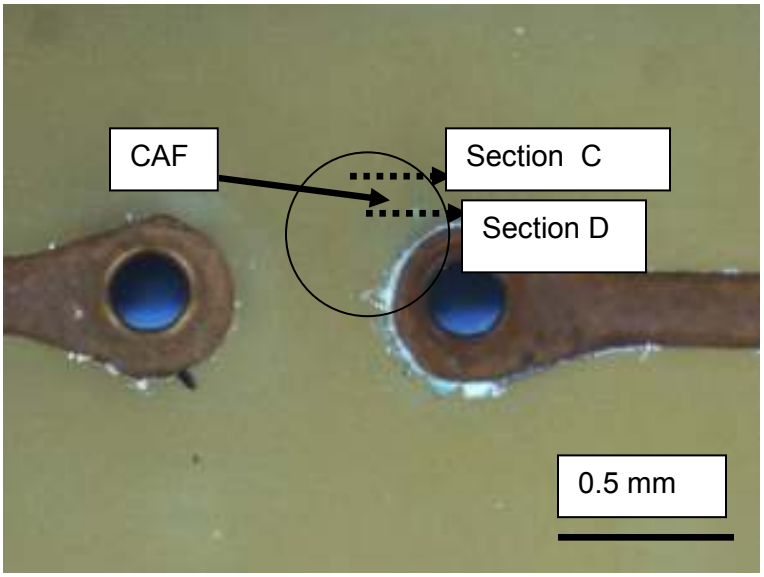

Figure 4.12: Optical image showing CAF for PEPG/Cl processed coupon.

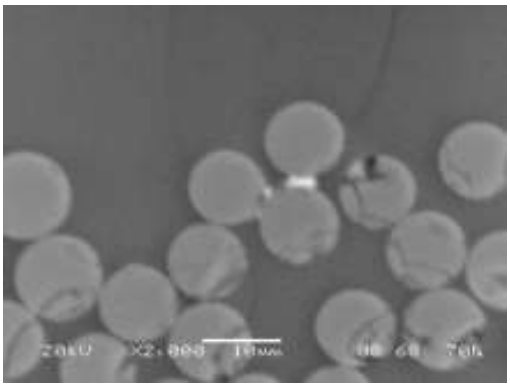

Figure 4.13: SEM image of section C, depicting CAF for a coupon processed with PEPG/Cl.

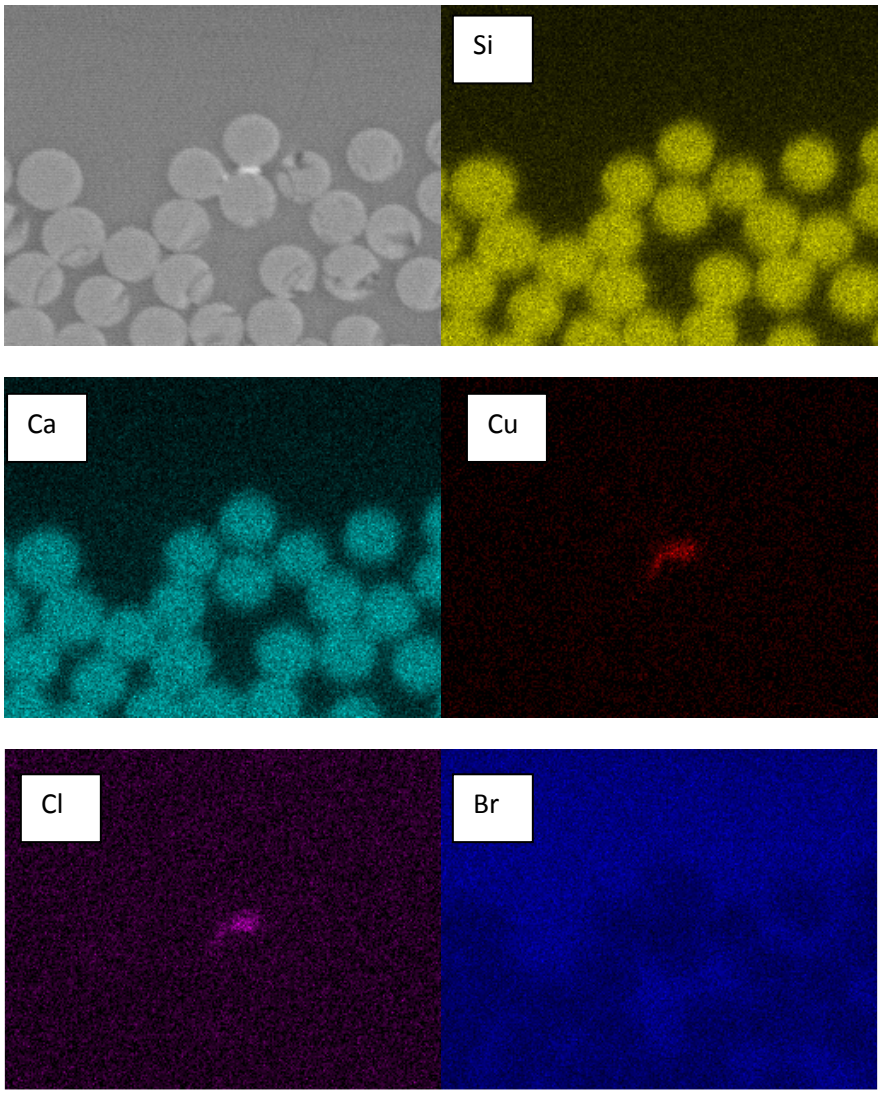

Figure 4.14: EDS map of section C for the PEPG/Cl processed coupon confirming the presence of copper and chlorine.

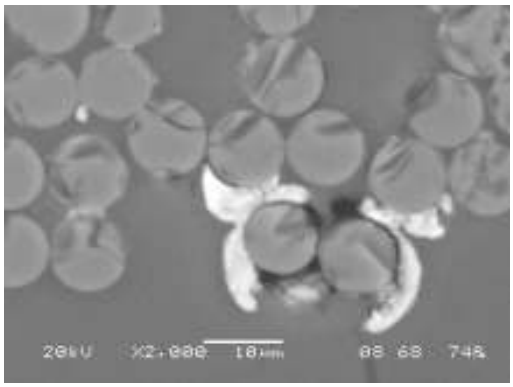

Figure 4.15: SEM image of section D showing thicker CAF and the copper compound in the polymer matrix beginning to form for a coupon processed with PEPG/Cl.

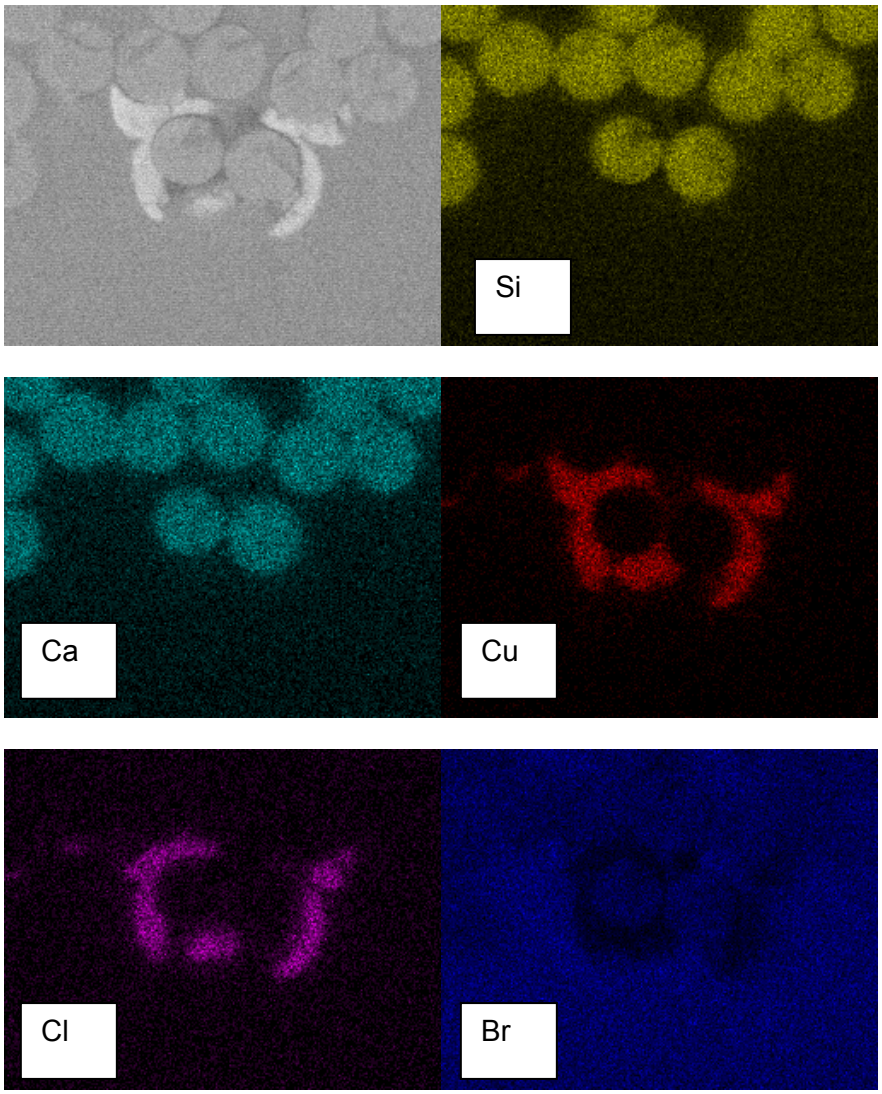

Figure 4.16: EDS map of section D for the PEPG/Cl processed coupon confirming the presence of copper and chlorine.

4.4.3 – Copper Compound in the Polymer Matrix for Coupons Processed with PEPG and PEPG/Cl

It was mentioned in Sections 4.4.1 and 4.4.2 that for coupons processed with PEPG and PEPG/Cl respectively, that in addition to CAF, a copper containing compound was observed in the polymer matrix.

4.4.3.1 - SEM and EDS work showing the Copper Compound for PEPG Processed Coupons

For coupons processed with PEPG solder flux, in addition to CAF surrounding the epoxy/glass fiber interface, a copper-chloride containing compound was found in the epoxy matrix (confirmed by EDS in Figure 4.17). A second example of a copper-chloride compound found in the polymer matrix is presented in Figure 4.18. Additional examples of the copper-chloride compound found in the polymer matrix are illustrated in Appendix C where serial cross-sectioning was performed.

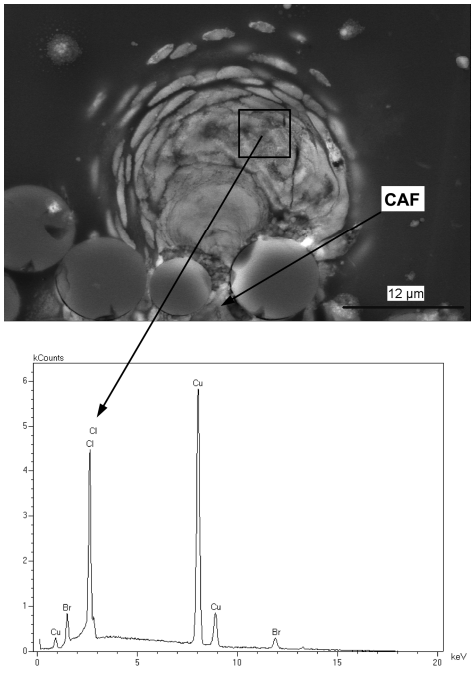

Figure 4.17: SEM and spot EDS of a typical copper-chloride containing compound found in the matrix for coupons processed with PEPG [33]. Source: Reprinted with kind permission of Springer Science and Business Media.

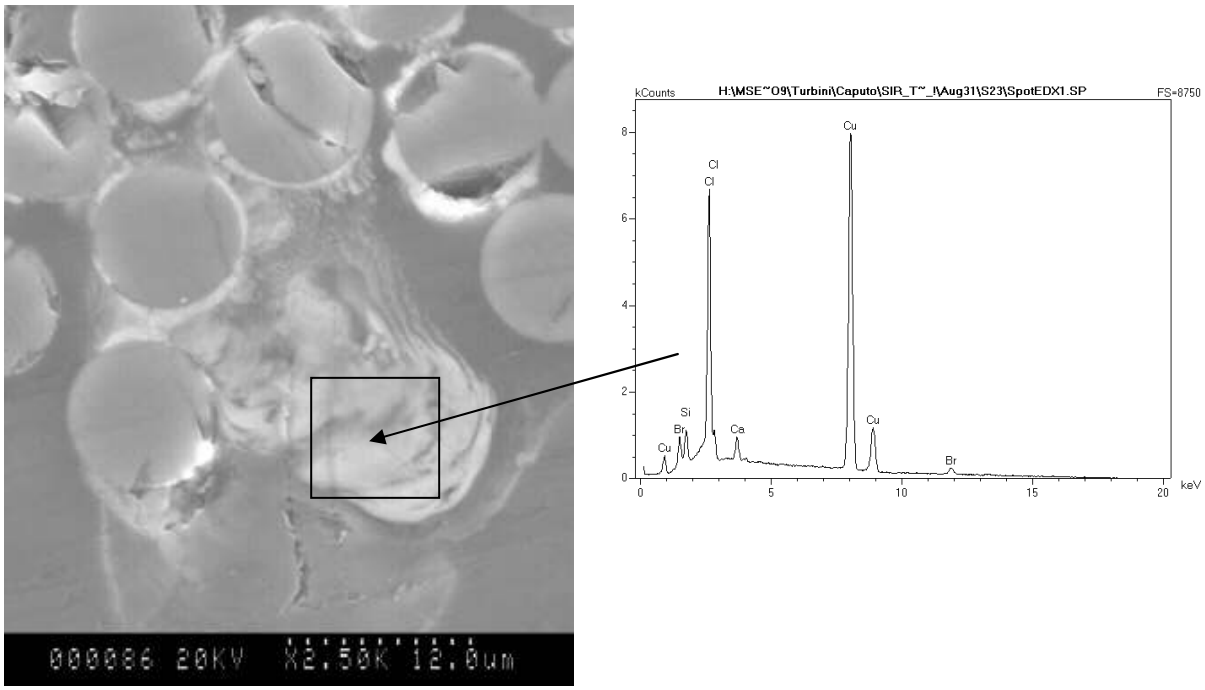

Figure 4.18: SEM and spot EDS of a typical copper-chloride compound found in the polymer matrix for coupons processed with PEPG.

4.4.3.2 - SEM and EDS Work showing the Copper Compound Found in the Polymer Matrix for PEPG/Cl Processed Coupons

Two separate examples of the copper compound found in the polymer matrix for PEPG/Cl processed coupons are shown in Figures 4.19 and 4.20. The spot EDS microanalysis confirms the presence of copper and chlorine. A third example is illustrated in the serial cross-sections in Appendix D.

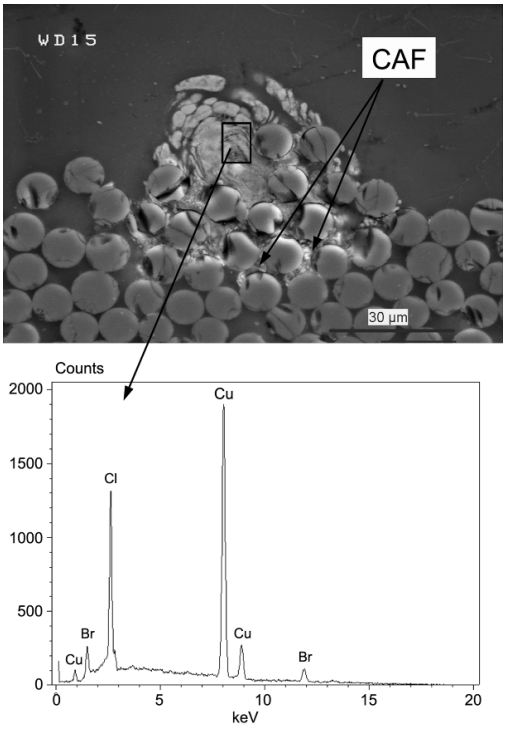

Figure 4.19: SEM and spot EDS of a typical copper-chloride containing compound found in the matrix for coupons processed with PEPG/Cl [33]. Source: Reprinted with kind permission of Springer Science and Business Media.

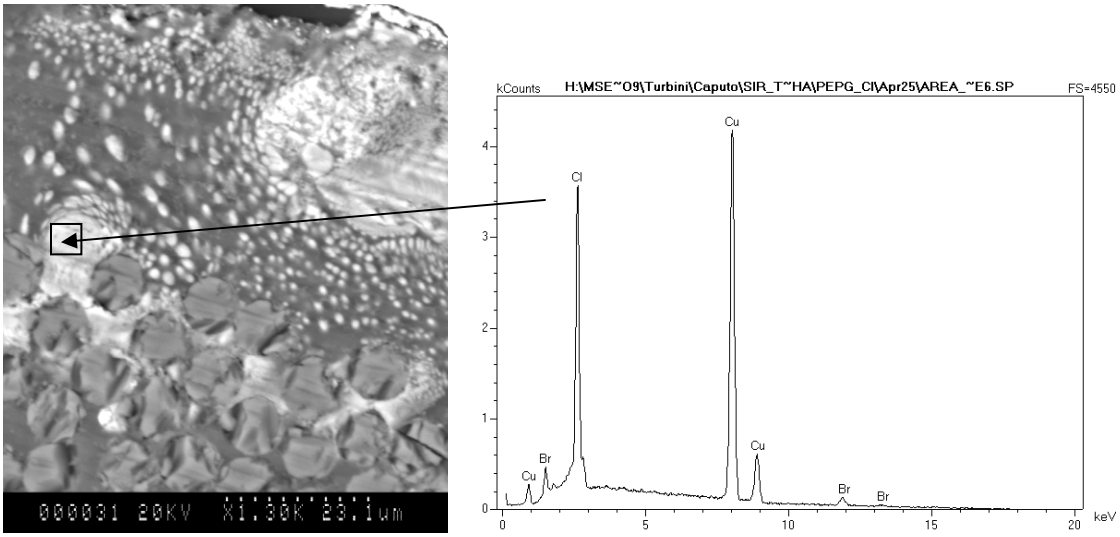

Figure 4.20: SEM and spot EDS of a typical copper-chloride containing compound found in the matrix for coupons processed with PEPG/Cl.

4.4.4 – PEG

For the PEG processed coupons only CAF was formed; no copper containing compound was observed in the polymer matrix. A typical example demonstrating CAF for a PEG coupon is found in Figure 4.21. The cross-section in Figure 4.21 was taken at the very tip of the CAF, illustrating it is very thin as it surrounds the epoxy-glass. The spot EDS microanalysis confirms the presence of copper and chloride. When further polished toward the anode the CAF appears thicker, as illustrated in the SEM images shown in Figure 4.22 (low magnification) and Figure 4.23 (high magnification). A second example of CAF for a coupon processed with PEG is illustrated in Figure 4.24. The cross-section was taken at the anode at (a) low magnification and (b) high magnification. The CAF is very thick at the anode. The spot EDS microanalysis (i.e. Figure 4.24 (c)) confirms the presence of copper and chlorine. Further examples showing CAF for a PEG processed coupon can be found in Appendix E.

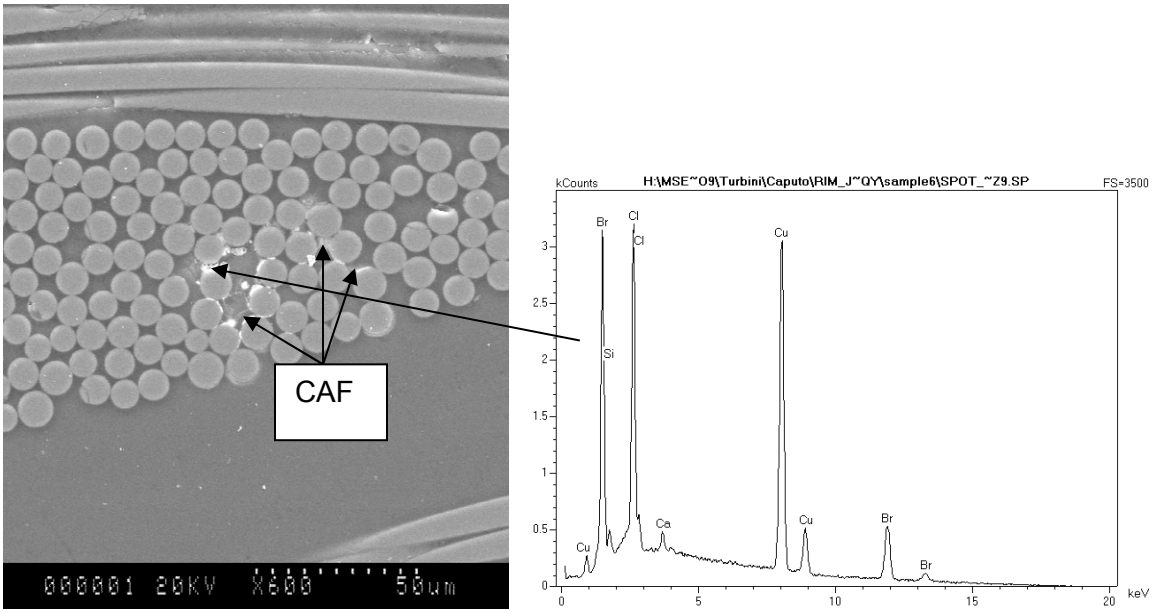

Figure 4.21: SEM image showing a cross-section at the CAF tip and a spot EDS for a PEG processed coupon confirming the presence of copper and chlorine.

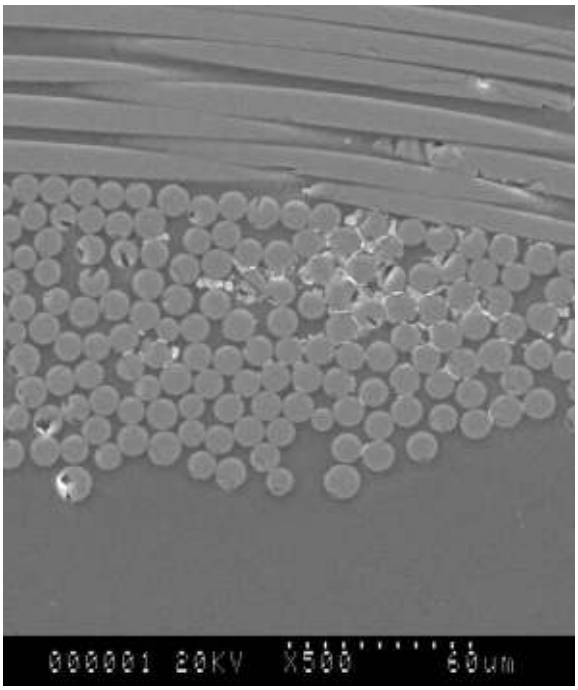

Figure 4.22: A low magnification SEM image presented in Figure 4.21 polished to the copper hole for a PEG processed coupon.

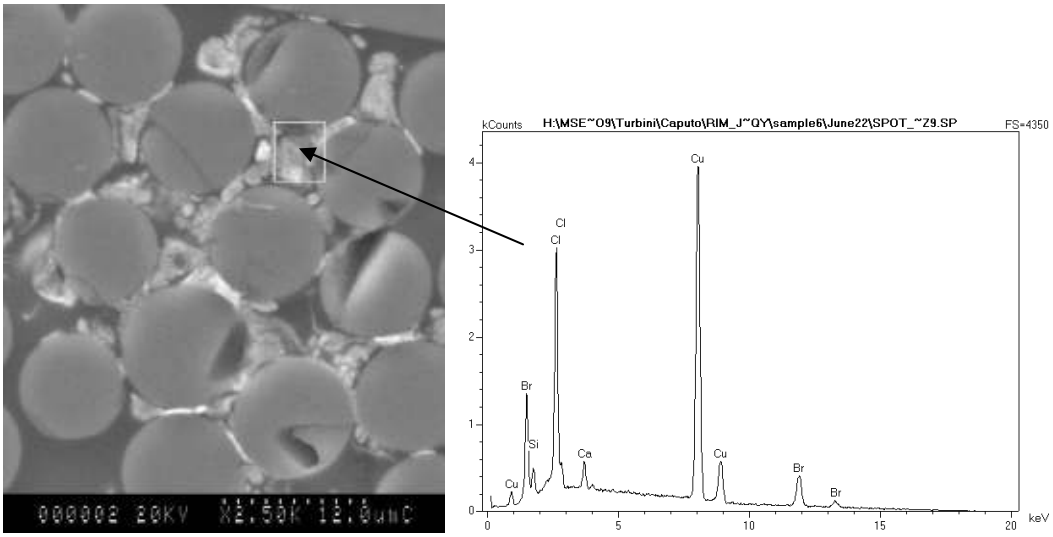

Figure 4.23: A high magnification SEM image of an area from Figure 4.22 showing the thicker CAF and a spot EDS confirming the presence of copper and chlorine for the PEG processed coupon [33]. Source: Reprinted with kind permission of Springer Science and Business Media.

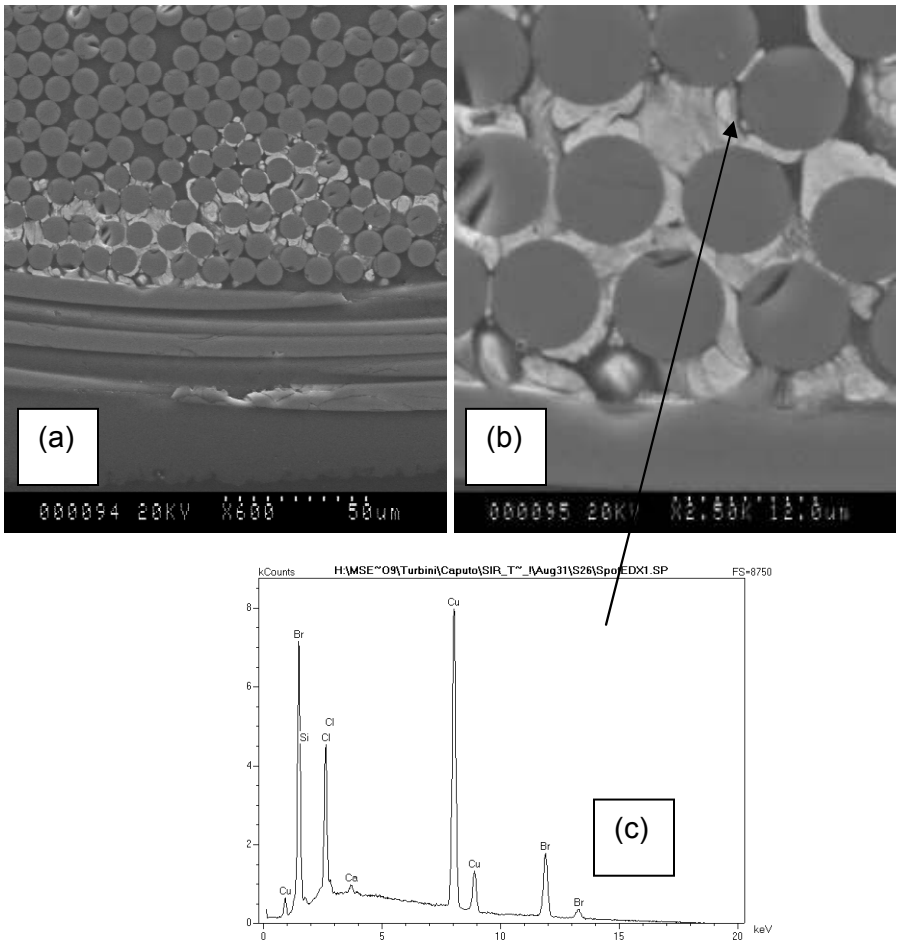

Figure 4.24: SEM image for a PEG processed coupon showing CAF that was polished to the copper hole at (a) low magnification, (b) high magnification, and (c) a spot EDS taken in Figure 4.24 (b).

4.4.5 - PEG/Cl

For the PEG/Cl processed coupons only CAF was formed. No copper compound was found in the polymer matrix. CAF surrounding the epoxy-glass is visible in Figure 4.25 for a PEG/Cl processed coupon. The spot EDS microanalysis confirms the presence of copper and chlorine. A second example of CAF is illustrated in Figure 4.26. It should be noted that the CAF in the second example is much thicker when compared to Figure 4.26. This is due to the fact that the sample in Figure 4.26 was polished to the anode. The spot EDS once again confirms the presence of copper and chlorine. An additional

example that was cross-section at the tip of the anode and then further polished to the anode is illustrated in Appendix F.

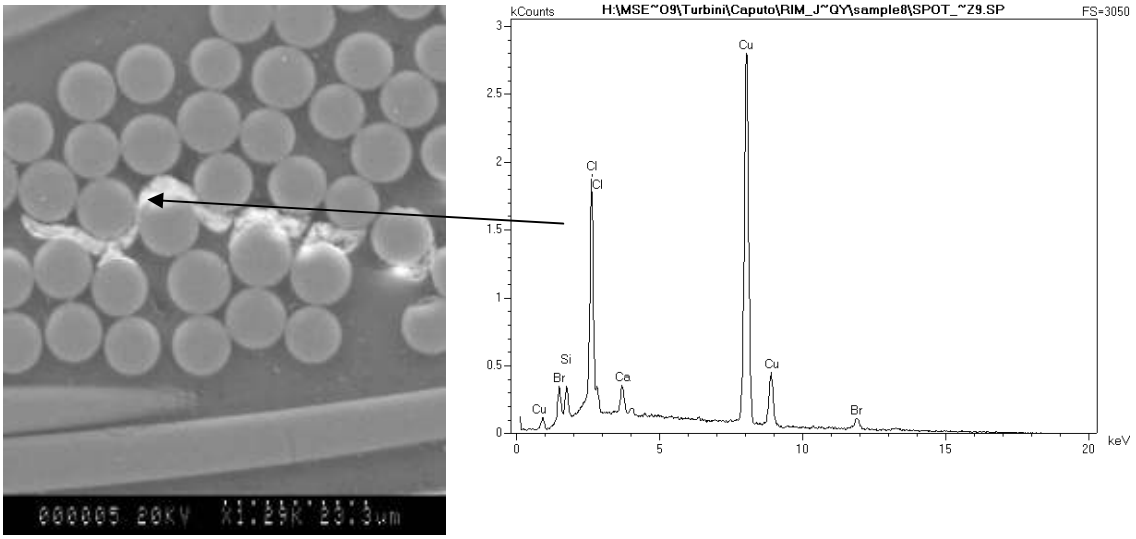

Figure 4.25: An SEM image showing CAF and spot EDS confirming the presence of copper and chlorine for a coupon processed with PEG/Cl [33]. Source: Reprinted with kind permission of Springer Science and Business Media.

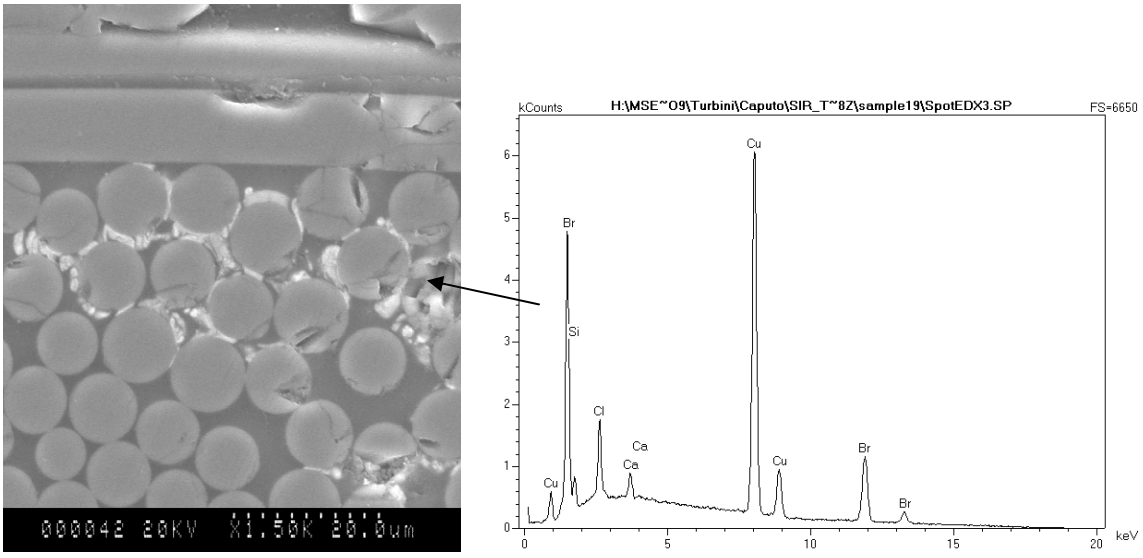

Figure 4.26: An SEM image for a PEG/Cl processed coupon polished to the copper hole depicting CAF and a spot EDS confirming the presence of copper and chlorine.

4.4.6 – HASL

SEM/EDS was performed on several CAF samples that were processed under 2 reflows with the HASL flux and exposed to temperature, humidity and bias conditions as highlighted in the Section 3.3. Serial cross-sectioning was performed to show that CAF became thicker as samples were polished closer to the anode.

4.4.6.1– SEM and EDS Work showing CAF for the HASL Processed Coupons

It has been previously shown that in addition to chloride CAF, coupons processed with a high bromide containing HASL fluid, could create bromide containing CAF. SEM/EDS was performed on several CAF samples that were processed under 2 reflows with the HASL fluid and exposed to temperature, humidity and bias conditions as highlighted in Section 3.3. The SEM/EDS confirms the presence of copper and bromine (Figures 4.27 and Figure 4.28). It must be noted that the TEM samples were prepared using FIB from the location where spot EDS spectra were obtained in Figures 4.27 and 4.28). Further examples of CAF for the HASL processed coupons can be found in Appendix G.

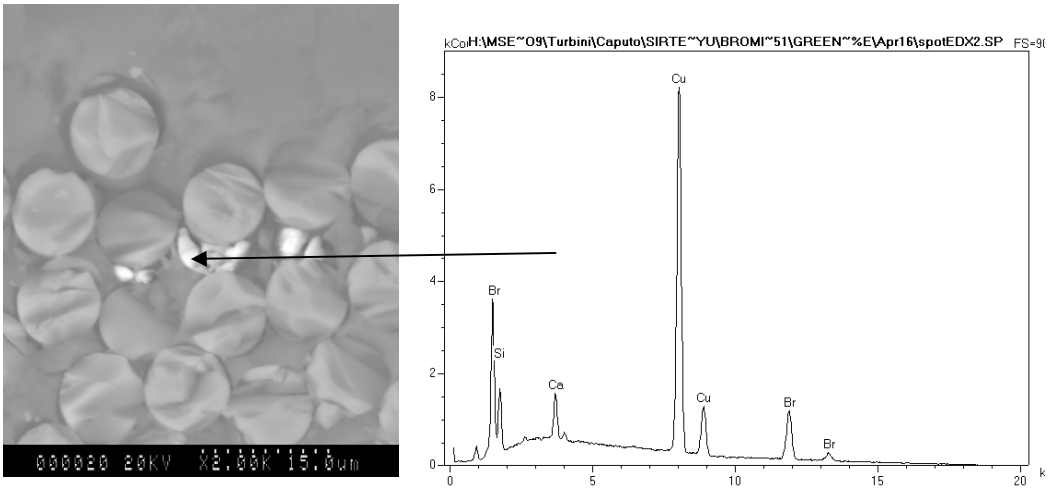

Figure 4.27: Image showing bromide CAF and a spot EDS for a HASL processed coupon.

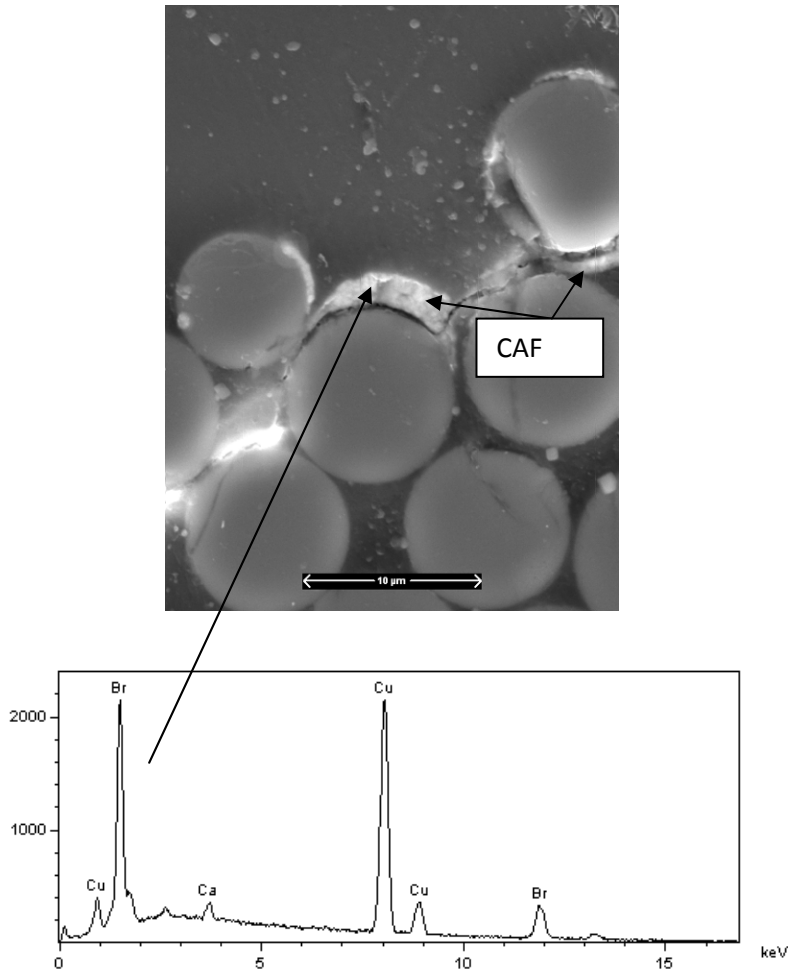

Figure 4.28: Image showing bromide CAF and a spot EDS for a HASL processed coupon.

4.4.6.2 – Optical Image showing the CAF Almost Bridging

An optical image for CAF represented electrically in IR spectra of Figure 4.1 generated using polarized light is shown in Figure 4.29. A higher magnification image is displayed in Figure 4.30. The serial cross-section illustrates that the CAF has almost bridged to the cathode.

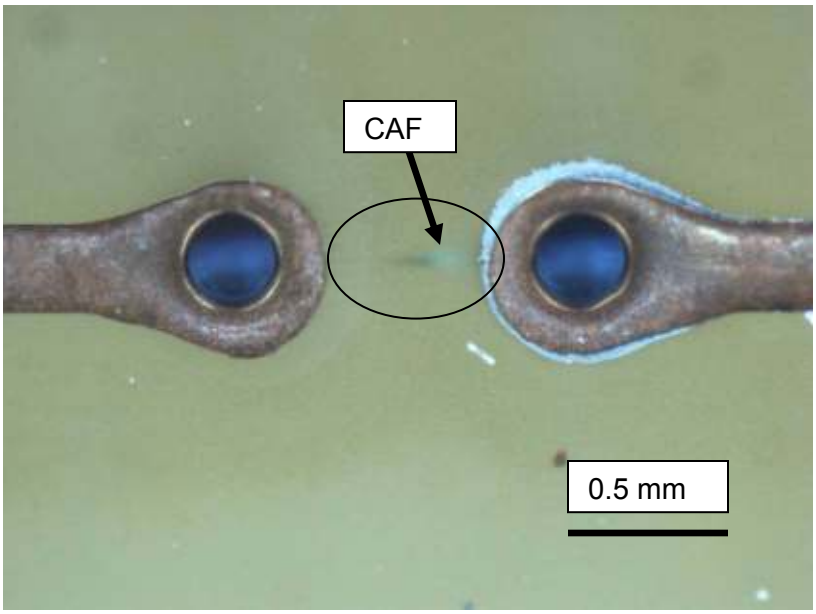

Figure 4.29: Optical image showing that CAF almost bridged for a HASL processed coupon.

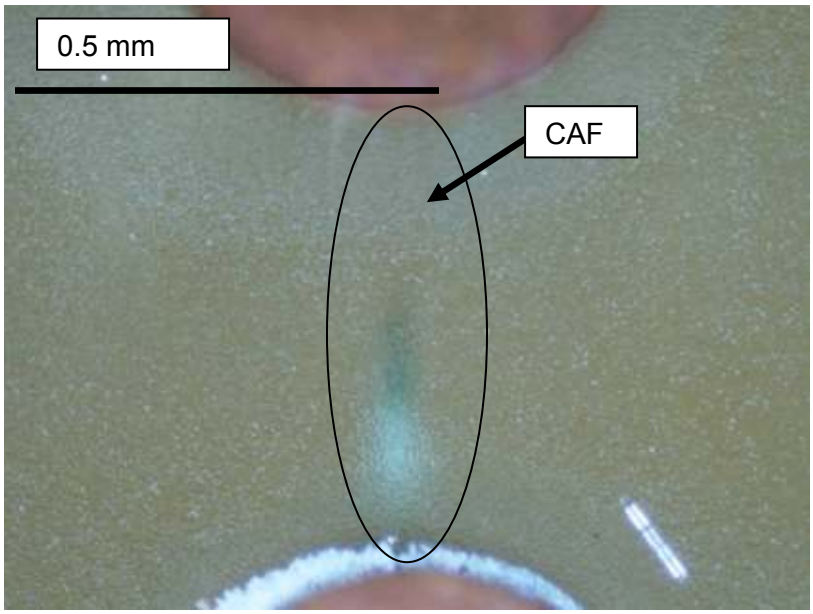

Figure 4.30: Higher Magnification optical image showing CAF almost bridging for a HASL processed coupon.

4.4.6.2.1 – Cross-Section and SEM Image showing that CAF almost Bridged

Figure 4.31 is an optical image that shows where the SEM cross-section was prepared for SEM. It can be seen that section E was located just past the cathode. The SEM image was generated using backscattered electrons as indicated in Section 3.4.2.

From the SEM image (Figure 4.32) CAF is indeed observed, thus confirming that the CAF almost bridged. EDS was performed to confirm the presence of copper, chlorine and bromine, which is not shown for brevity.

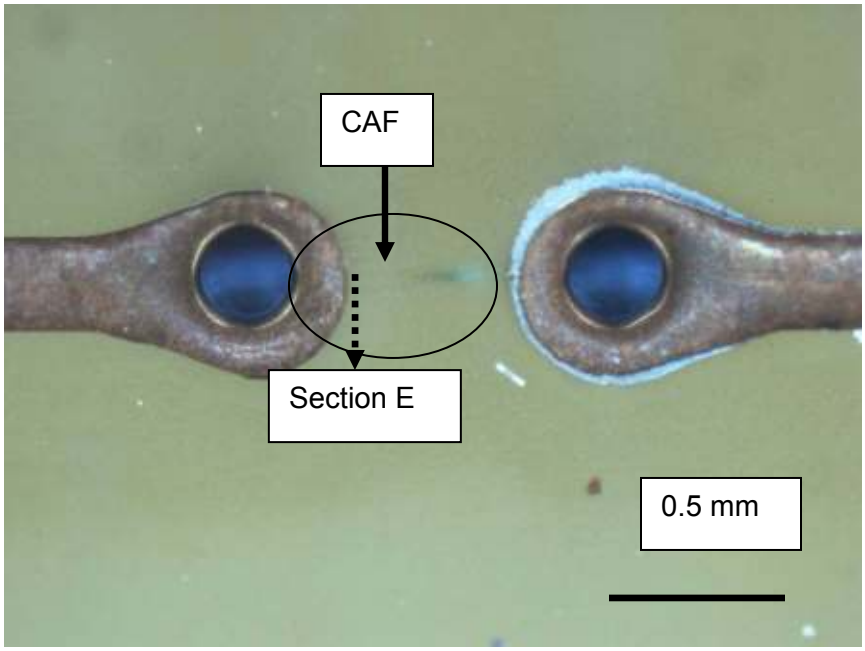

Figure 4.31: Optical image for the HASL processed coupon showing the location where an SEM cross-section was prepared for the CAF sample that almost bridged.

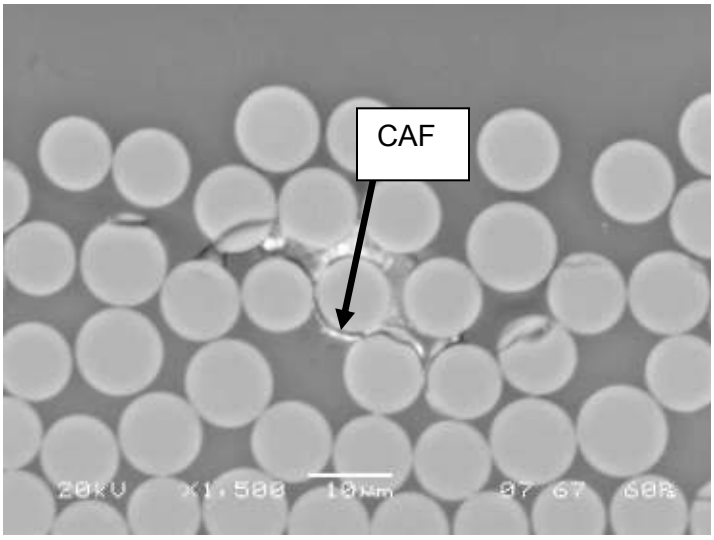

Figure 4.32: SEM image for the HASL processed coupon showing CAF for section E in Figure 4.31.

Sections F and G (in Figure 4.33) show CAF at two points. It is seen in section F (Figure 4.34) away from the anode and section G (Figure 4.36) close to the anode where the CAF becomes very thick. The EDS maps (Figures 4.35 & 4.37) show only the presence of copper and chlorine. This work shows that chloride CAF can be created in addition to bromide CAF for coupons processed with a high bromide containing flux. Further examples of CAF created for coupons processed with the HASL fluid can be found in Appendix G.

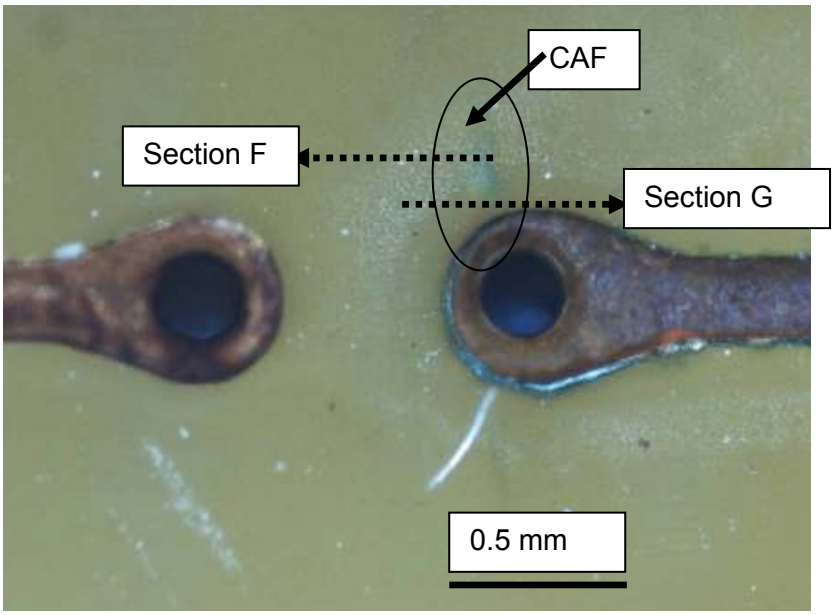

Figure 4.33: Optical image showing CAF for a HASL processed coupon.

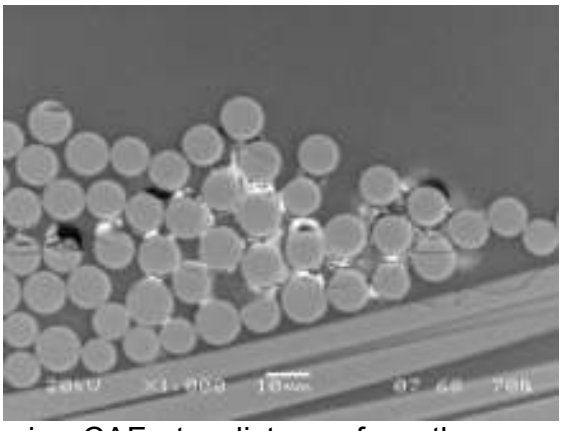
Figure 4.34: Image showing CAF at a distance from the copper anode (i.e. section F) for a HASL processed coupon.

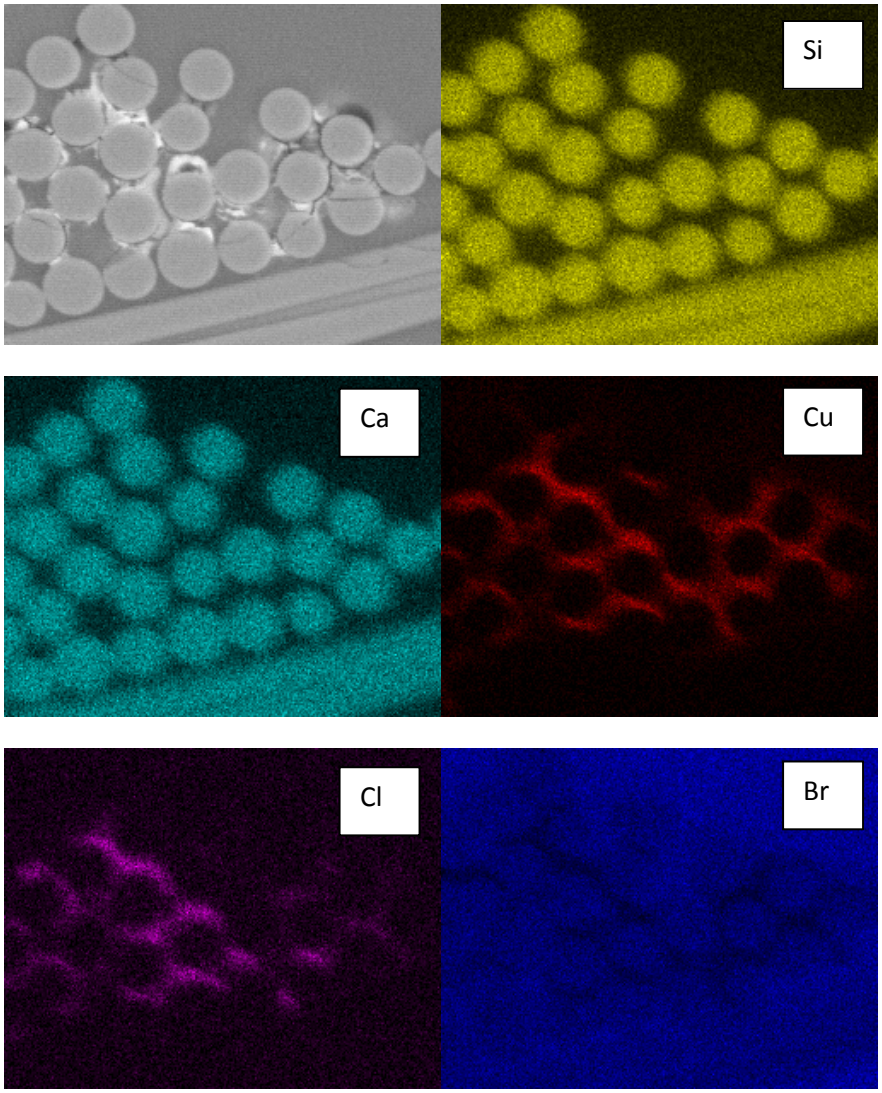

Figure 4.35: EDS map confirming the presence of copper and chlorine for the HASL processed coupon.

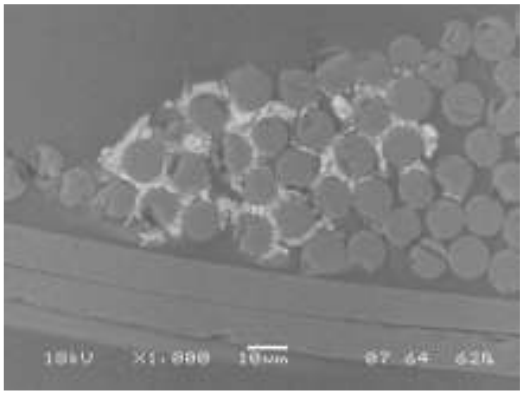

Figure 4.36: Image showing CAF where polishing was done to the copper hole (i.e. section G) for a HASL processed coupon.

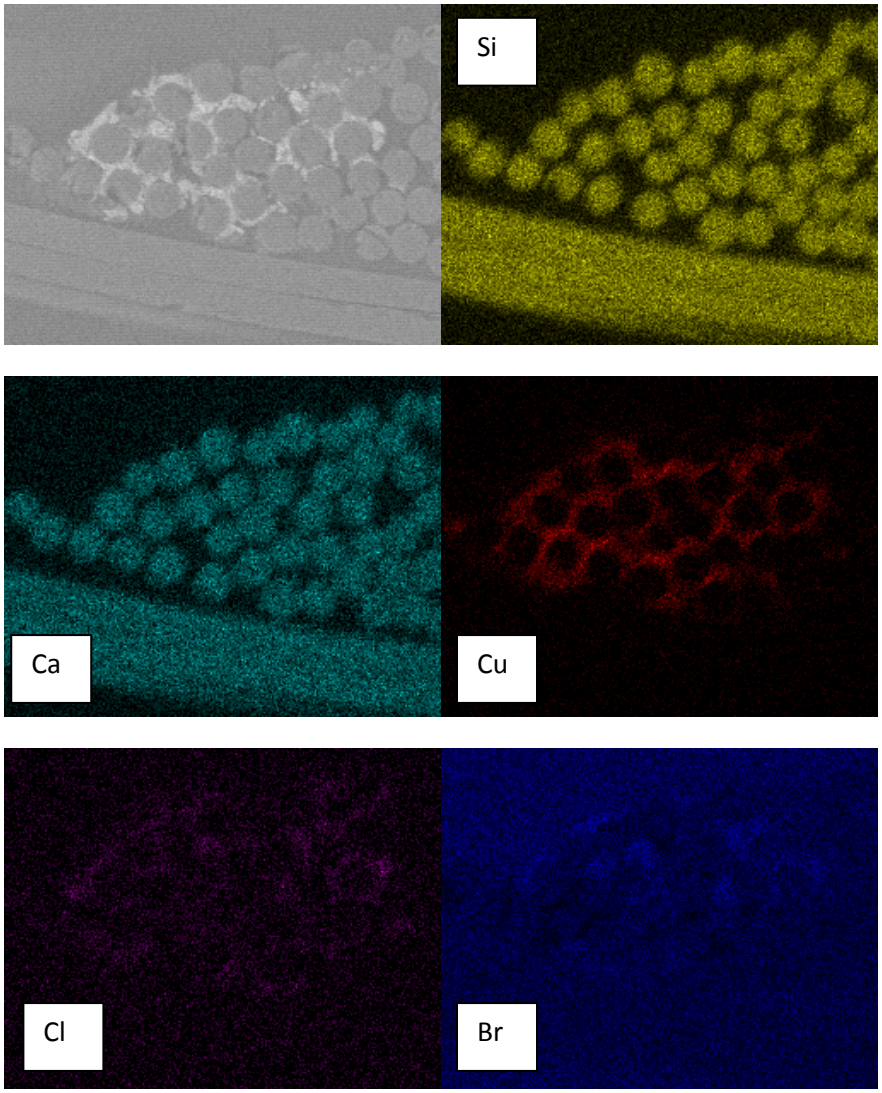

Figure 4.37: EDS map confirming the presence of copper, chlorine and bromine for section G that was HASL processed.

4.4.7 – Copper Compound in the Polymer Matrix for Coupons Processed with HASL Flux

For the coupons that were processed with the HASL fluid, a copper bromide compound was observed in the polymer matrix.

4.4.7.1 - SEM and EDS Work showing the Copper Compound for HASL Processed Coupons

An SEM image in Figure 4.38 shows that a compound was found in the polymer matrix for a HASL processed coupon. An EDS in the boxed area was performed that confirms that the compound contained copper and bromine. XPS performed on the compound formed in the epoxy matrix (Figure 4.38) is reported later in this chapter.

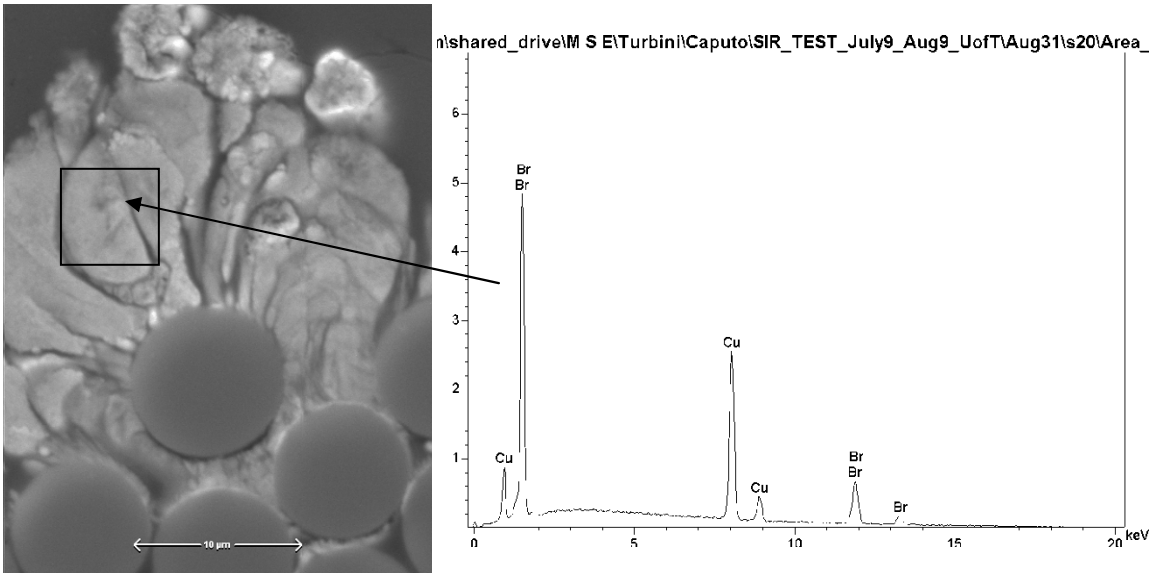

Figure 4.38: Area EDS illustrating copper and bromine in the polymer matrix for a coupon processed with HASL flux.

The optical image in Figure 4.39 illustrates a cross-section that was prepared at the anode (i.e. section H). In addition to CAF, a compound was observed in 3 different areas (Figure 4.40). For the purposes of illustrating the copper compound in the polymer matrix only area 3 will be presented in this section (Figure 4.41). The EDS map of area 3 (Figure 4.42) confirms the presence of two separate regions that are either copper-chloride or copper-bromide containing. The CAF, which surrounds the epoxy/glass fibers is copper-bromide containing in area 3. The reader can refer to Appendix G, Figures G.22 through G.28 for the entire SEM and EDS maps for section

H. It must be noted that the larger sized optical image (of Figure 4.39) is omitted in Appendix G and larger sized SEM/EDS images for Figures 4.40 through 4.42 (i.e. G.22, G.25 and G.28 respectively) are included in Appendix G.

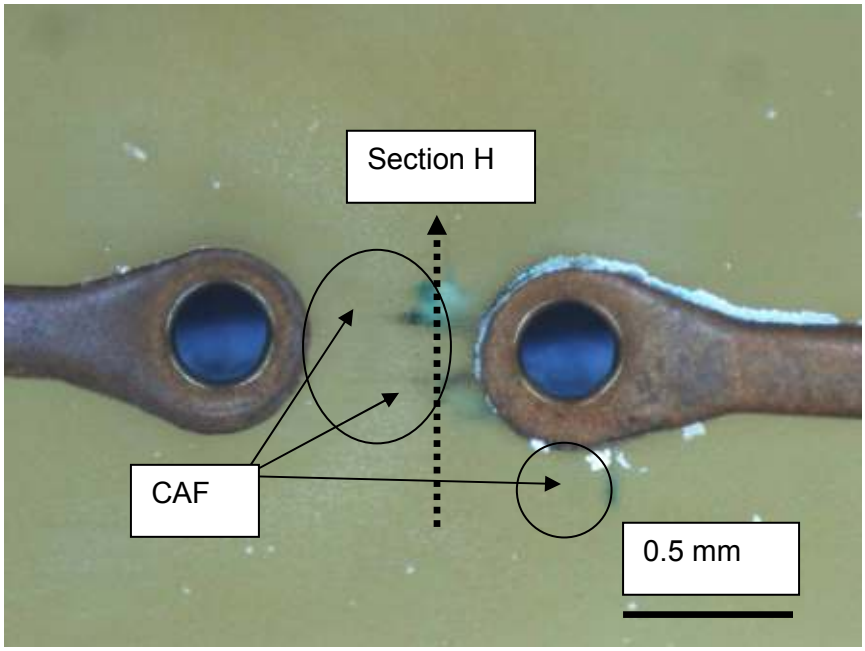

Figure 4.39: Optical image illustrating CAF for a HASL processed coupon.

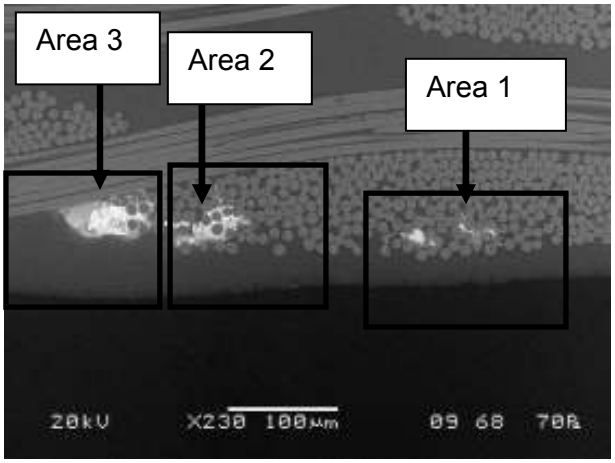

Figure 4.40: CAF and a copper compound in the polymer matrix in separate areas for section H that was HASL processed.

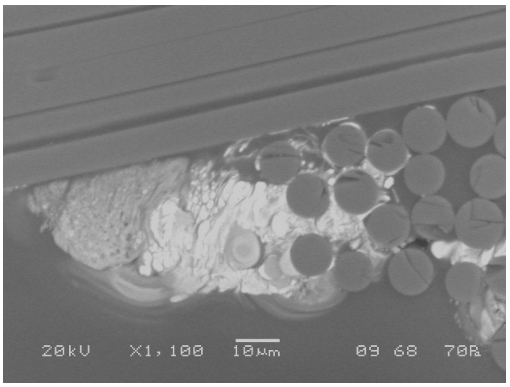

Figure 4.41: CAF and a copper compound in the polymer matrix in area 3 for section H that was HASL processed.

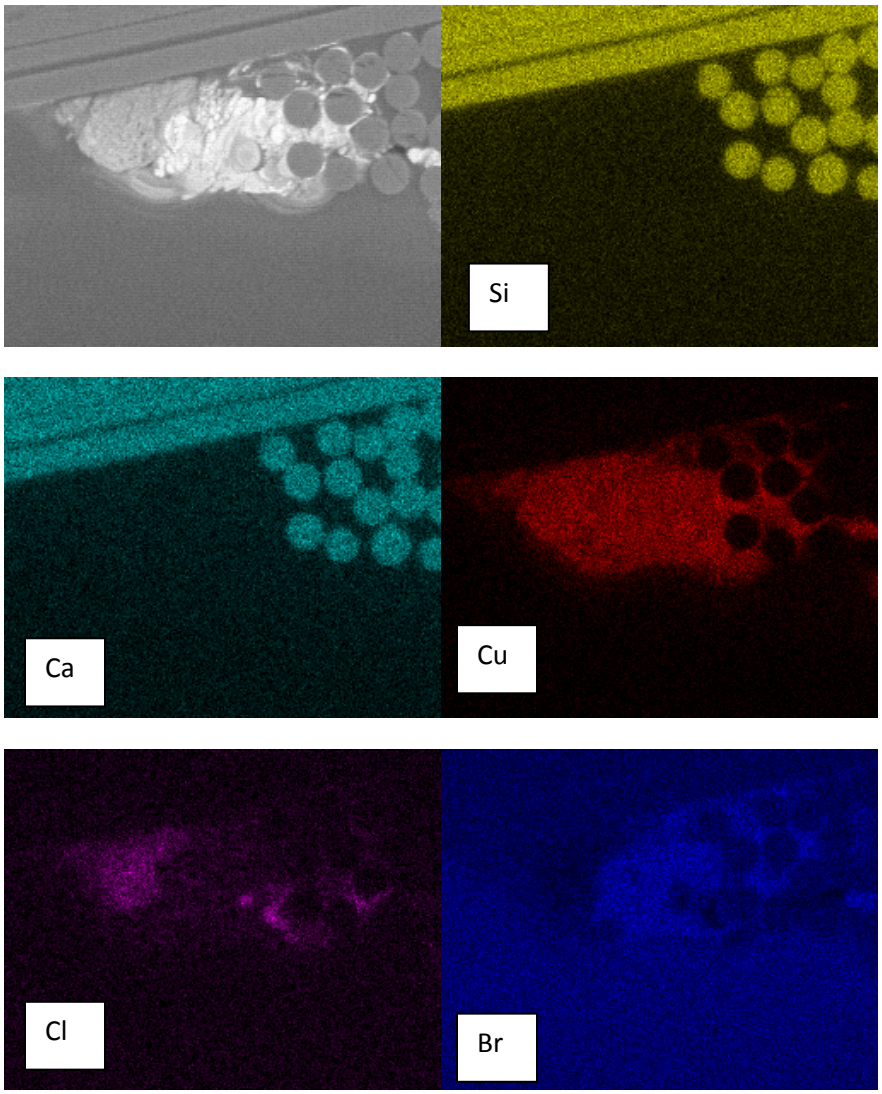

Figure 4.42: EDS map confirming the presence of copper, chlorine and bromine in area 3.

4.5 – X-ray Photoelectron Spectroscopy (XPS) Characterization of the Copper Compound in the Polymer Matrix

A copper containing compound formed in coupons processed with PEPG, PEPG/Cl, and the HASL fluxes. XPS was used to characterize this compound in detail.

4.5.1 - PEPG and PEPG/Cl

XPS was used to identify the copper-chloride compound found in the polymer matrix for coupons processed with PEPG and PEPG/Cl. The XPS spectra are shown in Figure 4.43 (PEPG) and Figure 4.44 (PEPG/Cl). The binding energies of the copper and the chloride are listed in Table 4.3. These values are the expected energies for Cu(I)Cl showing that this is the compound in the polymer matrix. The XPS spectra from the PEPG and PEPG/Cl samples were previously shown in Figures 4.17 and 4.19, respectively.

Table 4.3 – Binding Energies for PEPG and PEPG/Cl

Flux	Binding Energy (eV) Cu	Binding Energy (eV) Cl	Atom Percent (at%)	
			Cu	Cl
PEPG	933.1 (for Cu 2p3/2)	199.0 (for Cl 2p3/2)	55	45
PEPG/Cl	933.1 (for Cu2p3/2)	199.0 (for the Cl2p3/2)	46.6	53.4

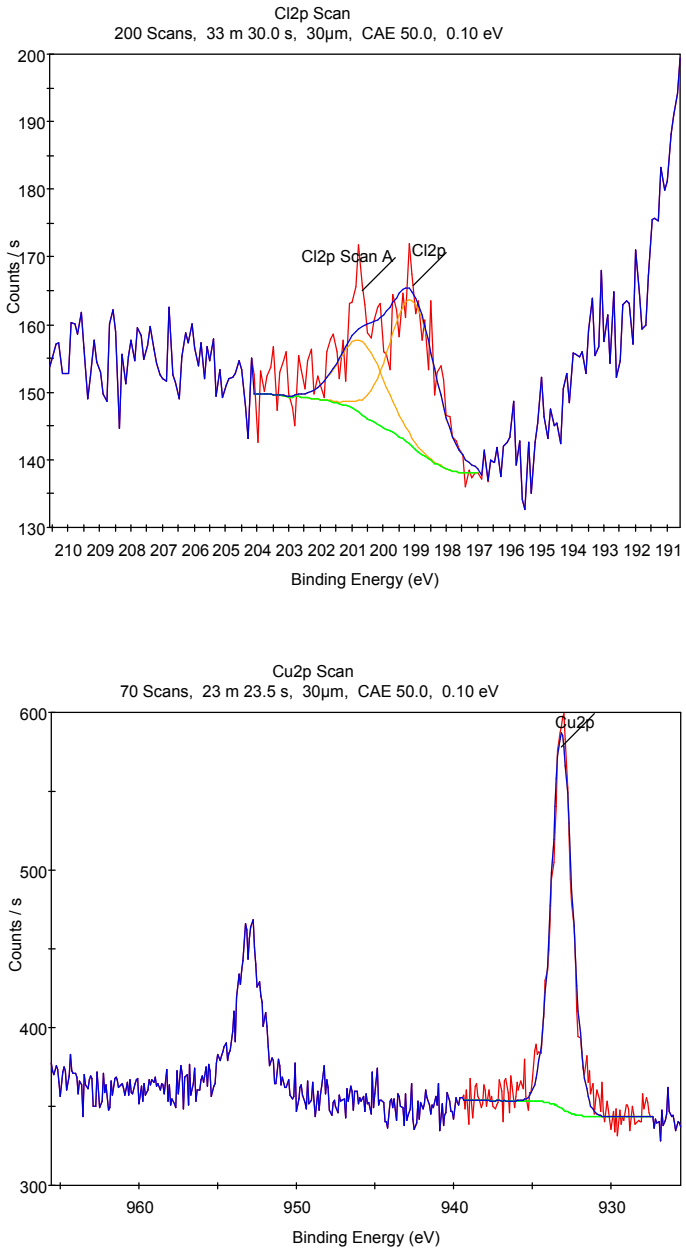

Figure 4.43: XPS spectra for the copper-chloride compound found in the polymer for coupons processed with PEPG [33]. Source: Reprinted with kind permission of Springer Science and Business Media.

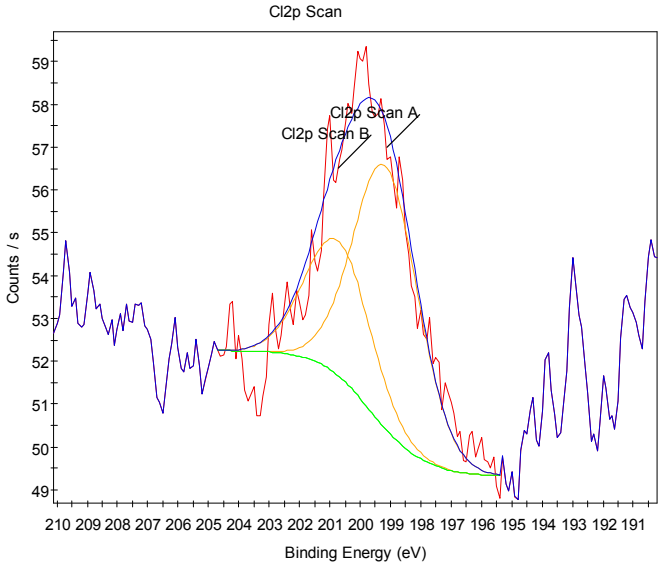

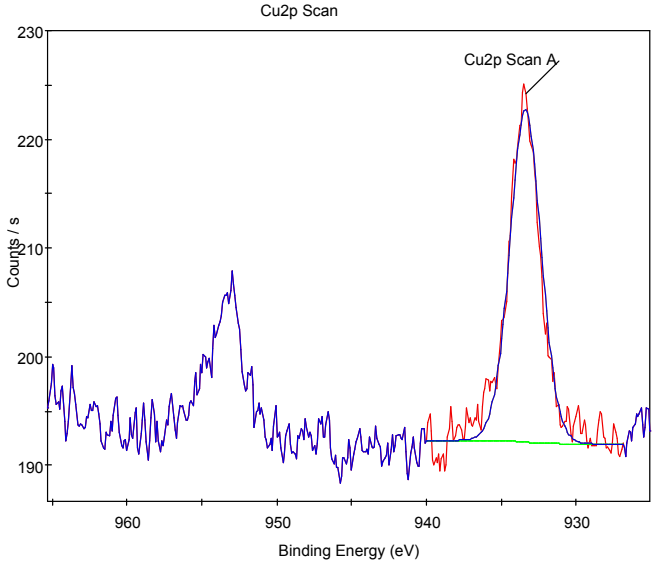

Figure 4.44: XPS spectra for the copper-chloride compound found in the polymer for coupons processed with PEPG/Cl [33]. Source: Reprinted with kind permission of Springer Science and Business Media.

4.5.2 – HASL

The copper-bromide compound found in the polymer matrix in Figure 4.38 was analyzed using XPS and the spectra are illustrated in Figure 4.45. The binding energies are summarized in Table 4.4. These values are the expected binding energies for

Cu(I)Br. The concentrations for the copper-bromide compound have been omitted since they are not realistic of the bromide levels in the compound due to the epoxy being brominated.

Table 4.4 – Binding Energies for HASL Flux

Flux	Binding Energy (eV) for Cu	Binding Energy (eV) for Br
HASL	933.18 (for Cu 2p3/2)	68.9 (for Br 3d5/2)

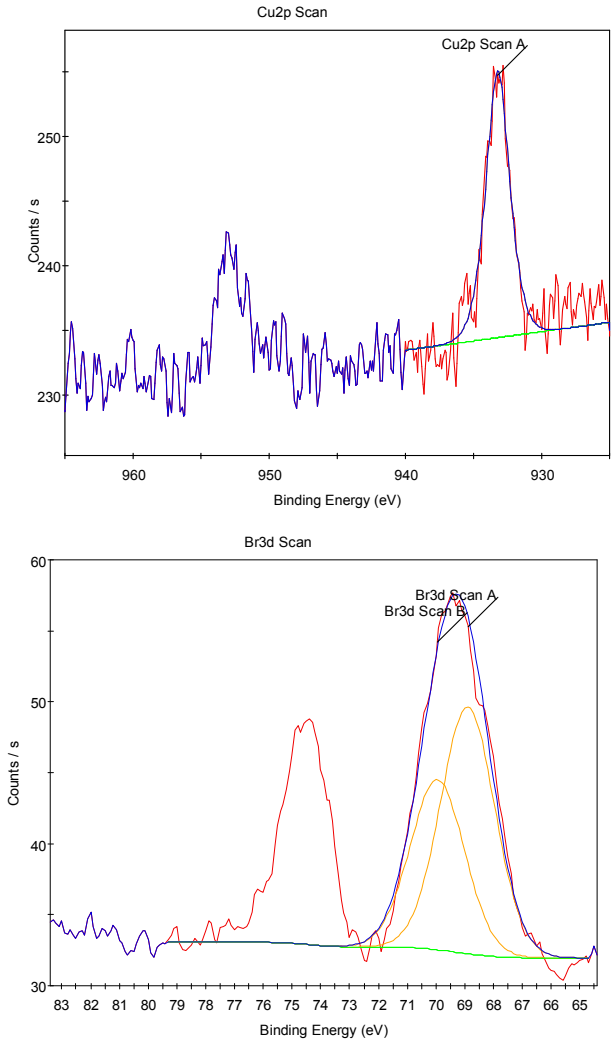

Figure 4.45: XPS spectra for the copper-bromide compound found in the polymer for coupons processed with the HASL flux.

4.6 – TEM Characterization of Bromide CAF

SEM/EDS results were presented in Section 4.6.1 for CAF containing copper, and bromine for some of the coupons processed with a high bromide containing flux. This section will identify bromide containing CAF using TEM.

4.6.1 – TEM Samples that were Prepared Using FIB

Two separate bromide CAF samples (i.e. prepared from Figures 4.27 and 4.28) were prepared for transmission electron microscopy (TEM) analysis using the Leo 1540 focused ion beam (FIB)/SEM cross beam microscope at the University of Western Ontario. An SEM/EDS chemical map (Figure 4.46) indicates where the section for sample 1 was prepared (i.e. Figure 4.27).

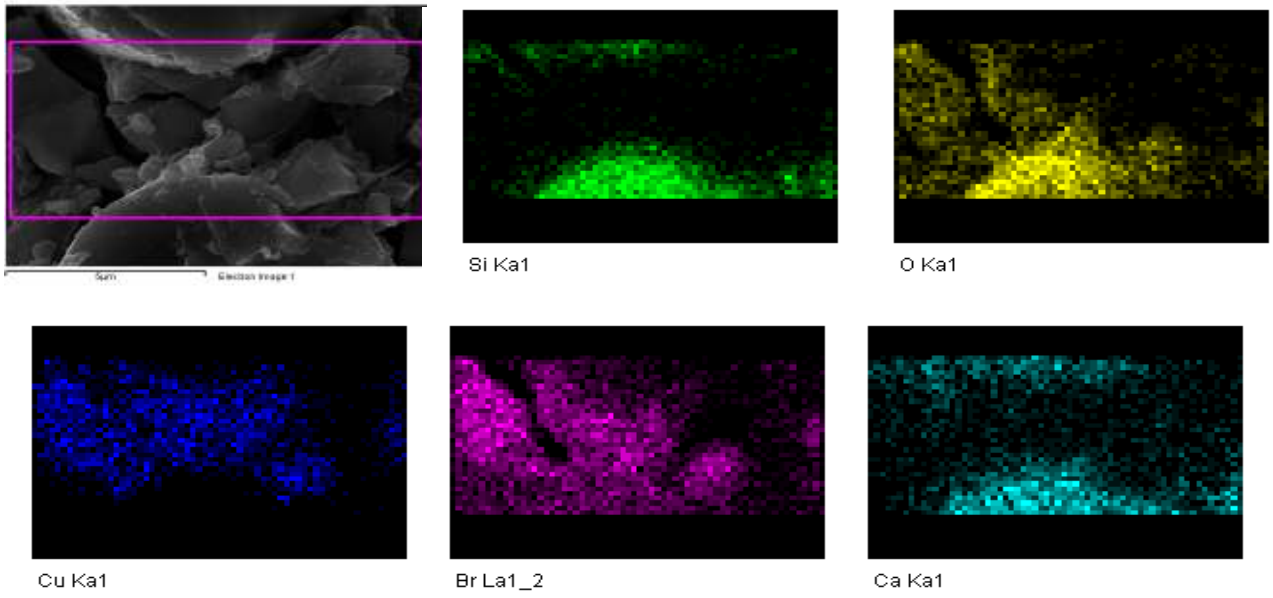

Figure 4.46: SEM/EDS elemental map of bromide CAF from Figure 4.27 where a TEM section was prepared using FIB.

The sequential milling of the bromide CAF for sample 1 is depicted in Figures 4.47. In Figure 4.46, the bromide containing CAF is presented where sample 1 was obtained (Figure 4.47 (a)). Figures 4.47 (b) and (c) illustrate the milling of the FIB section. Figure 4.47 (d) illustrates the sample before the final polishing and thinning stage. Figure 4.48 shows the preparation of sample 2. In a similar manner to sample 1, the bromide containing CAF is milled. The final polished and thinned sample 2 has been shown in Figure 4.48 (c).

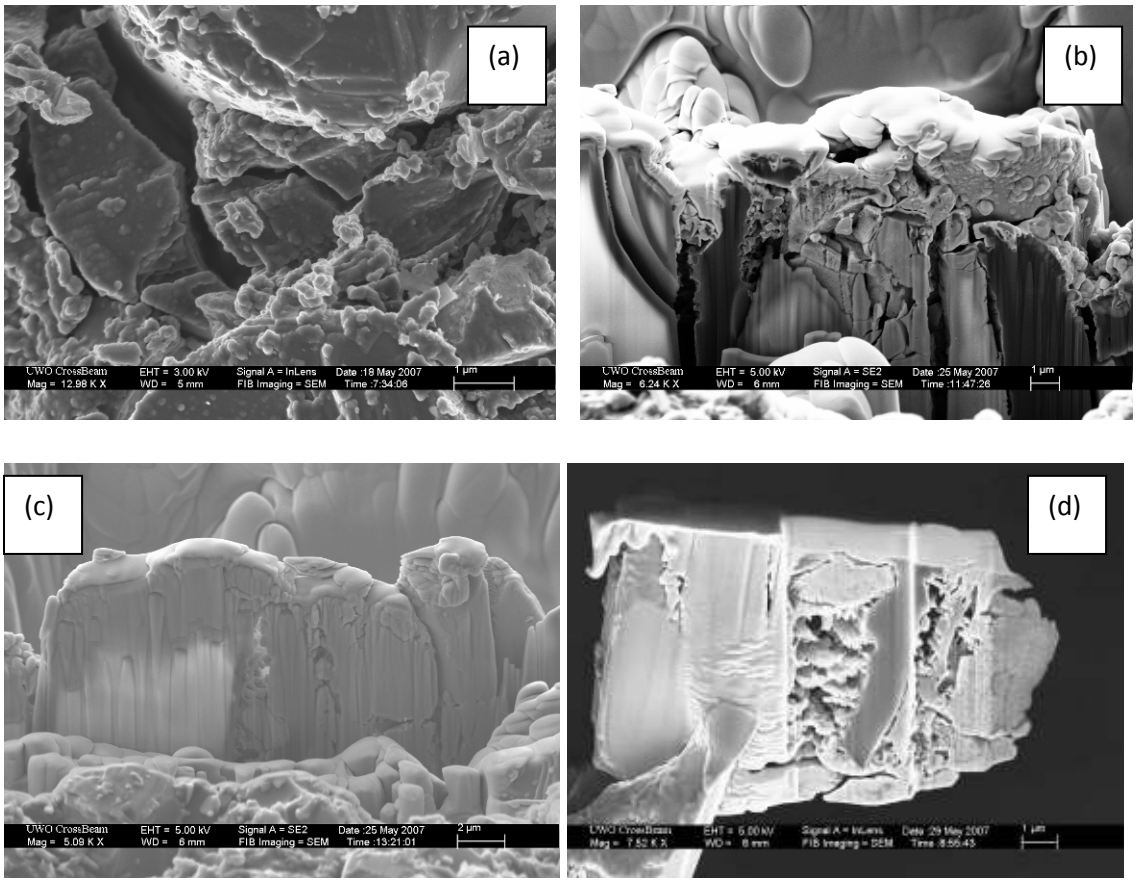

Figure 4.47: FIB sample preparation for sample 1 where (a) is the bromide CAF sample where the FIB sample was created, (b) the initial milling of the FIB sample, (c) continuation of milling, and (d) the FIB sample plucked out before the final polishing and thinning stage.

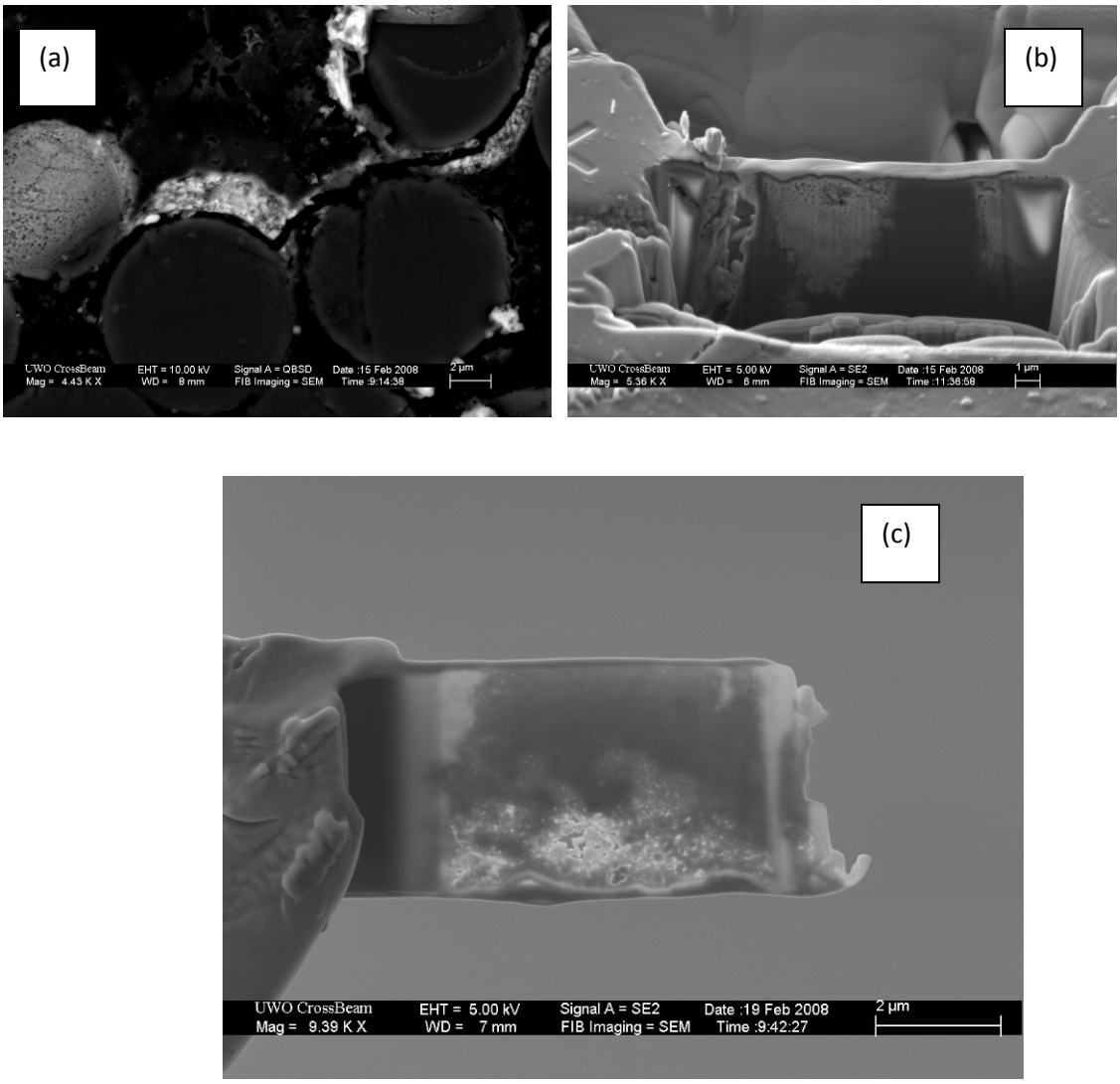

Figure 4.48: FIB sample preparation for sample 2 where (a) is the bromide CAF sample where the FIB sample was created, (b) the milling of the FIB sample, and (c) the FIB sample plucked out and polished and thinned.

4.6.2 – TEM-EDS

Figures 4.49 and 4.50 are the TEM sections for the two separate bromide-containing CAF samples. The circled area for each sample is where EDS was taken in the TEM before electron diffraction was performed. The EDS spectra in both figures confirm the presence of copper, oxygen, and bromide. The molybdenum peak is an artifact from the sample holder.

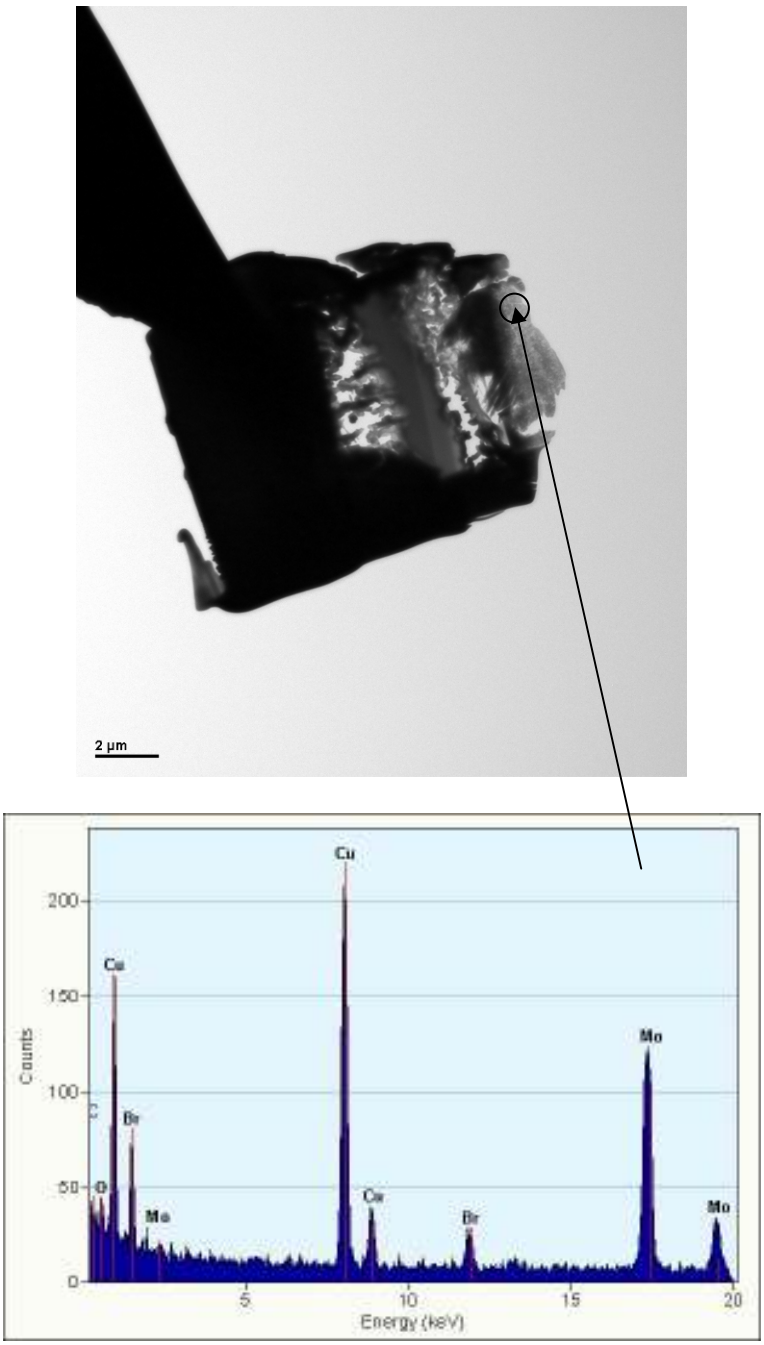

Figure 4.49: EDS in the circled area for the TEM section of sample 1.

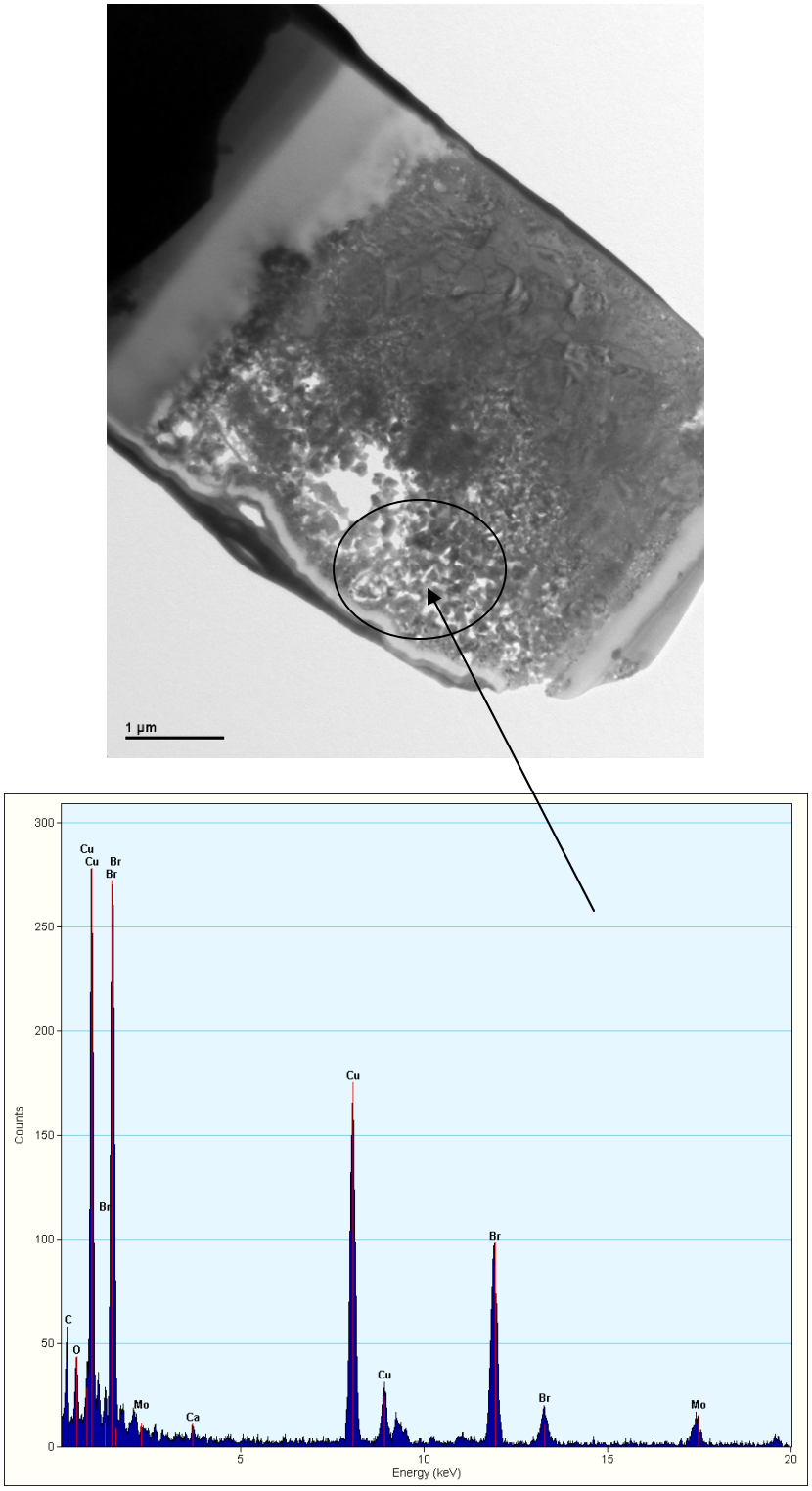

Figure 4.50: EDS in the circled area for the TEM section of sample 2.

4.6.3 – Selected Area Electron Diffraction

Electron diffraction patterns were generated on both samples where EDS was performed (Figure 4.51). From Figure 4.51 it can be seen that very clear diffraction patterns were generated to be indexed and matched with the accepted compound found in the diffraction database.

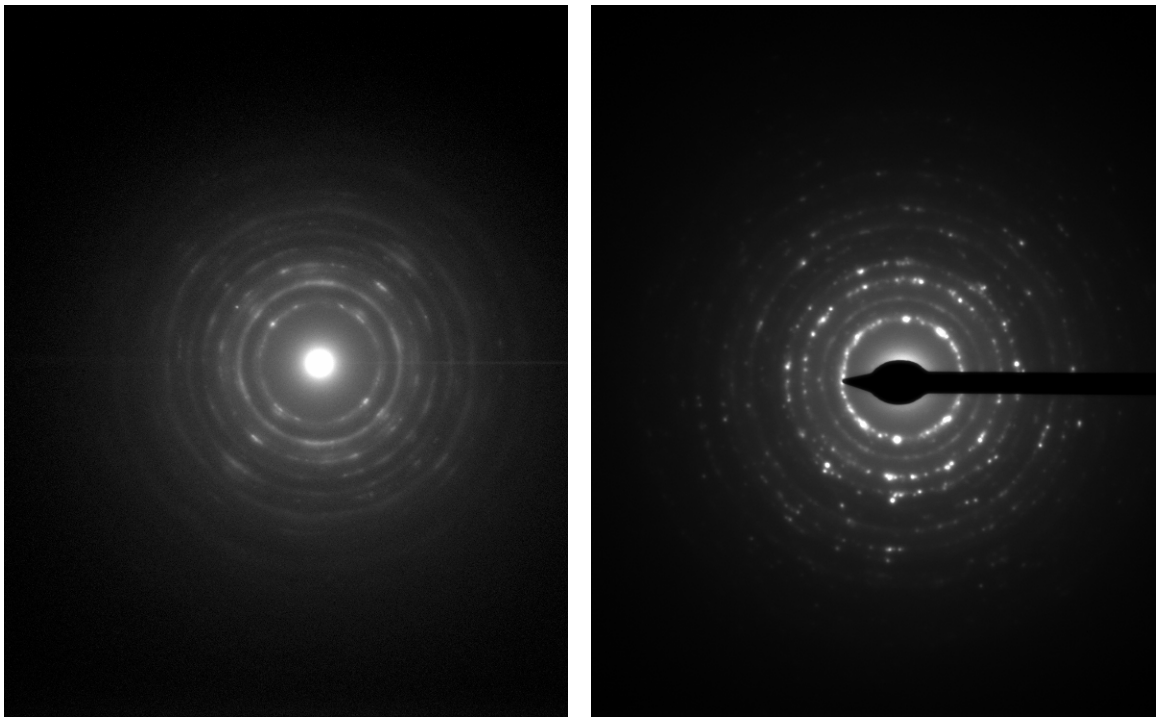

(a) (b)

Figure 4.51: TEM diffraction patterns for (a) sample 1, and (b) sample 2 in the area where EDS was performed.

4.6.4 – Indexing of the Diffraction Patterns

The diffraction patterns in Figure 4.51 were indexed according to the following relationship:

$$rd = \lambda L_{CL} \qquad (1)$$

where r is the measured ring radius from the diffraction pattern in mm, d is the interplanar spacing in nm, λ is the wavelength of incident radiation and L_{CL} is the camera length. The λL_{CL} term is constant and was determined to be 13.04 mm·nm using a standard gold diffraction pattern. The tabulated values were then compared to the standard accepted d values published by the International Centre for Diffraction Data (ICDD). Table 4.5 summarizes the tabulated d values and compares them to those found for $Cu_2(OH)_3Br$, Card Number 00-045-1309 [30]. The tabulated values match the accepted values for $Cu_2(OH)_3Br$. Therefore, the bromide-containing CAF is identified as $Cu_2(OH)_3Br$.

Table 4.5 – Indexed Patterns for Samples 1 & 2 Compared to the Accepted Data for $Cu_2(OH)_3Br$

Ring #	Sample 1	Sample 2	ICDD Card Number (00-045-1309) [$Cu_2(OH)_3Br$]
1 (d_{hkl}) Å	3.32	3.32	3.356
2 (d_{hkl}) Å	2.51	2.53	2.4966
3 (d_{hkl}) Å	2.04	2.05	2.045
4 (d_{hkl}) Å	1.75	1.73	1.751

4.7 - Chapter Summary

This chapter has presented a sample set of insulation resistance data for control coupons, and coupons processed with either PEPG, PEPG/Cl, PEG, PEG/Cl or HASL flux. The control coupons showed the highest insulation resistance data (i.e. in the order of $10^{11}\Omega$). The coupons processed with either PEPG, PEPG/Cl, or HASL flux had insulation resistance values an order of magnitude lower than the control coupons, while the PEG or PEG/Cl processed coupons showed insulation resistance values two orders of magnitude lower than the control coupons. For the coupons processed with PEPG, PEPG/Cl, PEG, and PEG/Cl, SEM and EDS data were presented to demonstrate chloride containing CAF. In addition, for the coupons processed with either PEPG or PEPG/Cl, a copper containing compound was observed in the bulk polymer, while for both PEG and PEG/Cl this same copper containing compound was not observed in the polymer matrix. For the coupons that were processed with the high bromide containing flux, CAF that contained either chloride or bromide was formed. The bromide containing CAF was characterized using SEM/EDS and TEM to be $Cu_2(OH)_3Br$. Also, a copper compound was observed for the coupons processed with the high bromide containing flux. XPS was used to characterize the copper containing compound found in the polymer matrix. For the coupons processed PEPG or PEPG/Cl, the compound was found to be Cu(I)Cl, while for the coupons processed with the HASL fluid, this compound was found to be Cu(I)Br.

Chapter 5 – Discussion

5.0 – Overview

This chapter will discuss all fluxes tested in this work. The electrical data will be compared for coupons processed with each respective flux and control coupons (i.e. as received and processed with no flux). It will be shown that the organic flux constituents diffuse into the printed wiring board material during soldering for all flux formulations. SEM and EDS was used to show that in addition to CAF, a copper compound is observed in the polymer for certain fluxes. XPS was used to characterize the compound in the polymer matrix. Using the XPS data, an electrochemical mechanism for the formation of CAF will be proposed. Ion chromatography will be used to show that for a high bromide containing flux, the bromide diffuses into the board material and is the source in the creation of the bromide containing CAF compound. The bromide containing CAF compound was characterized using TEM and a mechanism for its formation will be discussed using XPS data for the compound in the polymer matrix.

5.1 - Characterization of Polyethylene Propylene Glycol Flux

In the electronics industry the electrical integrity of a material is tested using temperature, humidity, bias (T-H-B) testing. This section will discuss the electrical data, SEM/EDS, FTIR, and XPS test results after accelerated aging for test coupons processed with polyethylene propylene glycol (PEPG) containing fluxes.

5.1.1 –Electrical Properties of PEPG and PEPG/Cl

The average insulation resistance values for coupons processed with PEPG fluxes were more than half an order of magnitude lower than the control coupons. This result is not surprising since the flux interacts with the board material causing the material to absorb more moisture during T-H-B testing lowering the electrical resistance and accelerating CAF growth. The creation of CAF at 4 out of the 12 potential sites for PEPG and 5 out of the 12 test sites for PEPG/Cl is a clear example of the interaction between the flux and the board material, while no CAF was created on the control coupons.

5.1.2 – Extraction of Organic Flux Residues and FTIR Analysis

As mentioned in Chapter 4, test coupons processed with PEPG-containing fluxes were cleaned after soldering, then they were soaked in acetonitrile for 24 hours [31]. The FTIR spectra of the extract (i.e. Figure 4.2) for the most part showed a match between the extract and the raw material demonstrating that the polyglycol from the flux had diffused into the substrate. One difference noted in the extract FTIR spectra is the presence of the carbon-oxygen stretch near 1720 cm^{-1} for the processed materials (i.e. Figures 4.2a) which is indicative of an aldehyde. The presence of this peak suggests that the terminal hydroxyl group of the polyglycols degraded thermally during processing to form the aldehyde which is consistent with previous reports in the literature [32-34]. It must be noted that the presence of chloride does not affect the FTIR spectra between PEPG and PEPG/Cl, since we are looking at the organic constituents (i.e. the PEPG vehicle), thus resulting in similiar FTIR spectra for both the PEPG and PEPG/Cl in the as received fluxes (i.e. Figure 4.2b and B.1b in Appendix B).

5.1.3 - SEM and EDS Characterization of PEPG and PEPG/Cl

Using SEM analysis this work has shown that PEPG and PEPG/Cl processed coupons formed CAF at the epoxy/glass fiber interface (Figure 4.5 - PEPG and Figure 4.11 & 4.13 - PEPG/Cl). The EDS confirmed the presence of both copper and chlorine. The presence of silicon and calcium in all EDS work is from the glass fibers and will not be mentioned further. The presence of bromine for processed coupons is from the brominated epoxy backbone. It must be noted that for Figures 4.6 (PEPG) and 4.12 (PEPG/Cl), CAF grows from the side, as opposed to between the adjacent hole-hole conductors. This is due to the direction of the electric field between the two holes which is most concentrated between the adjacent conductor but also present from the side of the conductor anode (Figure 5.1). This field diagram is valid for all coupons tested in this work.

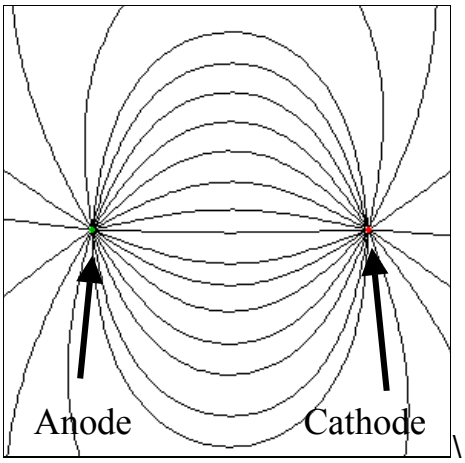

Figure 5.1: Electric field diagram between the anode and cathode for a hole-to-hole test coupon [9].

It was noted that as the polishing approached the anode, a compound appeared in the bulk polymer matrix for both the PEPG and PEPG/Cl processed coupons (i.e. Figure 4.7 and 4.9 for PEPG and Figure 4.15 for PEPG/Cl). The EDS confirmed the presence of

copper and chlorine for both the CAF and the copper compound in the bulk polymer matrix.

The fact that CAF becomes thicker at the anode is consistent with work by Ready et al [35] who used microtomography to show that the filament is thicker at the anode and thinner as it grows away from the anode.

5.1.4 – Pourbaix Diagram of the Copper-Chloride-Water System

Lando et al [3] noted that the electrolysis of water creates a PH gradient between the anode (i.e. acidic) and the cathode (i.e. basic). The creation of CAF and its growth from the anode can be best understood by examining the copper-chloride-water Pourbaix diagram (Figure 5.2) [36]. In this diagram we see that the atacamite compound, $3Cu(OH)_2 \cdot CuCl_2$ is insoluble below PH 4. Thus, in an acidic medium it precipitates out – thus growing from the anode.

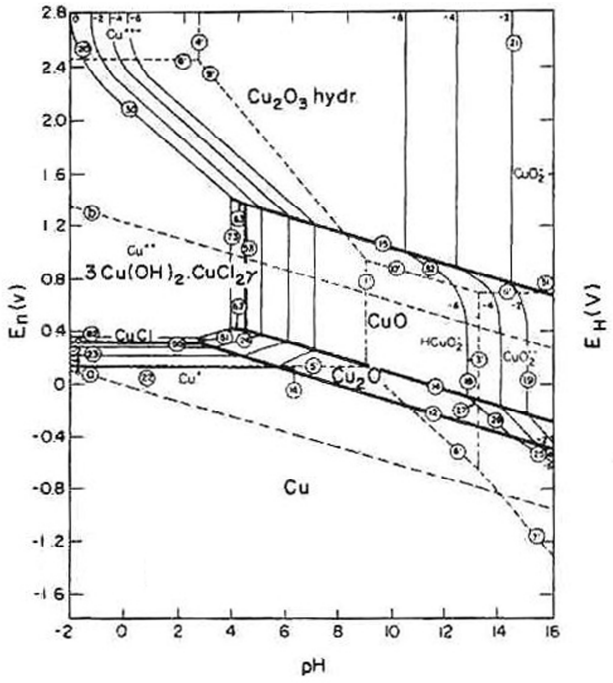

Figure 5.2: Pourbaix diagram for the copper-chloride-water system [36]. Source: Reprinted with kind permission of Springer Science and Business Media.

5.1.5 – Interaction between PEPG and PEPG/Cl with the Polymer Matrix

Using SEM and EDS this work has shown that a copper compound formed in the bulk polymer matrix for coupons processed with both PEPG and PEPG/Cl. This compound is not to be confused with CAF, as CAF is a salt which surrounds the epoxy/glass fiber interface. Figures 4.17 and 4.18 show for the PEPG processed coupons a copper compound in the bulk polymer (i.e. the area where no fibers are present) while CAF is seen surrounding the epoxy glass. For the PEPG/Cl processed coupons, (Figures 4.19 and 4.20), a copper compound is also observed in the bulk polymer matrix, while CAF occurs at the epoxy/glass fiber interface. This work used XPS [33] to characterize the compound in the polymer matrix to be Cu(I)Cl for both PEPG and PEPG/Cl processed coupons.

This further confirms the work by Zado [37] and Brous [31, 38] who pointed out that there was an interaction between the solder flux and laminate material. They recognized that this affected the electrical properties of the laminate material, but did not relate it to CAF. Ready [9, 10] used SEM and EDS to show that boards processed with no flux formed CAF only at the epoxy/glass fiber interface. However, for boards processed with the PEPG fluxes a copper compound was found in the bulk polymer matrix.

5.2 Characterization of PEG and PEG/Cl Fluxes

This section will discuss the electrical data, SEM/EDS, FTIR, and XPS test results after accelerated aging for test coupons processed with PEG or PEG/Cl.

5.2.1 - Early Studies by Zado and Brous

The effect of water soluble fluxes on CAF formation has been studied for over 30 years. Zado [37] was the first to identify the importance of flux interaction with board material. He found that the PEG processed comb patterns had an insulation resistance 3 orders of magnitude lower than the control coupons. In the present work coupons processed with PEG show insulation resistance values were approximately 1.5 orders of magnitude lower when compared to the control coupon. The difference in the insulation resistance values between this work and the work of Zado [37] is attributed to conductor patterns used.

In a separate study, Brous [31, 38] extracted the flux residues using acetonitrile. He then evaporated the acetonitrile solution and used FTIR to confirm that the PEG had diffused into the processed coupons. The present work has also extracted the organic constituents from boards processed with PEG and PEG/Cl and used FTIR to match the spectra for each of the extracts of the as received fluxes to the thermal decomposition residues which were similar but contained an aldehyde terminal group. This shows that the organic residues from the various fluxes used in this study diffused into the PWB [33].

5.2.2 – Electrical Properties

For both the PEG and PEG/Cl fluxed coupons, the average insulation resistance value is 1.5 orders of magnitude lower than the control coupons. Lower insulation resistance values were also observed by Turbini and Bent [6] in their work. It is not surprising that CAF was created at 6 out of the 12 potential test sites for PEG. For the coupons processed with PEG/Cl, no CAF was created for the test presented in Table 4.1.

5.2.3 – Extraction of Organic Flux Residues and FTIR Analysis

As mentioned in Chapter 4, test coupons processed with PEG and PEG/Cl fluxes were cleaned after soldering, then they were soaked in acetonitrile for 24 hours. The PEG FTIR spectra (i.e. Figure 4.3) for the most part showed a match between the extract and the raw material demonstrating that the polyglcol from the flux has diffused into the substrate. As was the case for the PEPG and PEPG/Cl fluxes there was a carbon-oxygen stretch near 1720 cm^{-1} for the processed materials (i.e. Figures 4.3a) which is indicative of an aldehyde group formed by some thermal degradation of the PEG.

5.2.4 – Interaction between PEG and PEG/Cl with the Laminate

For coupons processed with either PEG or PEG/Cl, CAF was created. It was observed in several tests that for the PEG processed coupons, CAF formation is more likely to occur as compared with PEG/Cl processed coupons. For the insulation resistance tests in Table 4.1 (samples prepared at RIM) CAF was only observed for the PEG flux. However, coupons processed at George Brown College show CAF on coupons processed with PEG/Cl. Turbini et al [6] used optical microscopy to observe CAF on comb patterns processed with PEG and aged. The variation among these 3 tests is the temperature profile experienced by the coupons. Thus CAF could be created under certain temperature processing profiles for PEG/Cl.

5.2.5 – Inhibition of the Copper Compound for PEG and PEG/Cl Processed Coupons

A model [33] has been developed to explain the hindering effect of chloride in the presence of PEG on CAF formation based on the work of Yokoi et al [39] and Feng et al [40].

Coupons processed with PEG show no copper-chloride compound in the bulk polymer matrix. This is due to the fact that copper is weakly bound in the presence of PEG. Yokoi et al [39] have proposed that in the absence of chloride, PEG binds weakly to the surface of copper forming a crown ether (Figure 5.3 and 5.4(a)).

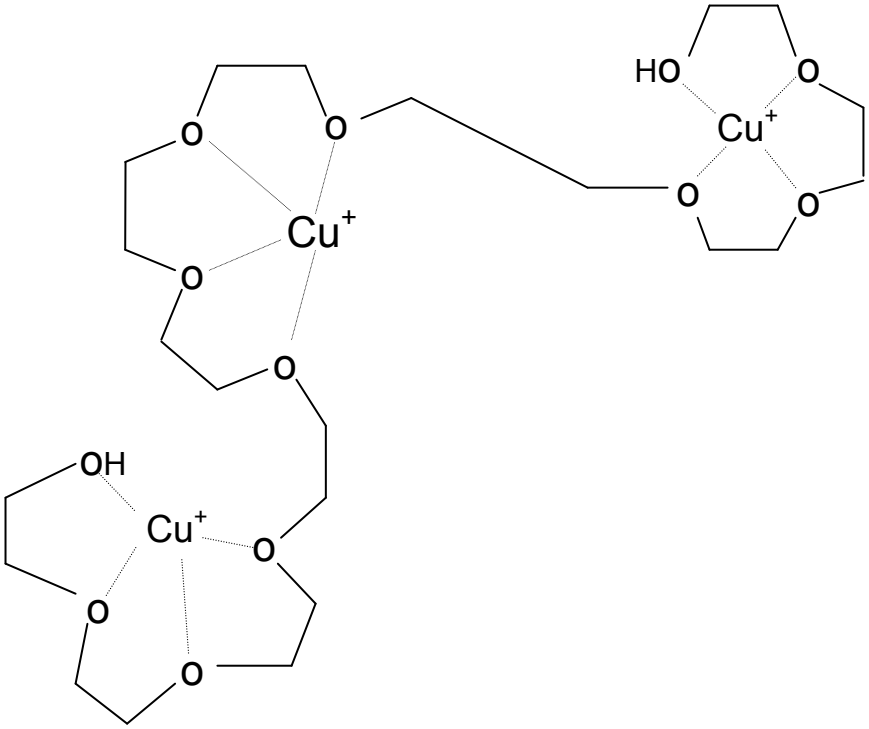

Figure 5.3: Cu^+ forms crown ethers with PEG [33]. Source: Reprinted with kind permission of Springer Science and Business Media.

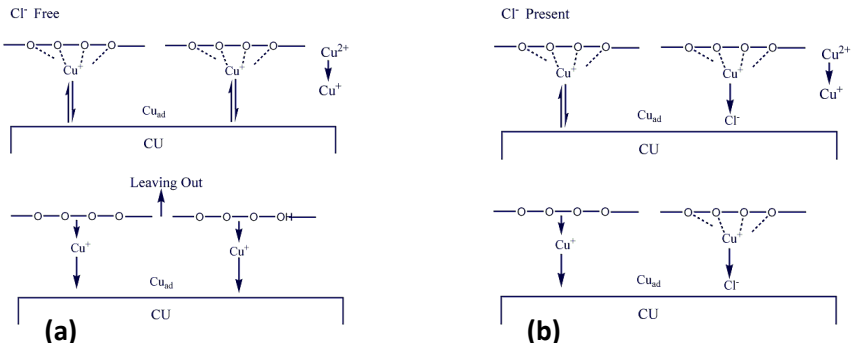

Figure 5.4: Cu^+ forms (a) weakly bound crown ethers in the absence of chloride with PEG , and (b) tightly bound PEG-Cu-Cl complex in the presence of chloride [33].

Several studies [39-42] have also shown that when chloride is present, a PEG-Cu-Cl complex forms [40], acting as a barrier which limits Cu diffusion from the anode (Figure 5.4(b) and 5.5). Since CAF is observed for PEG processed coupons, it is proposed that the copper and chloride for its formation are derived from this PEG-Cu-Cl complex. The absence of CuCl in the polymer matrix suggests that this PEG-Cu-Cl complex restricts the availability of copper ions in the PEG-saturated epoxy matrix.

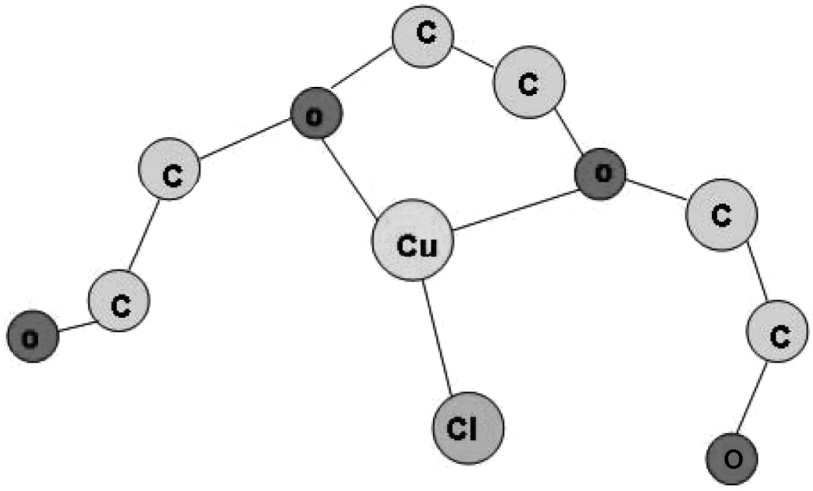

Figure 5.5: Copper binding to the PEG-Cu-Cl system [33]. Source: Reprinted with kind permission of Springer Science and Business Media.

5.3 – Formation of $Cu_2(OH)_3Cl$

The work of DerMarderosian [17] proved that CAF is formed by an electrochemical process. Ready et al identified CAF to be atacamite, (i.e. $Cu_2(OH)_3Cl$) [10]. This section will propose an electrochemical mechanism for CAF formation using XPS data.

5.3.1 – Proposed Chemical Reaction Forming Chloride CAF

The creation of CAF and its growth from the anode can be understood by examining the copper-chloride-water Pourbaix diagram (Figure 5.1) [36] discussed in section 5.1.3.

Atacamite, $3Cu(OH)_2 \cdot CuCl_2$ (which is equivalent to $Cu_2(OH)_3Cl$) is insoluble below PH 4. Thus, once this compound is formed, it precipitates – thus growing from the anode. The formation of CAF (i.e. atacamite) can proceed if Equations (5.1) or (5.2) predominate:

$$12CuCl_2^- + 3\ O_2 + 6\ H_2O = 4Cu_2(OH)_3Cl + 4Cu^{2+} + 20Cl^- \quad (5.1)$$

or

$$12CuCl + 3O_2 + 6H_2O = 4Cu_2(OH)_3Cl + 4Cu^{2+} + 8Cl^- \quad (5.2)$$

XPS data [33] has shown that the compound in the polymer is CuCl. The analysis clearly reveals that the copper is in the +1 state. This gives strong support to the proposal that the precursor in CAF formation is CuCl, which is converted to $Cu_2(OH)_3Cl$ according to Equation 5.2 [43].

In addition, if CuCl forms Cu^{+2} according to reaction 5.3:

$$CuCl \rightarrow Cu^{2+} + Cl^- + 1e^- \quad (5.3)$$

then atacamite formation will follow reaction 5.4:

$$2CuCl^+ + 3H_2O = Cu_2(OH)_3Cl + 3H^+ + Cl^- \quad (5.4)$$

5.3.2 – Studies Investigating the Oxidation of Copper in Chloride

The formation of atacamite, $Cu_2(OH)_3Cl$ has been previously observed in printed wiring board assemblies (PWAs) [44] and in the atmospheric corrosion of copper in the form of patinas found on statues and roof tops [45].

5.3.3 – Electro-dissolution Mechanisms of Copper in Chloride Media

A number of electrochemical/corrosion studies have reported on the behaviour of copper in a chloride medium [46-66]. The main difference in the model from each study lies in the initial electro-dissolution reaction(s) of copper. These reactions are believed to be reversible and are assumed to be under mixed kinetics (charge transfer and mass transport controlled).

The first group of researchers [47-51] defined the electro-dissolution to occur in a single step according to the following reaction:

$$Cu + 2Cl^- \Leftrightarrow CuCl_2^- + 1e^- \quad (5.5)$$

The second group of researchers [52-57] defined the electro-dissolution of copper to occur in two steps according to the following reactions:

$$Cu \Leftrightarrow Cu^+ + 1e^- \quad (5.6)$$

$$Cu^+ + 2Cl^- \Leftrightarrow CuCl_2^- \quad (5.7)$$

A third group of researchers [58-65] defined the electro-dissolution of copper to occur in two steps according to the following reaction:

$$Cu + Cl^- \Leftrightarrow CuCl + 1e^- \quad (5.8)$$

$$CuCl + Cl^- \Leftrightarrow CuCl_2^- \quad (5.9)$$

The important point to note in each of these mechanisms is that the copper is found in the +1 valence state in the form of the copper chloride complex $CuCl_2^-$. According to

this work, the XPS data gives strong support that the precursor to CAF is the formation of CuCl (Equation 5.8).

5.3.3.1 – Single – Step Oxidation Mechanism for Copper in Chloride Media

Bacarella and Griess [47] extended the original work of Lal and Thirsk by performing electrochemical corrosion experiments at different chloride concentrations and temperatures. They found that for a range of NaCl concentrations (0.124 M, 0.372 M and 1.24 M) at either 29 ^{o}C or 101 ^{o}C, the copper dissolves as $CuCl_2^-$ according to reaction 5.5. Brossard [48] investigated the corrosion of copper in LiCl ranging in concentration between 0.2 M and 10 M and pH from 3 to 7 and also confirmed that copper dissolves to the form the $CuCl_2^-$ complex, consistent with reaction 5.5. Faita et al [49] found that for the corrosion of copper in a 0.5 M solution of NaCl and pH of 3, that the main dissolved copper species were $CuCl_2^-$ and $CuCl_3^{2-}$. The reaction paths occurred according to reaction 5.10 where x was either 2 or 3.

$$Cu + xCl^- + 1e^- \rightarrow CuCl_x^{(1-x)} \quad (5.10)$$

Their work showed that the passivation of the copper surface was due to the precipitation of CuCl. The CuCl film gives very poor protection of the copper surface due to the oxidation of copper to Cu^{2+}. They concluded since the Cl^- was high, the diffusion of either $CuCl_2^-$ and $CuCl_3^{2-}$ was the rate limiting step.

The single step mechanism proposed in section 5.3.3.1 is not consistent with the XPS results which do not support the formation of CAF from the $CuCl_2^-$ complex. CAF can form from this complex based on Equation 5.1, however, the presence of CuCl in the

XPS data suggests the chloride concentration present is insufficient to form the $CuCl_2^-$ complex in a single step.

5.3.3.2 - Two – Step Oxidation Mechanism for Copper in Chloride Media

The formation of the $CuCl_2^-$ complex can also occur in two-steps based on previous studies. This section will discuss previous works where the formation of the $CuCl_2^-$ complex can occur from reaction from either (i) Cu^+ and Cl^- (Equations 5.6 & 5.7) or (ii) CuCl and Cl^- (Equations 5.8 & 5.9).

5.3.3.2.1 – Formation of $CuCl_2^-$ from Cu^+ and Cl^-

Taylor [57] investigated the copper oxidation and reduction on Au in 0.5 M NaCl. In 0.5 M NaCl, the Cu corrosion was present solely via Cu^+ in chloride media to form the $CuCl_2^-$ complex.

Braun and Nobe [52] proposed that the diffusion of chloride ions is the rate determining step. The results indicate that in solutions less than 0.75 M, $CuCl_2^-$ is favoured, while in solutions with higher chloride concentrations, $CuCl_3^{2-}$ dominates. In addition, their work suggests that for chloride ion concentrations less than 0.05 M, a considerable amount of copper is dissolved as Cu^{2+}.

5.3.3.2.2 – Formation of $CuCl_2^-$ from CuCl and Cl^-

Flatt and Brook [60] investigated the corrosion of copper for a range of NaCl concentrations at 25 ^oC and pH of 3. They found that the CuCl thickness increased with potential and decreased with increasing NaCl concentration. For the 1% NaCl solution, they observed that two competing reactions occur, with the dissolution to a soluble ion, either Cu^+ or $CuCl_2^-$ being superseded by reaction 5.11:

$$Cu + Cl^- \rightarrow CuCl + 1e^- \quad (5.11)$$

These results are in agreement with the CuCl resulting in passivation over a critical thickness. If the potential was further increased, the current rise resulted in the breakdown of the film. This breakdown can be the result of the direct oxidation of Cu to Cu^{2+} or the CuCl oxidation to Cu^{2+}. The latter is the preferred mechanism due to what was observed, reaction 5.12.

$$CuCl \rightarrow Cu^{2+} + Cl^{-} + 1e^{-} \quad (5.12)$$

It is possible however for film dissolution to take place at preferential sites, thus exposing the metal and favoring reaction 5.13. This does support the evidence of localized pitting.

$$Cu \rightarrow Cu^{2+} + 2e^{-} \quad (5.13)$$

Lee and Nobe [62, 63] found that Cu electro-dissolution is independent of H^{+} concentration at chloride concentrations of 1M and 5M. The rate of electro-dissolution increases as chloride concentration increases between 0.1-4 M. The results indicate that for less than 1M Cl^{-}, $CuCl_2^{-}$ is the dominant cuprous species, however, above 1M Cl^{-}, substantial amounts of $CuCl_3^{2-}$ exists. It has been shown above the limiting current region Cu^{2+} is detected, and Cu^{2+} formation decreases with increasing Cl^{-} concentration. This finding is consistent with the work of Sharkey and Lewin [67], who found that the presences of higher order copper-chloride complexes are present with increasing chloride concentration.

The presence of CuCl in the polymer matrix provides evidence that there is insufficient chloride media in CAF formation to create the $CuCl_2^{-}$ complex. This gives strong evidence that the localized chloride concentration in CAF formation is less than 0.1 M,

thus providing an insufficient chloride media, resulting in Equation 5.2 to being favoured in CAF formation.

5.3.4 – Meeker and LuValle's Two- Step Kinetic Model for CAF Formation

Earlier, Meeker and LuValle [16] had attempted to develop an appropriate chemical model for the growth of CAF. Based on previous work [68, 69] in which chlorine (and sometimes other) salts remain in a printed wiring board after manufacturing, they developed the following model for CAF formation [16] (Figure 5.6) in which two competing reactions lead to two different chlorine-containing compounds.

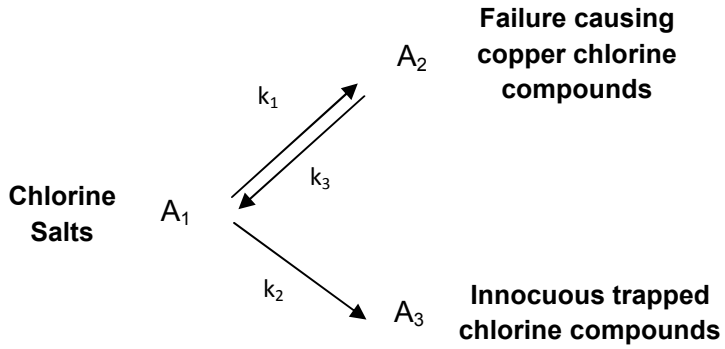

Figure 5.6: Kinetic model for CAF failure. Source: Reprinted with kind permission of Springer Science and Business Media.

They described three special cases for CAF failure:

Model 1: $k_1 >> k_2, k_3$ results in the formation of a failure-causing chlorine compound – CAF, as the dominant failure reaction.

$$A_1 \xrightarrow{k_1} A_2 \qquad (5.14)$$

Model 2: k_1, k_2 >> k_3 results in a *non-reversible* competition between CAF formation, and the formation of an innocuous compound that traps chlorine.

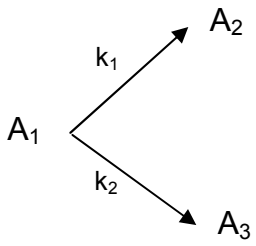

(5.15)

Model 3: k_1, k_3 >> k_2 results in a reversible failure reaction creating CAF.

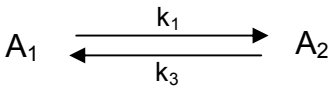

(5.16)

The solutions for Models 2 and 3 have the same basic form, differing only in rate constants [16]. Using time-to-failure data from constant-humidity experiments it would be difficult to distinguish between these two models. LuValle did show that if both the cumulative damage rate and the stress level changed as a function of time one could distinguish between the two. Since their experimental work did not include varying the stress levels, they focused only on Model 2.

In our work the failure causing copper-chlorine compound has been identified as $Cu_2(OH)_3Cl$. However there was no evidence of any “innocuous trapped chlorine compounds”. Thus the physical evidence shows that Model 1 is the more appropriate explanation for CAF failure in PWBs [43]:

$$3O_2 + 6H_2O + 12CuCl \xrightarrow{k_1,\ H^+} 4Cu_2(OH)_3Cl + 4Cu^{2+} + 8Cl^- \quad (5.17)$$

This is backed up by the previously reported work of Ready [9] which used a linear circuit for periodically measuring insulation resistance values of test coupons which have been under 150 to 200V bias. A switching system periodically moved the electrical circuit from the high voltage bias circuit to the low voltage linear circuit for measurement. The data collection system was programmed to read the resistance value for each test site, and to remove the voltage from any site where the resistance was low, indicating that the CAF had reached the anode. In the initial setup, the data acquisition system was programmed to check the resistance value periodically at all test points, even those that had the high voltage bias turned off in previous measurements. If the resistance of these test points increased to an acceptable level, bias was reapplied. Samples examined optically at the end of the experiment showed that test points which had been turned off and on a number of times during the test exhibited burn-out between anode and cathode because once the CAF becomes thick enough it conducts current from the cathode to the anode, heating the polymer to the point of charring. In the case where the bias voltage is turned off, the anode is no longer acidic and the CAF dissolves. When the voltage is reapplied, the CAF continues to grow and thicken, finally causing the burn-out. The burnout happens quickly since $Cu_2(OH)_3Cl$ has semiconductor properties. Thus, Equation 5.17 is the correct mechanism for CAF formation as the above work proves that acid catalyzes the growth of CAF.

5.4 – Characterization of the HASL Flux

It had previously been reported by Ready and Turbini [8, 70] that the halide content effects the chemical nature of CAF. When coupons are processed with either no flux or flux containing 2 wt% chloride or 2 wt% bromide, CAF contains both copper and chlorine. This copper-chloride containing CAF compound was investigated using transmission electron microscopy (TEM) and identified as atacamite, $Cu_2(OH)_3Cl$. However, when a flux containing 15 wt% bromide was used, Ready et al [8] found that bromide containing CAF could be created. Test coupons were processed with a HASL flux containing 15 wt% bromide in order to create and characterize brominated CAF.

5.4.1 – Electrical Properties Comparing IR Readings of HASL Versus Control Coupons

For the high bromide containing (i.e. HASL fluid) fluxed coupons (Table 4.1) the average insulation resistance value is an order of magnitude lower than the control coupons. The polyglycol vehicle in the HASL fluid, as well as the high bromide content appears to have a direct effect of lowering the insulation resistance. CAF was created at 11 out of the 12 potential test sites.

5.4.2 – Example of CAF Almost Forming a Bridge

For the HASL processed coupons Figure 4.1 shows that the insulation resistance dropped periodically as CAF almost bridged between the anode and cathode. When CAF bridges at the cathode, there is a sudden drop in insulation resistance followed by a self healing (restoration) of the insulation resistance. This insulation resistance degradation followed by restoration took place 7 times in the 28 day period but the CAF was not thick enough to form a complete short during that time. This is due to the fine tip of the filament going back into solution. Ready and Turbini showed that taking

readings at 15 minute intervals compared to 120 minute intervals also exhibited this phenomena. Further, Ready and Turbini used a linear circuit and showed resistance was self healing (i.e. increased above the threshold), the bias was reapplied to that specific site and the CAF resumed growing and thickening. This process of lowering of the insulation resistance occurred 3 or 4 times during the insulation resistance test until the resistance maintained the low value when retested. The electrical readings in the present study were only taken every 8 hours and therefore no drop in readings were not observed.

The optical images in Figure 4.29 and Figure 4.30 show that the CAF almost bridged. Due to the lighting source of the microscope the CAF near the cathode is not clearly seen. However, when a cross-section (i.e. section E in Figure 4.31) was prepared just beyond the cathode, the CAF in Figure 4.30, was observed by SEM (i.e. Figure 4,32), thus supporting the electrical data.

5.4.3 – Interaction between HASL Flux with the Polymer Matrix

This work has shown using SEM and EDS that a copper compound was present in the bulk polymer matrix for coupons processed with the HASL flux. Figure 4.38 shows the copper compound found in the bulk polymer.

5.4.3.1 – Extraction of Organic Flux Residues and FTIR Analysis

The polyglycol from the HASL processed coupons was extracted and analyzed as outlined in the experimental section (i.e. 3.4.7). The FTIR spectra for the processed coupons after 1 or 2 reflows and the unprocessed coupon were compared to the spectra of the HASL fluid. The polyglycol spectra for the HASL flux for the most part showed a match to the polyglycol spectra of the extract from the processed coupons (Figure 4.4). This shows that the polyglycol from the HASL flux diffused into the

substrate during soldering. As was the case for the PEPG based fluxes, a carbon-oxygen stretch peak appeared near 1720 cm^{-1} representing the aldehyde formed by thermal decomposition during soldering.

5.4.4 - Ion Chromatography of Flux and Processed Coupons

Ionic contamination was removed from control and flux treated coupons as described in Chapter 4 and ion chromatography was used to determine the levels of chloride and bromide ions (Table 4.2). For the control boards, the chloride ion source has been shown previously [68, 69] to be the epiclorhydrin which is the reagent used in the synthesis of epoxy. The bromide comes from residues from the bromination of the epoxy backbone. The PEPG and PEG processed coupons contained trace amounts of chloride, while the PEPG/Cl and the PEG/Cl contained only slightly more chloride. For the coupons processed with the HASL flux, the amount of chloride remained low even though the flux contained chloride, but the bromide concentration increased approximately 1000 times compared to the control coupon, showing that bromide ions diffused into the epoxy. These bromide ions from the HASL flux are the source of the brominated CAF.

5.4.5 - SEM and EDS Characterization for the HASL Processed Coupons

SEM and EDS work show that bromide containing CAF was created (Figures 4.27 & 4.28). In addition to bromide CAF, samples that were processed with the HASL flux, resulted in the creation of chloride CAF (Figures 4.35 & 4.37). This result is consistent with the work by Ready [8] who found that both chloride and bromide CAF can be created when this high bromide HASL flux was used.

5.4.6 – Pourbaix Diagram for the Copper-Bromide-Water System

As is the case with chloride CAF formation, bromide containing CAF also precipitates out in an acidic medium. The Pourbaix diagram for the Cu-Br-H_2O system [71] is shown in Figure 5.7 showing that both copper (I) bromide and copper-hydroxy-bromide are insoluble in acid.

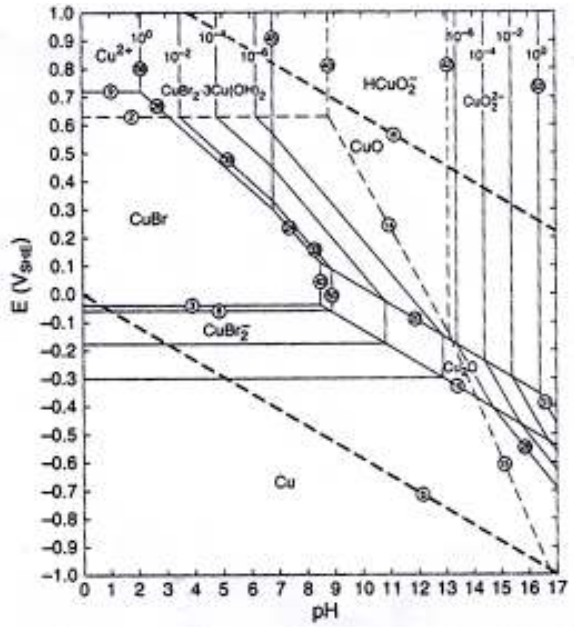

Figure 5.7: Pourbaix diagram for the copper-bromide-water system [71]. © NACE International 2004

5.5 – Formation of $Cu_2(OH)_3Br$

The TEM diffraction patterns in this work show that bromide CAF is $Cu_2(OH)_3Br$. The XPS results provide strong support that CuBr compound is formed in the polymer matrix. This section will propose a mechanism for the formation of brominated CAF.

5.5.1- Proposed Chemical Reaction for the Formation of Bromide CAF

The Pourbaix diagram (Figure 5.5) shows that $Cu_2(OH)_3Br$ is insoluble in acid. In addition, the electrochemical corrosion of copper in both bromide (i.e. reactions 5.19 &

5.20) and chloride (i.e. 5.8 & 5.9) media behave similarly [72, 73]. The bromide CAF forms according to reaction 5.18:

$$4CuBr + O_2 + 4H_2O \rightarrow 2Cu_2(OH)_3Br + 2Br^- + 2H^+ \quad (5.18)$$

5.5.2 – Studies Investigating the Oxidation of Copper in Bromide Media

A number of studies have reported on the corrosion of copper in chloride media. To date much less work has been reported on the copper-bromide system. In the last 25 years [71-82] the copper-bromide system has gained interest due to its application in copper heat exchangers which use LiBr as an absorbing agent [80]; with the bulk of the studies being done in the last 10 years [71, 76-82]. All studies of the copper-bromide system have shown that it behaves similar to the copper-chloride system [72, 73].

5.5.3 - Electro-dissolution Mechanisms of Copper in Bromide Media

The work by Brossard [73] as well as, Aben and Troman [72] found that corrosion of copper occurred according to the following reactions:

$$Cu + Br^- \rightarrow CuBr + e^- \quad (5.19)$$

$$Cu + 2Br^- \rightarrow CuBr_2^- + e^- \quad (5.20)$$

The XPS confirmed that the copper (I) bromide is in the polymer matrix. This indicated that copper dissolution was consistent with reaction (5.19), where copper is attacked anodically by bromide ions forming CuBr. The hydrogen ions are readily available at the anode according to the following reaction

$$H_2O = 0.5O_2 + 2H^+ + 2e^- \quad (5.21)$$

and provide the acidic medium in which CuBr is insoluble according to the Pourbaix diagram.

5.6 – Solubility Product for CuBr Versus CuCl

The solubility product (K_s) for CuBr and CuCl are different – the CuBr is approximately 25-50 times lower than that of CuCl. These differences are summarized in Table 5.1.The solubility product shows that both CuCl and CuBr are highly insoluble, thus giving evidence for the presence of these compounds in the polymer matrix. Cu^+ is readily available from the electrochemical corrosion of the copper and either Cl^- and possibly Br^- ions, depending on whether or not a high bromide flux is used to process the coupons.

Table 5.1 - The Solubility Product for CuBr and CuCl

Compound	Solubility Product (K_s) [72, 83]
CuBr	$10^{-8.3}$
CuCl	$10^{-6.84}$

5.7- Gibbs Free Energy of Formation for $CuBr_2^-$ Versus $CuCl_2^-$

It is known from previous work [84, 85] that dissolved copper forms an intermediate CuCl precipitate which undergoes complexation reactions with chloride. In the presence of bromide ions the reaction conditions are modified. If the Gibb's standard free energy($\Delta G°_{298}$) is considered for both $CuBr_2^-$ is (i.e. -189.12 $kJmol^{-1}$) [72] and the $CuCl_2^-$ is (-240.5$kJmol^{-1}$) complexes, the overall reaction paths for both $CuBr_2^-$ and $CuCl_2^-$ (Equations 5.22 and 5.23, respectively) result in a unfavorable formation of either

$CuBr_2^-$ and $CuCl_2^-$ from the direct attack of either chloride or bromide ions on copper (Table 5.2). This provides strong evidence that these complexes are not likely to form by this attack (i.e. 5.5). In addition, it is also thermodynamically unfavourable to form the copper di-chloro complex according to Equation 5.9. This gives strong support that reaction 5.2 is more likely to proceed with conversion of CuCl to atacamite. This also holds true for bromide CAF.

Table 5.2 – $\Delta G°$ for $CuBr_2^-$ and $CuCl_2^-$ Reactions

Reaction	$\Delta G°$ ($kJmol^{-1}$) [75]
$Cu + 2Br^- \rightarrow CuBr_2^-$ (5.22)	18.8
$Cu + 2Cl^- \rightarrow CuCl_2^-$ (5.23)	21.6
$CuCl + Cl^- \Leftrightarrow CuCl_2^-$ (5.24)	10.6

5.8 - $\Delta G°$ for $CuCl_2 \cdot 3Cu(OH)_2$ Versus $CuBr_2 \cdot 3Cu(OH)_2$

The spontaniety of a reaction can be determined by calculating the Gibbs free energy change as follows:

$$\Delta G^\circ = \Sigma n \Delta G^\circ_{f(products)} - \Sigma m \Delta G^\circ_{f(reactants)} \quad (5.25)$$

Table 5.3 summarizes the standard free energies of formation ($\Delta G°_f$) for the constituents in Equations 5.2 (chloride CAF) and 5.18 (bromide CAF). Using Equation 5.25, the standard free energy change for a reaction (ΔG°), for chloride CAF is -3287.4 KJ and -1420.4 KJ for bromide CAF. From these values, it can be concluded that both reactions are thermodynamically favoured to proceed, however, the chloride CAF

reaction is more highly favoured than the bromide CAF. This is why high bromide content is needed to form bromide CAF, and even in this case, as the results show, chloride CAF and a copper-chloride compound can be found in the polymer matrix.

Table 5.3 – Standard Gibbs Free Energies of Formation ($\Delta G°_f$) at 25 °C

Compound	ΔG°_f (KJ·mol^{-1})
$CuCl_2 \cdot 3Cu(OH)_2$ (s)	-1340.3 [86]
$CuBr_2 \cdot 3Cu(OH)_2$ (s)	-1282.0 [71]
CuCl (s)	-119.9 [87]
CuBr (s)	-100.8 [87]
Cl^- (aq)	-131.2 [87]
Br^- (aq)	-104.0 [87]
Cu^{2+} (aq)	65.5 [87]
H_2O (l)	-237.1 [87]
H^+ (aq)	0 [87]
O_2 (g)	0 [71, 86]

5.9 – Chapter Summary

This chapter has discussed the electrical and SEM/EDS results that were obtained for coupons processed with PEPG, PEPG/Cl, PEG, PEG/Cl and the HASL processed coupons. FTIR was used to show that the flux vehicle diffuses in the polymer matrix during the soldering process. Ion chromatography was used to show that the bromide source in bromide CAF is from the flux. For the PEPG, PEPG/Cl, and the HASL fluxes, in addition to CAF, a copper compound was observed in the bulk polymer matrix. XPS

was used to characterize this compound as CuCl for PEPG and PEPG/Cl fluxes, and CuBr for the HASL flux. Based on the XPS results, chemical mechanisms for the formation of both chloride and bromide CAF were proposed. For the PEG and PEG/Cl fluxes, no copper compound was observed in the bulk polymer matrix. A model explaining this result was proposed. In addition, the Meeker and LuValle two-step model was discussed, and based on the results of the present research a single non-reversible reaction model was proposed to explain CAF formation. TEM was used to show that bromide CAF is $Cu_2(OH)_3Br$.

Chapter 6 - Summary and Conclusions

The major contributions of this thesis are:

1. The copper compound found in the polymer matrix has been characterized for the first time using XPS to be CuCl. This is the first work to show that this compound is the same for coupons processed with PEPG and PEPG/Cl. This is the first work to show that for coupons fluxed with PEG and PEG/Cl, no copper-chloride compound is found in the polymer matrix. This work has also been the first to propose a model to explain why CAF forms at the epoxy/glass fiber interface and not in the polymer matrix for coupons processed with PEG and PEG/Cl [33].

2. This work is the first work to identify using XPS that the precursor to CAF formation is CuCl, and propose an electrochemical mechanism for the formation of chloride containing CAF, $Cu_2(OH)_3Cl$. In addition, it is the first work to propose that the competing reactions proposed by Meeker and LuValle are better represented by a single non-reversible reaction [43].

3. This is the first work to identify bromide containing CAF as $Cu_2(OH)_3Br$ using TEM. This is the first work to show that a copper containing compound can form in the polymer matrix for processed coupons using a high bromide containing flux, and using XPS, identify this compound as CuBr. The XPS data is the first to show that in CAF formation, whether it be chloride or bromide containing, the corrosion processes follow a similar electrochemical mechanism.

Chapter 7 – Industrial Significance and Impact

CAF failure is most favoured for hole-to-hole conductor orientations. CAF failure occurs in two steps, where initially the epoxy glass interface is weakened, followed by CAF growth from the anode. The weakening of the epoxy glass fiber interface can be caused by thermal processing (i.e. soldering), moisture uptake of the board which further weakens the epoxy glass fiber interface, water soluble fluxes, and mechanical hole drilling. Trends in modern day electronics are towards smaller much more compact board designs. It is projected by IPC that hole-hole spacings will reach 0.175 mm by 2016. These closer spacings pose a serious reliability threat when it comes to CAF failure. CAF resistant materials tend to be more expensive and will be used for high reliability applications. These materials tend to be more brittle and extra care must be taken into account in design and hole drilling. The board thickness, glass style, and resin content all affect the brittleness of substrate materials. Many studies have evaluated CAF resistant materials using hole-to-hole spacings as small as 0.076 mm. The drill bit thickness and spacing have a clear affect in reducing the amount of mechanical stress. Laser drilling is a potential alternative to mechanical drilling; however, it is limited to small diameter holes with low aspect ratios. Mechanical drilling remains the predominant method, and spacings below 0.5 mm can result in cracking between barrels. Hole-to-hole separations no smaller than 0.5 mm are recommended unless special methods are used to eliminate cracking through the barrel.

CAF is an electrochemically induced failure mode in which a conductive copper-containing salt grows subsurface from the anode to the cathode along the epoxy-glass

fiber interface. CAF has previously been identified as $Cu_2(OH)_3Cl$. According to the Pourbaix diagram it is insoluble in acid, causing it to grow from the anode.

The present work has evaluated coupons processed with water soluble fluxes based on PEG and PEPG with and without chloride. For both of these flux systems, the flux residues were extracted using acetonitrile and FTIR was used to confirm that the PEG and PEPG diffused into the board during processing. This work shows that for coupons processed with PEPG a copper chloride containing compound was found in the polymer matrix in addition to the CAF at the epoxy/glass interface. This work identified this compound as CuCl using XPS.

For PEG no copper chloride compound was found in the polymer matrix. Based on previous studies by others, it is proposed that a PEG-Cu-Cl complex formed at the copper anode which limits the creation of copper ions, and the ones that are formed react to form CAF at the epoxy/glass interface.

Several electrochemical studies have examined the corrosion of copper in an aqueous chloride solution and have shown that the precursor to atacamite can be either CuCl or $CuCl_2^-$. The present study uses XPS data to identify the precursor as CuCl, and is the first work to propose the complete electrochemical mechanism for CAF formation.

Earlier, Meeker and LuValle had suggested that there are two competing reaction products in CAF formation–a corrosive copper chloride compound and some innocuous trapped chlorine compounds. We have found no evidence for the innocuous chlorine compounds, so we conclude that the formation of CAF proceeds in a single non-reversible reaction.

Copper-bromide containing CAF has been created and this work identified this compound as $Cu_2(OH)_3Br$. The polyglycol from the flux has been extracted from the processed coupons and it has been shown by FTIR to be present within the board. Ion chromatography has confirmed the bromide from the flux diffuses into the board and is the main source in the formation of bromide containing CAF. The corrosion of copper in bromide media behaves similar to that in chloride media. This is consistent with the XPS data which has been used to identify and characterize this copper-bromide compound in the polymer matrix to be CuBr for coupons processed with high-bromide containing flux.

Either chlorine or bromine is required in order to form CAF. The chlorine source has been shown to be present in the board from the chemicals used in the manufacture of the epoxy. If resins that are chlorine free are used, then chloride CAF formation can be prevented. In the case of the brominated CAF, it has been shown that the bromide source is from the high bromide containing HASL flux. If HASL fluxes that are low in bromide content are used on epoxy FR-4 boards, the formation of brominated CAF can be eliminated.

Chapter 8 – Future Work

The present work has evaluated the interaction of solder flux and traditional FR-4 using a hole to hole test coupon. The emergence of both CAF resistant and halogen free materials has resulted in a need for the electronics industry to study the susceptibility of CAF failure for these new materials using various conductor orientations found in today's electronic circuits (see Table 1 below). Thus it is essential in the future to evaluate the effect of these different conductor orientations on CAF formation for newer substrates processed at lead-free soldering temperatures.

Table 8.1 – Different Conductor Orientations, Spacing and Voltages

Conductor orientation
hole-hole (drilled)
Microvia-microvia (laser formed)
power plane – plated through hole (inner layers)
trace - trace (inner layers)
trace - plane (inner layers)

References

[1] P. J. Boddy*, et al.*, "Accelerated Life Testing of Flexible Printed Circuits: Part I: Test Program and Typical Results," in *14th Annual Proc. Reliability Physics*, 1976, pp. 108-117.

[2] J. N. Lahti*, et al.*, "The Characteristic Wearout Process in Epoxy-Glass Printed Circuits for High Density Electronic Packaging," in *17th Annual Proc. Reliability Physics*, 1979, pp. 39-43.

[3] D. J. Lando*, et al.*, "Conductive Anodic Filaments in Reinforced Polymeric Dielectrics: Formation and Prevention," in *17th Annual Proc. Reliability Physics*, 1979, pp. 51-63.

[4] T. L. Welsher*, et al.*, "Conductive Anodic Filament: An Electrochemical Failure Mechanism of Reinforced Polymeric Dielectrics," *Annual Report of the Conference on Electrical Insulation and Dielectric Phenomena*, 1980, pp. 234-238.

[5] T. L. Welsher*, et al.*, "CAF in Composite Printed-Circuit Substrates: Characterization, Modeling and a Resistant Material," in *17th Annual Proc. Reliability Physics*, 1980, pp. 235-237.

[6] L. J. Turbini*, et al.*, "Impact of Higher Melting Lead-free Solders on the Reliability of Printed Wiring Assemblies," *Journal of Surface Mount Technology,* vol. 13, pp. 10-14, 2000.

[7] J. A. Jachim, "The Examination of the Effect of Three Water Soluble Fluxes on Biased Comb Patterns to High Humidity or Condensing Environments," Master of Science in Metallurgy, Materials Science and Metallurgical Engineering, Georgia Institute of Technology, Atlanta, 1994.

[8] W. J. Ready, "Factors Which Enhance Conductive Anodic Filament (CAF) Formation," Master of Science in Metallurgy, Materials Science and Metallurgical Engineering, Georgia Institute of Technology, Atlanta, 1997.

[9] W. J. Ready, "Reliability Investigation of Printed Wiring Boards Processed With Water Soluble Flux Constituents," Ph.D, Materials Science and Metallurgical Engineering, Georgia Institute of Technology, Atlanta, 2000.

[10] W. J. Ready and L. J. Turbini, "The Effect of Flux Chemistry, Applied Voltage, Conductor Spacing, and Temperature on Conductive Anodic Filament Formation," *J. Electron. Mater.,* vol. 31, pp. 1208-1224, 2002.

[11] W. W. Wang, "Advanced Materials for Printed Circuit Boards," *Materials Research Symposium Proceedings,* vol. 108, pp. 125-138, 1988.

[12] IPC T-50 Terms and Definitions published by the IPC-Association Connecting Electronics Industries, Bannockburn, IL 60015, 1996.

[13] B. Rudra*, et al.*, "Assessing Time-to-Failure Due to Conductive Filament Formation in Multi-Layer Organic Laminates," *IEEE Transactions on Components, Packaging, and Manufacturing Techniques - Part B,* vol. 17, pp. 269-276, 1994.

[14] M. W. Jawitz, Ed., *Printed Circuit Board Materials Handbook*. New York: McGraw Hill, 1997.

[15] P. D. Döring, *Halogen-free Flame Retardants in E&E Application*. Karlsruhe Germany: Forschungszentrum Karlsruhe GmbH, 2007.
[16] W. Q. Meeker and M. J. LuValle, "An Accelerated Life Test Model Based on Reliability Kinetics," *Technometrics,* vol. 37, p. 133, 1995.
[17] A. DeMarderosian, "Raw Material Evaluation Through Moisture Resistance Testings," in *IPC*, San Francisco, 1976, pp. 1-53.
[18] Joint Committee for Powder Diffraction Standards, Powder Diffraction File, International Center for Diffraction Data, Swarthmore, PA, (Card Number 23-948, 1971).
[19] Joint Committee for Powder Diffraction Standards, Powder Diffraction File, International Center for Diffraction Data, Swarthmore, PA, (Card Number 23-269,1972).
[20] IPC National Technology Roadmap for Electronic Interconnect and Assemblies 2006/2007 published by the IPC-Association Connecting Electronics Industries 3000 Lakeside Drive, Bannockburn, IL 60015.
[21] K. Sauter, "Electrochemical Migration Testing Results: Evaluating PWB Design, Manufacturing Process, and Laminate Material Impacts on CAF Resistance," *CircuitTree,* vol. 15, pp. 10-19, 2002.
[22] K. L. Rogers and M. G. Pecht, "A Variant of Conductive Filament Formation Failures in PWBs with 3 and 4 mil Spacings," *Circuit World,* vol. 32, pp. 11-18, 2006.
[23] B. K. Hinds and M. Treanor, "Drilling of Printed Circuit Boards: Factors Limiting The Use of Smaller Drill Sizes," *Proc. Instn. Mech. Engrs. Part B,* vol. 214, pp. 35-45, 2000.
[24] H. Murai*, et al.*, "The Evaluation of CAF Property for Narrow TH Pitch PCB," in *IPC Printed Circuits Expo, APEX and the Designers Summit*, Las Vegas, Nevada, 2008.
[25] L. Gopalakrishnan*, et al.*, "Condcutive Anodic Filament Formation - Effect of Feature Sizes on Product Reliability," in *SMTA International*, 2004, pp. 429-437.
[26] K. Karavakis and S. Bertling, "Conductive Anodic Filament (CAF): The Threat to Miniaturization of the Electronics Industry," *Circuitree,* vol. 17, pp. 70-73, 2004.
[27] G. Parry*, et al.*, "The Effect of Manufacturing Parameters on Board Design for CAF Evaluation," in *Proceedings of the International Conference on Lead-free Soldering*, Toronto, Ontario, May 26, 2005.
[28] A. Caputo*, et al.*, "Design Limitations Related to Conductive Anodic Filament (CAF) Formation in a Micro-World," *Microsystem Technologies,* vol. 15, pp. 39-44, 2009.
[29] L. A. Giannuzzi and F. A. Stevie, *Introduction to Focused Ion Beams : Instrumentation, Theory, Techniques, and Practice*. New York: Springer, 2005.
[30] Joint Committee for Powder Diffraction Standards, Powder Diffraction File, International Center for Diffraction Data, Swarthmore, PA, (Card Number 00-045-1309,1986).
[31] J. Brous, "Electrochemical Migration and Flux Residues - Causes and Detection," in *NEPCON West*, 1992, pp. 386-393.

[32] H. Arisawa and T. B. Brill, "Flash Pyrolysis of Polyethylene Glycol Part I: Chemometric Resolution of FTIR Spectra of the Volatile Products at 370-550°C," *Combustion and Flame,* vol. 109, pp. 87-104, 1997.
[33] A. Caputo*, et al.*, "Conductive Anodic Filament (CAF) Formation Part I: The Influence of Water-Soluble Flux on Its Formation," *Journal of Electronic Materials,* vol. 39, pp. 85-91, 2010.
[34] X. Han*, et al.*, "Effects of Fullerenes on Thermal Behaviors of Polyethylene Glycol," *Journal of Thermal Analysis and Calorimetry,* vol. 93, pp. 927-933, 2008.
[35] W. J. Ready*, et al.*, "Microstructure of Conductive Anodic Filaments Formed during Accelerated Testing of Printed Wiring Boards," *Circuit World,* vol. 21, pp. 5-9, 1995.
[36] M. Pourbaix, "Lectures on Electrochemical Corrosion," ed. New York: Plenum Press, 1973.
[37] F. M. Zado, " Effects of Non-ionic Water Soluble Flux Residues," *AT & T, The Engineer,* vol. 27, pp. 41-48, 1983.
[38] J. Brous, "Water Soluble Flux and its Effect on PC Board Insulation Resistance," *Electronic Packaging and Production,* vol. 21, p. 80, 1981.
[39] M. Yokoi*, et al.*, "Adsorption Behavior of Polyoxyethylene on the the Copper Surface in an Acid Copper Sulfate Bath," *Denki Kagaku,* vol. 52, p. 218, 1984.
[40] Z. V. Feng*, et al.*, "Inhibition due to the Interaction of Polyethylene Glycol, Chloride, and Copper in Plating Baths: A Surface-Enhanced Raman Study," *J. Phys. Chem. B,* vol. 107, pp. 9415-9423, 2003.
[41] J. W. Gallaway and A. C. West, "PEG, PPG, and Their Copolymers as Suppressors in Copper Electroplating," *Journal of The Electrochemical Society,* vol. 155, pp. D632-D639, 2008.
[42] K. R. Hebert*, et al.*, "Chemical Mechanism of Suppression of Copper Electrodeposition by Poly(ethylene glycol)," *Journal of The Electrochemical Society,* vol. 152, pp. C324-C329, 2005.
[43] A. Caputo*, et al.*, "Conductive Anodic Filament Formation Part II: Electrochemical Reactions Leading to CAF," *Journal of Electronic Materials,* vol. 39, pp. 92-96, 2010.
[44] A. J. Raffolovich, "Corrosive Effects of Solder Flux on Printed-Circuit Boards," *IEEE Trans. Parts, Hybrids,Packag.,* vol. 7, p. 155, 1971.
[45] H. Strandberg and L. G. Johansson, "Some Aspects of the Atmospheric Corrosion of Copper in the Presence of Sodium Chloride," *J. Electrochem. Soc.,* vol. 145, p. 1093, 1998.
[46] P. M. May*, et al.*, "The Corrosion of Copper in Ethylene Glycol-Water Mixtures Containing Chloride Ions," *Journal of Applied Electrochemistry,* vol. 21, pp. 358-364, 1991.
[47] A. L. Bacarella and J. C. Griess, "The Anodic Dissolution of Copper in Flowing Sodium Chloride Solutions Between 25 ^{o}C and 175 ^{o}C," *Journal of the Electrochemical Society,* vol. 120, pp. 459-465, 1973.
[48] L. Brossard, "Anodic Dissolution of Copper in Concentrated LiCl Solution at pH between 3 and 7," *Journal of the Electrochemical Society,* vol. 130, pp. 403-405, 1983.

[49] G. Faita, *et al.*, "Copper Behaviour in Acid and Alkaline Brines - I. Kinetics of Anodic Dissolution in 0.5M NaCl and Free-Corrosion Rates in the Presence of Oxygen," *Corrosion Science,* vol. 15, pp. 383-392, 1975.
[50] M. Georgiadou and R. Alkire, "Modelling Copper Etching in Aerated Chloride Solutions," *Journal of Applied Electrochemistry,* vol. 28, pp. 127-134, 1998.
[51] S. R. D. Sanchez and D. J. Schiffrin, "The Use of High Speed Rotating Disc Electrodes for the Study of Erosion-Corrosion of Copper Base Alloys in Sea Water," *Corrosion Science,* vol. 28, pp. 141-151, 1988.
[52] M. Braun and K. Nobe, "Electrodissolution Kinetics of Copper in Acidic Chloride Solutions," *J. Electrochem. Soc.,* vol. 126, pp. 1666-1671, 1979.
[53] P. A. Lush and M. J. Carr, "Copper Dissolution in Sea Water Under Mixed Activation and Diffusion Control," *Corrosion Science,* vol. 19, pp. 1079-1088, 1979.
[54] F. Mansfield, *et al.*, "The Corrosion Behavior of Copper Alloys, Stainless Steels and Titanium in Seawater," *Corrosion Science,* vol. 36, pp. 2063-2095, 1994.
[55] S. R. D. Sanchez and D. J. Schiffrin, "The Flow Corrosion Mechanism of Copper Base Alloys in Sea Water in the Presence of Sulphide Contamination," *Corrosion Science,* vol. 22, pp. 585-607, 1982.
[56] W. H. Smyrl, "Digital Dependance of Faradic Analysis," *Journal of the Electrochemalical Society,* vol. 132, pp. 1555-1562, 1985.
[57] A. H. Taylor, "The Corrosion Behavior of Cu and Naval Brass in 0.5M NaCl Solutions at Ambient Temperature," *Journal of the Electrochemical Society,* vol. 118, pp. 854-859, 1971.
[58] F. K. Crundwell, "The Anodic Dissolution of Copper in Hydrochloric Acid Solutions," *Electrochimica Acta,* vol. 37, pp. 2707-2714, 1992.
[59] C. Deslouis and B. Tribollet, "Electrochemical Behaviour of Copper in Neutral Aerated Chloride Solution - I. Steady-State Investigation," *Journal of Applied Electrochemistry,* vol. 18, pp. 374-383, 1988.
[60] R. K. Flatt and P. A. Brook, "The Effects of Anion Concentration on Anodic Polarization of Copper, Zinc, and Brass," *Corrosion Science,* vol. 11, pp. 185-196, 1971.
[61] F. King, *et al.*, "Oxygen Reduction of Copper in Neutral NaCl solution," *Journal of Electroanalytical Chemistry,* vol. 385, 1995.
[62] H. P. Lee and K. Nobe, "Kinetics and Mechanisms of Cu Electrodissolution in Chloride Media," *Journal of the Electrochemical Society,* vol. 133, pp. 2035-2043, 1986.
[63] H. P. Lee, *et al.*, "Film Formation and Current Oscillations in the Electrodissolution of Cu in Acidic Chloride Media," *Journal of the Electrochemical Society,* vol. 132, pp. 1031-1037, 1985.
[64] C. H. Bonfiglio, *et al.*, "The Kinetics of the Anodic Dissolution of Copper in Acid Chloride Solutions," *Corrosion Science,* vol. 13, pp. 717-724, 1973.
[65] M. E. Walton and P. A. Brook, "The Dissolution of Cu-Ni Alloys in Hydrochloric Acid - I. Rotating Disk Electrode Measurements," *Corrosion Science,* vol. 17, pp. 317-328, 1977.
[66] G. Kear, *et al.*, "Electrochemical Corrosion of Unalloyed Copper in Chloride Media - A Critical Review," *Corrosion Science,* vol. 46, pp. 109-135, 2004.

[67] J. B. Sharkey, and S.Z. Lewin, "Conditions Governing the Formation of Atacamite and Paratacamite," *American Minerologist,* vol. 56, pp. 179-192, 1971.
[68] C. F. Coombs, *Printed Circuits Handbook*, 5th ed. New York: McGraw-Hill, 2001.
[69] D. R. Lefebvre*, et al.*, "Degradation of Epoxy Coatings in Humid Environments: The Critical Relative Humidity for Adhesion Loss," *J. Adhesion Sci. Technol.,* vol. 5, p. 201, 1991.
[70] W. J. Ready*, et al.*, "Conductive Anodic Filament Enhancement in the Presence of a Polyglycol-Containing Flux," in *IEEE International Reliability Physics Symposium Proceedings*, Dallas, TX, 1996, pp. 267-273.
[71] M. J. Munoz-Portero*, et al.*, "Pourbaix Diagrams for Copper in Aqueous Lithium Bromide Concentrated Solutions," *Corrosion,* vol. 60, pp. 749-756, 2004.
[72] T. Aben and D. Tromans, "Anodic Polarization Behavior in Aqueous Bromide and Bromide/Benzotriazole Solutions," *J. Electrochem. Soc.,* vol. 142, pp. 398-404, 1995.
[73] R. L. Brossard, "L'electrodissolution du Cuivre dans les Solutions Bromurees," *Can. J. Chem,* vol. 62, 1984.
[74] B. Hibbert*, et al.*, "The Kinetics and Mechanism of the Corrosion of Copper in Acidified Copper (II) Bromide Solution," *Corrosion Science,* vol. 30, pp. 367-376, 1990.
[75] Z. H. Gu*, et al.*, "Comparison of Dynamic Behaviour of the Anodic Dissolution of Copper in Aqueous Chloride and Bromide Solutions," *Electrochimica Acta,* vol. 41, pp. 2045-2054, 1996.
[76] V. Perez-Herranz*, et al.*, "Effect of Fluid Velocity and Exposure Time on Copper Corrosion in a Lithium Bromide Solution," *Corrosion,* vol. 57, pp. 835-842, 2001.
[77] A. Igual-Munoz*, et al.*, "Galvanic Study of Zinc and Copper in Lithium Bromide Solutions at Different Temperatures," *Corrosion,* vol. 57, pp. 516-522, 2001.
[78] A. Igual-Munoz*, et al.*, "Corrosion Behavior and Galvanic Studies of Brass and Bronzes in Aqueous Lithium Bromide Solutions," *Corrosion,* vol. 58, p. 560569, 2002.
[79] M. Itagaki*, et al.*, "Anodic Dissolution and Disproportional Reaction of Copper in Bromide Solution Investigated by Channel Flow Electrode," *Corrosion Science,* vol. 45, pp. 1023-1036, 2003.
[80] M. Itagaki*, et al.*, "Electrochemical Reactions of Copper and Carbon Steel in Lithium Bromide Solution," *Corrosion Engineering,* vol. 53, pp. 359-374, 2004.
[81] M. J. Munoz-Portero*, et al.*, "Anodic Polarization Behavior of Copper in Concentrated Aqueous Lithium Bromide Solutions and Comparison with Pourbaix," *Corrosion,* vol. 61, pp. 464-572, 2005.
[82] M. T. Montanes*, et al.*, "Evolution with Exposure Time of Copper Corrosion in a Concentrated Lithium Bromide Solution. Characterization of Corrosion Products by Energy-Dispersive X-ray Analysis and X-ray Diffraction," *Corrosion,* vol. 62, pp. 64-73, 2006.
[83] D. Tromans and R. H. Sun, "Anodic Polarization Behavior of Copper in Aqueous Chloride/Benzotriazole Solutions," *J. Electrochem. Soc.,* vol. 138, pp. 3235-3244, 1991.
[84] Z. H. Gu*, et al.*, "The Oscillatory Behaviour of Anodic Copper Dissolution into a NaCl/KSCN Electrolyte " *Electrochimica Acta,* vol. 37, pp. 2637-2644, 1992.

[85] Z. H. Gu and T. Z. Fahidy, "An Experimental Study of Anodic Dissolution of Copper in Aqueous Sodium Chloride via Laser-Induced Image Processing," *J. Appl. Electrochem.,* vol. 19, pp. 354-360, 1989.
[86] A. I. Demidov, "Thermodynamics of Patina Formation," *Russian Journal of Applied Chemistry,* vol. 80, pp. 566-569, 2007.
[87] D. R. Lide, *CRC Handbook of Chemistry and Physics : A Ready-Reference Book of Chemical and Physical Data*, 87th ed. New York: Taylor and Francis, 2006.

Appendices

Appendix A: Insulation Resistance Data

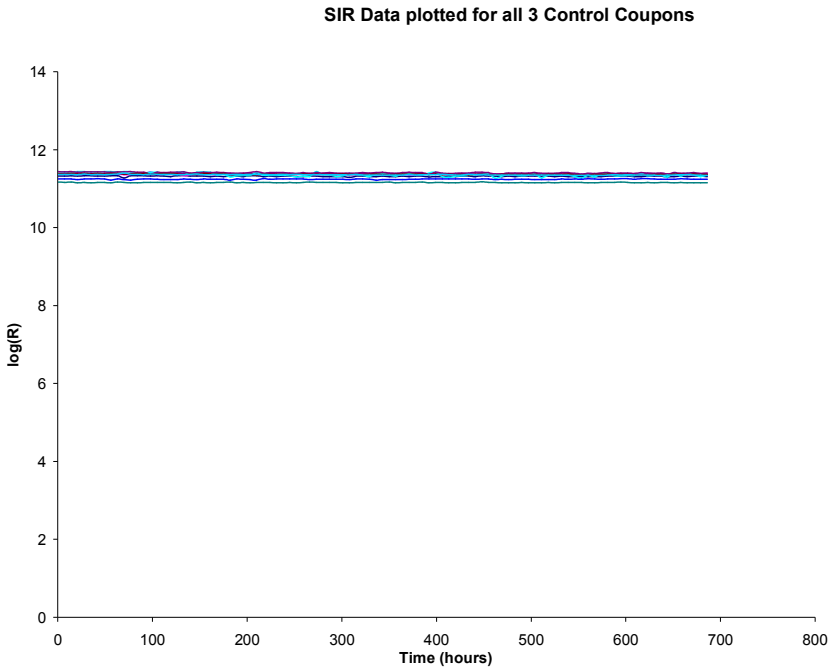

Figure A.1 – Summary of the insulation resistance data for the control coupons

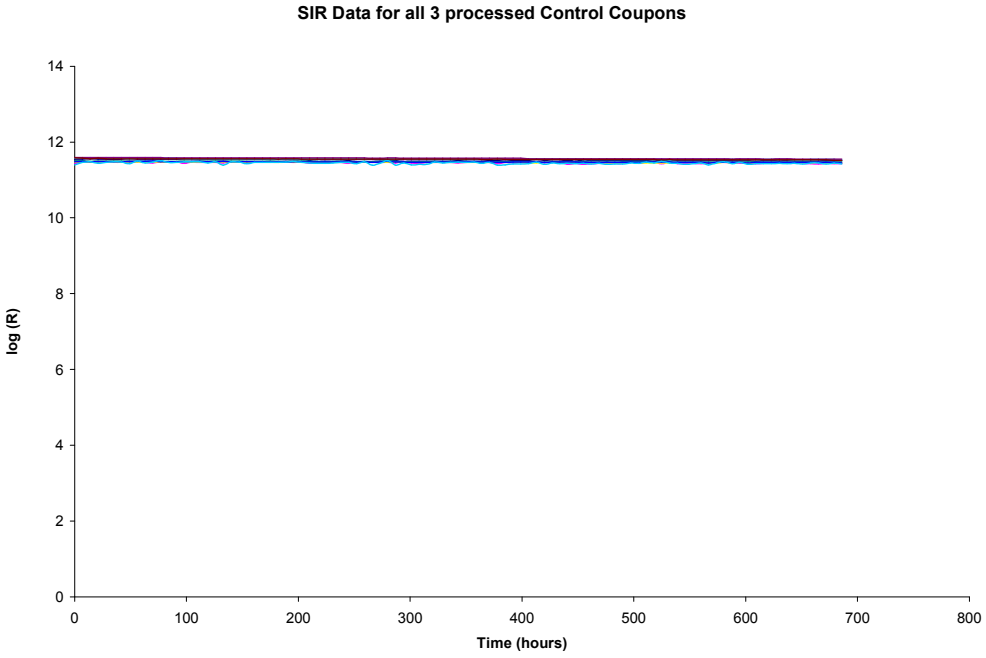

Figure A.2 – Summary of the insulation resistance data for the coupons processed with no flux.

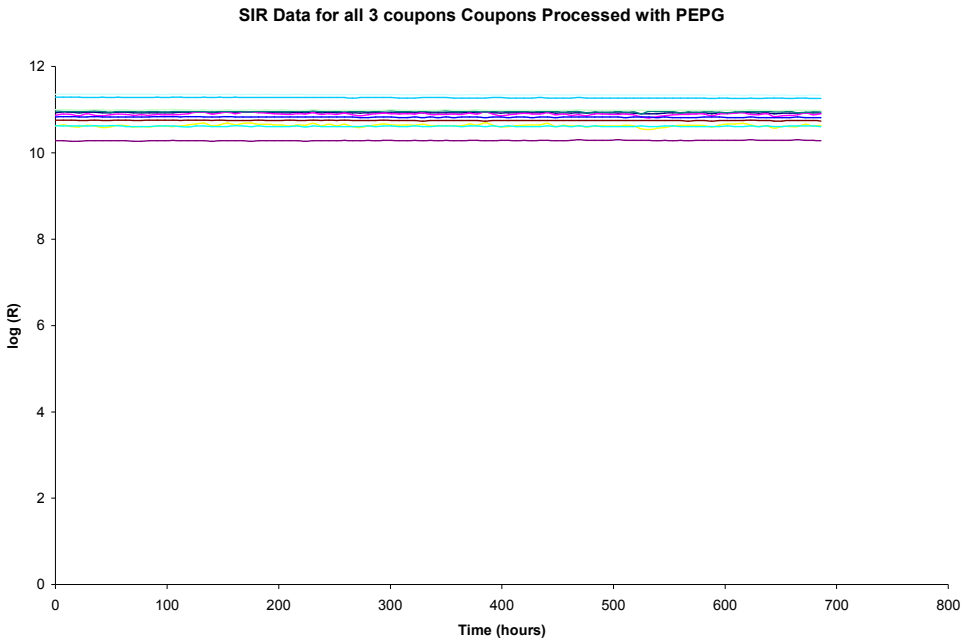

Figure A.3 – Summary of the insulation resistance data for the coupons processed with PEPG flux.

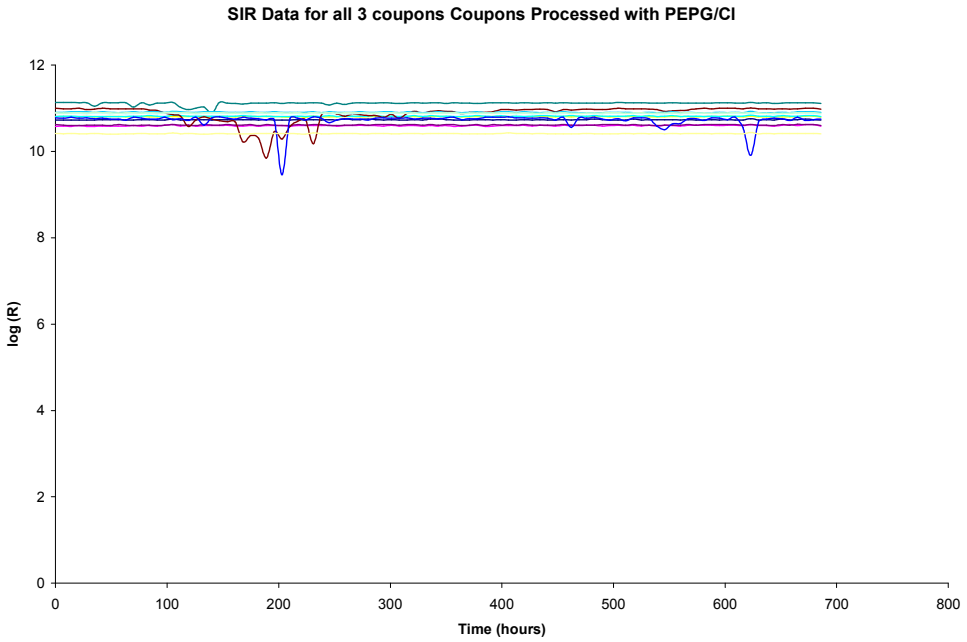

Figure A.4 – Summary of the insulation resistance data for the coupons processed with PEPG/Cl flux.

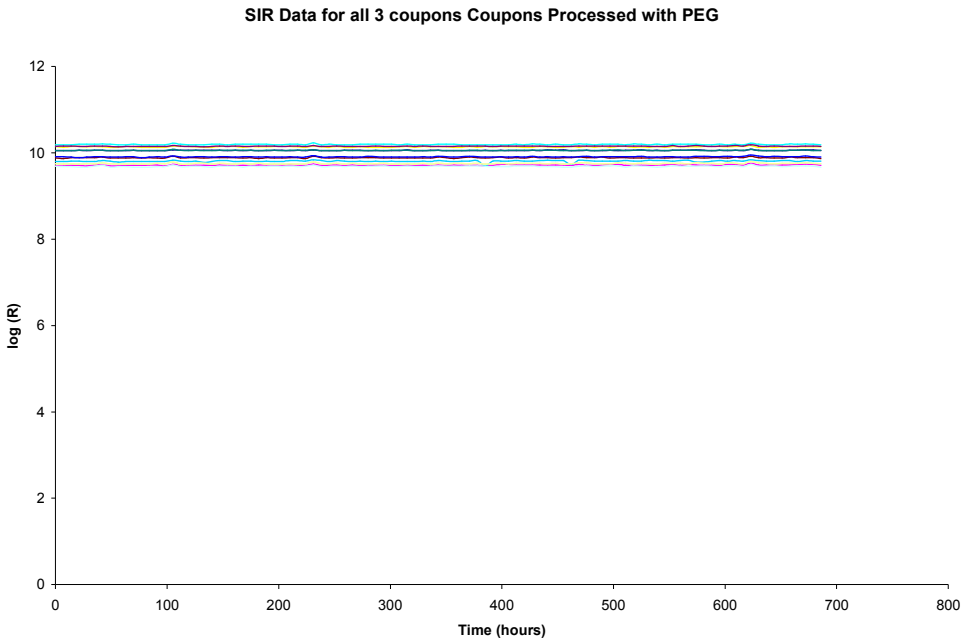

Figure A.5 – Summary of the insulation resistance data for the coupons processed with PEG flux.

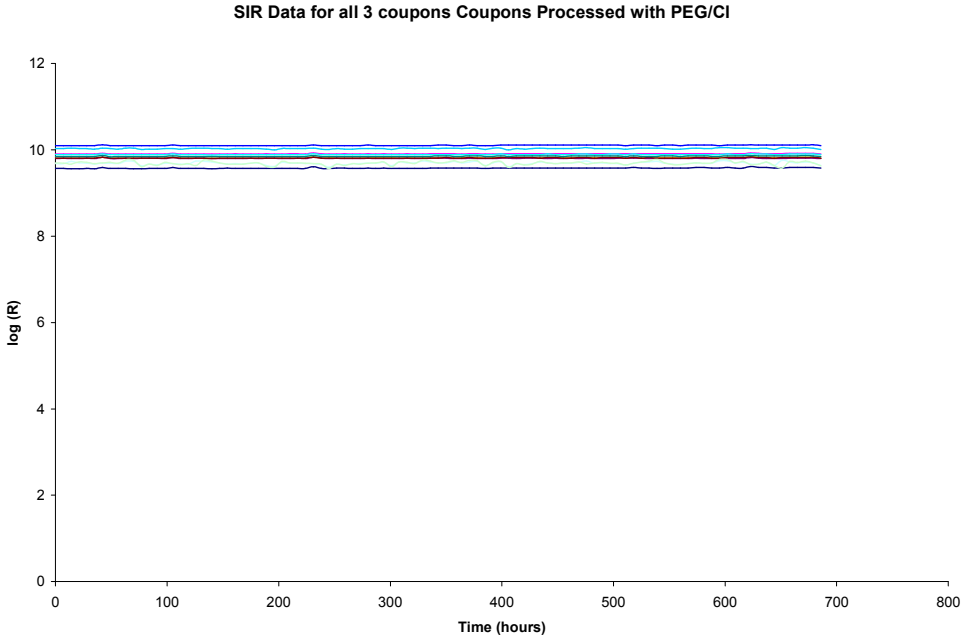

Figure A.6 – Summary of the insulation resistance data for the coupons processed with PEG/Cl flux.

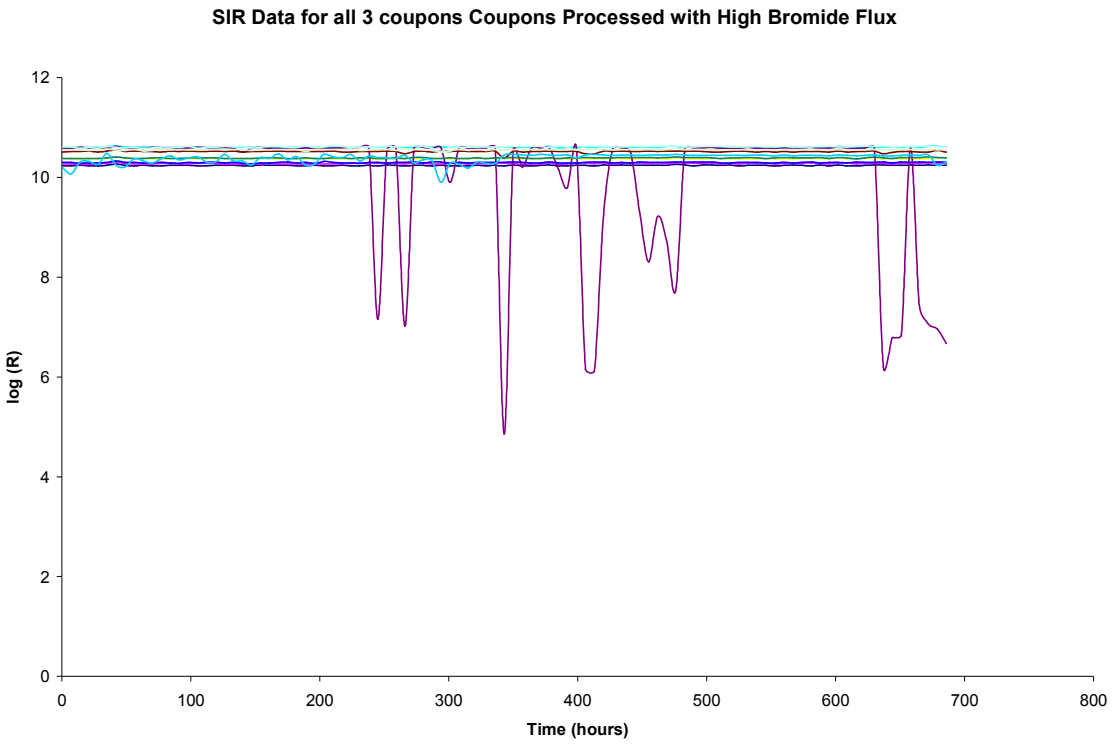

Figure A.7 – Summary of the insulation resistance data for the coupons processed with the high bromide containing flux (i.e. HASL fluid).

Appendix B: FTIR spectra for PEPG/Cl and PEG/Cl

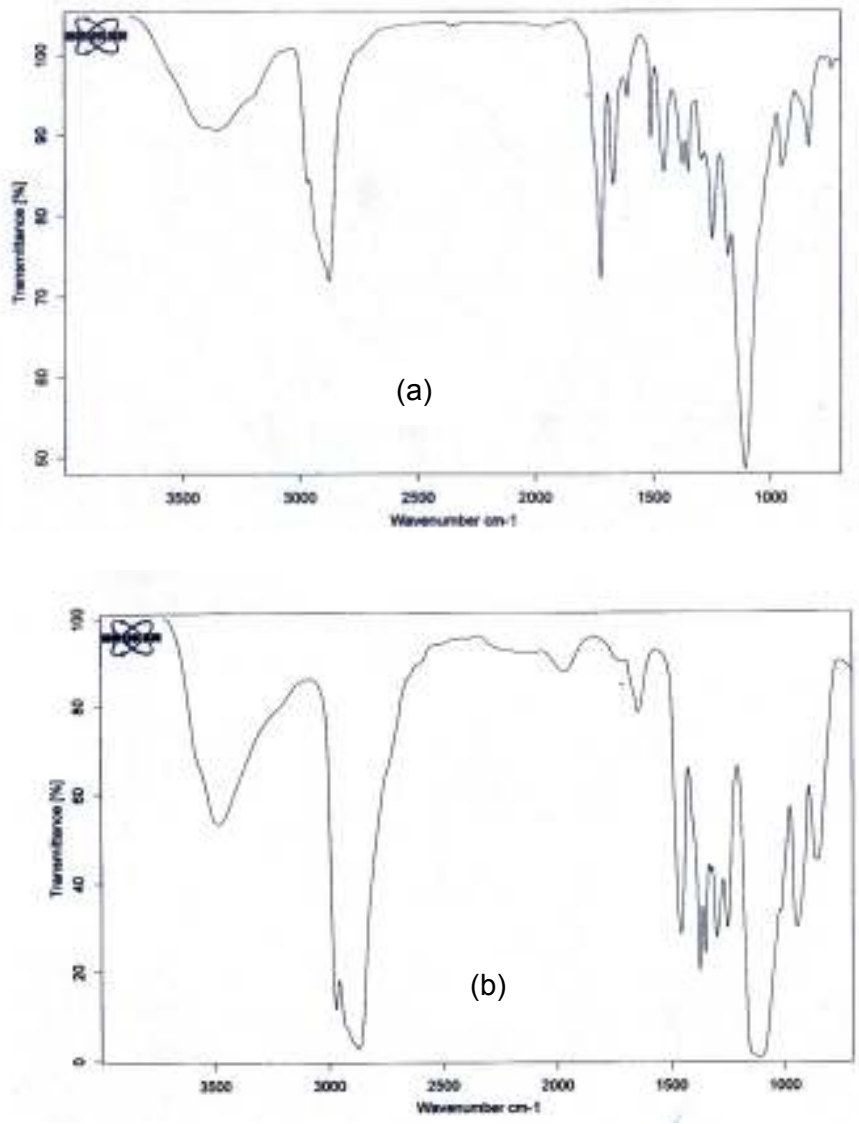

Figure B.1: FTIR spectra for (a) PEPG/Cl flux extracted from processed coupon, and (b) PEPG/Cl flux.

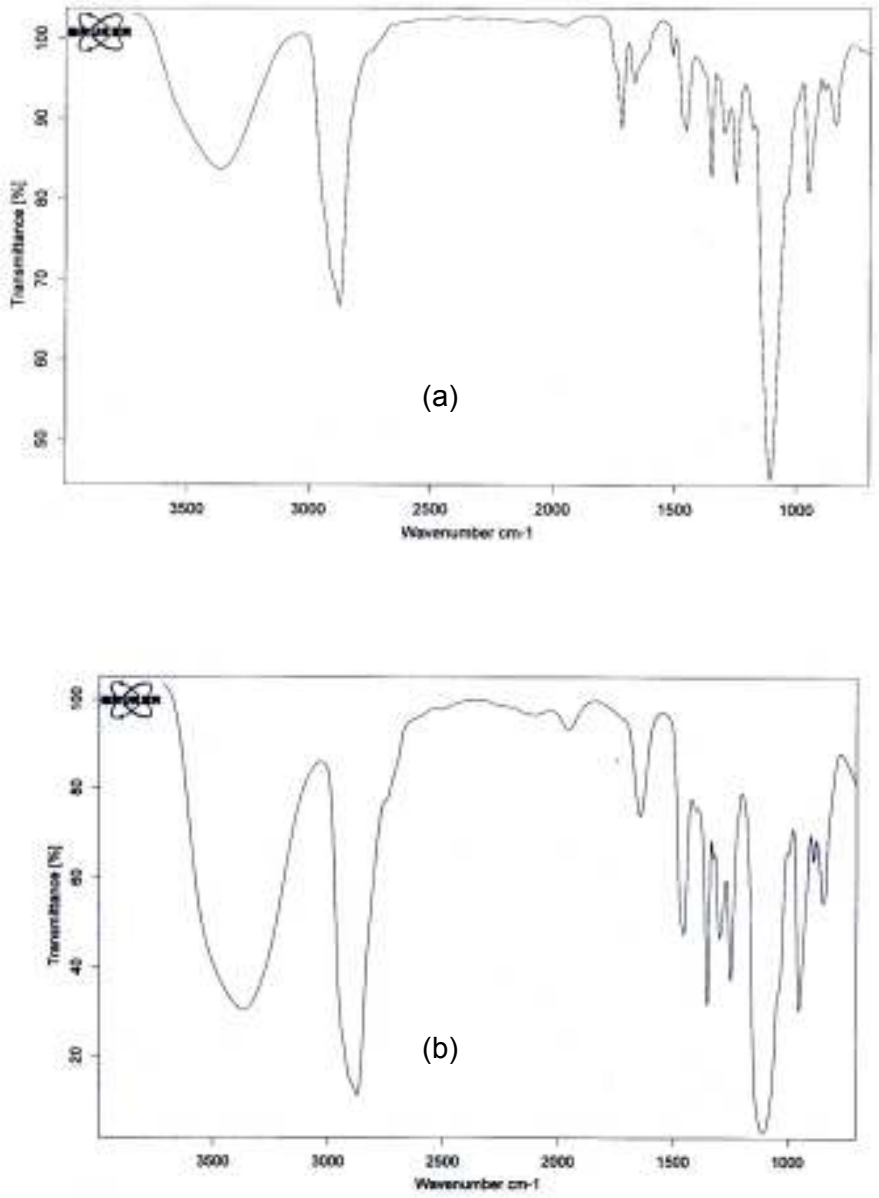

Figure B.2: FTIR spectra for (a) PEG/Cl flux extracted from processed coupon, and (b) PEG/Cl flux.

Appendix C: PEPG processed coupons

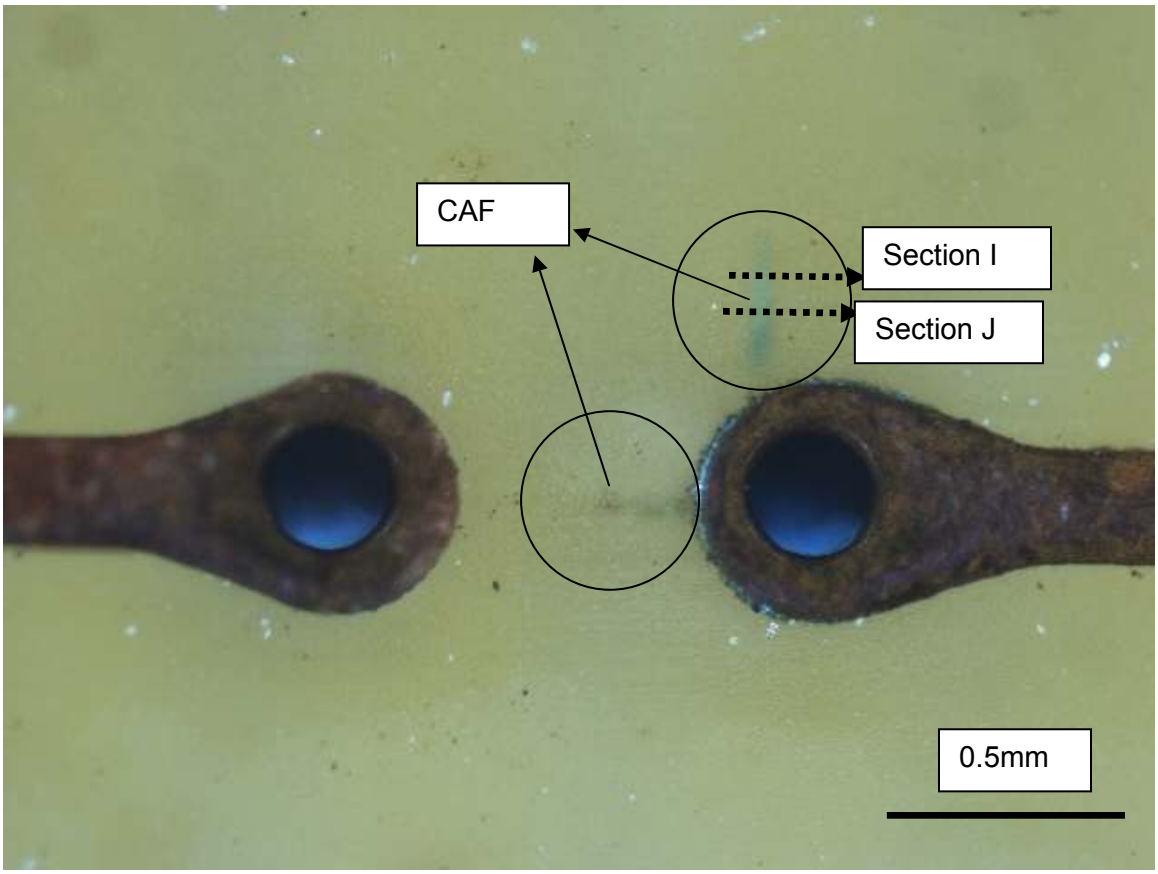

Figure C.1: Optical image showing CAF for PEPG processed coupon.

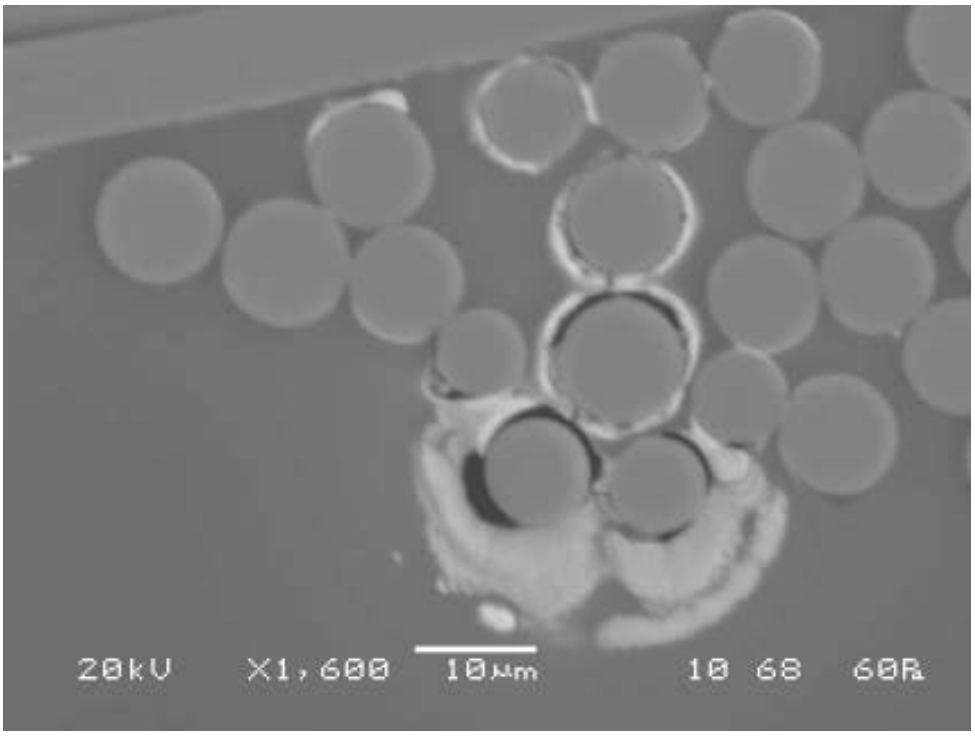

(a)

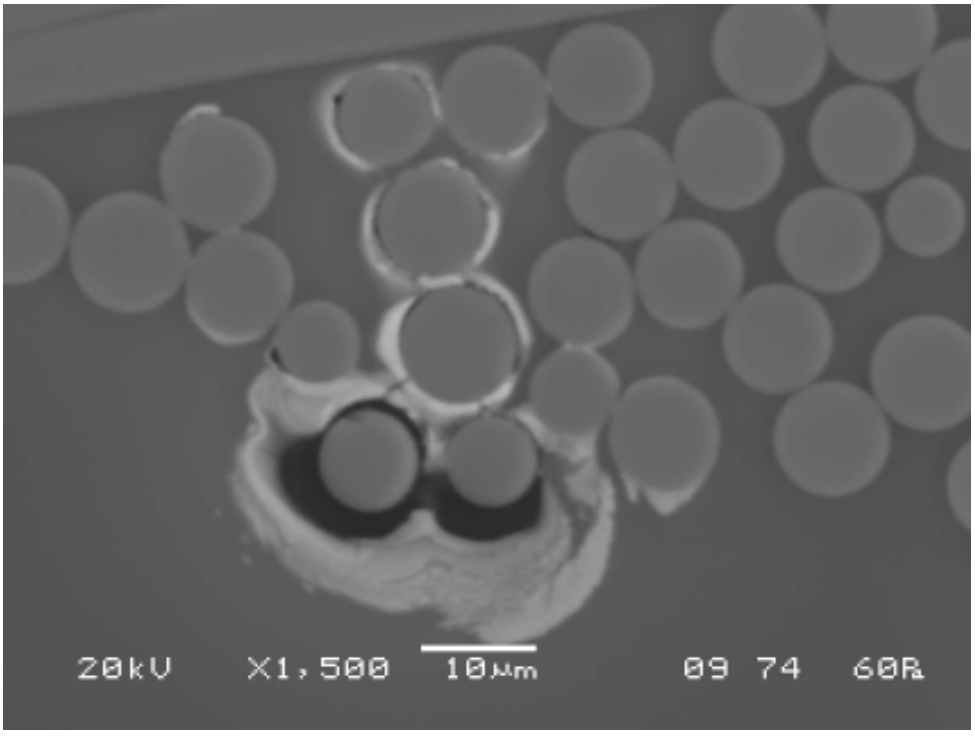

(b)

Figure C.2: A PEPG processed coupon showing a copper compound in the polymer matrix and CAF at the epoxy-glass for (a) section I and (b) section J.

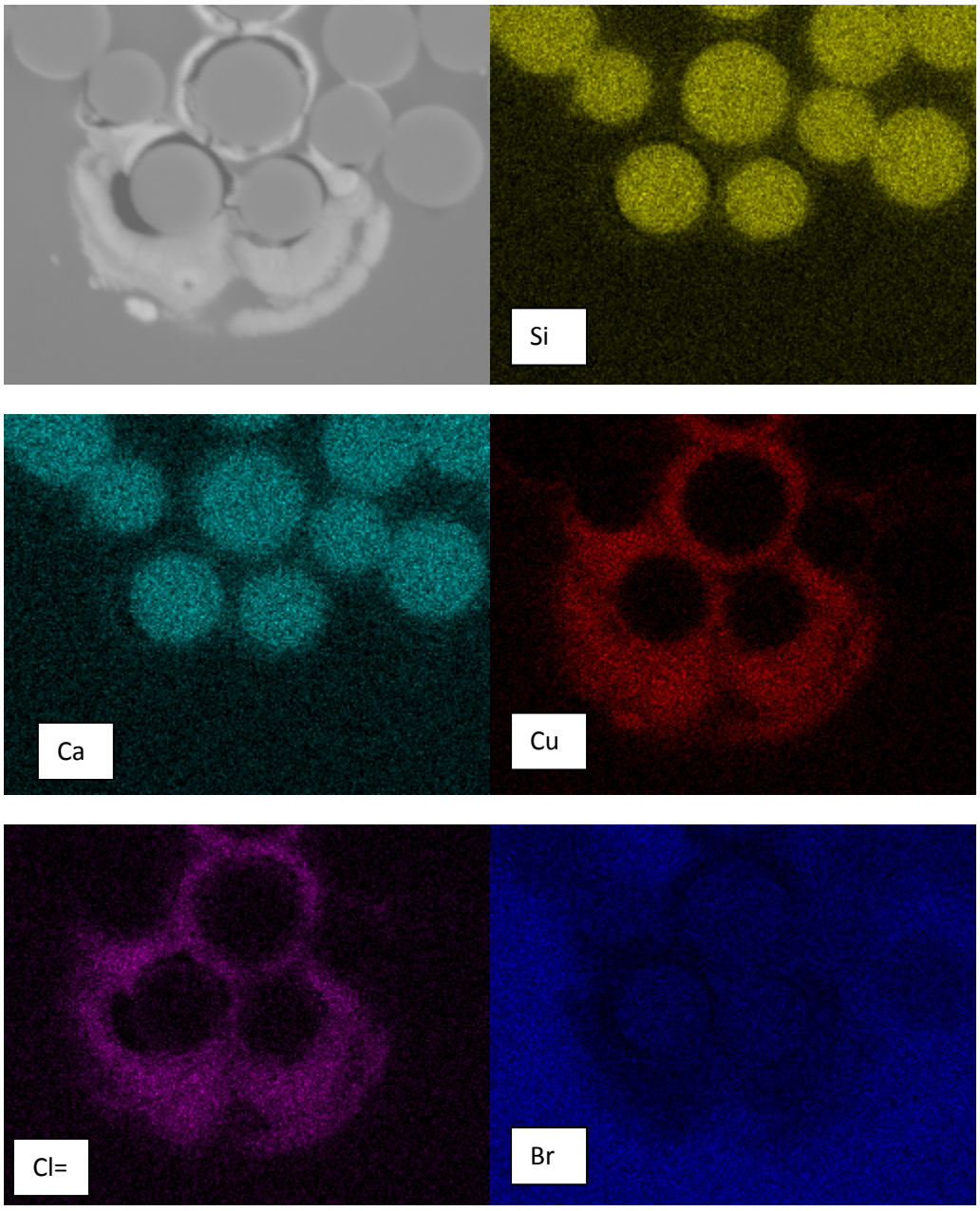

Figure C.3: EDS map of the PEPG processed coupon for section I.

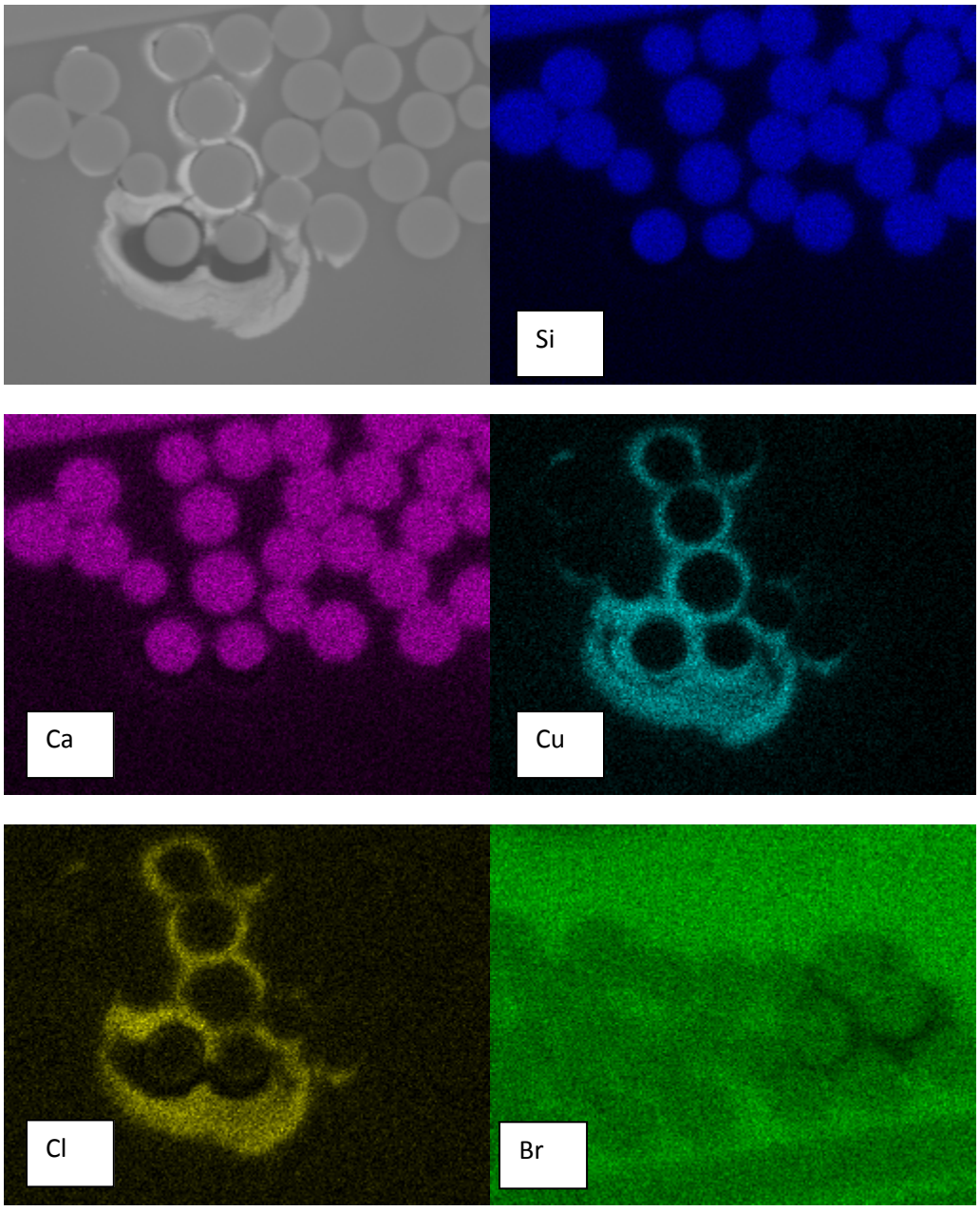

Figure C.4: EDS map of the PEPG processed coupon for section J.

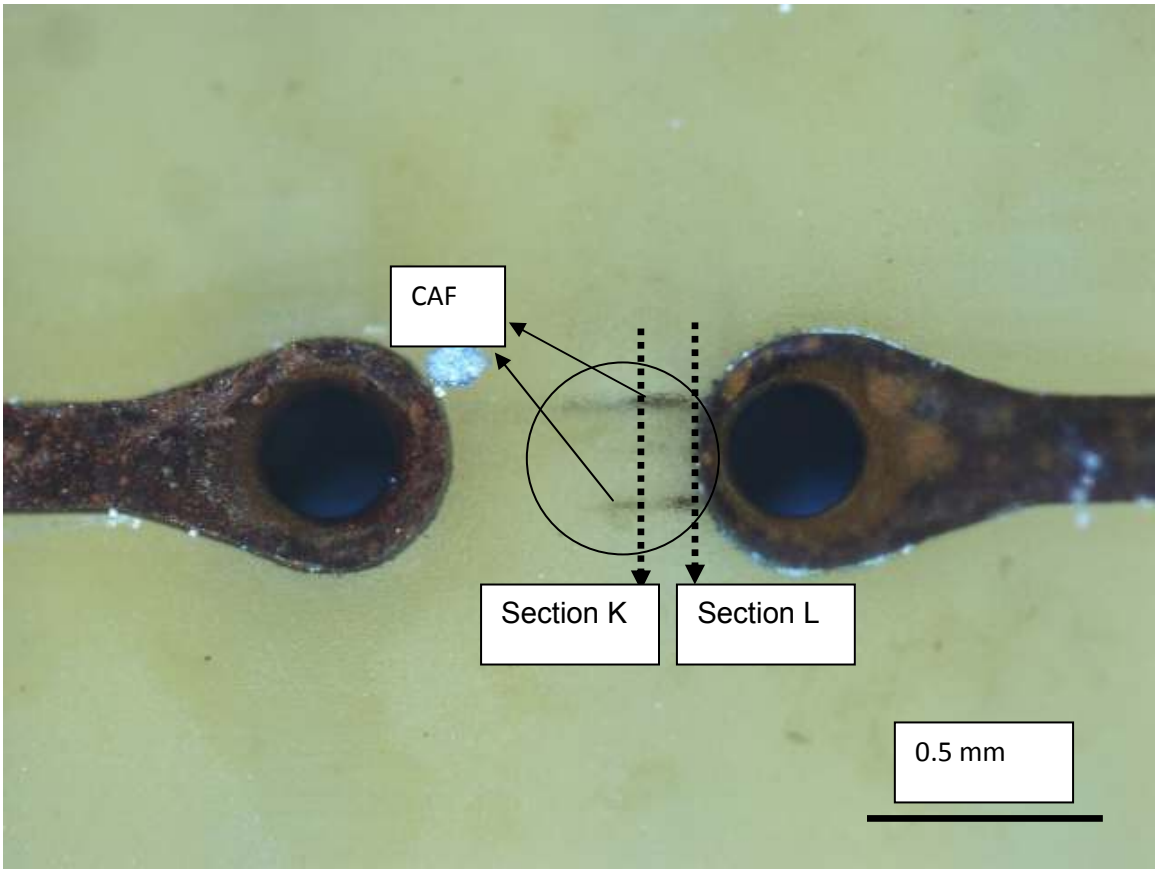

Figure C.5: Optical image illustrating CAF for a PEPG processed coupon.

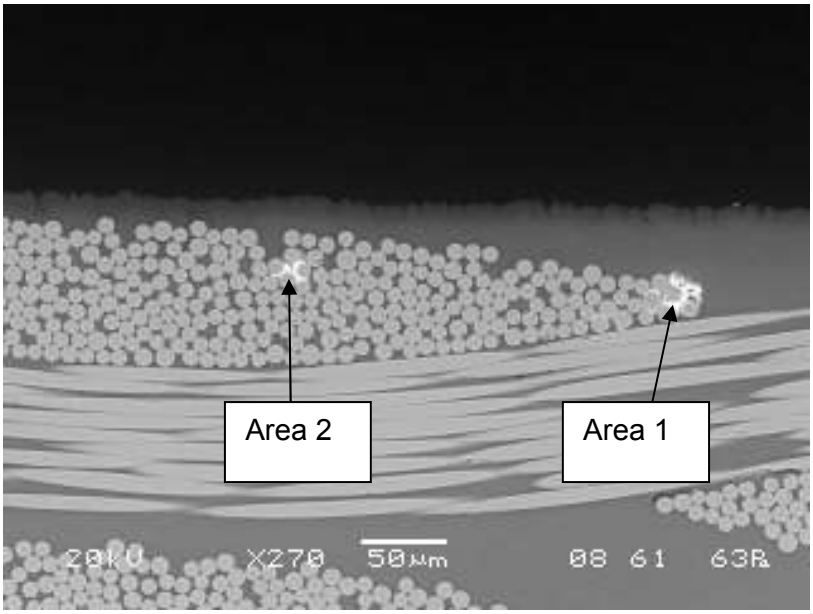

Figure C.6: A PEPG processed coupon showing a copper compound in the polymer matrix and CAF for section K.

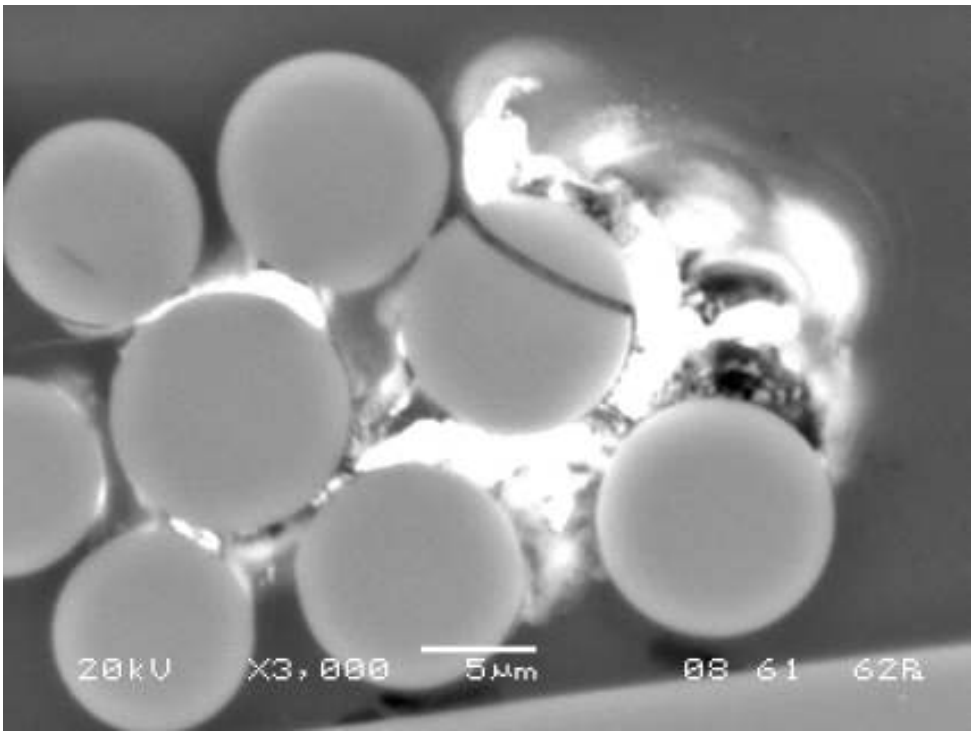

(a)

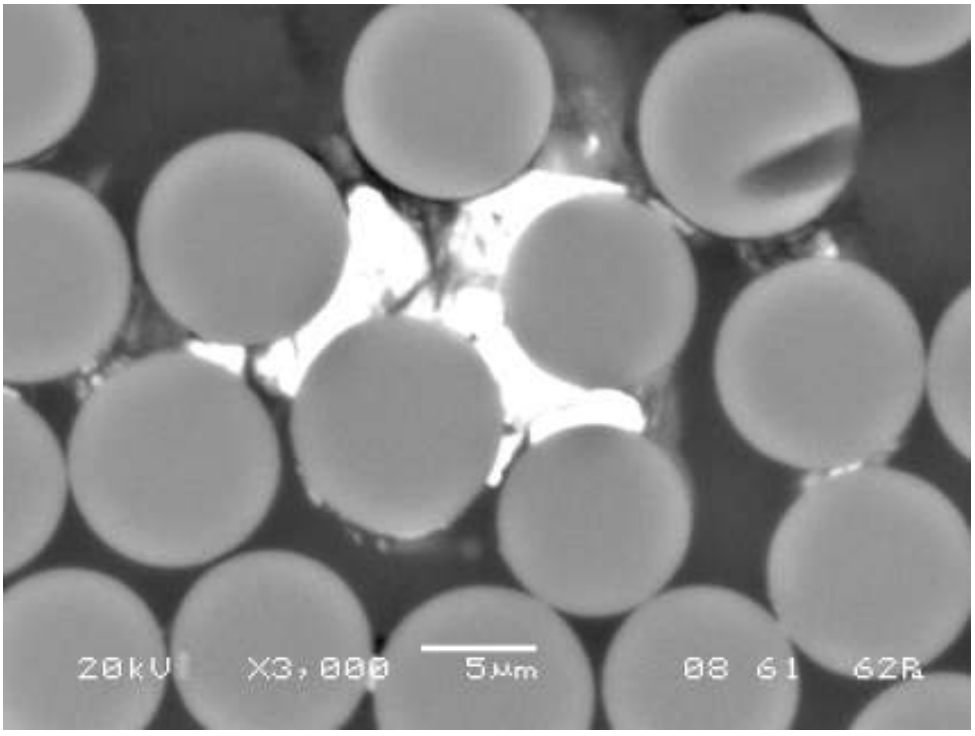

(b)

Figure C.7: The PEPG processed coupons showing a copper compound in the polymer matrix and CAF for section K in (a) area 1 and (b) area 2.

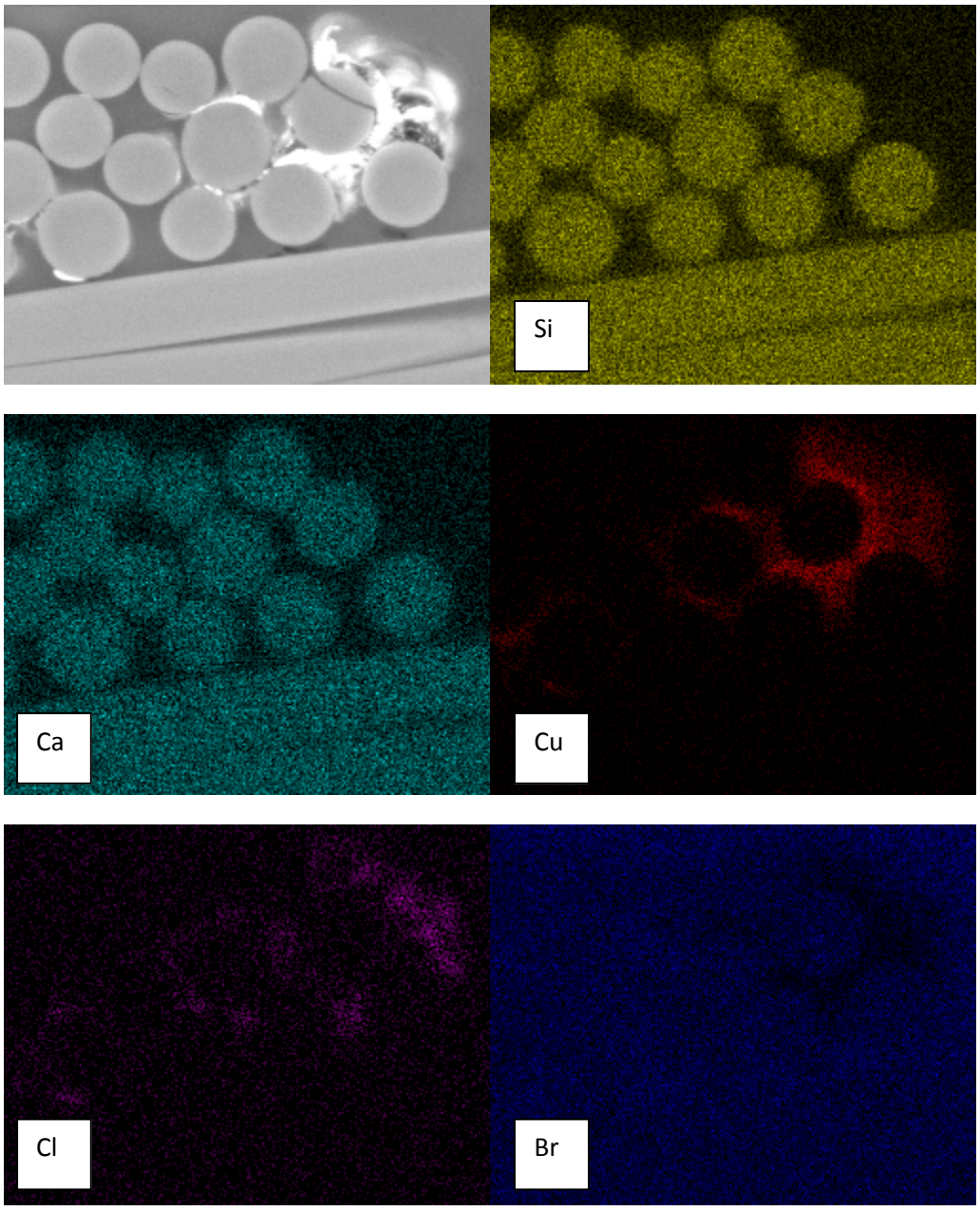

Figure C.8: EDS map of the PEPG processed coupon for the CAF and copper compound in the polymer matrix found in area 1 of section K.

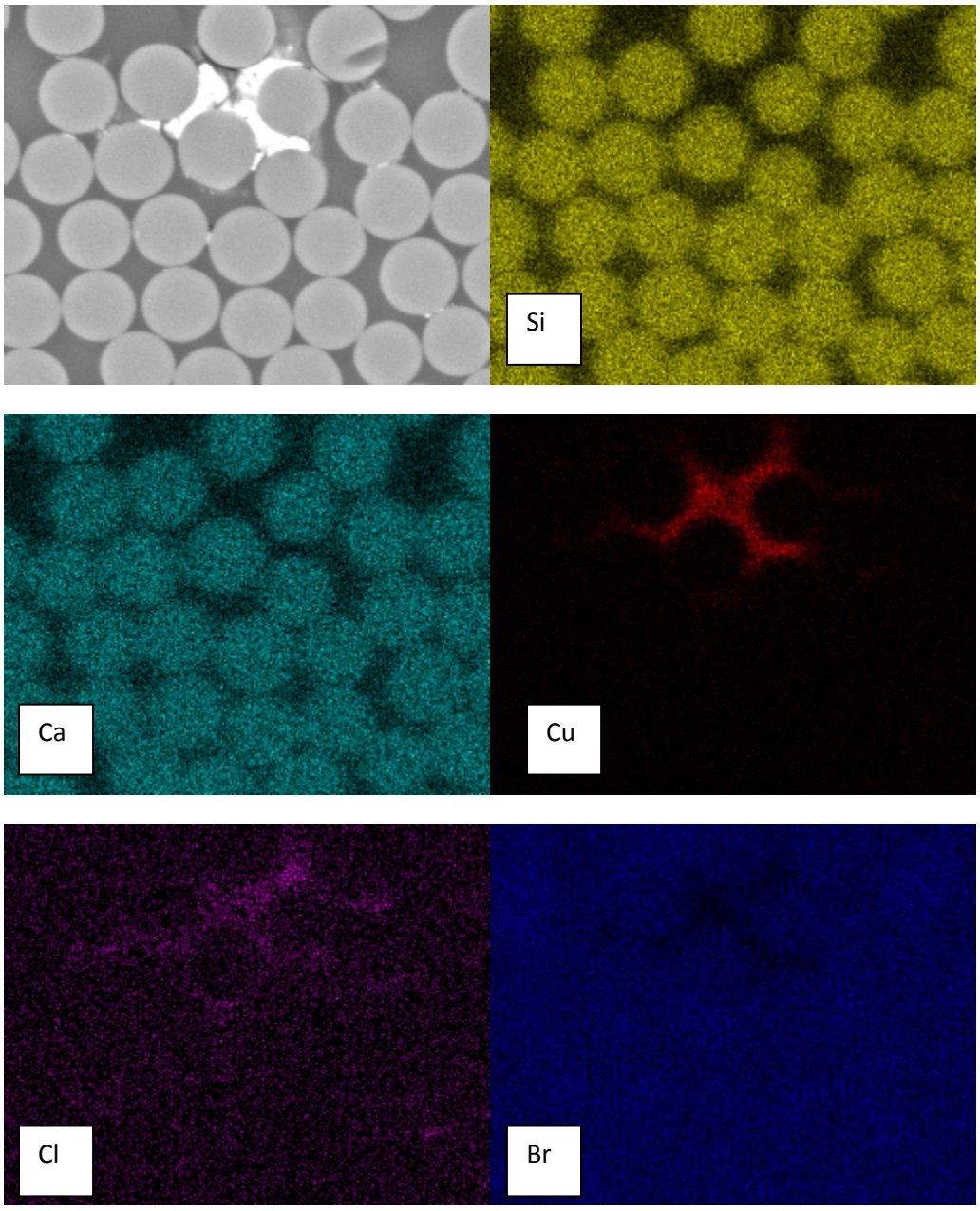

Figure C.9: EDS map of the PEPG processed coupon for the CAF and copper compound in the polymer matrix in area 2 for section K.

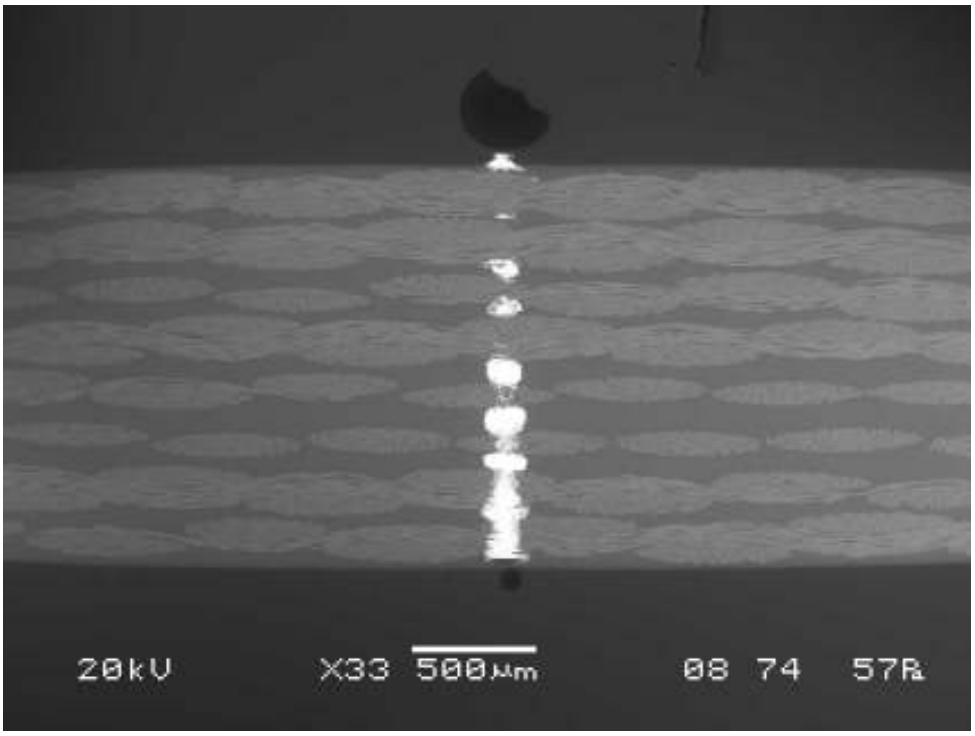

Figure C.10: A PEPG processed coupon showing the tip of the anode hole (i.e. section L).

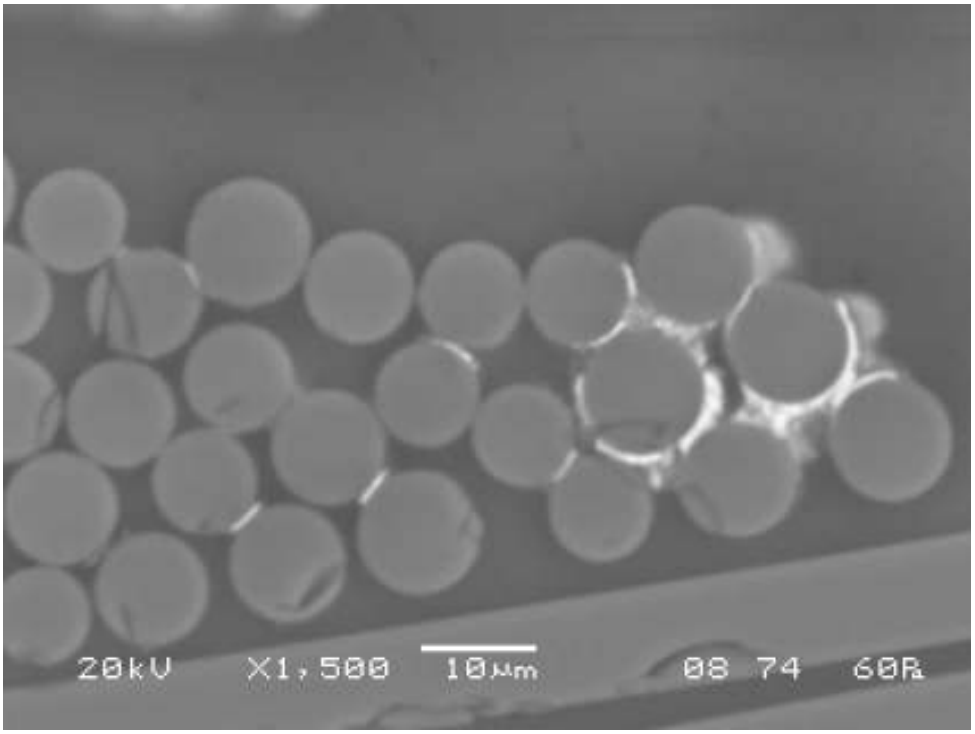

Figure C.11: A PEPG processed coupon showing CAF and a copper compound in the polymer matrix for section L in one area.

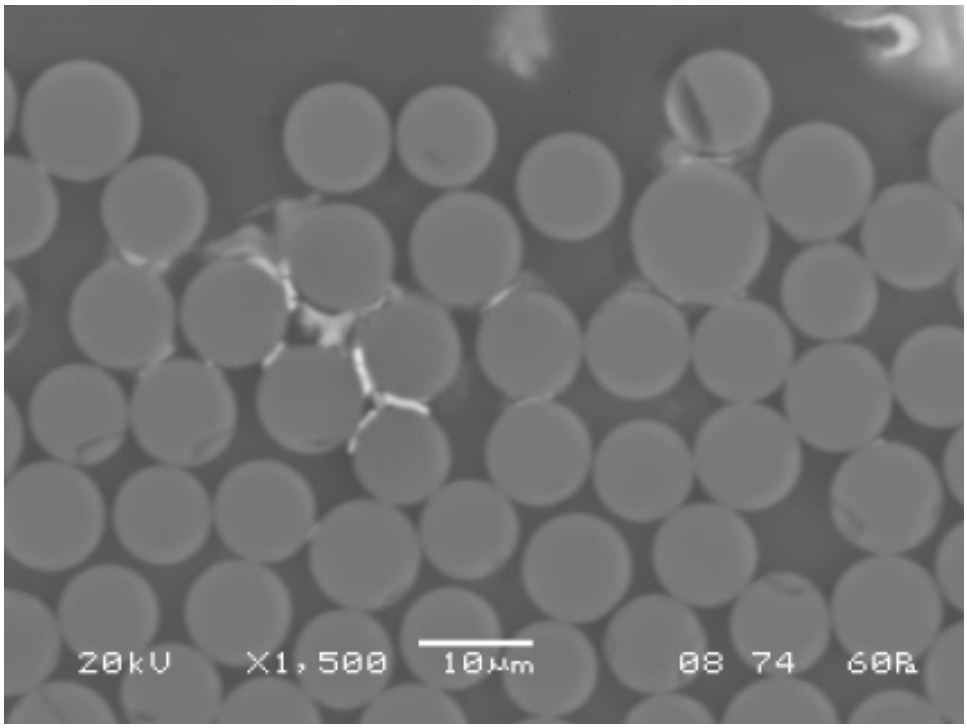

Figure C.12: A PEPG processed coupon showing CAF and a copper compound in the polymer matrix for section L in a second area.

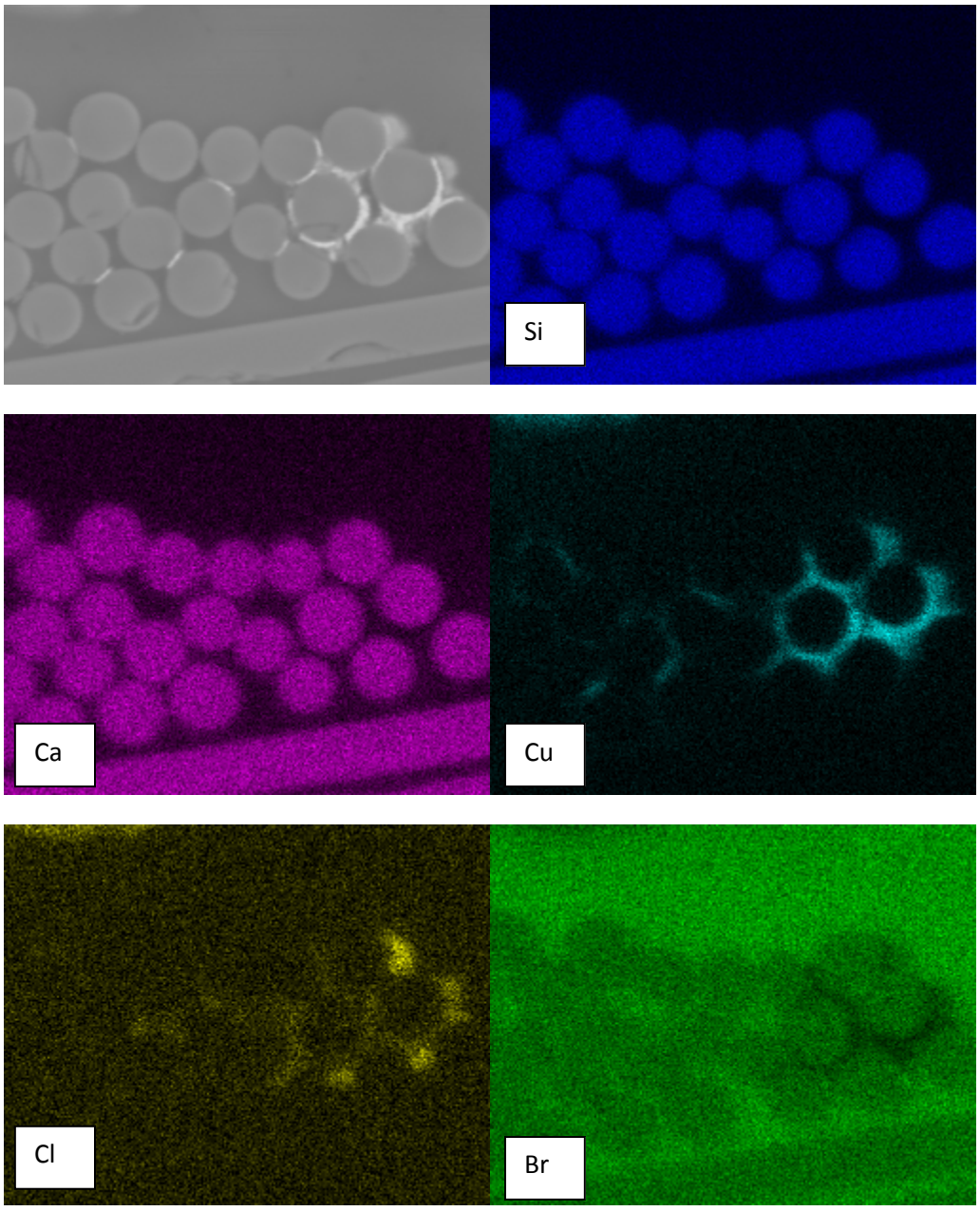

Figure C.13: EDS map of the PEPG processed coupon for the area shown in Figure C.11 (i.e. section L).

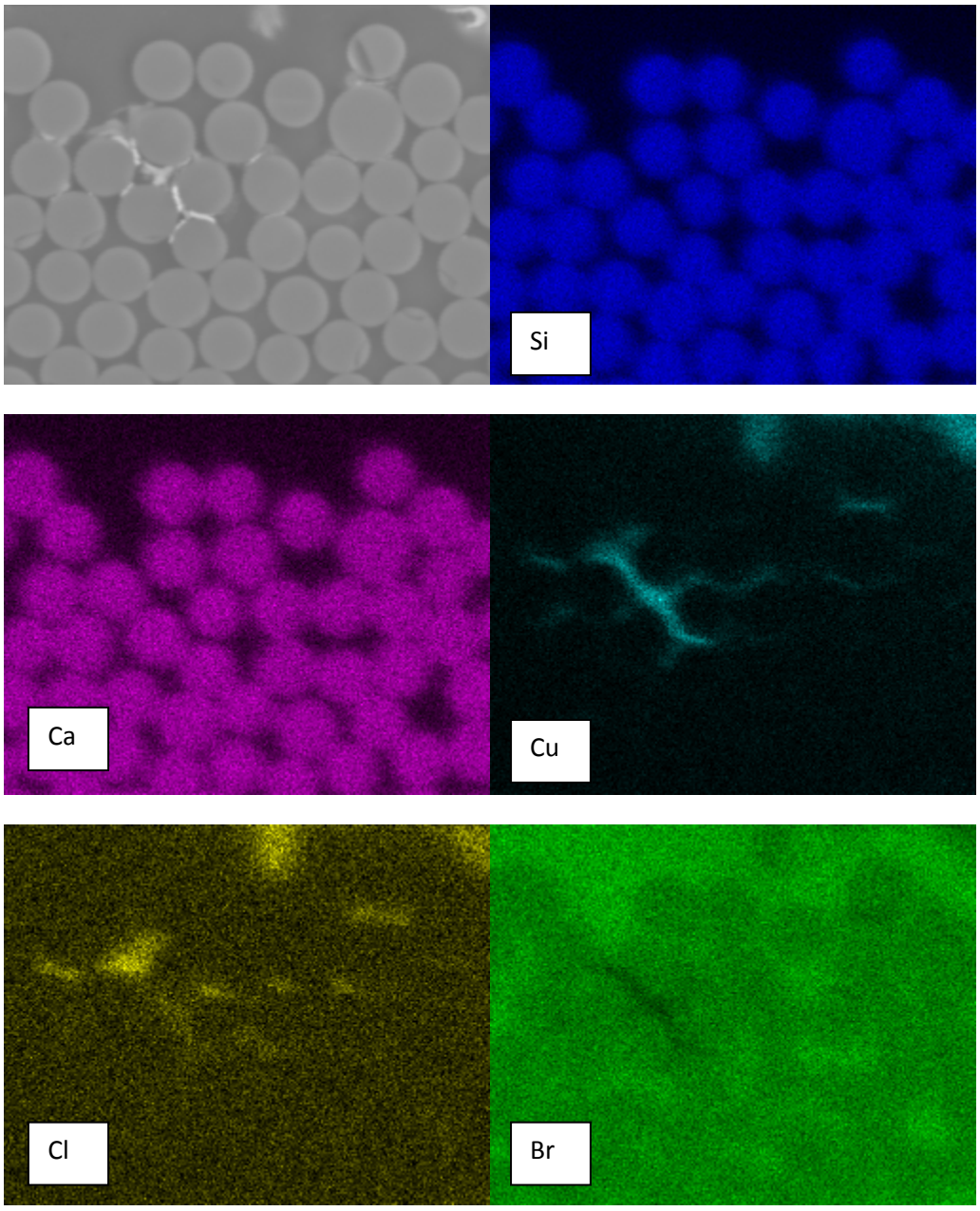

Figure C.14: EDS map of the PEPG processed coupon for the area shown in Figure C.12 (i.e. section L).

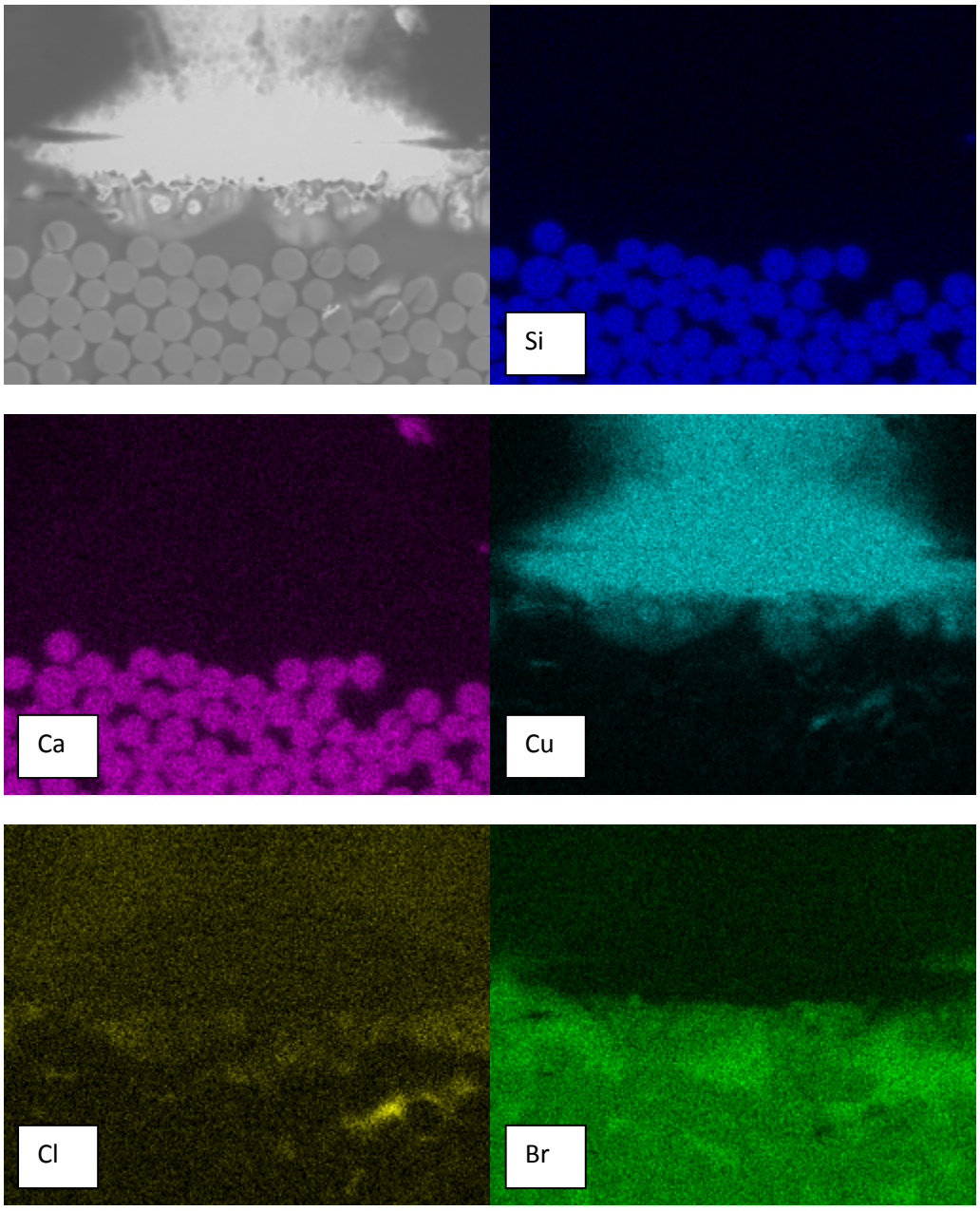

Figure C.15: EDS map of the PEPG processed coupon at the anode tip for section L.

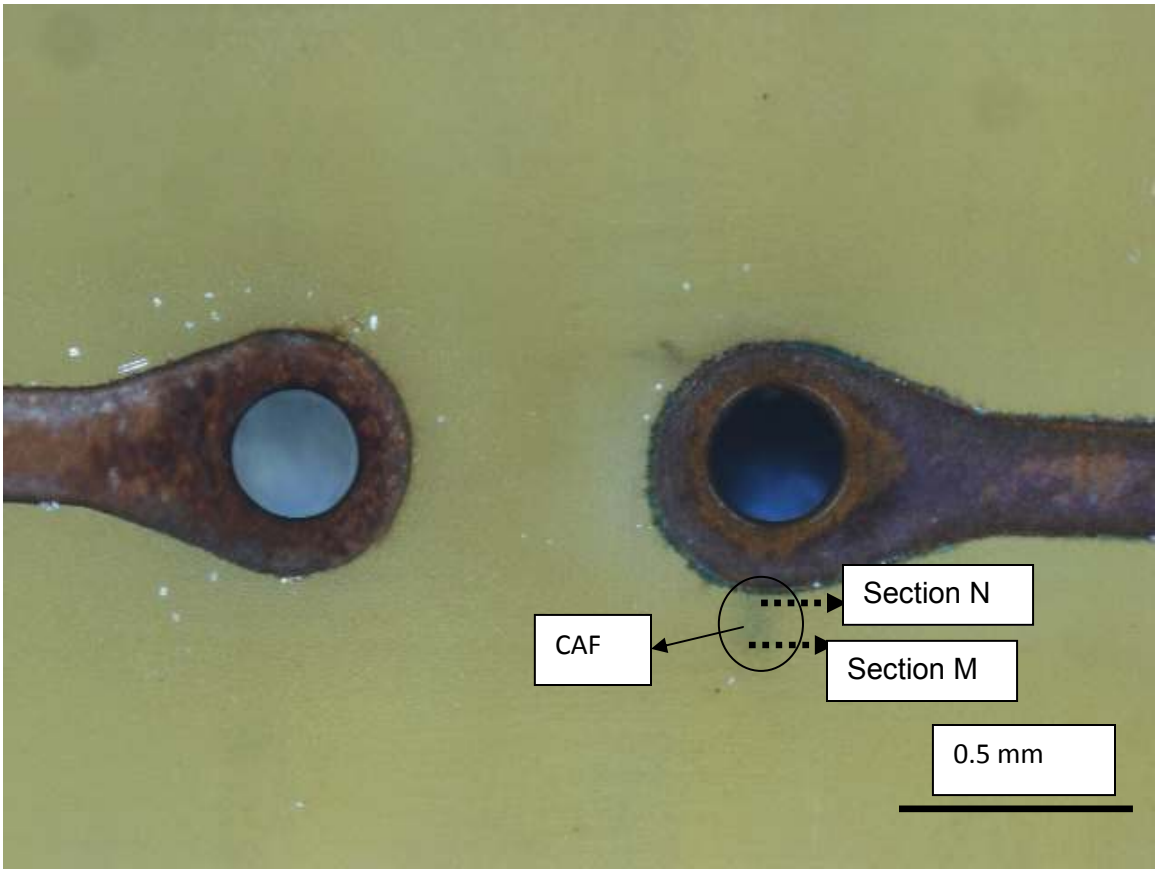

Figure C.16: Optical image illustrating CAF for a PEPG processed coupon.

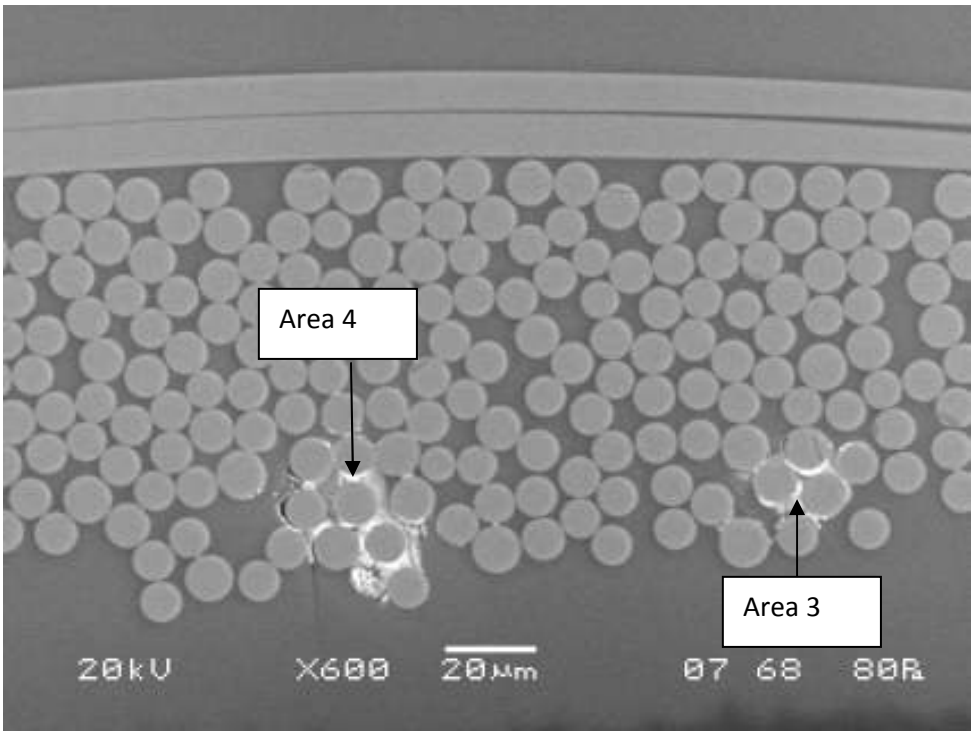

Figure C.17: A PEPG processed coupon showing a copper compound in the polymer matrix and CAF in two separate areas for section M.

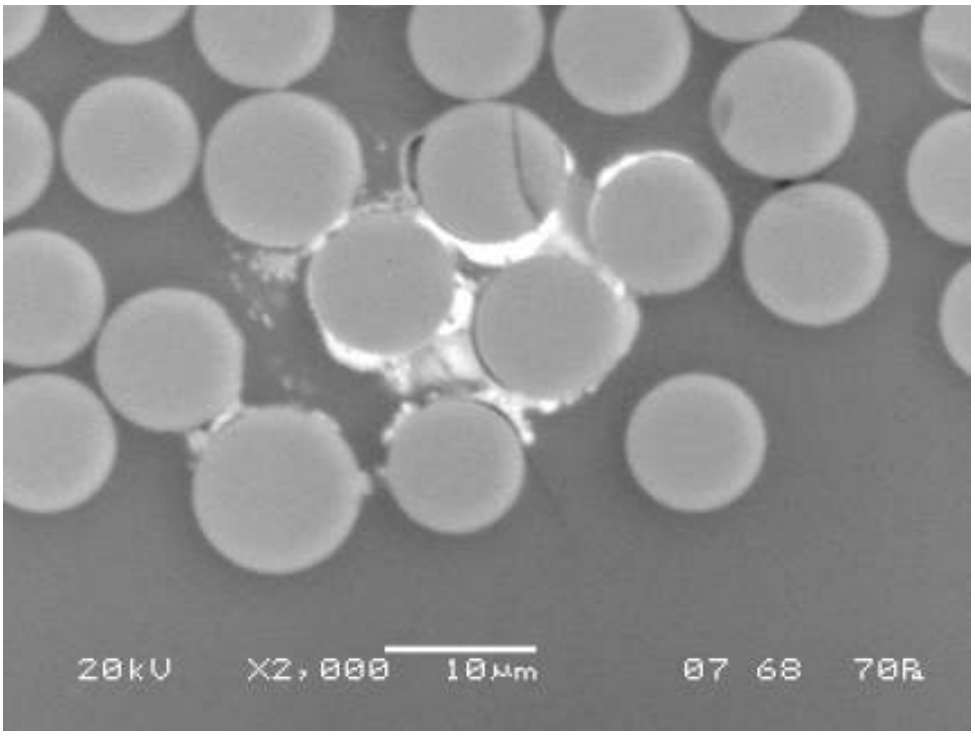

(a)

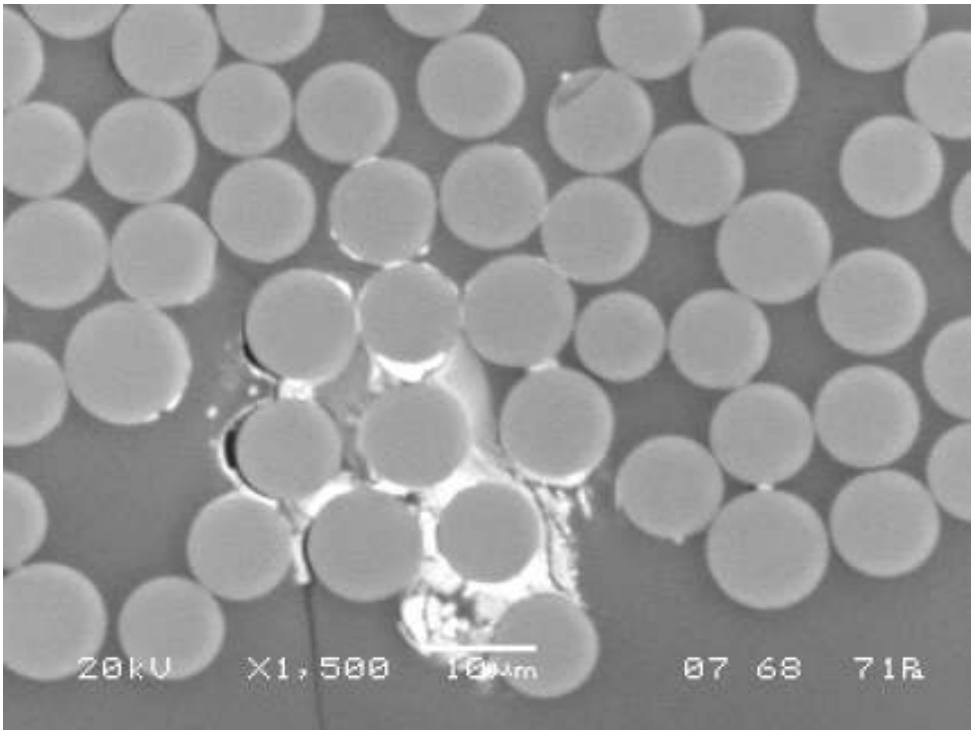

(b)

Figure C.18: A higher magnification image of the PEPG processed coupon of the copper compound in the polymer matrix and CAF for section M in (a) area 3 and (b) area 4.

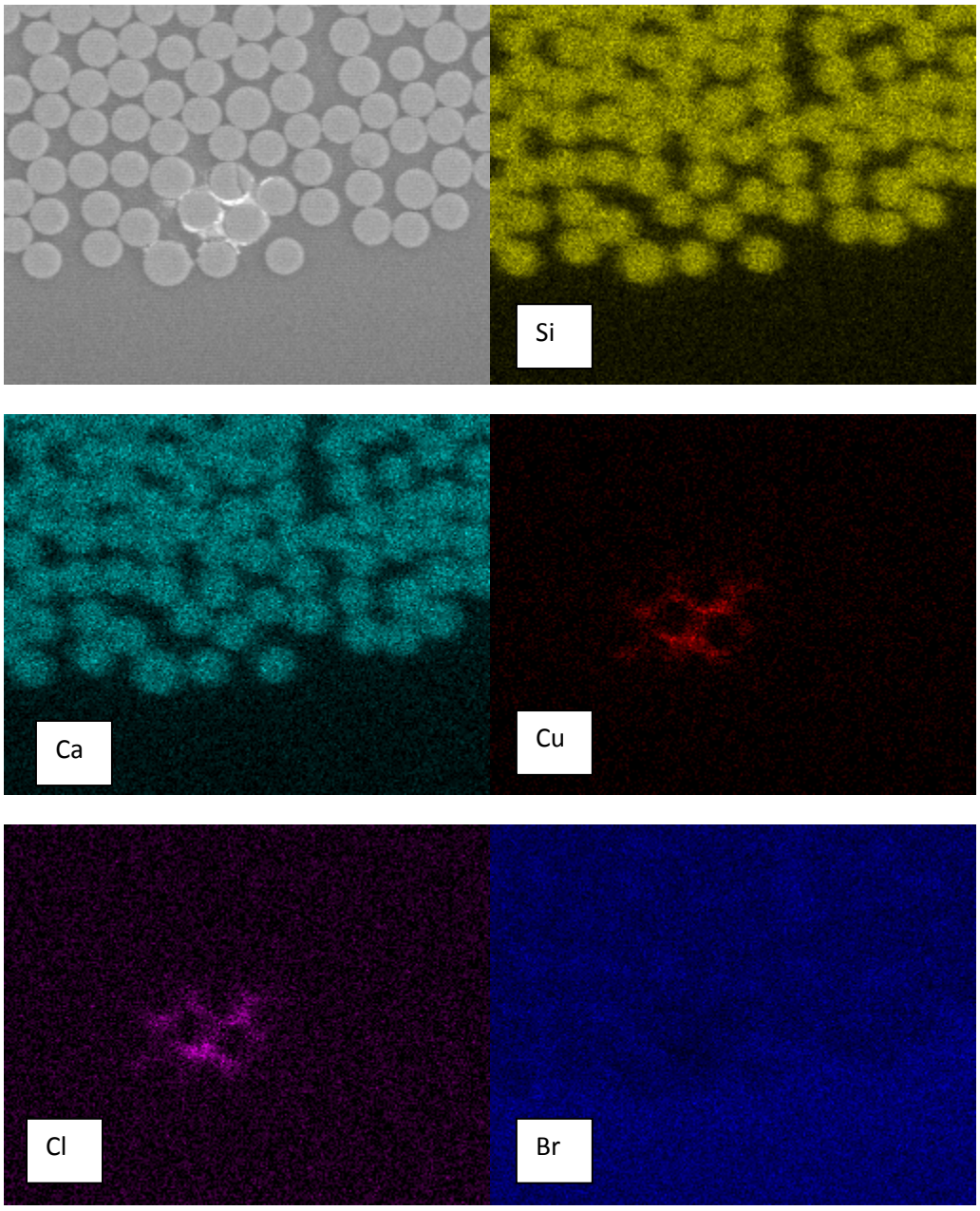

Figure C.19: EDS map of the PEPG processed coupon showing CAF and copper compound in the polymer matrix in area 3 for section M.

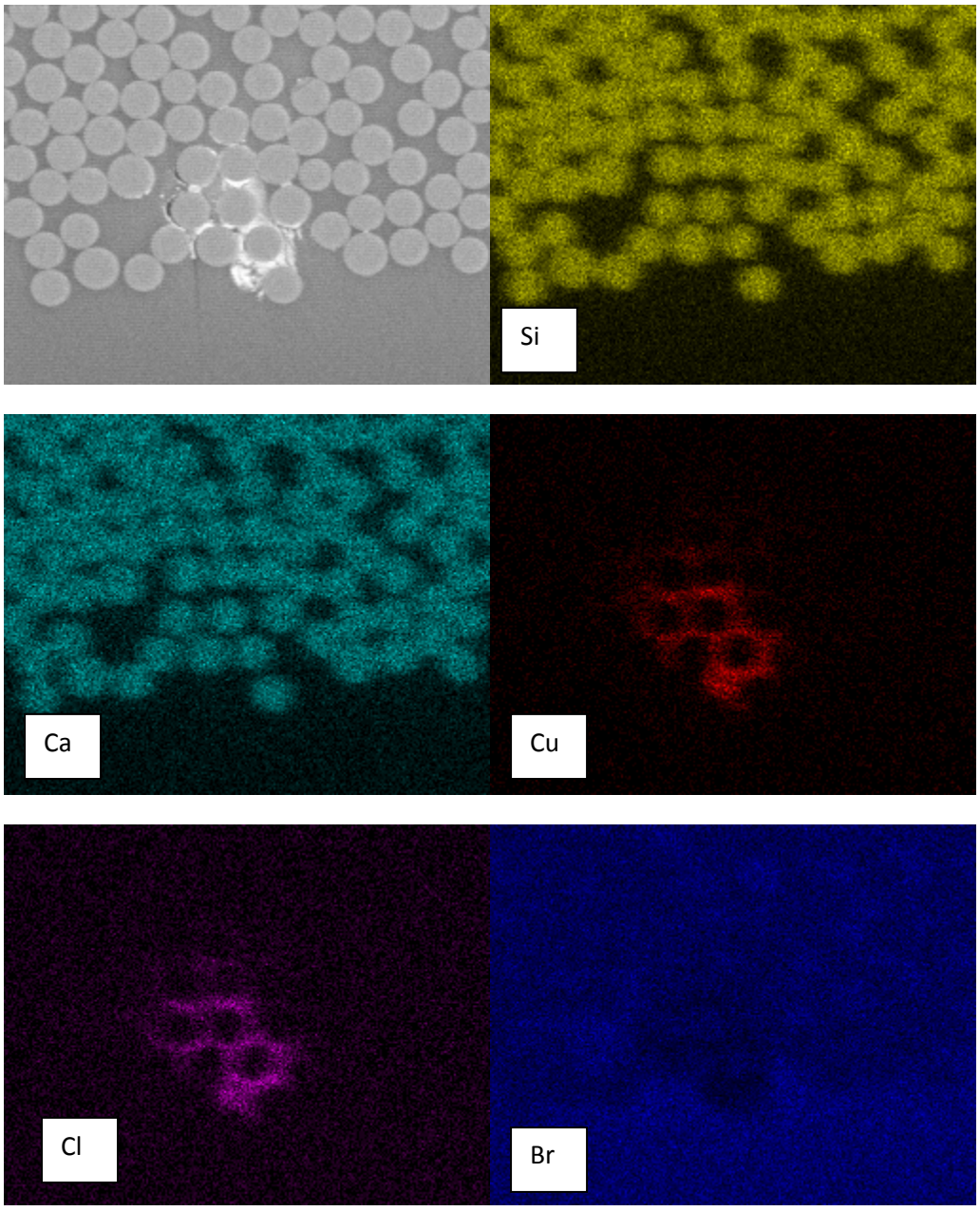

Figure C.20: EDS map of the PEPG processed coupon showing CAF and the copper compound in the polymer matrix for area 4 in section M.

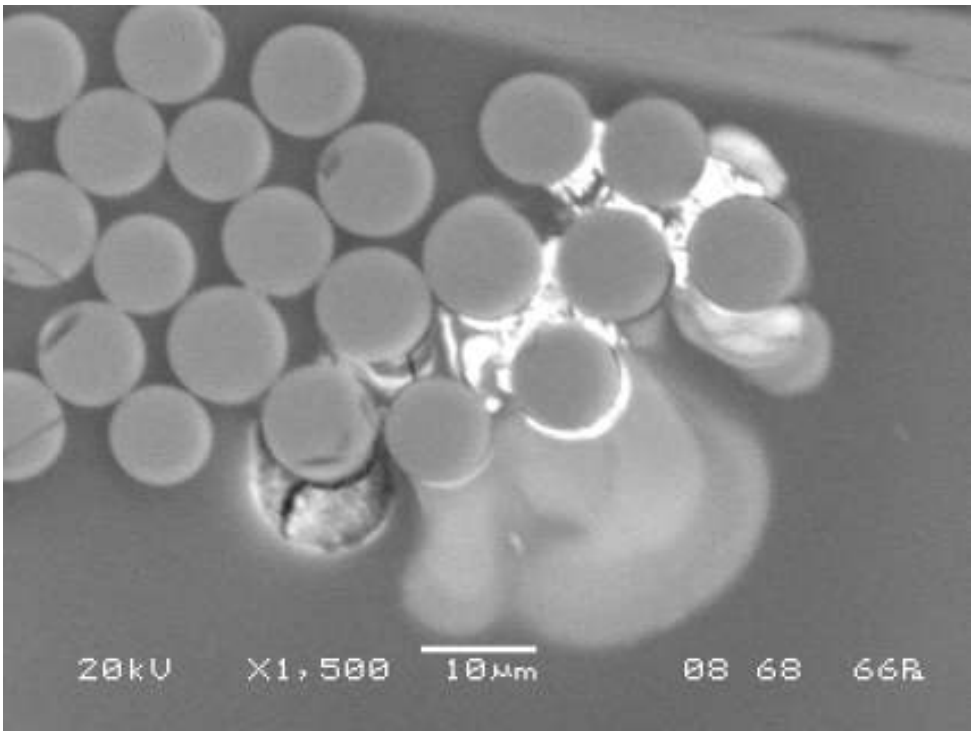

Figure C.21: A PEPG processed coupon showing CAF and a copper compound in the polymer matrix for section N.

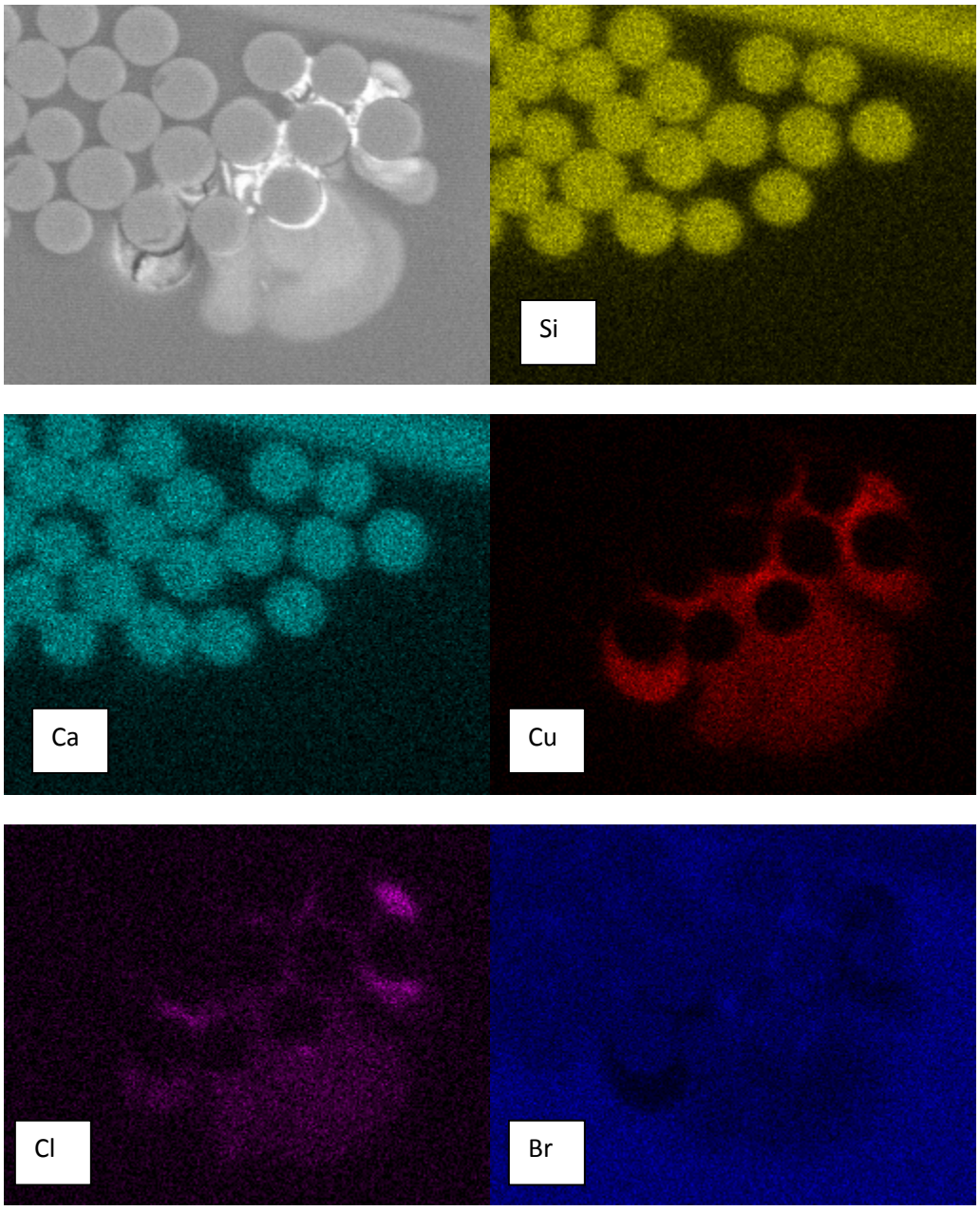

Figure C.22: EDS map of the PEPG processed coupon for the CAF and copper compound in the polymer matrix for section N.

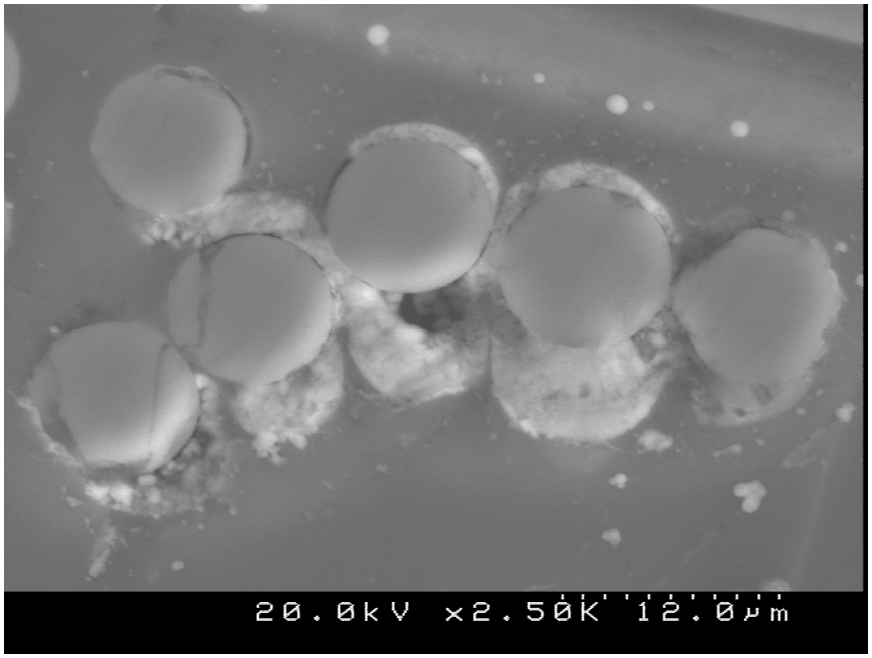

Figure C.23: A PEPG processed coupon showing CAF and a copper compound in the polymer matrix beginning to form.

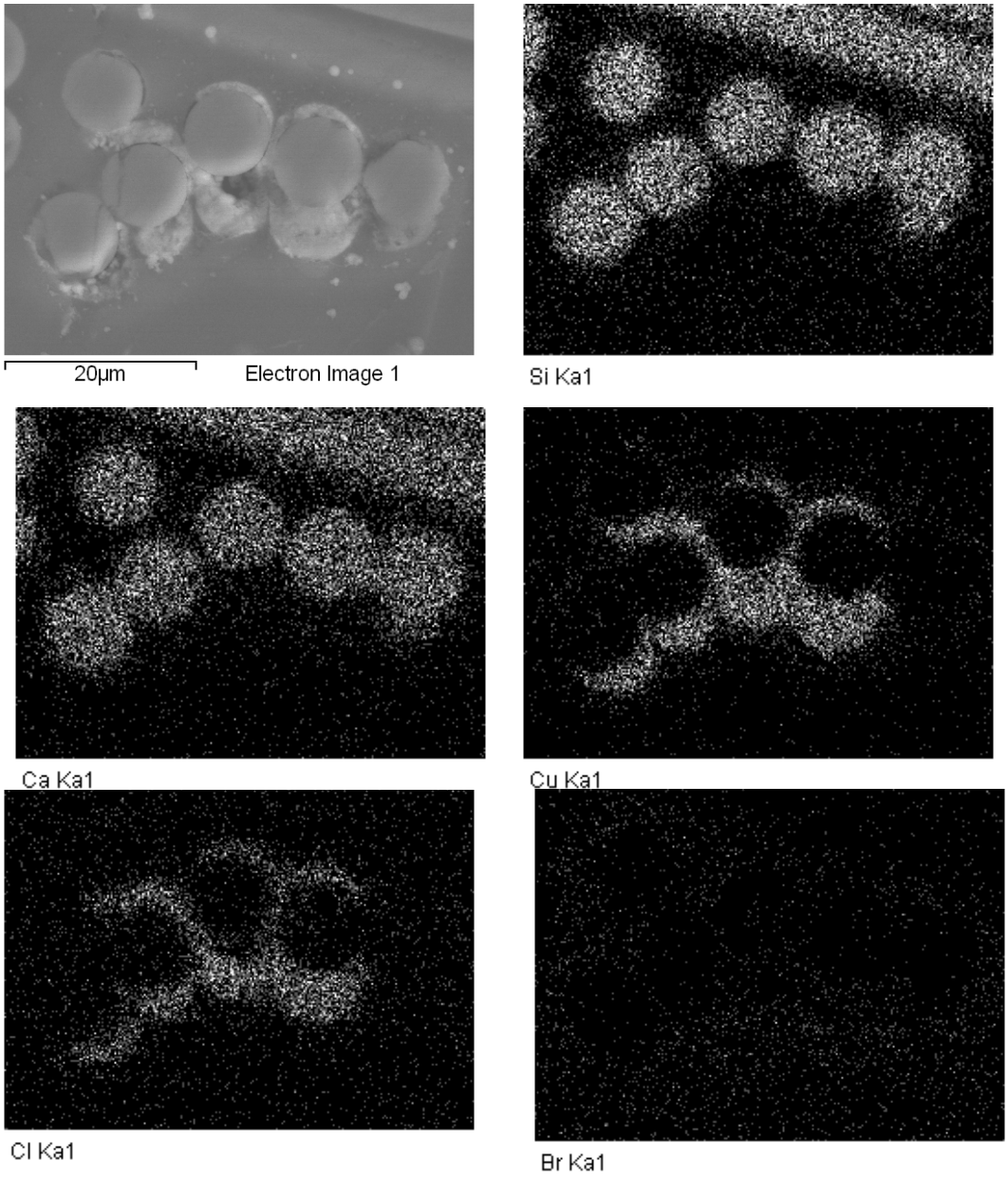

Figure C.24: EDS map of PEPG processed coupon presented in Figure C.23.

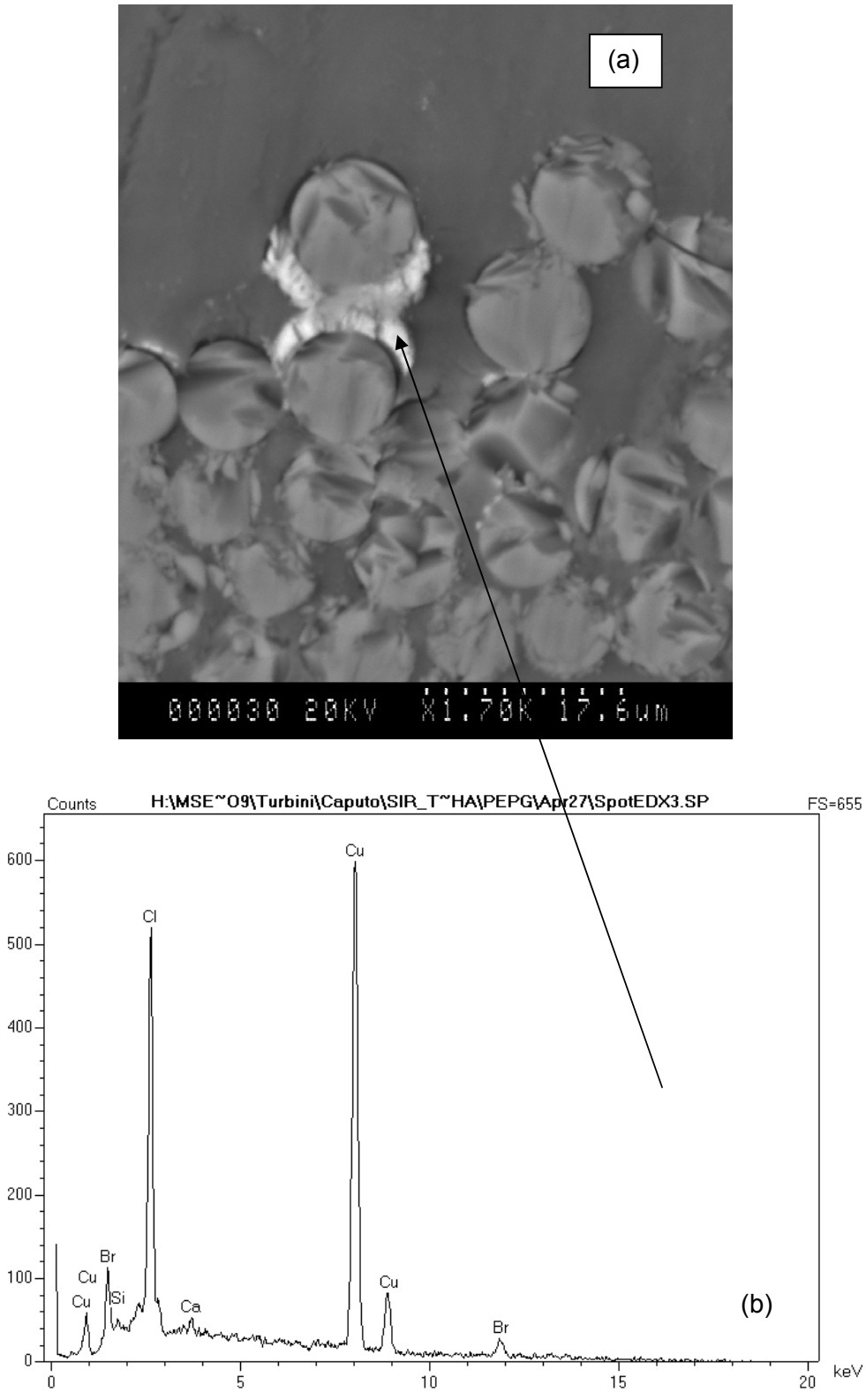

Figure C.25: SEM image and spot EDS for a PEPG a processed coupon.

Appendix D: PEPG/Cl Processed coupons

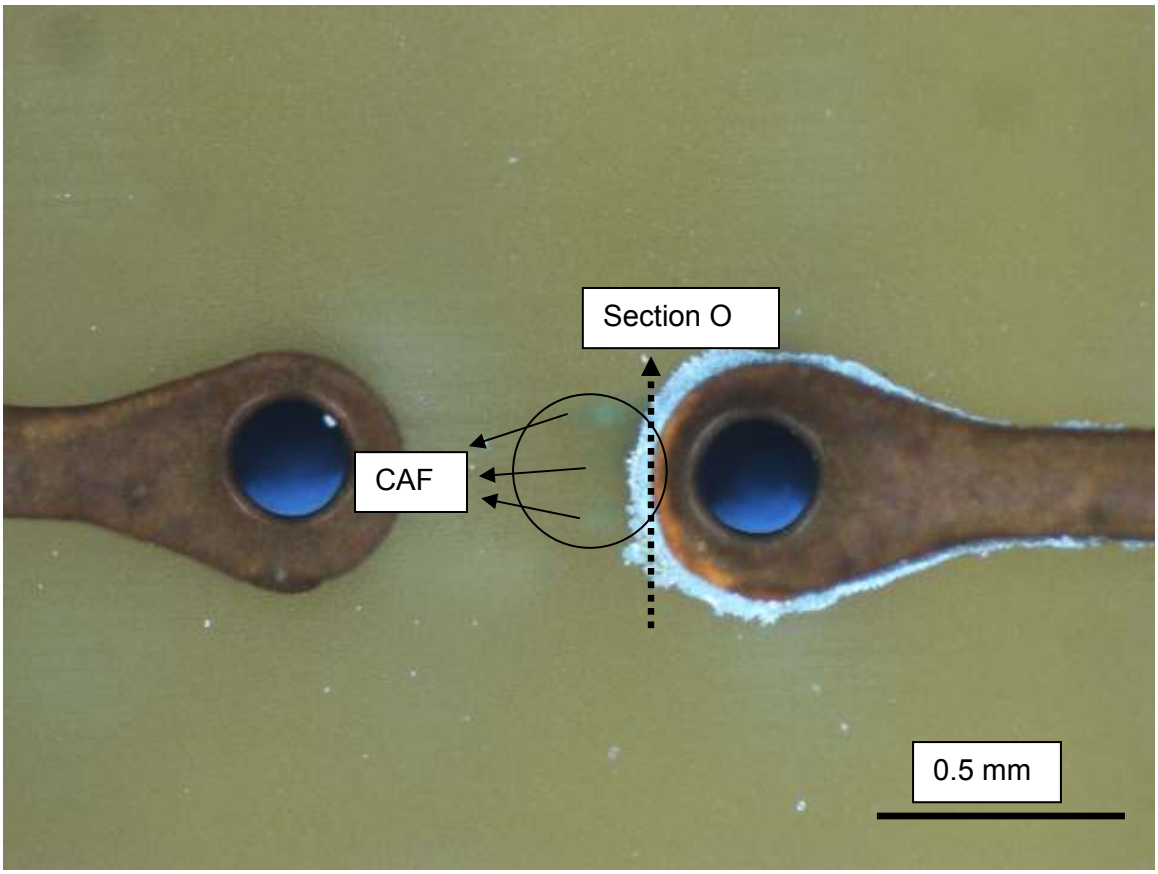

Figure D.1: Optical image showing CAF for a PEPG/Cl processed coupon.

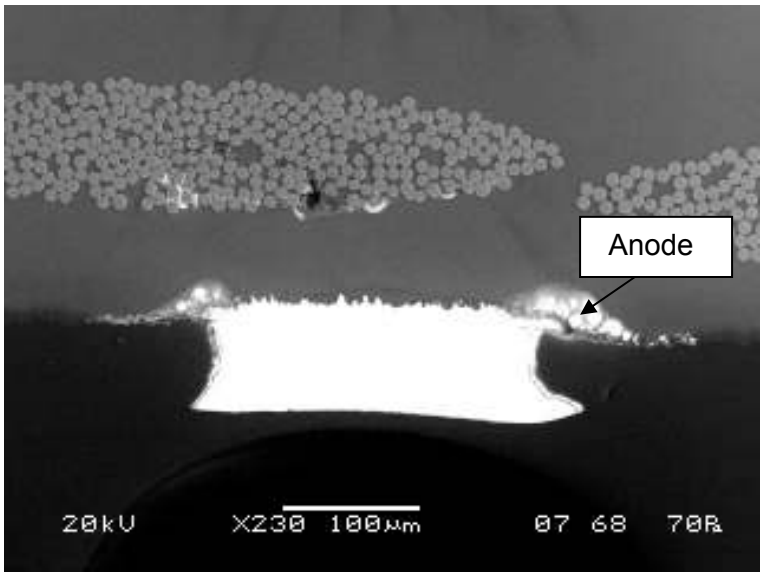

Figure D.2: Low magnification SEM image of section O, illustrating CAF and the copper compound observed in the polymer matrix for a coupon processed with PEPG/Cl.

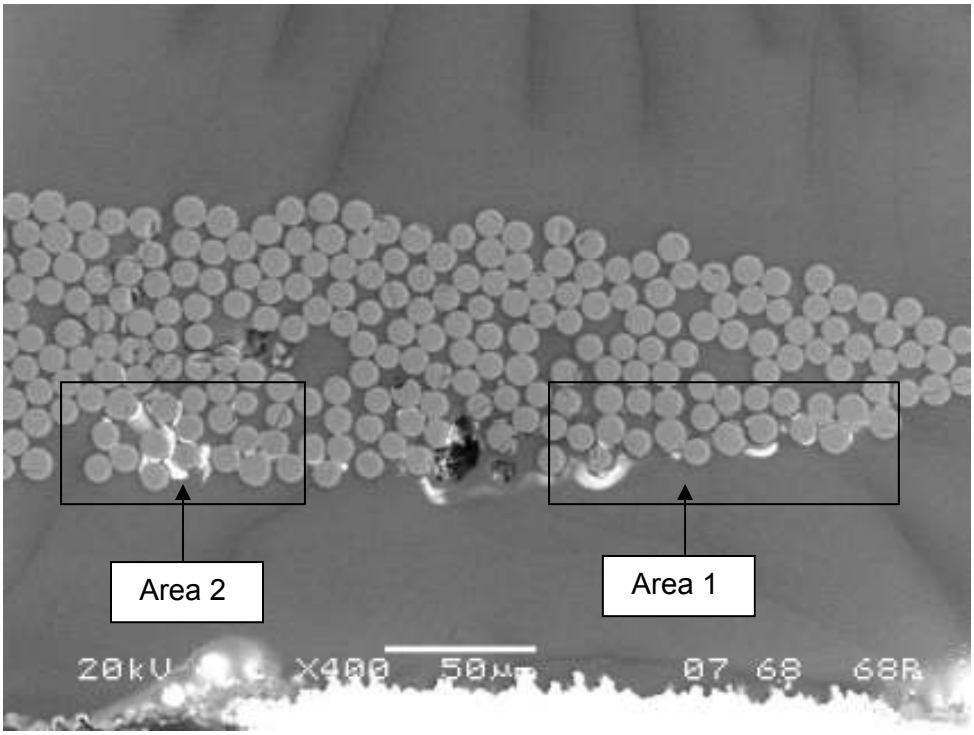

Figure D.3: Higher magnification SEM image of section O in Figure D.2, showing CAF and the copper compound in the polymer matrix found in two separate areas for the PEPG/Cl processed coupon.

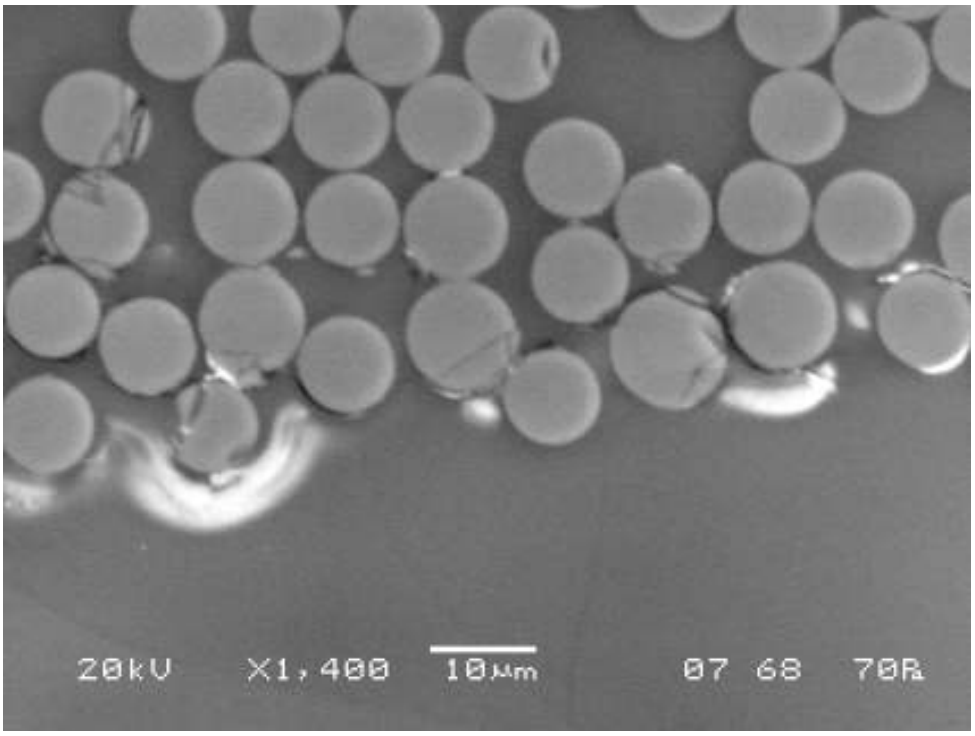

Figure D.4: CAF and the copper compound in the polymer matrix found in area 1 for the PEPG/Cl processed coupon (i.e section O).

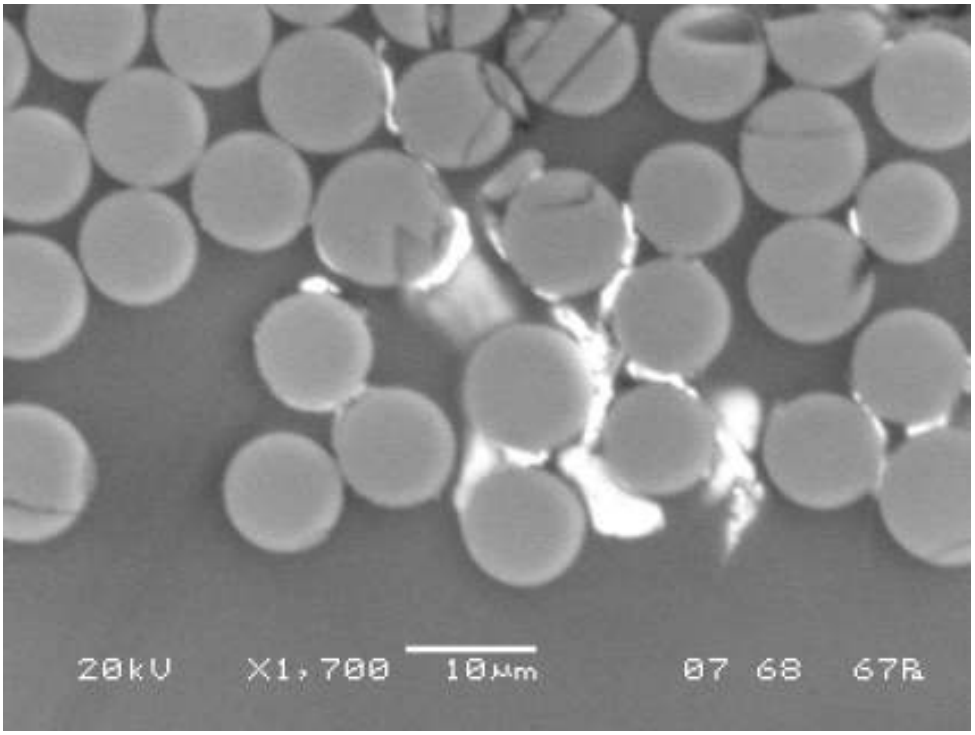

Figure D.5: CAF and the copper compound in the polymer matrix found in area 2 for the PEPG/Cl processed coupon (i.e section O).

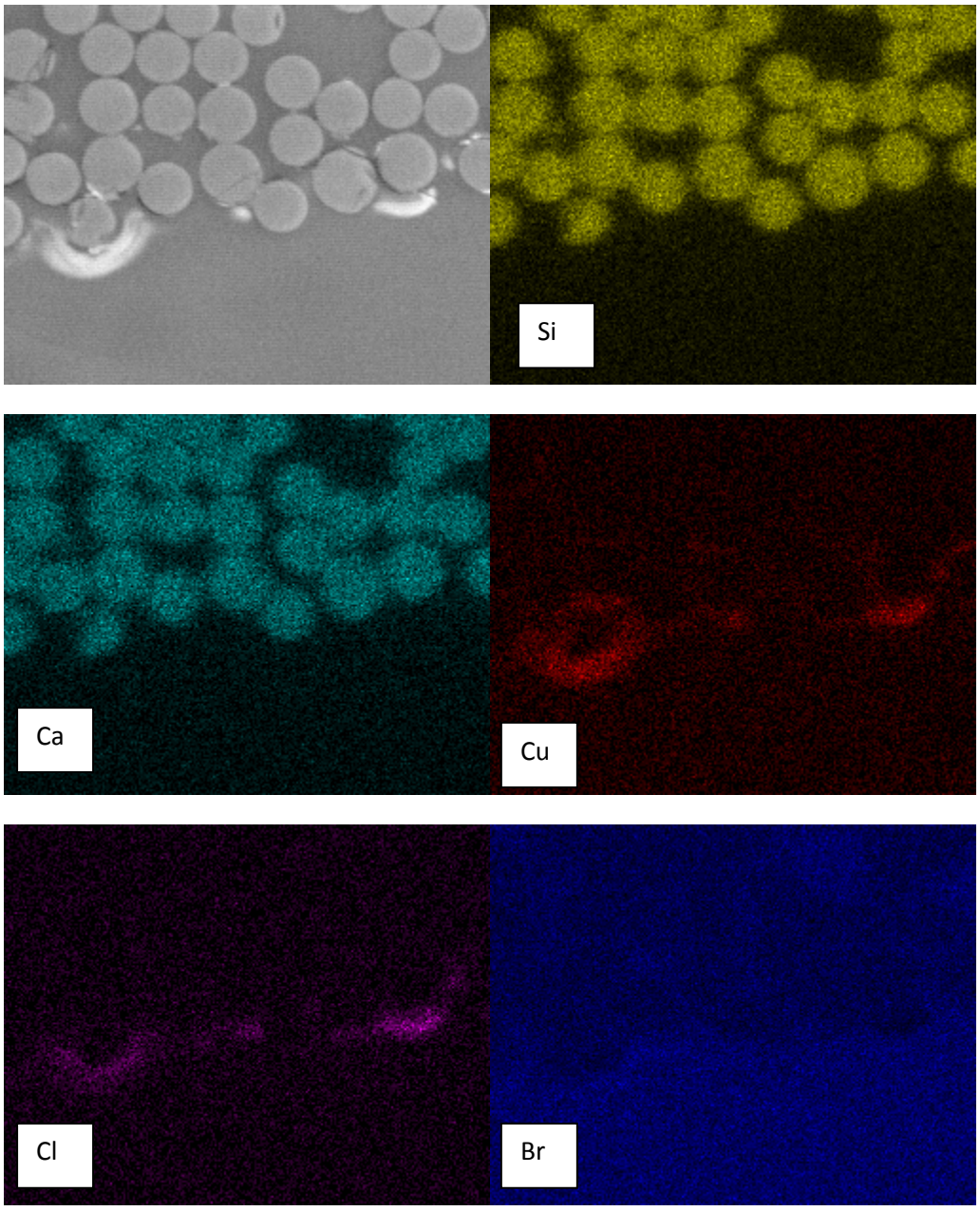

Figure D.6: EDS map of area 1 for section O confirming the presence of copper and chlorine for the PEPG/Cl processed coupon.

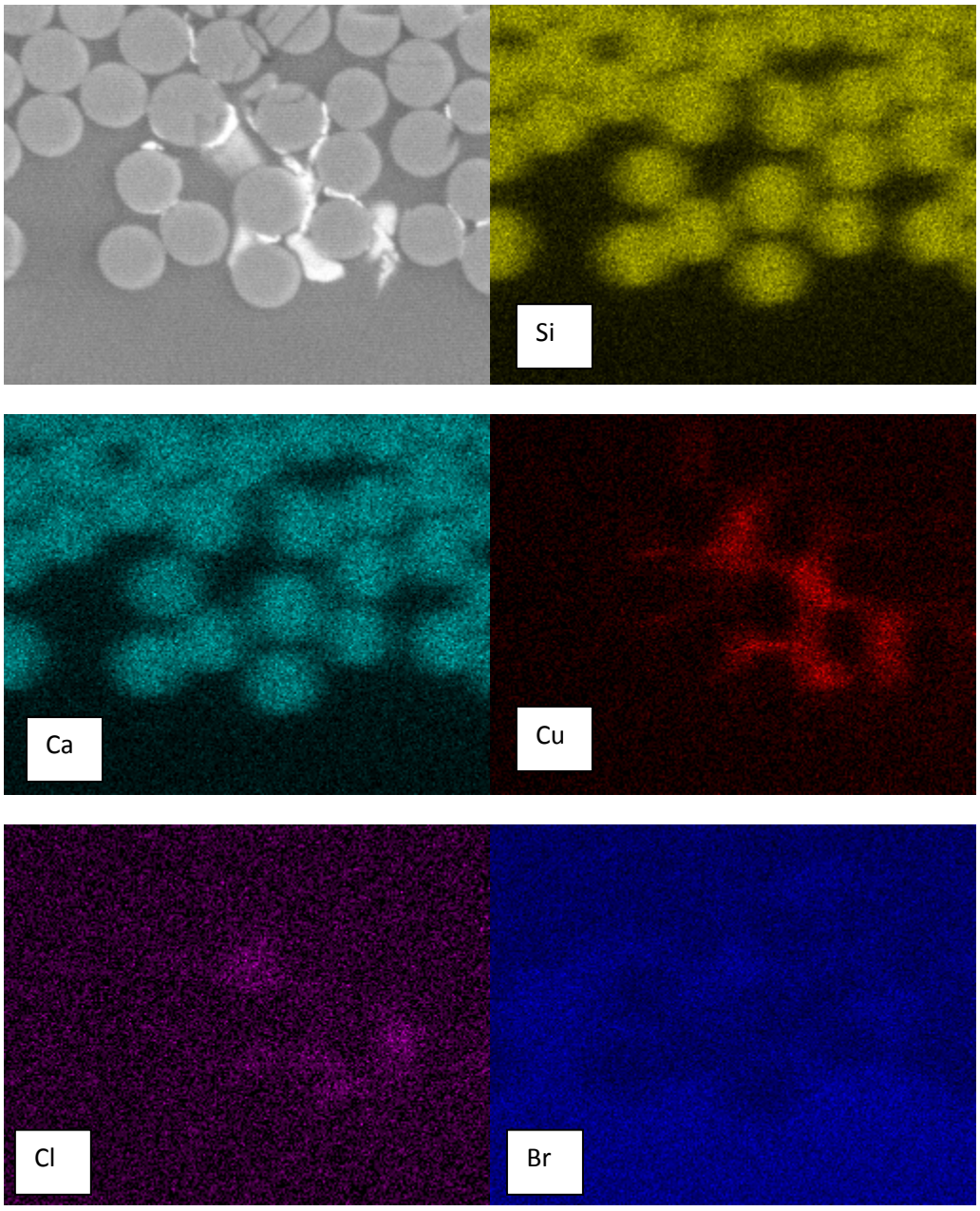

Figure D.7: EDS map of area 2 for section O confirming the presence of copper and chlorine for the PEPG/Cl processed coupon.

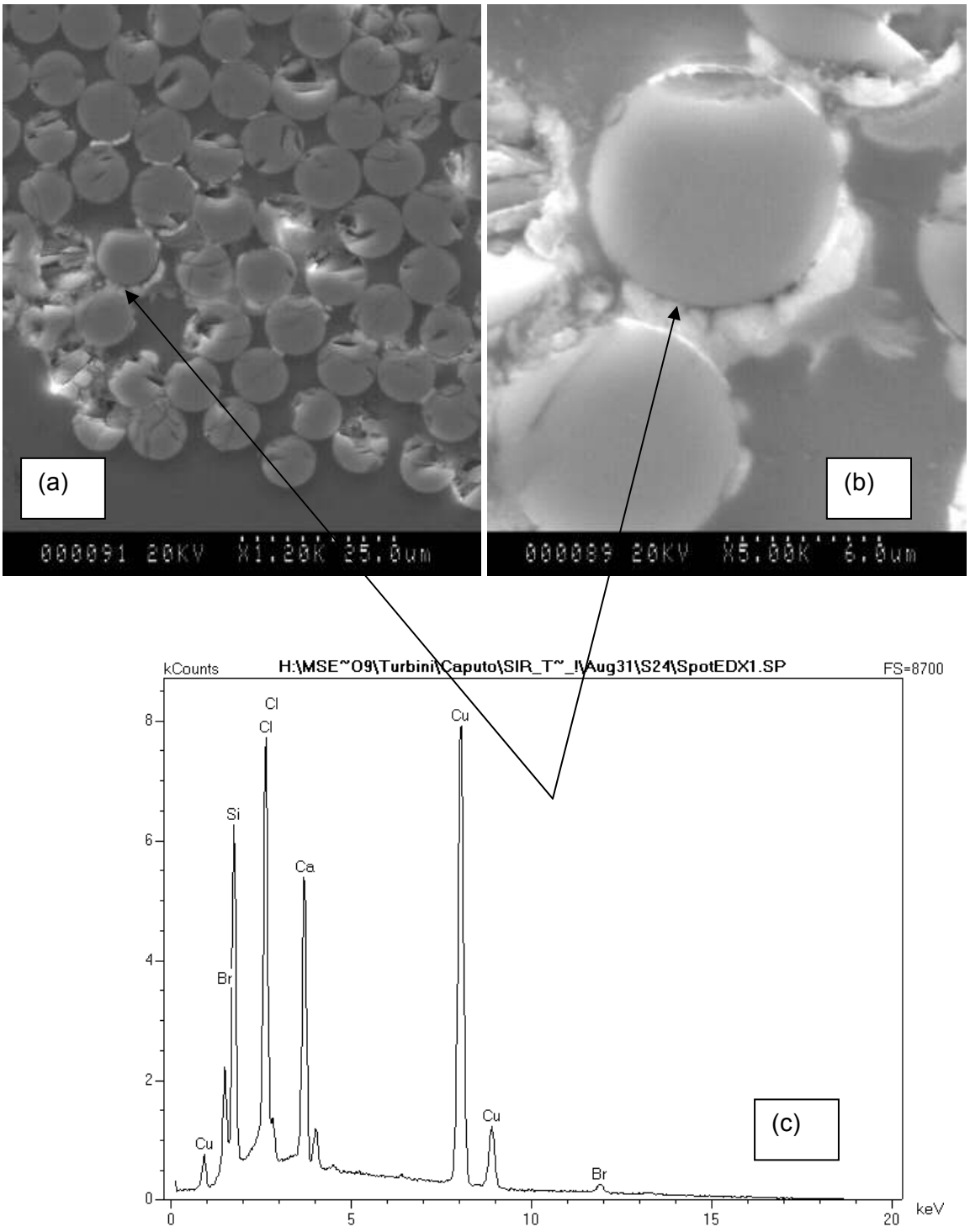

Figure D.8: SEM image at (a) low magnification, (b) high magnification of the area where a spot EDS was performed, and (c) spot EDS confirming the presence of copper and chlorine for a PEPG/Cl processed coupon where CAF was observed.

Appendix E: PEG processed coupons

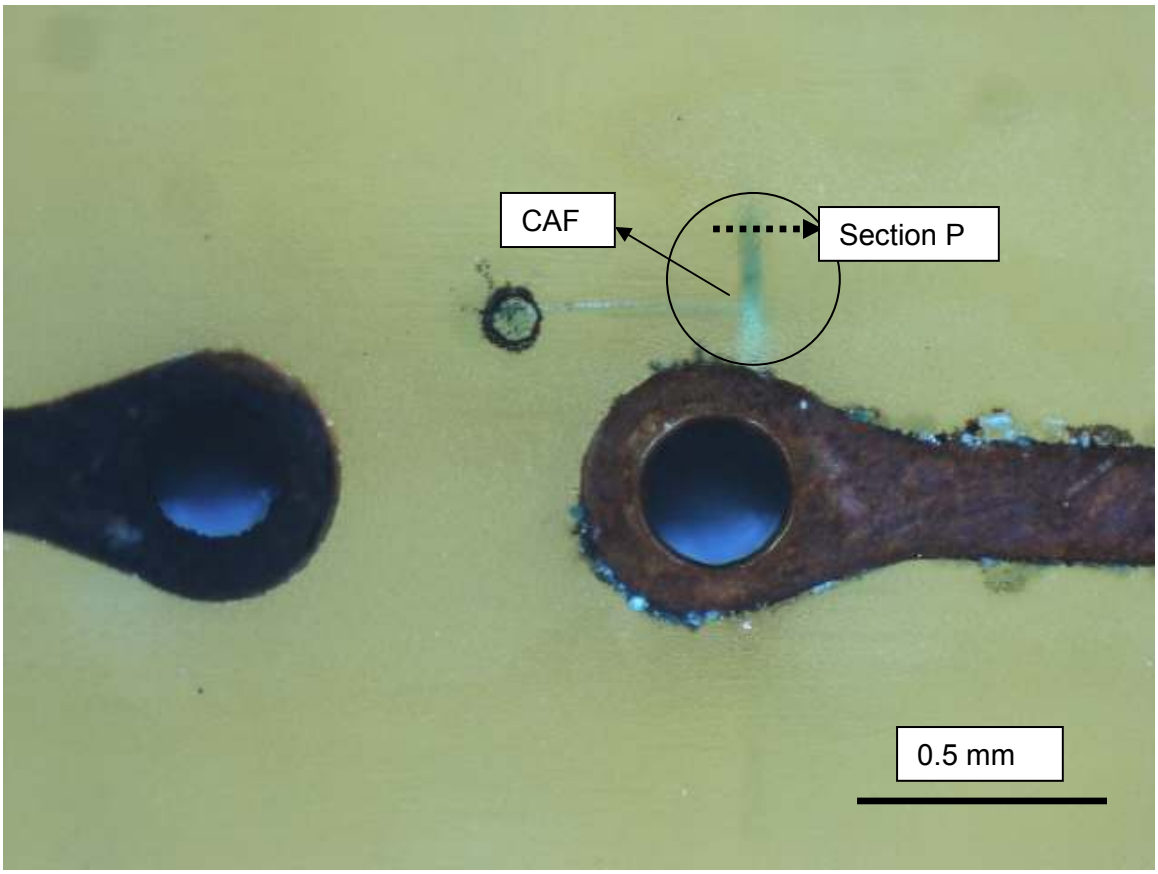

Figure E.1: Optical image illustrating CAF for a PEG processed coupon.

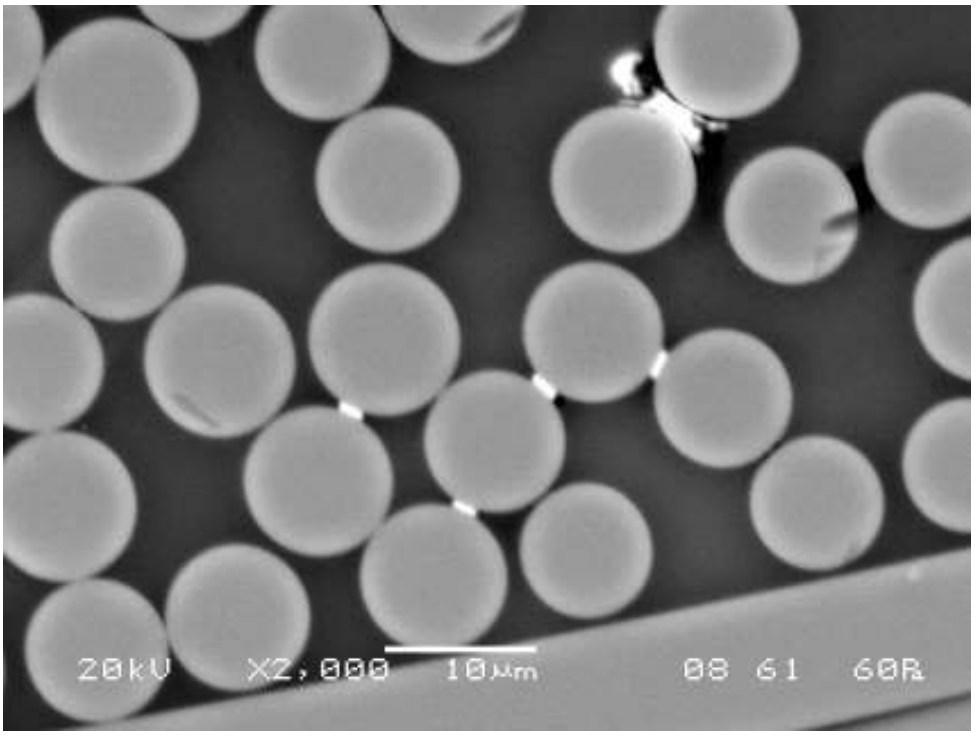

Figure E.2: SEM image of CAF for section P in Figure E.1.

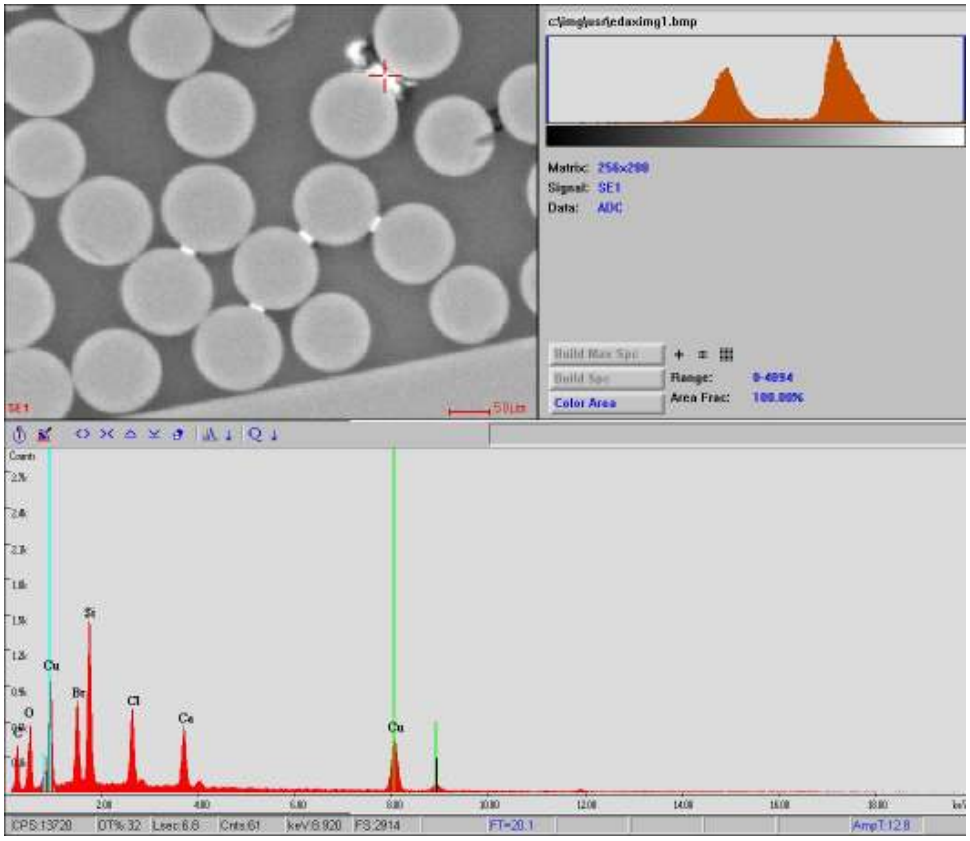

Figure E.3: Spot EDS confirming the presence of copper and chlorine for section P.

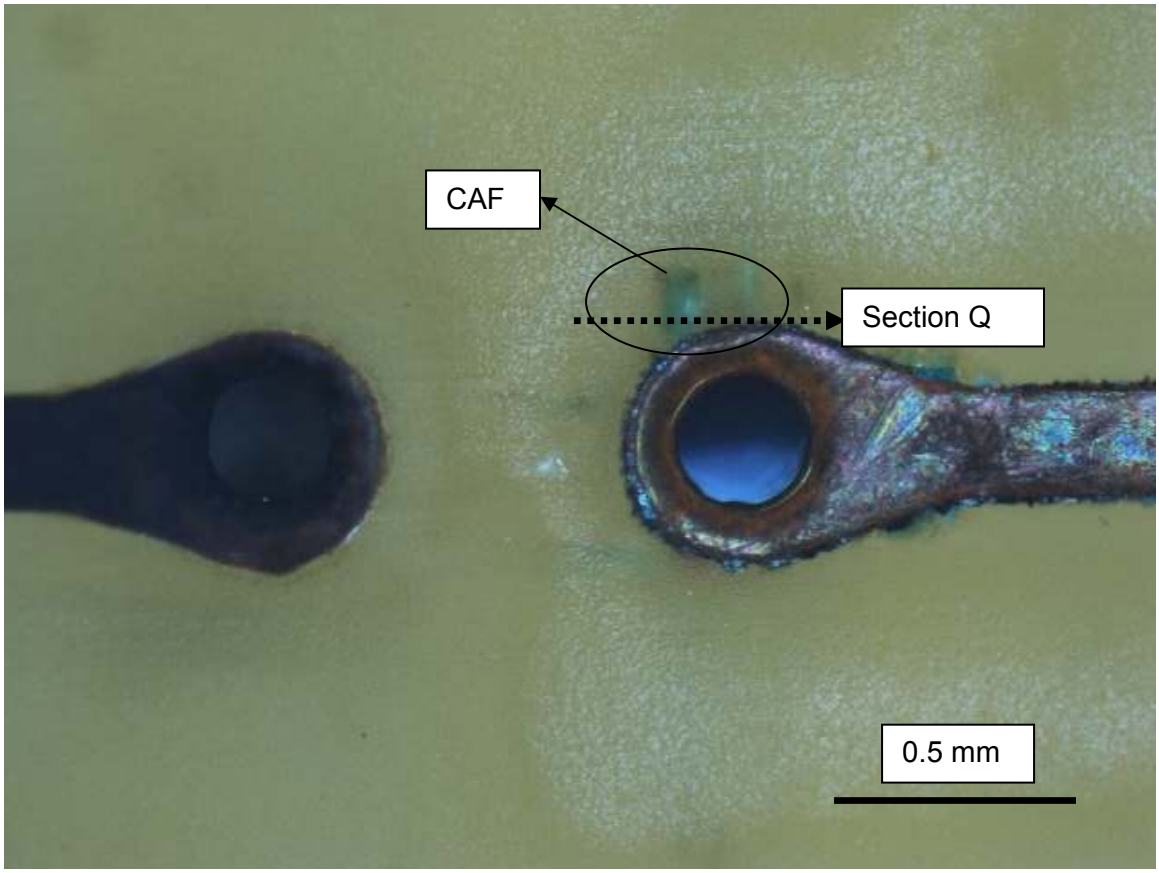

Figure E.4: Optical image illustrating CAF for a PEG processed coupon.

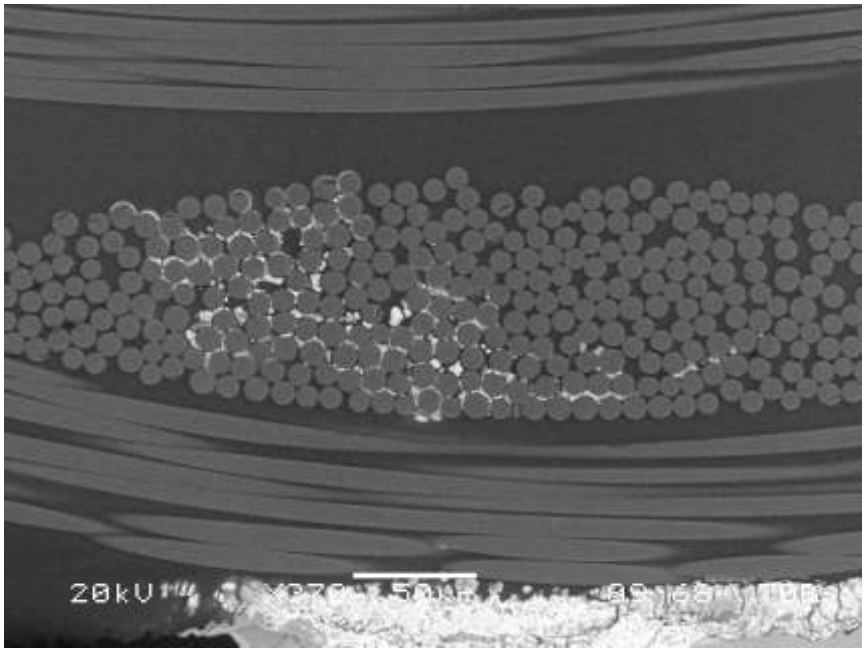

Figure E.5: Low magnification SEM image for section Q showing CAF for the PEG processed coupon.

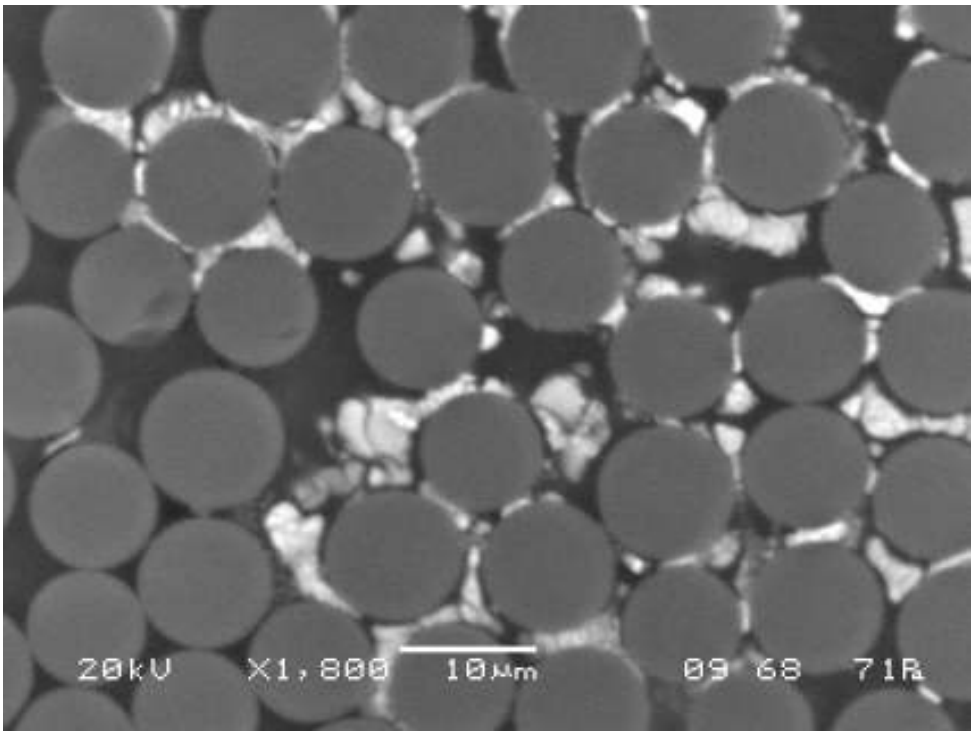

(a)

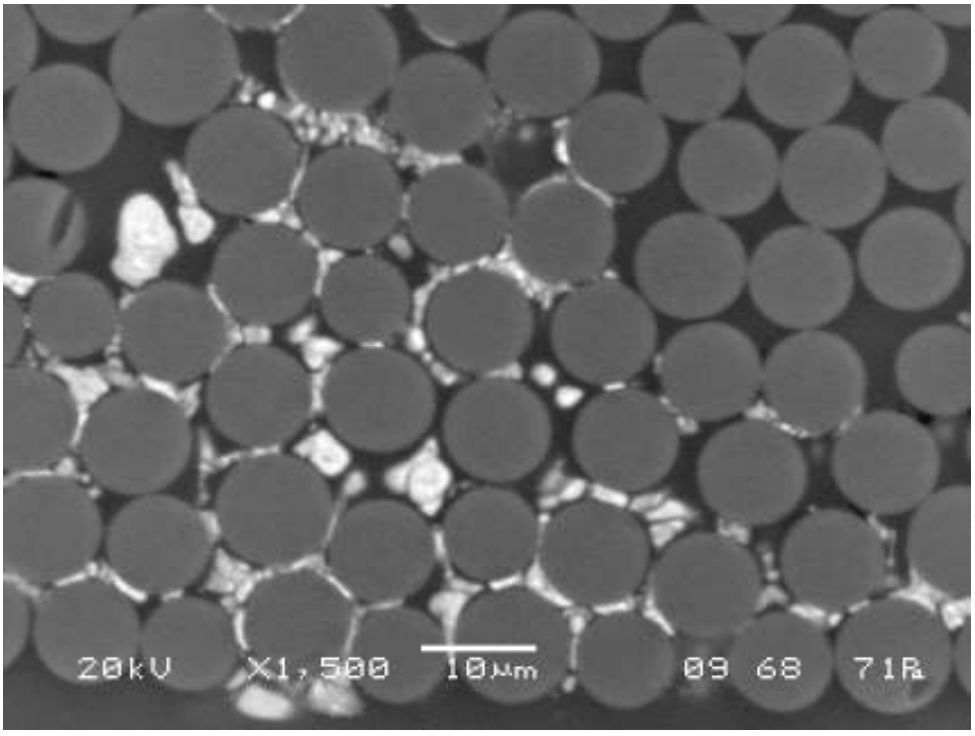

(b)

Figure E.6 High magnification SEM image for section Q showing CAF in two separate areas.

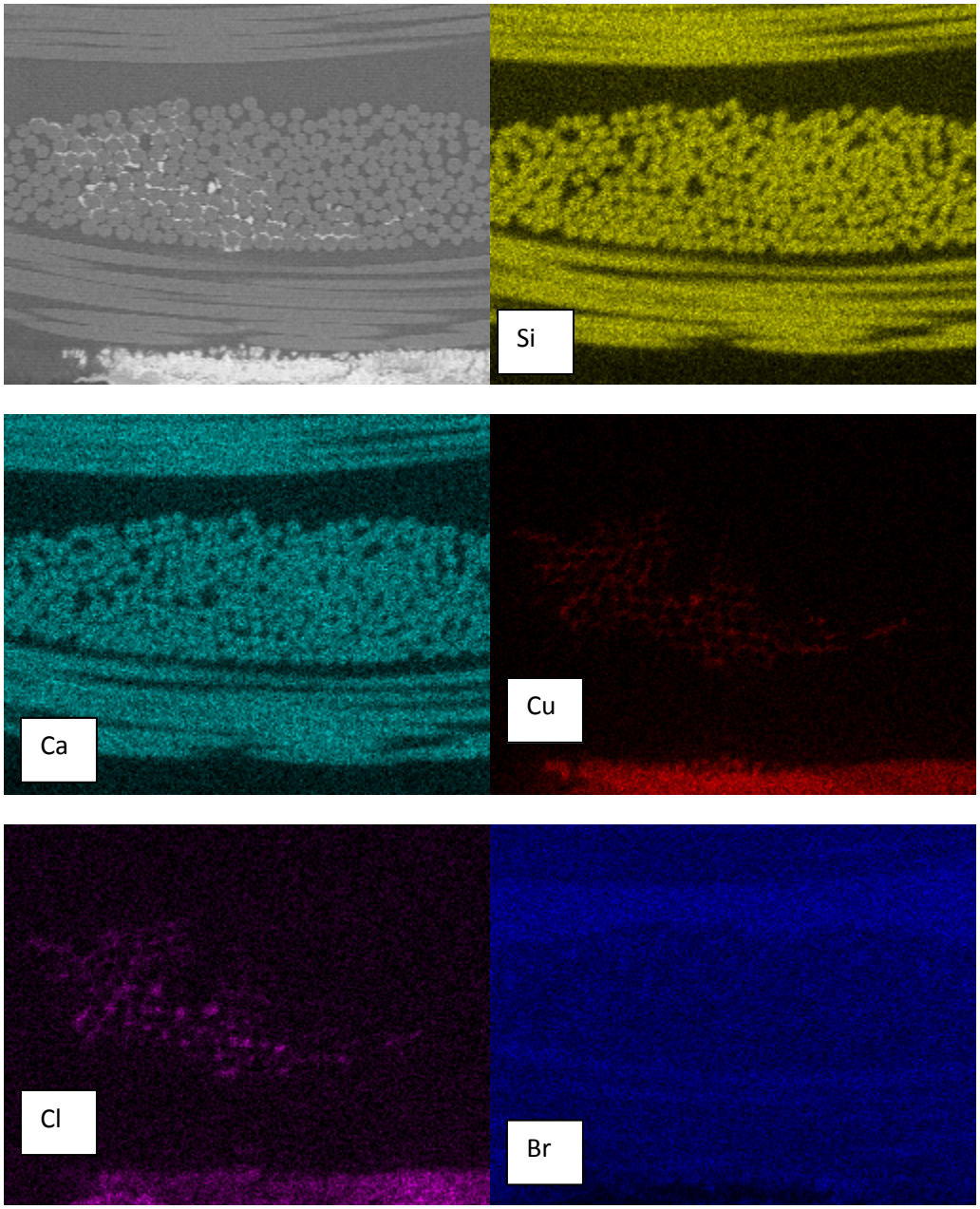

Figure E.7: EDS map at low magnification confirming the presence of copper and chlorine for section Q.

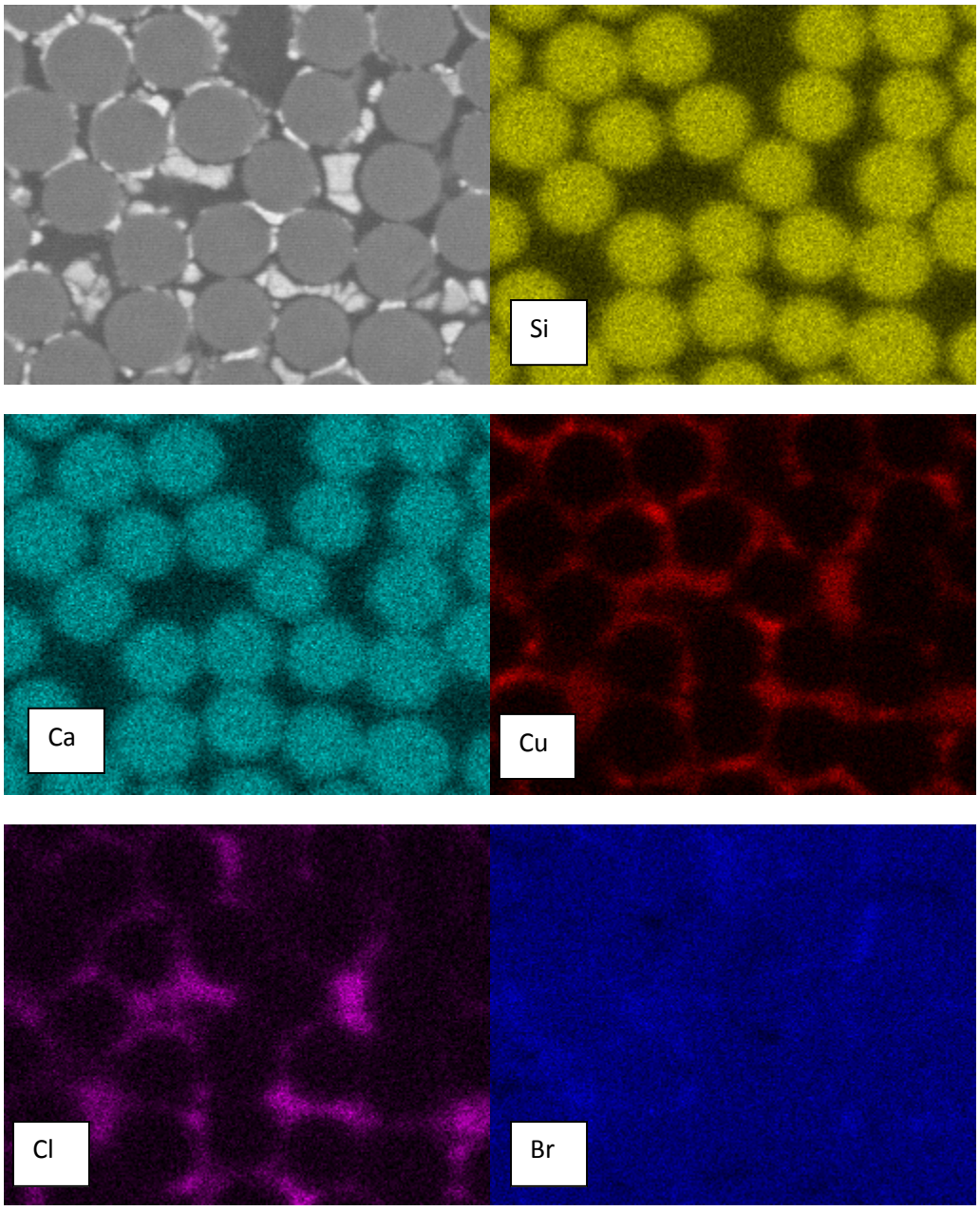

Figure E.8: EDS map at high magnification confirming the presence of copper and chlorine for section Q.

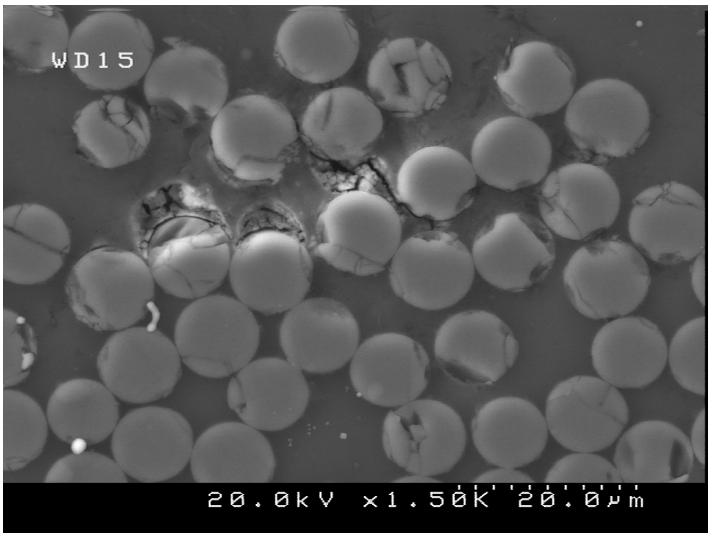

Figure E.9: SEM image illustrating CAF for a PEG processed coupon.

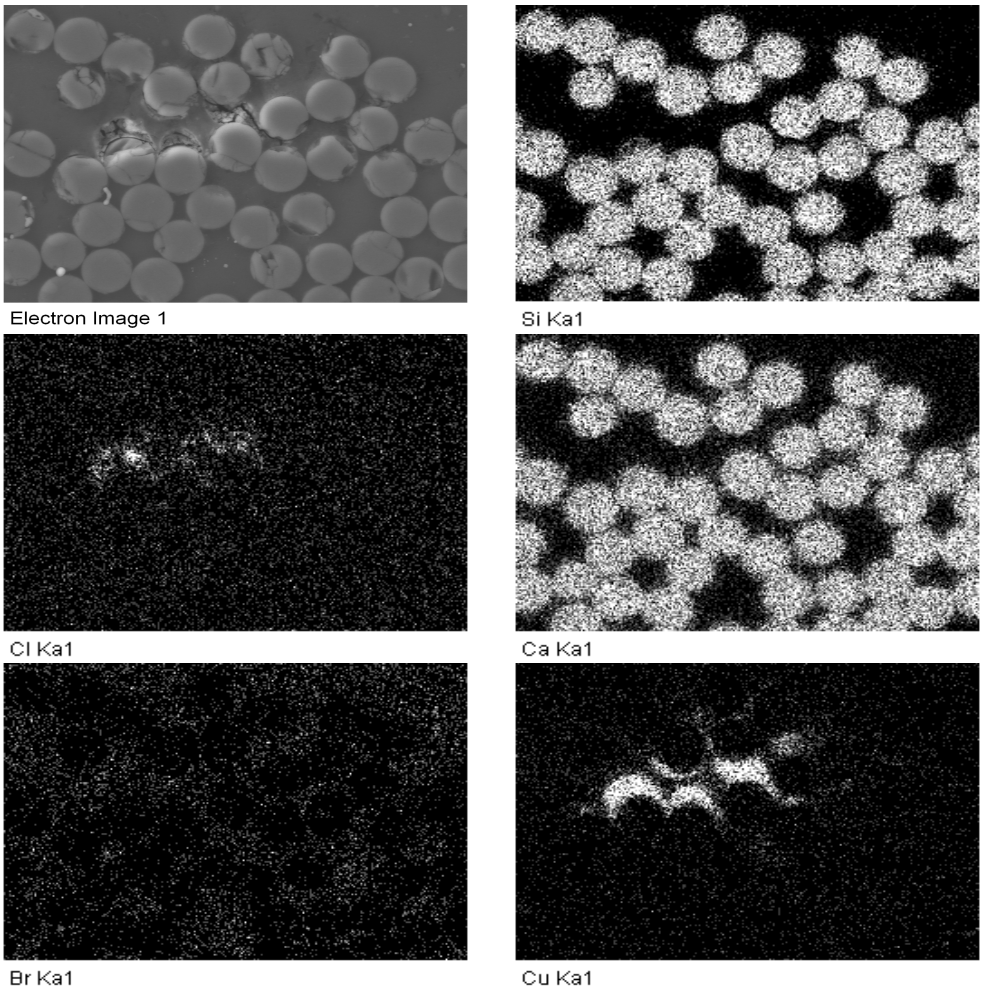

Figure E.10: EDS map at high magnification confirming the presence of copper and chlorine.

Appendix F: PEG/Cl Processed coupons

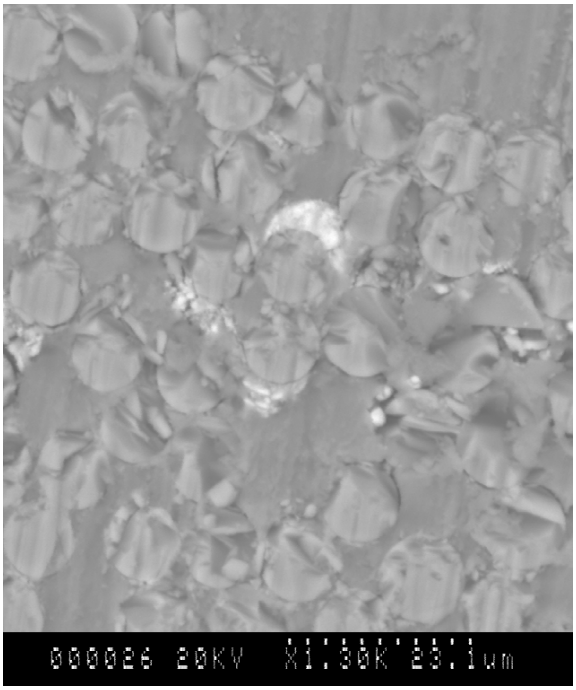

Figure F.1: An SEM cross-section illustrating CAF at a distance from the copper hole for a PEG/Cl processed coupon.

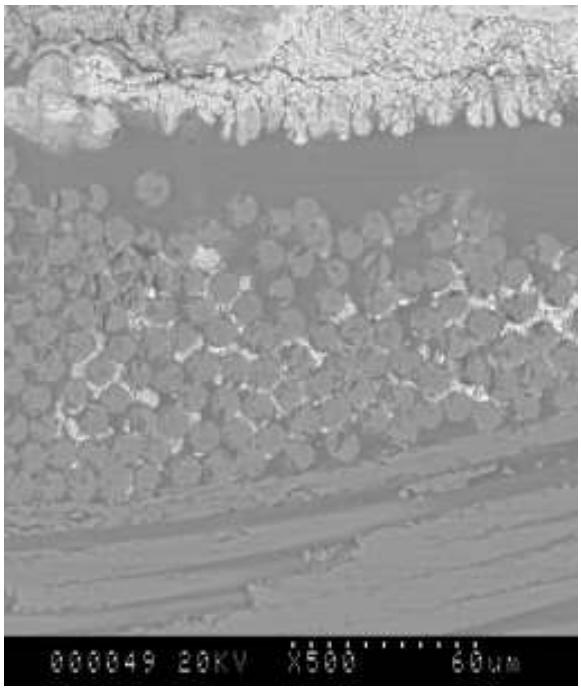

Figure F.2: The cross-section of Figure F.1 polished to the copper hole.

Appendix G: HASL Processed Coupons

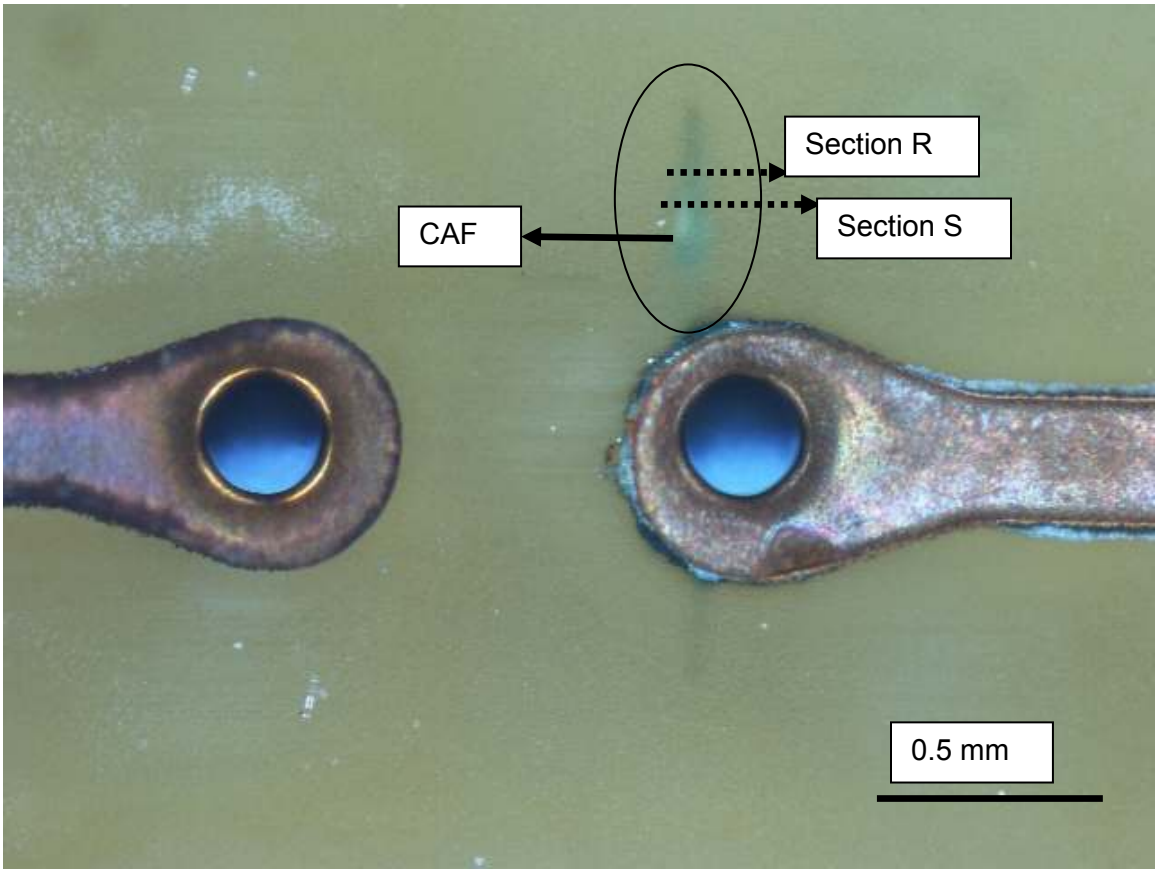

Figure G.1: Optical image illustrating CAF for a HASL processed coupon.

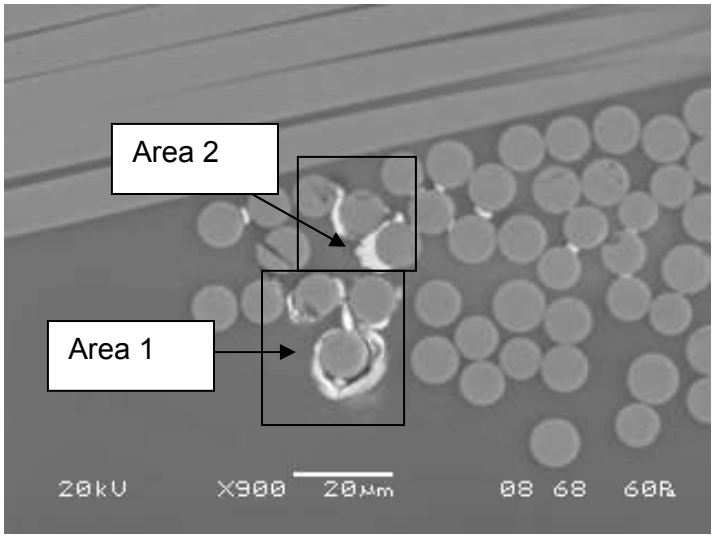

Figure G.2: Low magnification SEM image for section R demonstrating CAF for a HASL processed coupon.

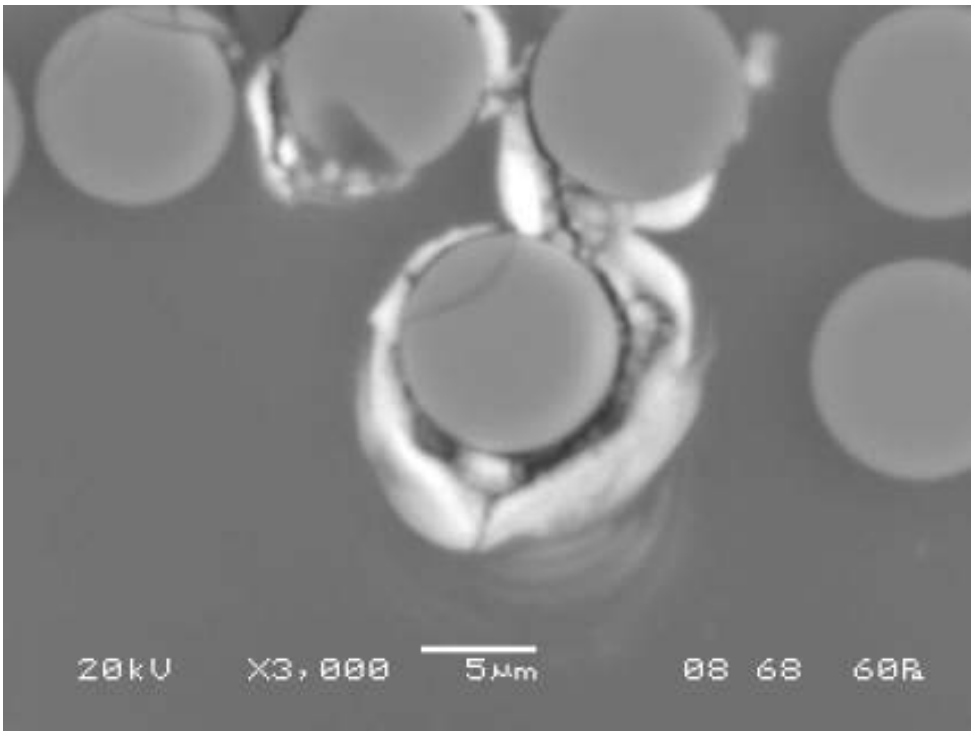

(a)

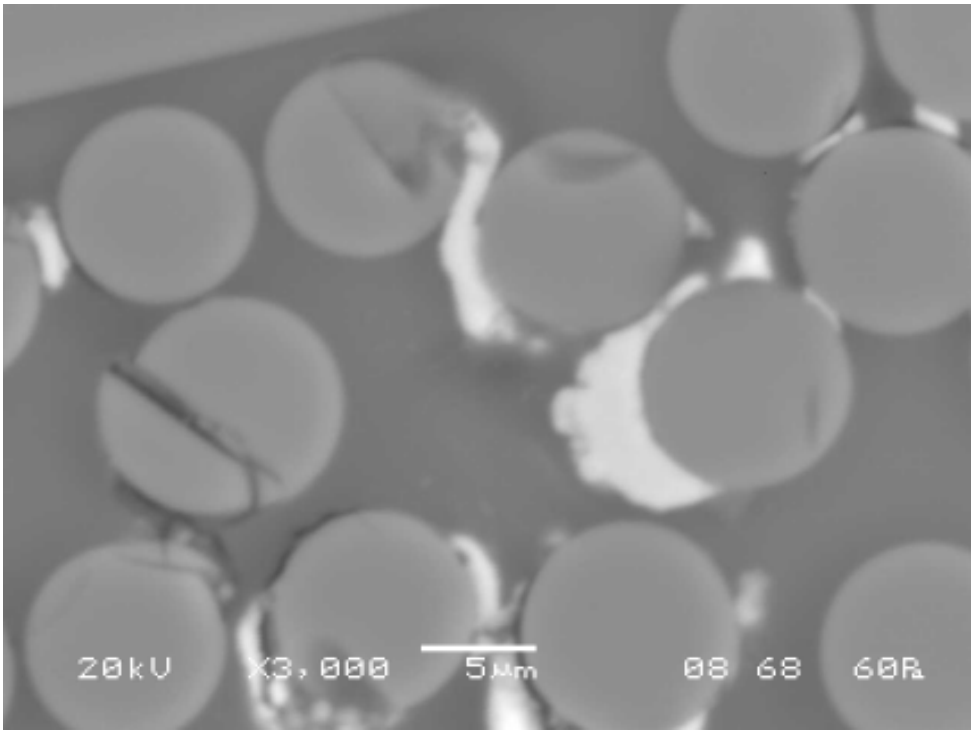

(a)

Figure G.3: High magnification SEM image for section R showing CAF in (a) area 1, and (b) area 2.

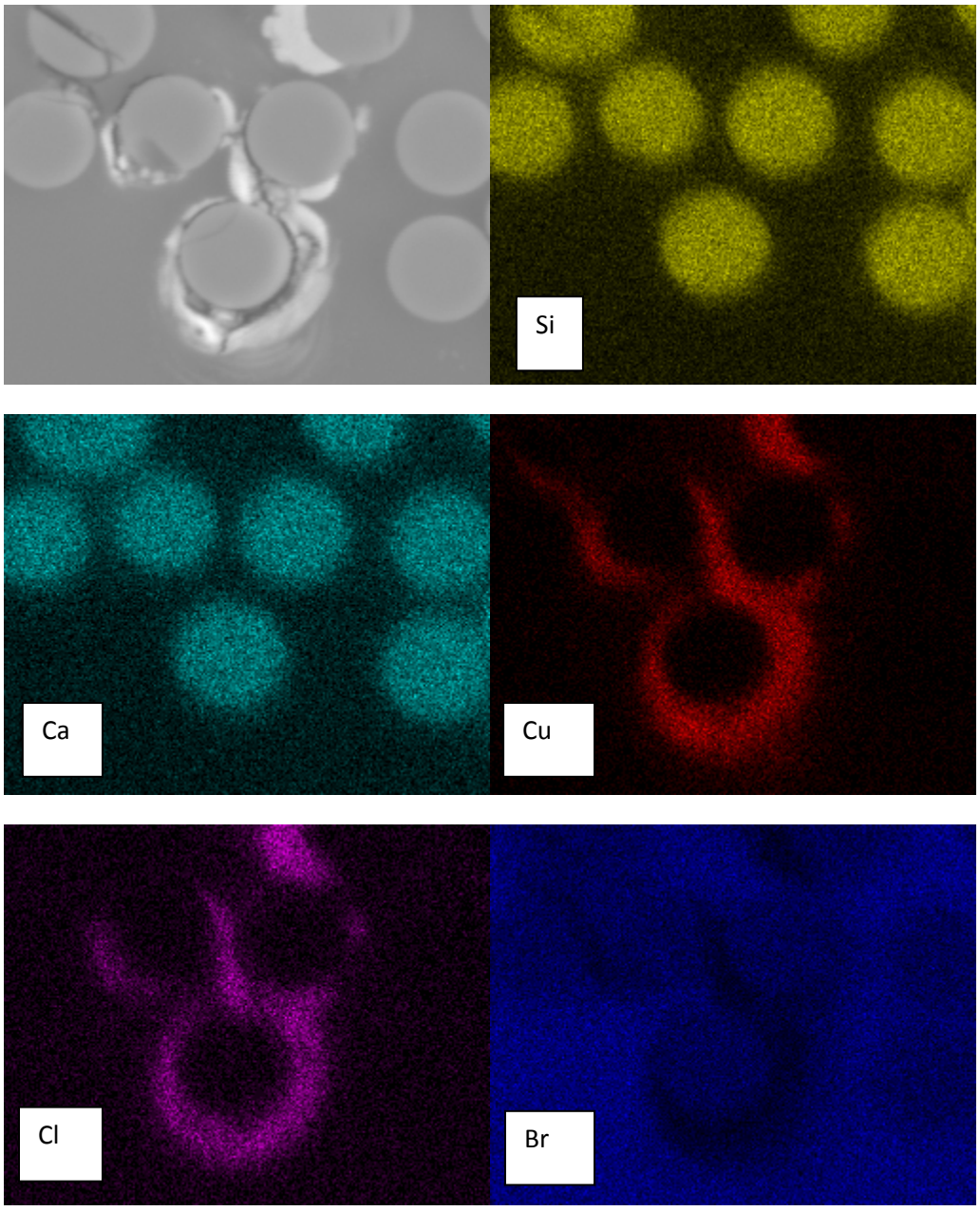

Figure G.4: EDS map of area 1 in section R confirming the presence of copper and chlorine.

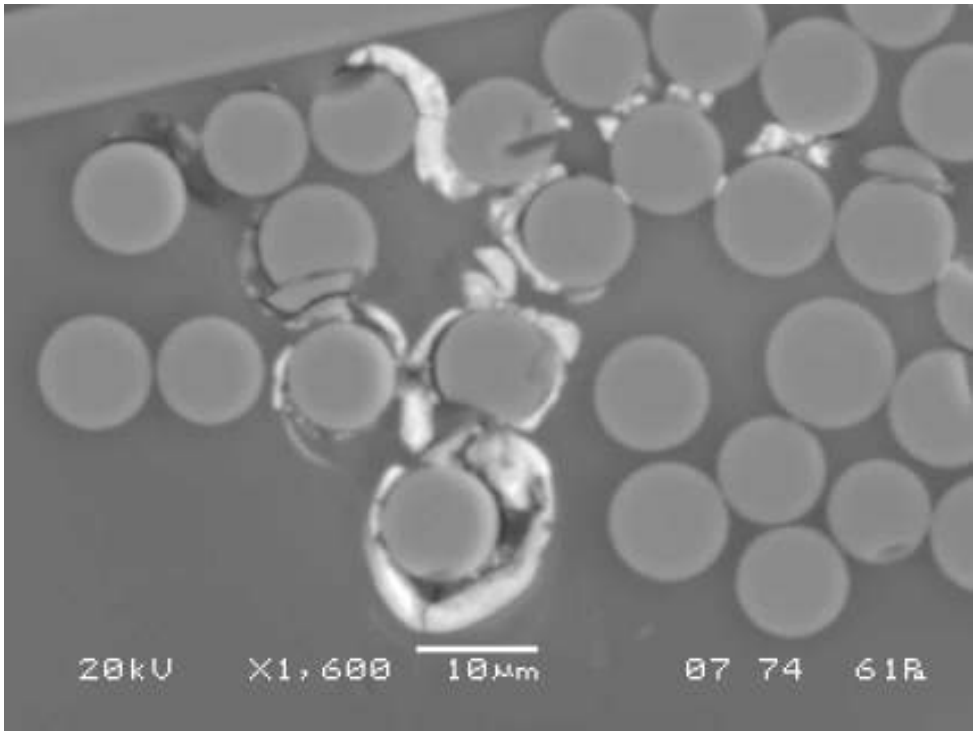

Figure G.5: SEM image of section S illustrating CAF.

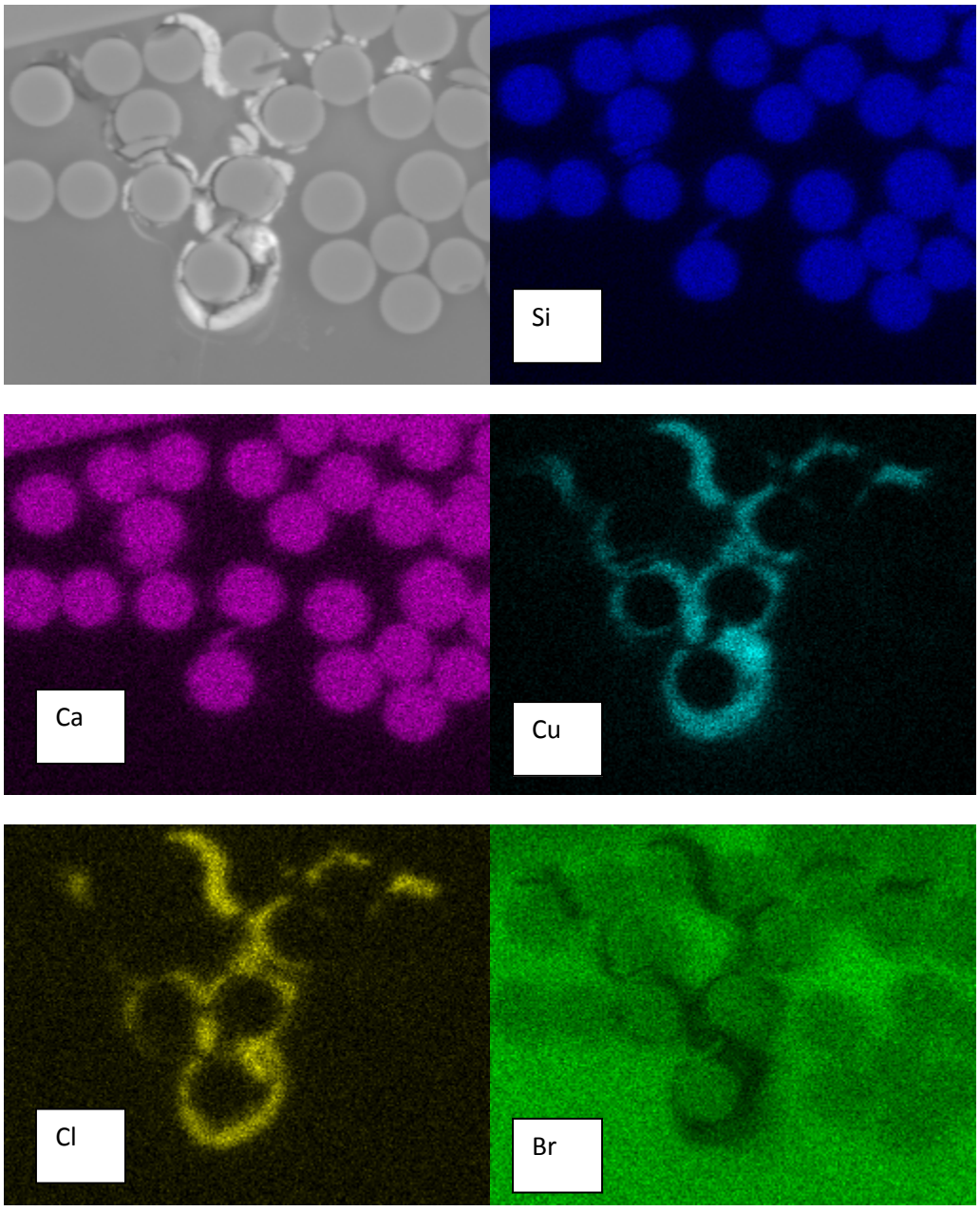

Figure G.6: EDS map for section S confirming the presence of copper, chlorine and bromine.

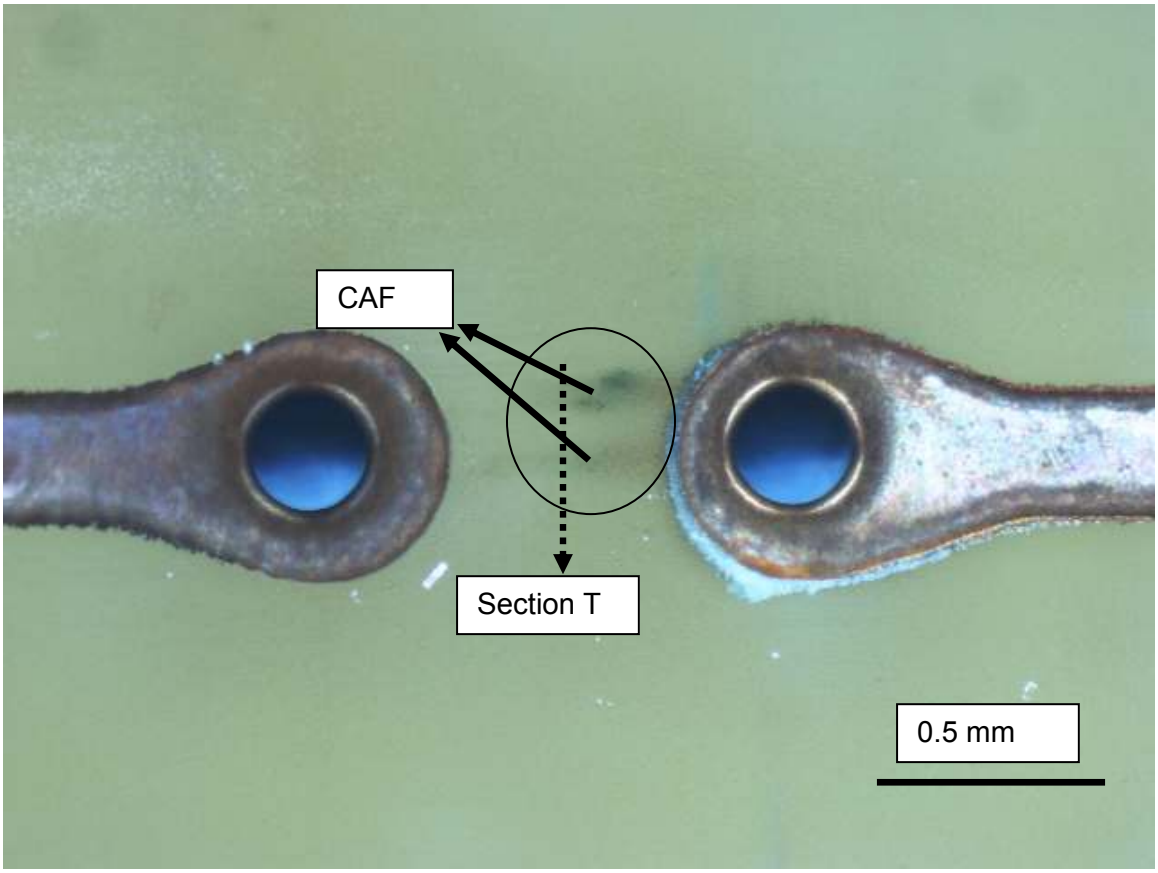

Figure G.7: Optical image illustrating CAF for a HASL processed coupon.

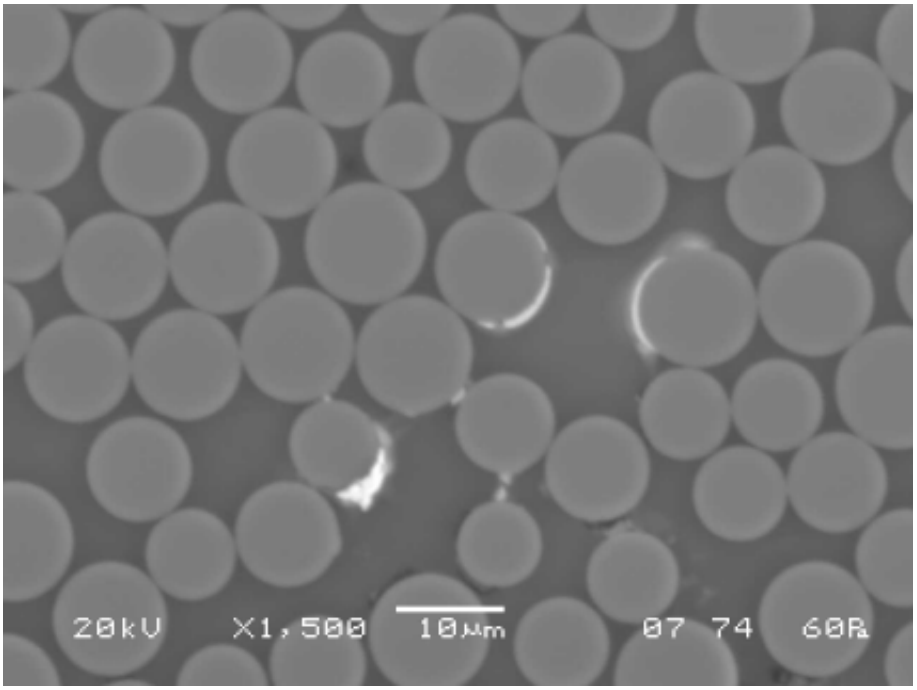

Figure G.8: SEM image showing CAF for a HASL processed coupon (i.e. section T).

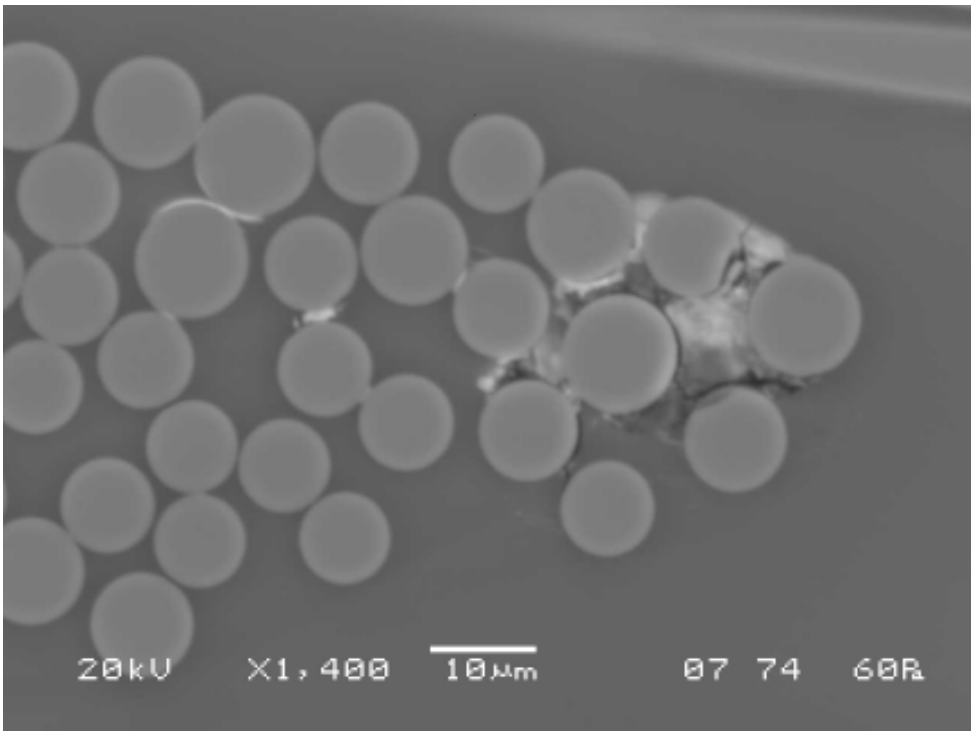

Figure G.9: SEM image for section T showing CAF for HASL processed coupons at a different point.

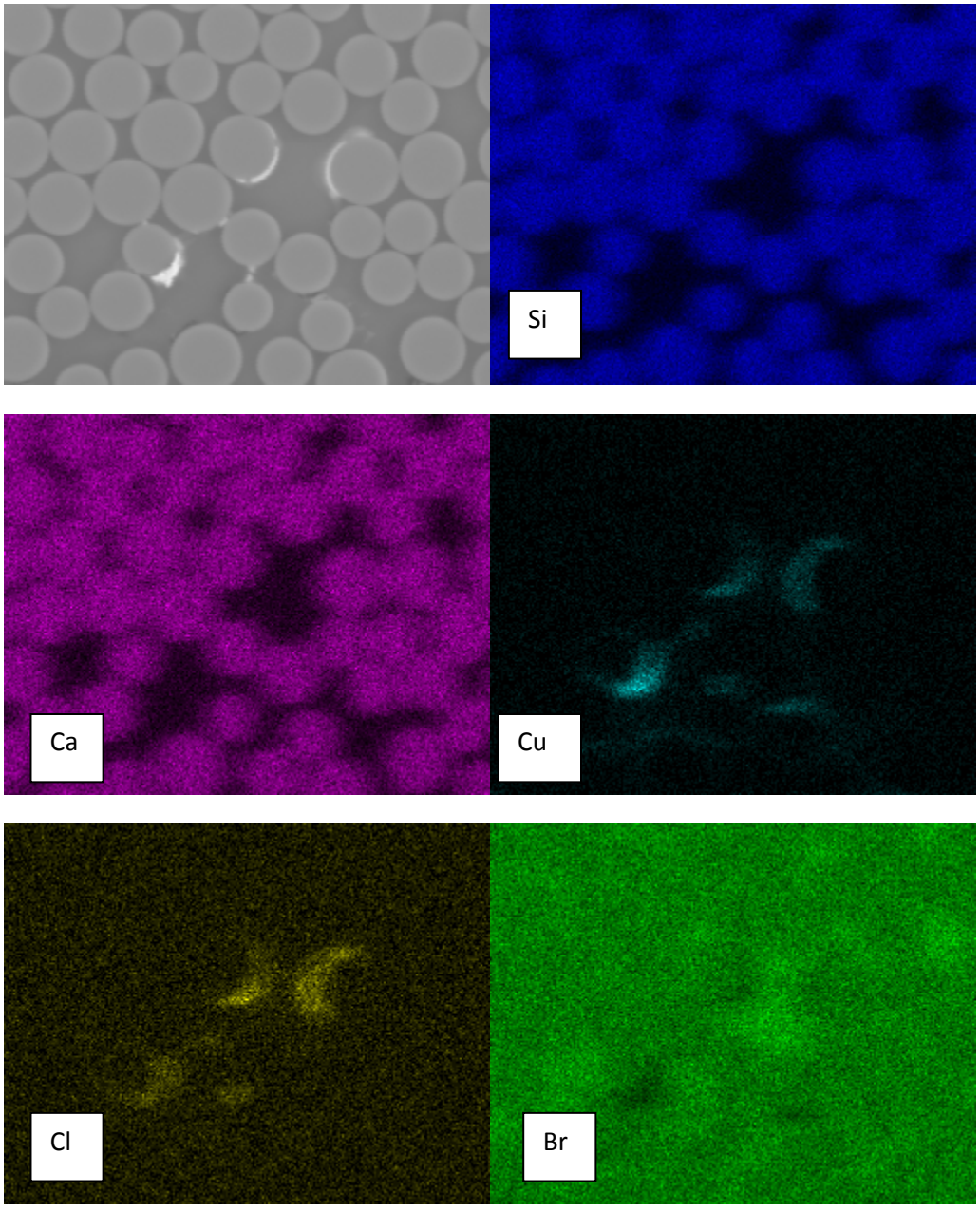

Figure G.10: EDS map confirming the presence of copper and chlorine for the CAF presented in Figure G.8.

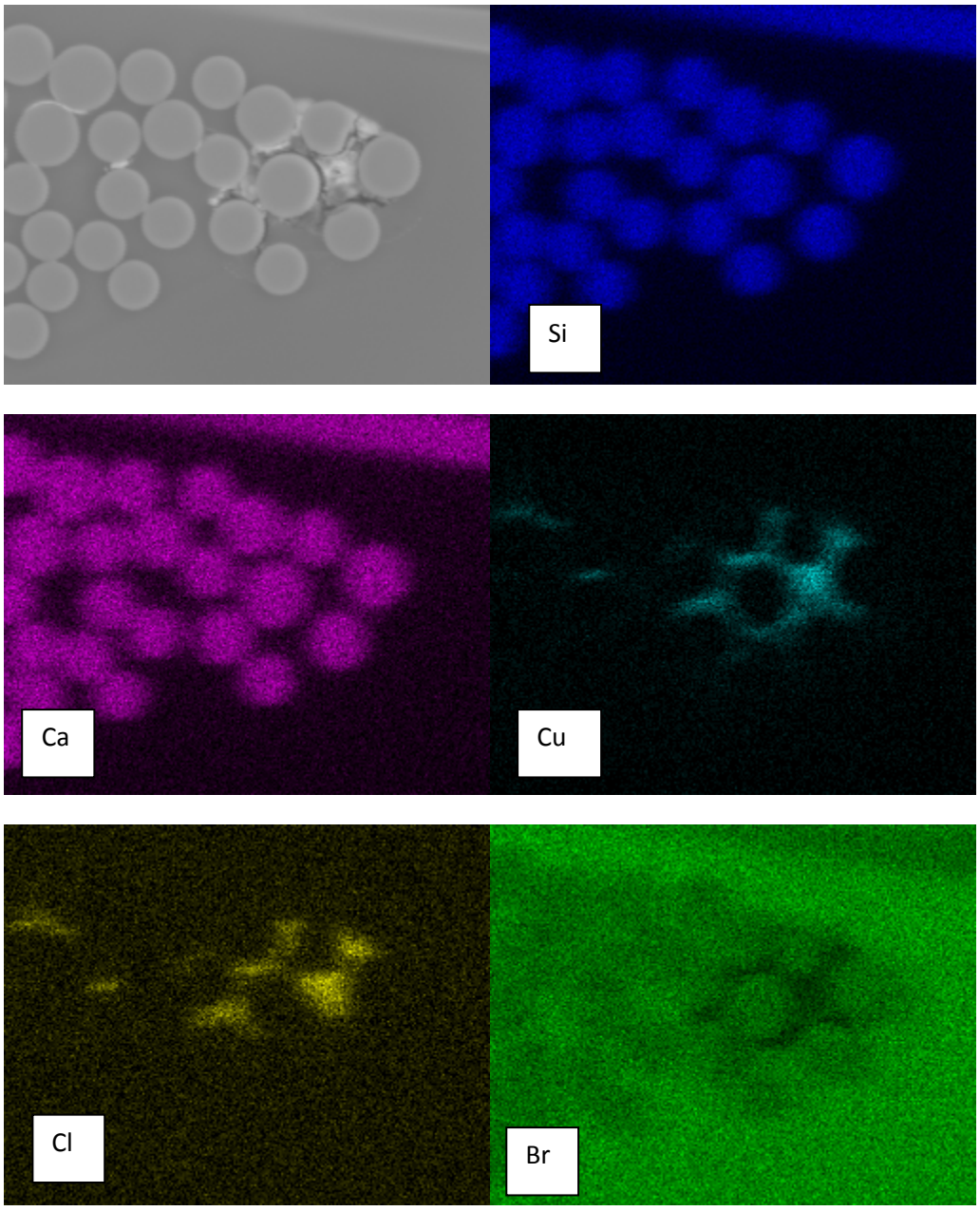

Figure G.11: EDS map confirming the presence of copper and chlorine for the CAF presented in Figure G.9.

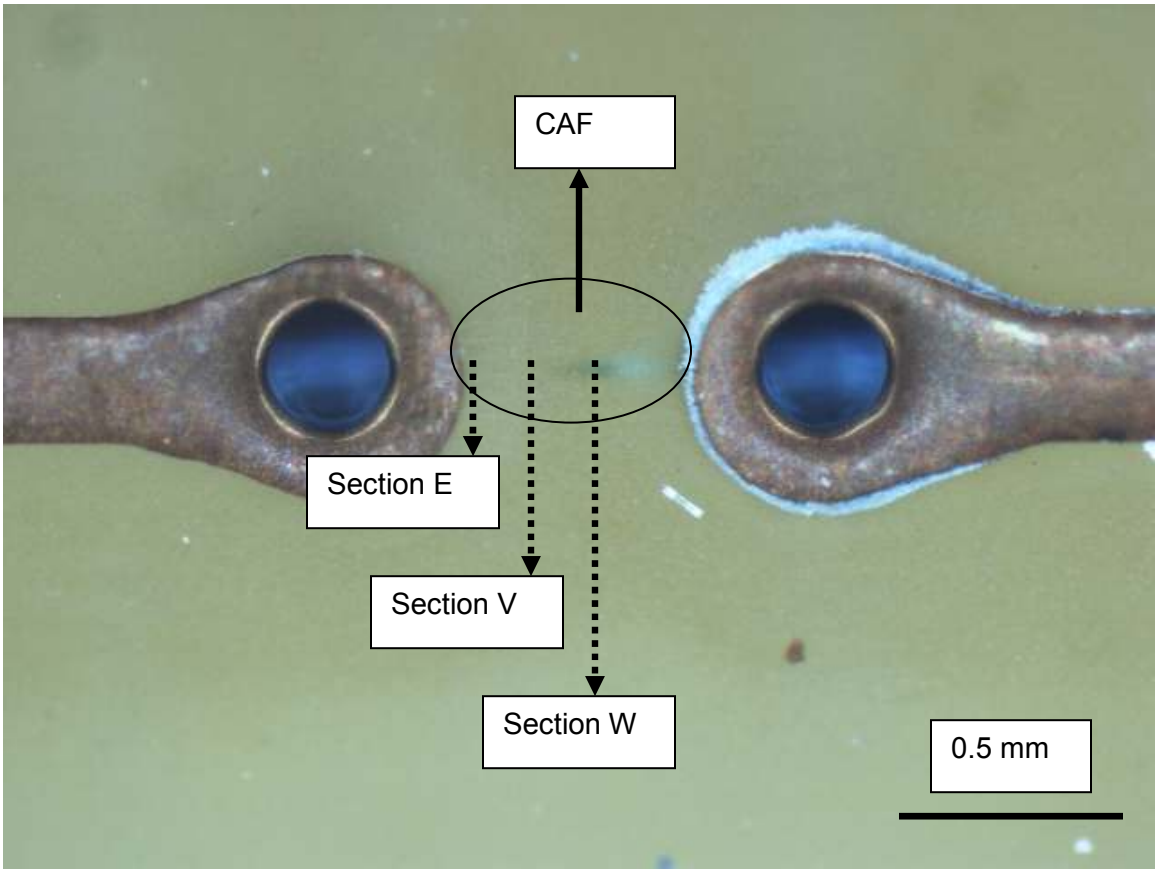

Figure G.12: Optical image illustrating CAF almost forming a bridge with the cathode for a HASL processed coupon.

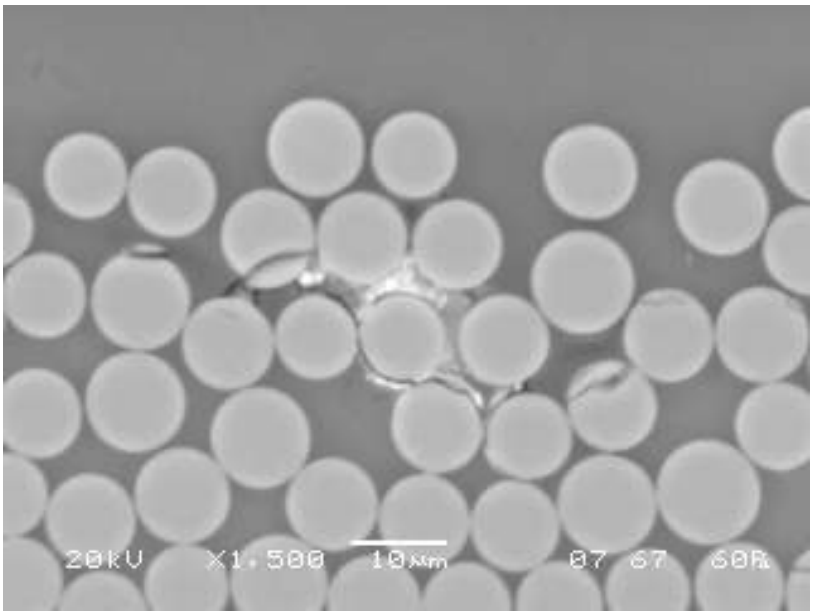

Figure G.13: CAF observed for section E.

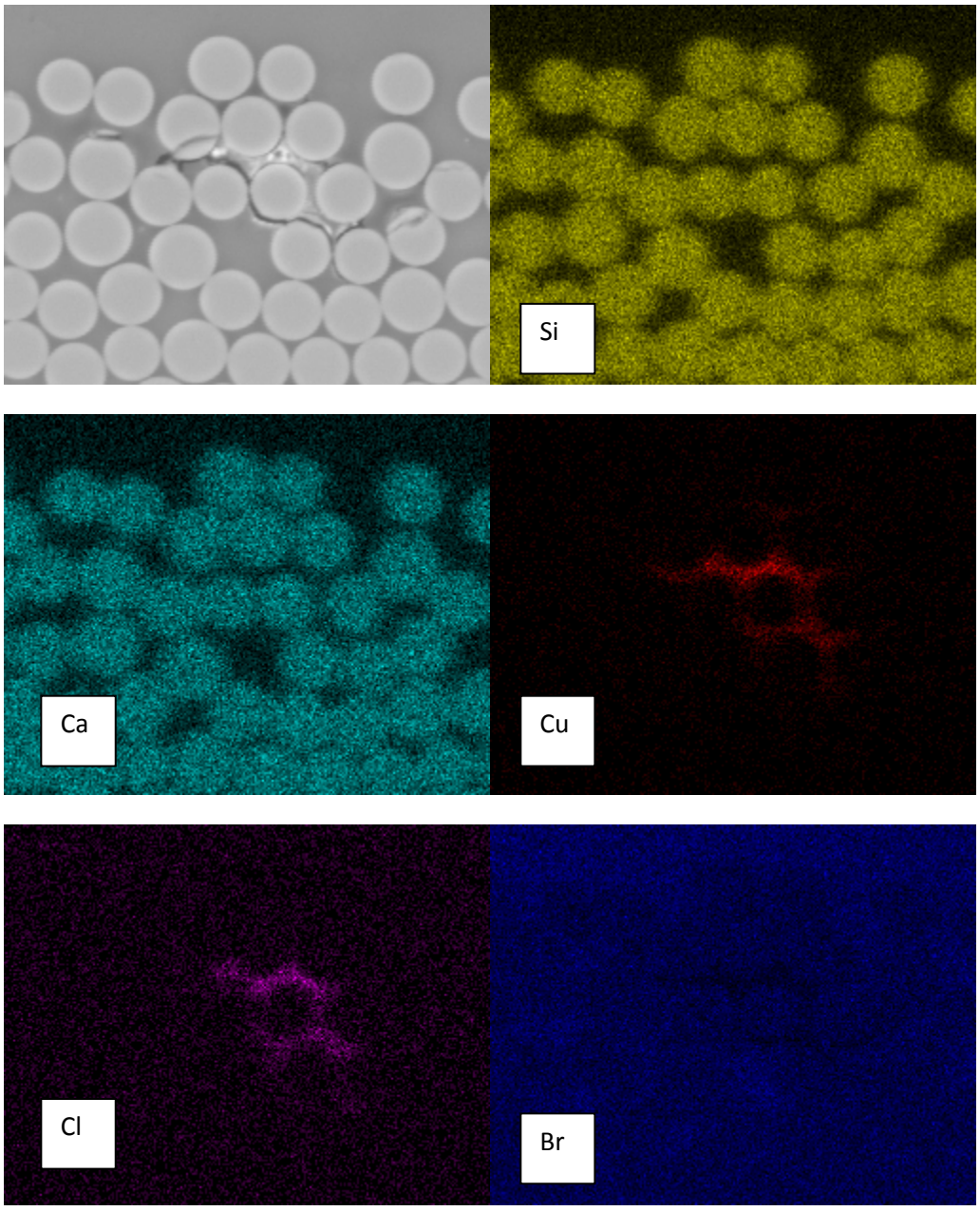

Figure G.14: EDS map confirming the presence of copper and chlorine in section E.

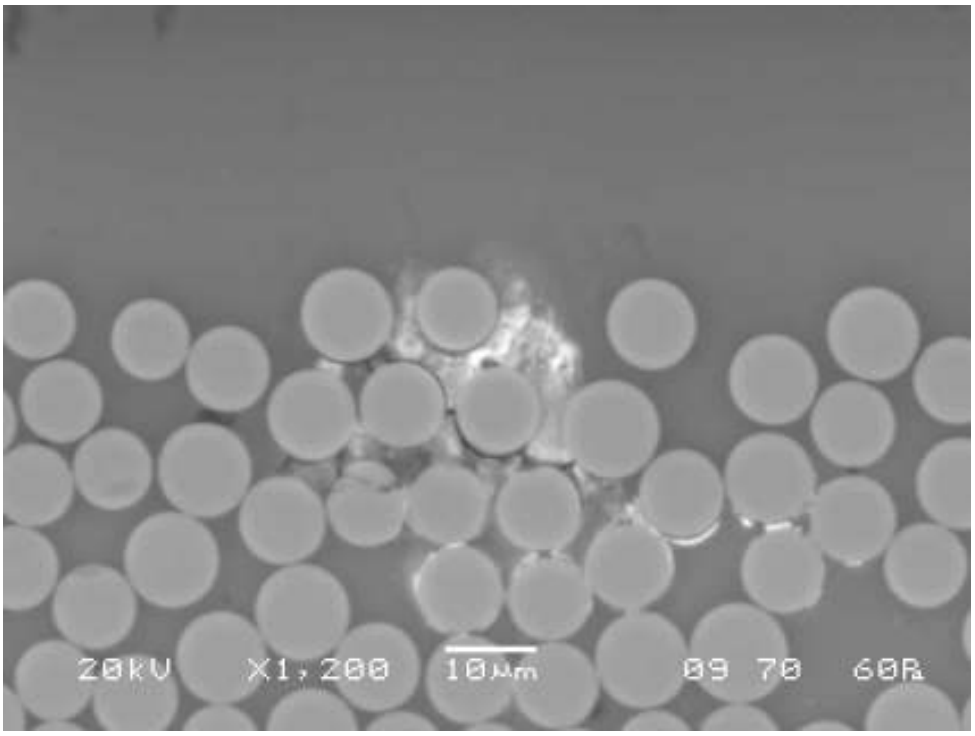

Figure G.15: CAF observed for section V.

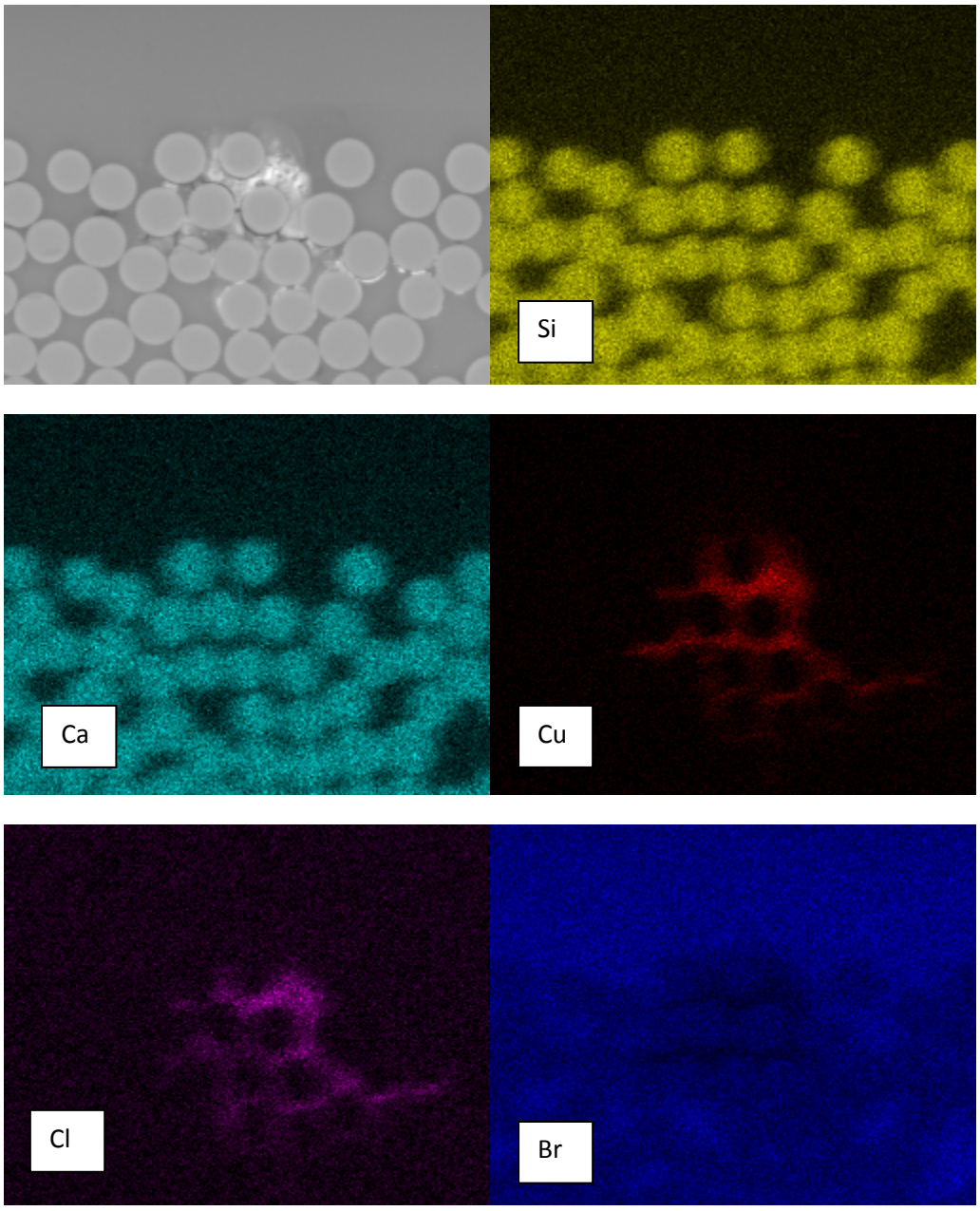

Figure G.16: EDS map confirming the presence of copper and chlorine in section V.

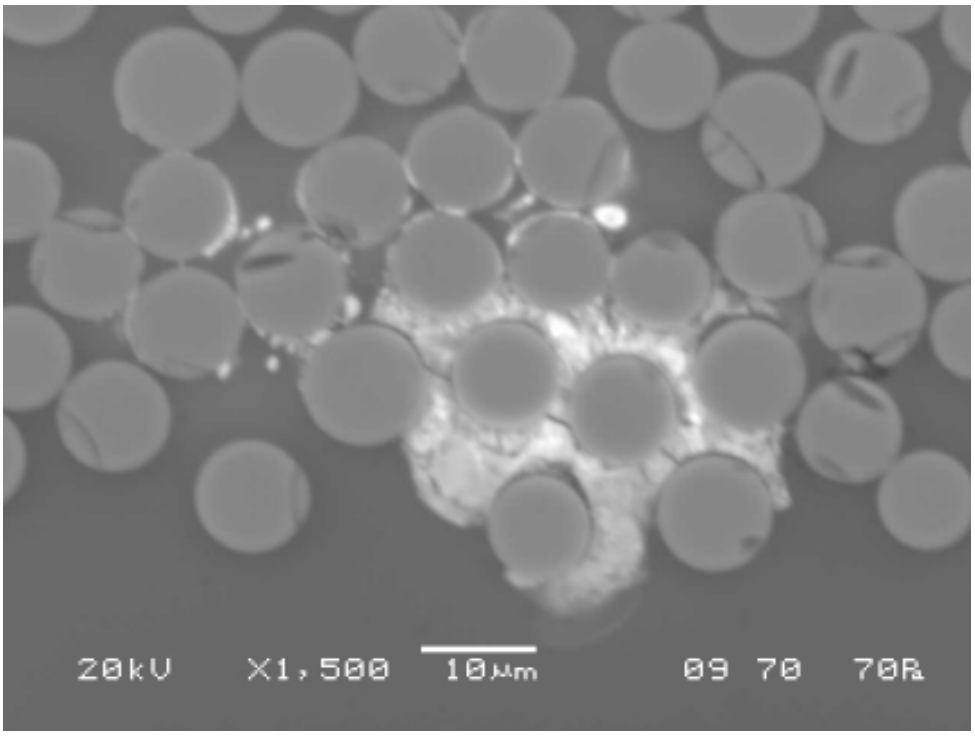

Figure G.17: CAF observed for section W.

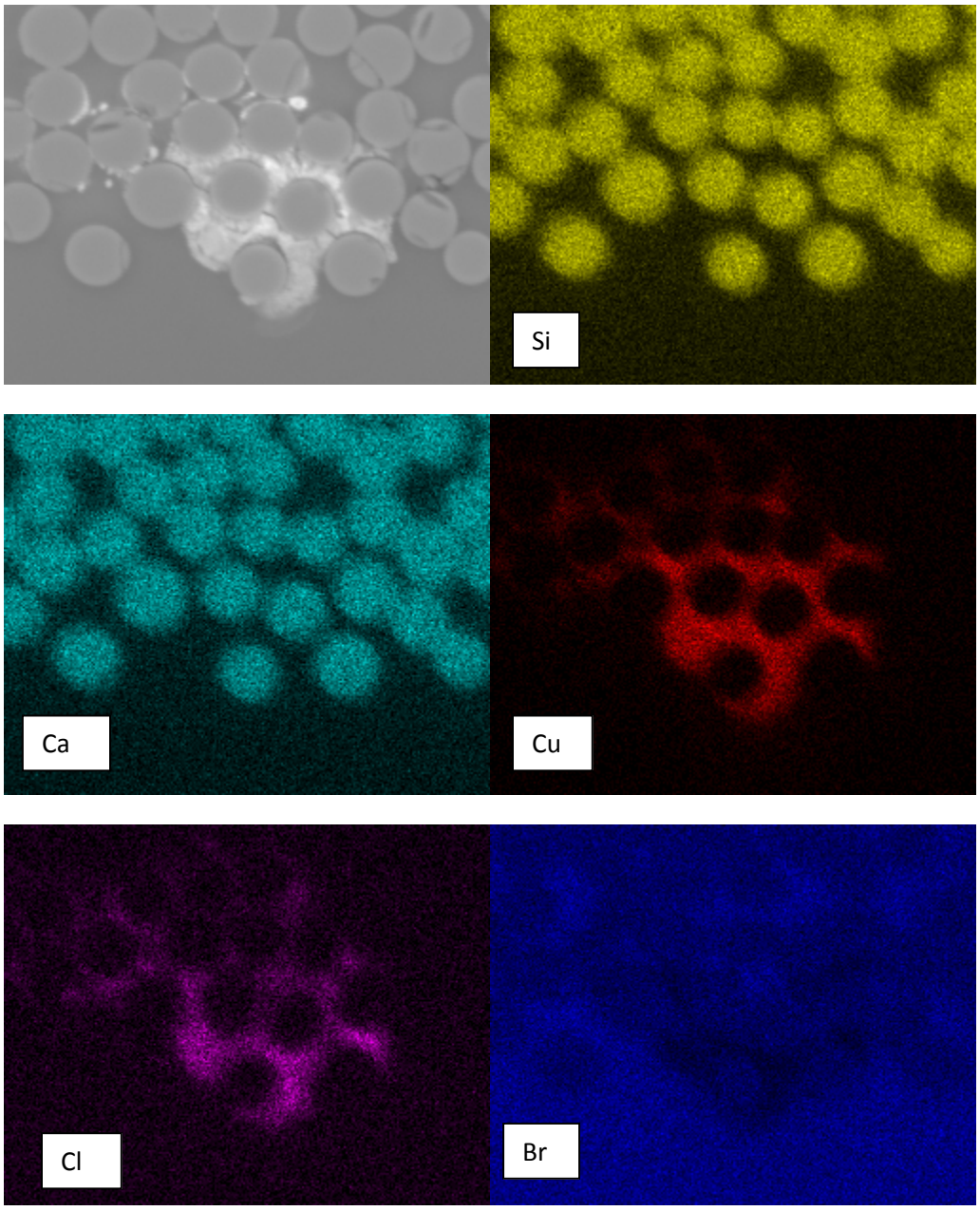

Figure G.18: EDS map confirming the presence of copper and chlorine for section W.

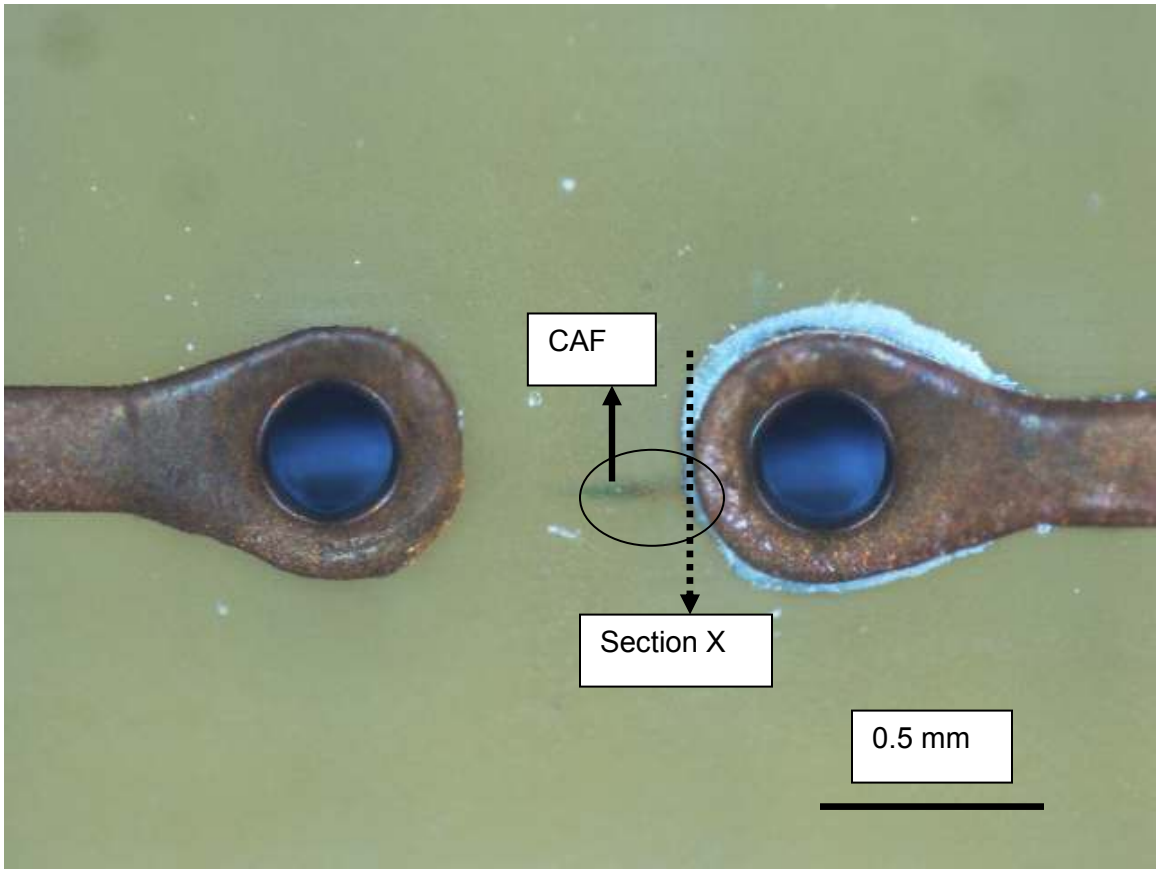

Figure G.19: Optical image illustrating CAF for a HASL processed coupon.

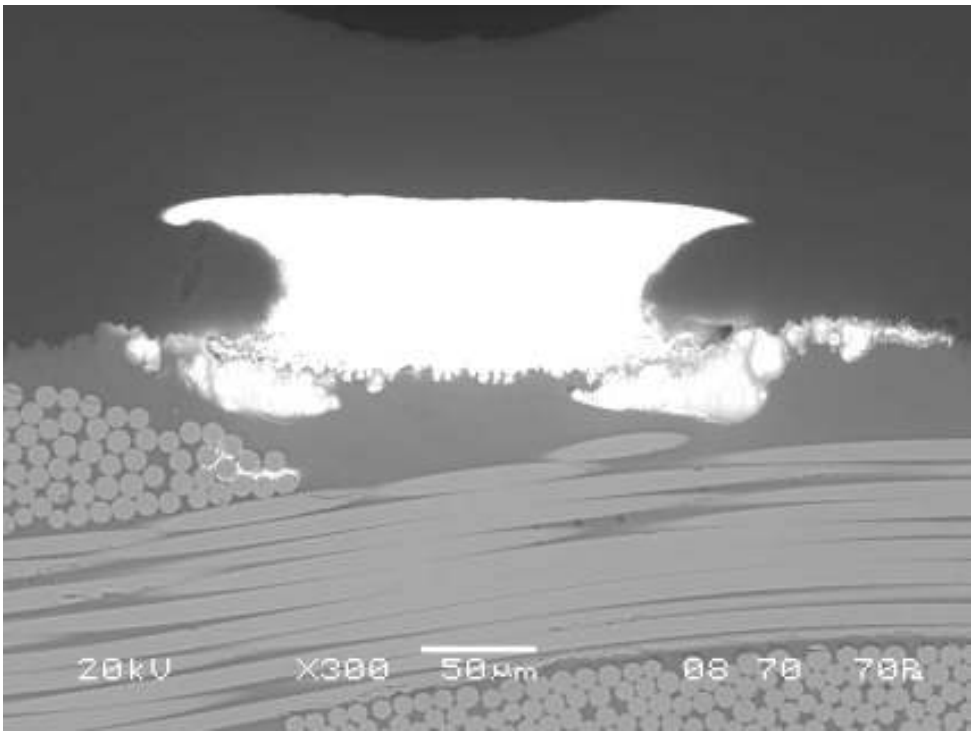

(a)

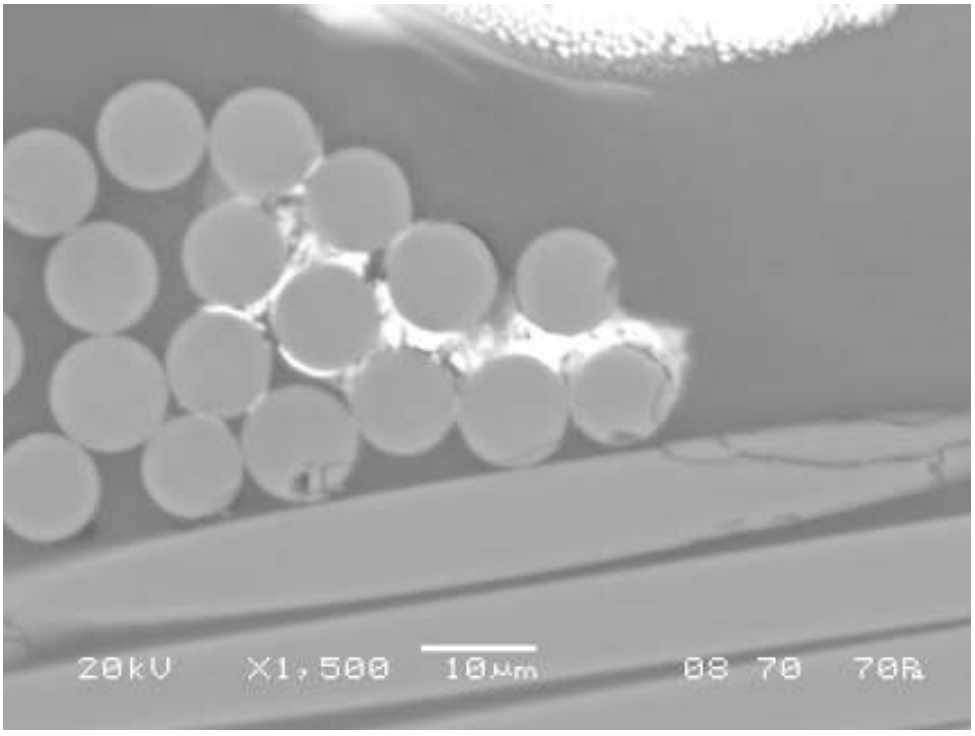

(b)

Figure G.20: SEM image illustrating CAF for section X at (a) low magnification and, (b) high magnification.

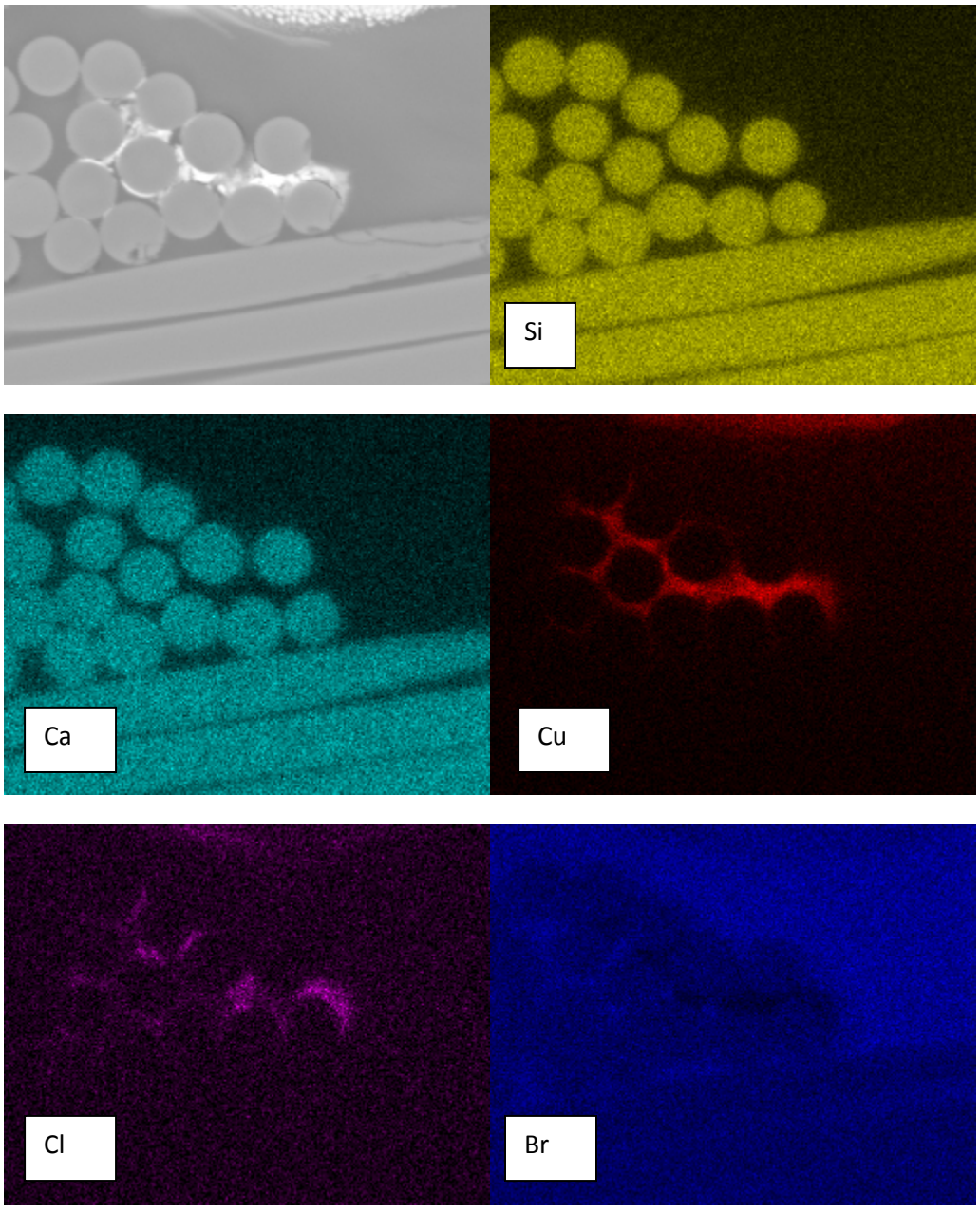

Figure G.21: EDS map confirming the presence of copper and chlorine for section X.

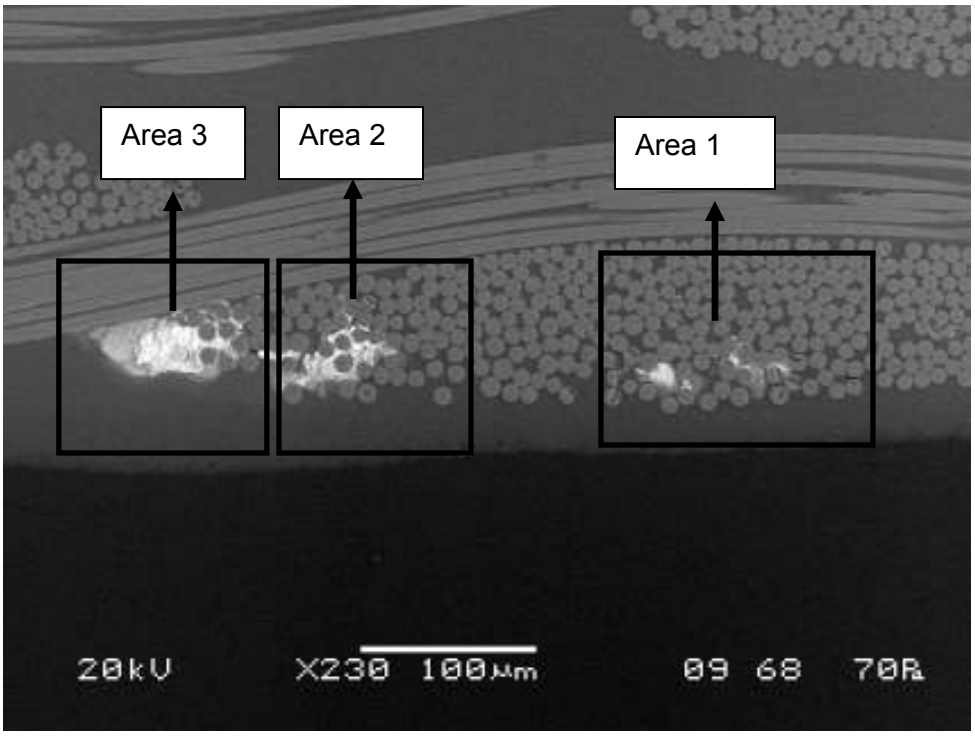

Figure G.22: CAF and a copper compound in the polymer matrix in separate areas for section H.

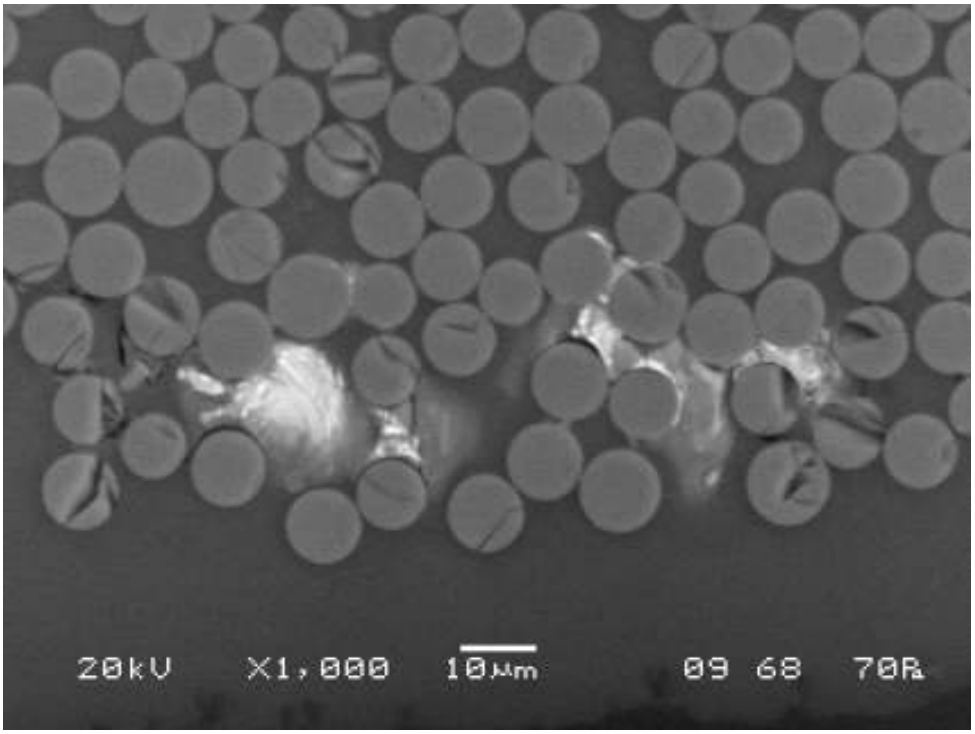

Figure G.23: CAF and a copper compound in the polymer matrix in area 1 for section H.

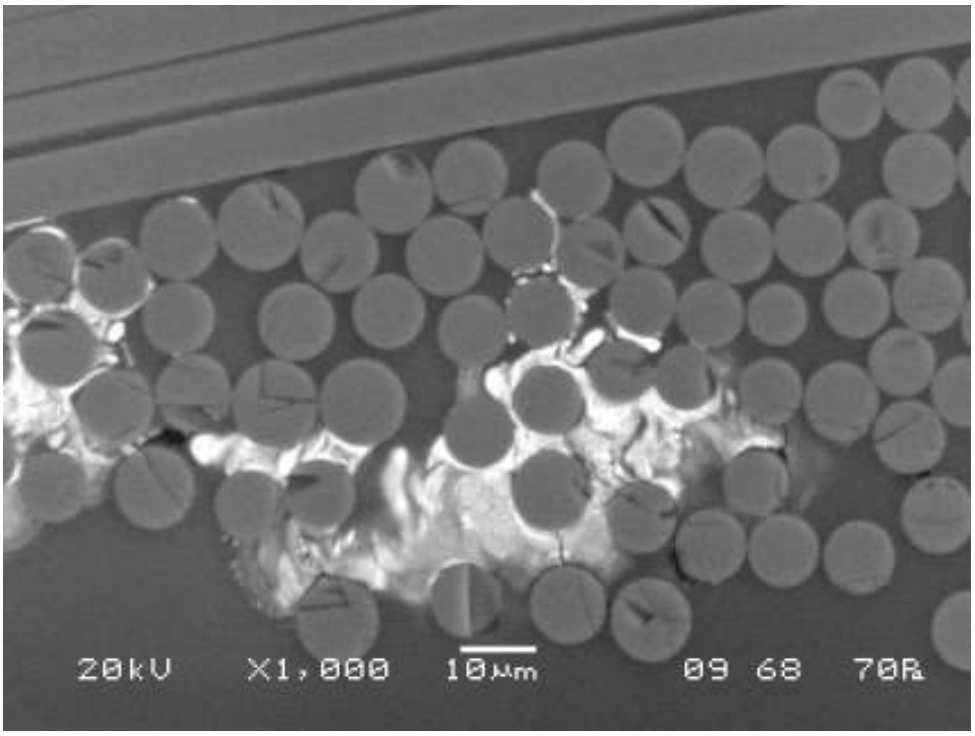

Figure G.24: CAF and a copper compound in the polymer matrix in area 2 for section H.

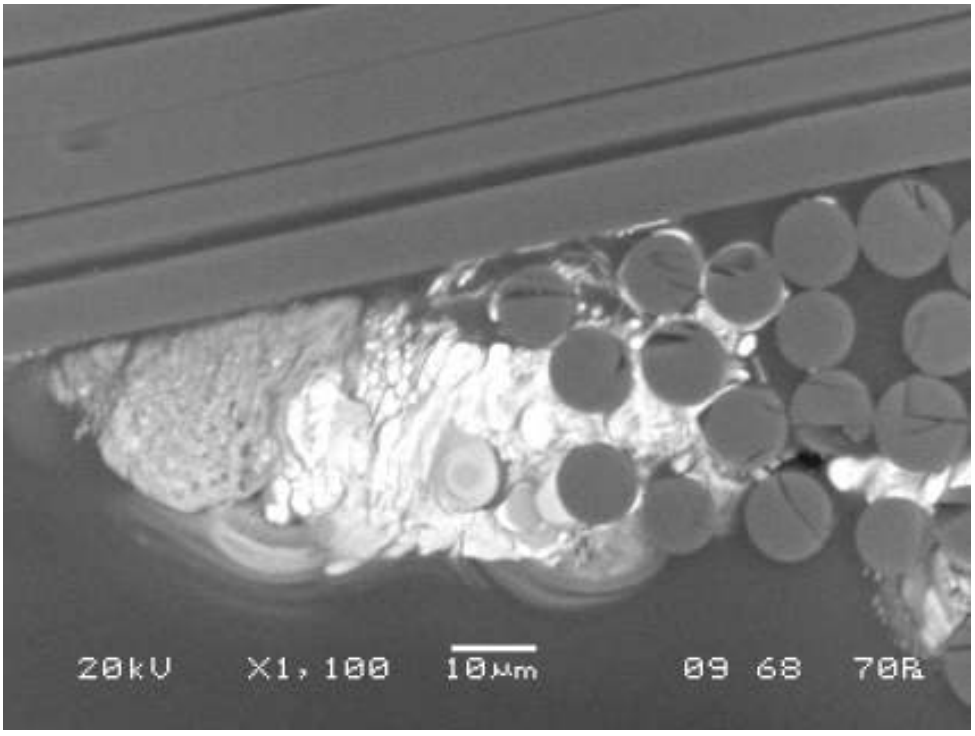

Figure G.25: CAF and a copper compound in the polymer matrix in area 3 for section H.

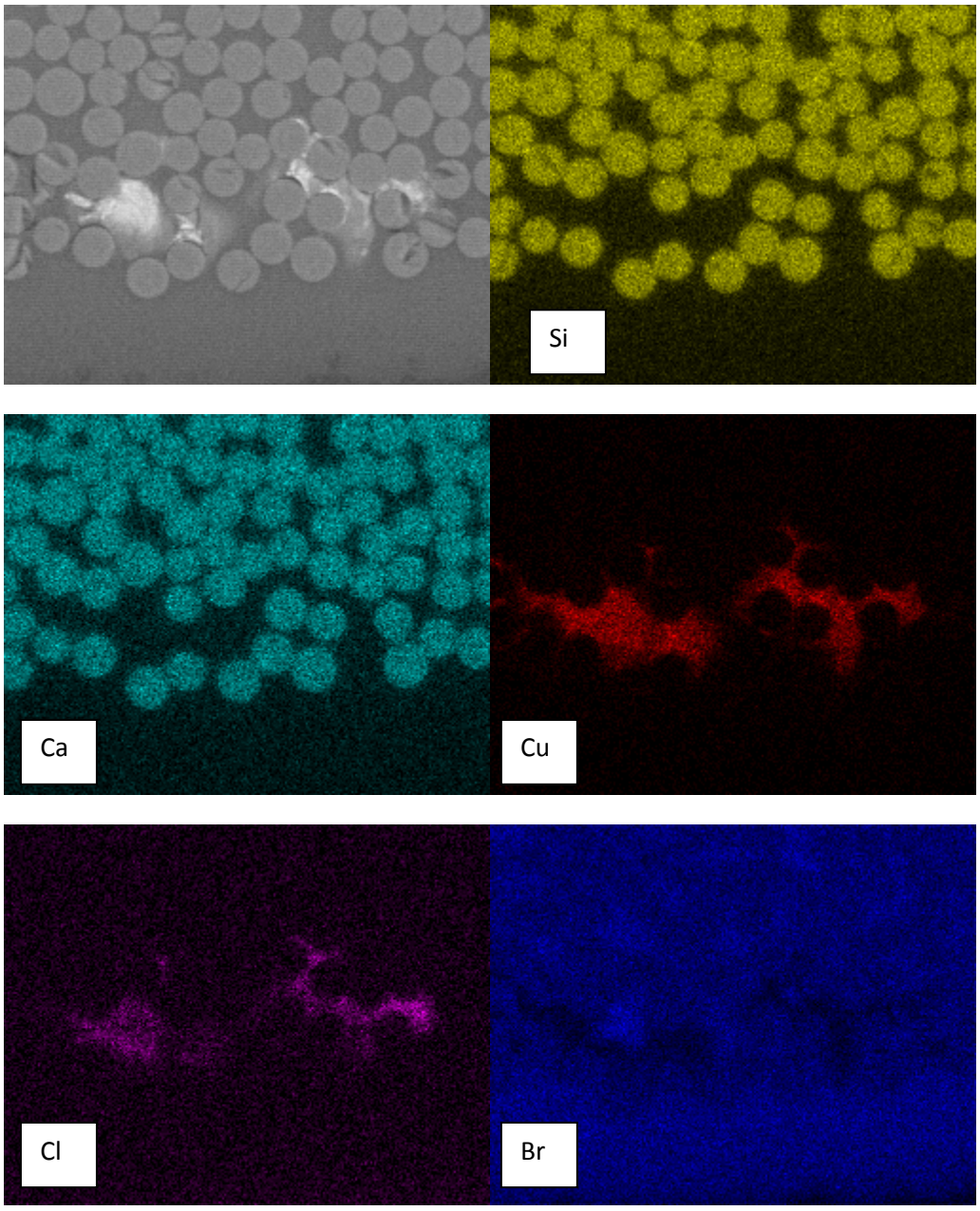

Figure G.26: EDS map confirming the presence of copper, chlorine and bromine in area 1 for section H.

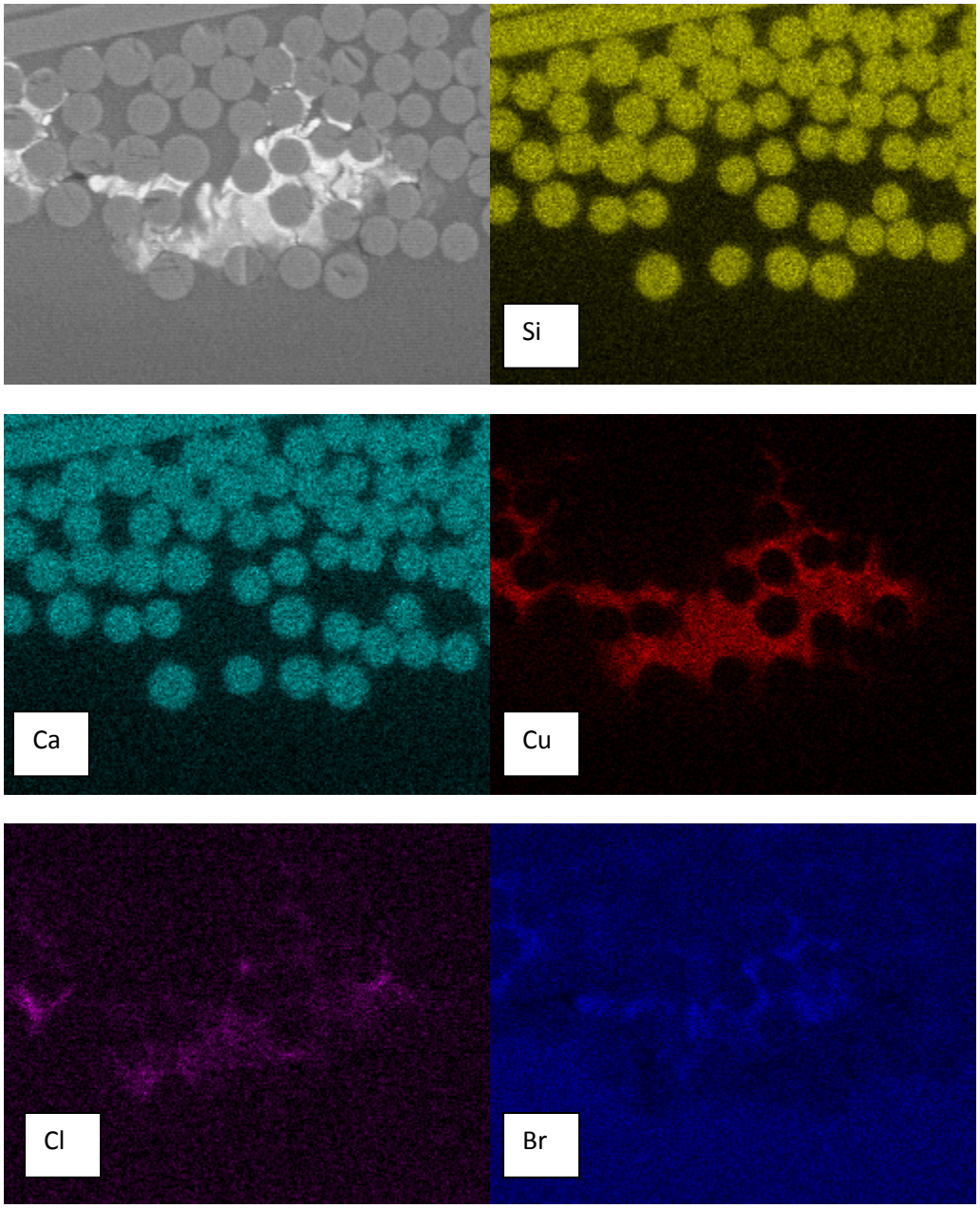

Figure G.27: EDS map confirming the presence of copper, chlorine and bromine in area 2 for section H.

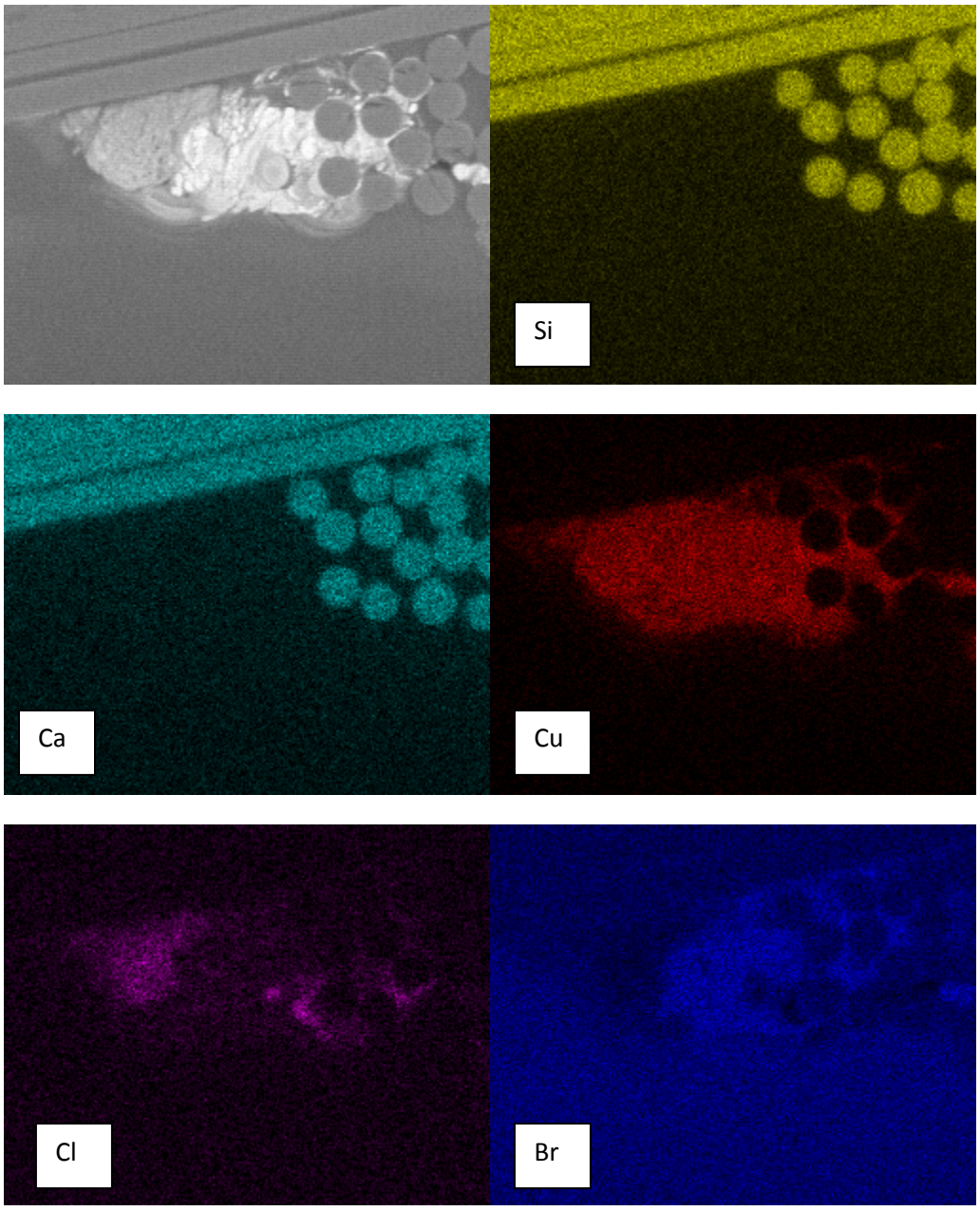

Figure G.28: EDS map confirming the presence of copper, chlorine and bromine in area 3 for section H.